The Roles of SOX9 and SOX10 in Therapy Resistance in $BRAF^{V600E}$-Induced Melanoma

John Abou-Hamad

Department of Cellular and Molecular Medicine

Faculty of Medicine

University of Ottawa

Ottawa, Ontario, Canada

This thesis is submitted to the University of Ottawa as a partial fulfilment of the Ph.D. program in Cellular and Molecular Medicine

Abstract

SOX9 and SOX10 have both pro-and anti-tumourigenic functions. In melanoma, SOX9 and SOX10 expression are mutually exclusive, suggesting they play unique roles. Here we assessed the role of SOX9 and SOX10 on therapy resistance in BRAF V600E-driven melanoma. We used a panel of syngeneic murine YUMM (Yale University Murine Melanoma) cell lines and demonstrated that these YUMM cells indeed have mutually exclusive expression of SOX9 and SOX10, correlated with their vemurafenib resistance (a BRAFV600E inhibitor). Unexpectedly, exogenous expression of SOX9 or SOX10 did not alter resistance to vemurafenib. Interestingly, SOX9 knockout cells that underwent a vemurafenib treatment regimen didn't transition to a resistant state and remained sensitive. Sox9 gene activation and Sox10 repression during the transition to the resistant state were in part due to chromatin remodeling. To further explore the role of SOX10 in resistance, we treated vemurafenib resistant YUMM lines with the oncolytic virus VSVΔ51, an emerging therapy. We showed that these resistant cells were also resistant to oncolytic virotherapy. Furthermore, loss of SOX10 recapitulates both the vemurafenib and the oncolytic resistant state in melanoma. SOX10 deletion resulted in an upregulation of various interferon stimulated genes which could play key roles in this cross resistant state. To gain further insights into the role of SOX10 in melanoma, we generated Sox10 knock-out YUMM lines. We found that the loss of SOX10 alters tumour growth by two distinct mechanisms. The loss of SOX10 induces cancer stem cell-like (CSC) properties and lead to a downregulation of CEACAM1, an inhibitory immune receptor found on both immune and cancer cells. This SOX10-CEACAM1 axis led to a decrease in anti-tumour CD8+ T cell infiltration in melanoma tumours. Taken together, we find that SOX9 plays a gatekeeper role during the transition to a targeted therapy resistant state while SOX10 enhances immune evasion and the differentiated state.

Table of Contents

List of Figures

Supplemental Figures

List of Tables

Copyright Permissions

Open Access Brief Report

Sox10-Deficient Drug-Resistant Melanoma Cells Are Refractory to Oncolytic RNA Viruses

by John Abou-Hamad [1,2], Jonathan J. Hodgins [1,3], Edward Yakubovich [1,2], Barbara C. Vanderhyden [1,2], Michele Ardolino [1,3] and Luc A. Sabourin [1,2,*]

[1] Centre for Cancer Therapeutics, Ottawa Hospital Research Institute, 501 Smyth Road, Ottawa, ON K1H 8L6, Canada

[2] Department of Cellular and Molecular Medicine, University of Ottawa, Ottawa, ON K1H 8L6, Canada

[3] Department of Biochemistry, Microbiology and Immunology, University of Ottawa, Ottawa, ON K1H 8L6, Canada

[*] Author to whom correspondence should be addressed.

Cells **2024**, *13*(1), 73; https://doi.org/10.3390/cells13010073

Submission received: 28 November 2023 / Revised: 21 December 2023 / Accepted: 25 December 2023 / Published: 29 December 2023

Download Browse Figures Review Reports Versions Notes

Abstract

Targeted therapy resistance frequently develops in melanoma due to intratumor heterogeneity and epigenetic reprogramming. This also typically induces cross-resistance to immunotherapies. Whether this includes additional modes of therapy has not been fully assessed. We show that co-treatments of MAPKi with VSV-based oncolytics do not function in a synergistic fashion; rather, the MAPKis block infection. Melanoma resistance to vemurafenib further perturbs the cells' ability to be infected by oncolytic viruses. Resistance to vemurafenib can be induced by the loss of SOX10, a common proliferative marker in melanoma. The loss of SOX10 promotes a cross-resistant state by further inhibiting viral infection and replication. Analysis of RNA-seq datasets revealed an upregulation of interferon-stimulated genes (ISGs) in SOX10 knockout populations and targeted therapy-resistant cells. Interestingly, the induction of ISGs appears to be independent of type I IFN production. Overall, our data suggest that the pathway mediating oncolytic resistance is due to the loss of SOX10 during acquired drug resistance in melanoma.

Keywords: melanoma; SOX10; BRAFV600E; oncolytics; vemurafenib; drug resistance

MDPI Open Access Information and Policy

Permissions

Abbreviations

4-OHT	4-hydroxytamoxifen
5-Aza	5-azacytidine
AKT	Protein kinase B
ATAC-seq	Assay of Transposase-Accessible Chromatin using sequencing
ATP	Adenosine triphosphate
BSA	Bovine serum albumin
BAC	Bacterial artificial chromosome
C57	C57BL/6
Cas9	CRISPR-associated protein 9
CD	Cluster of differentiation
CDKN2a	Cyclin dependent kinase inhibitor 2A
cDNA	Complementary DNA
CEACAM	Carcinoembryonic antigen-related cell adhesion molecule
ChIP	Chromatin immunoprecipitation
CM	Cutaneous melanoma
CNV	Copy number variation
CR	Conserved region
CRD	Cysteine-rich domain
CRISPR	Clustered regularly interspaced short palindromic repeats
CSC	Cancer stem cell
DCT	Dopachrome tautomerase

DIM	Dimerization domain
DMEM	Dulbecco’s modified eagle media
DNA	Deoxyribonucleic acid
DTT	Dithiothreitol
EMT	Epithelial–mesenchymal transition
ERK	Extracellular signal-regulated kinase
FBS	Fetal bovine serum
GDP	Guanosine diphosphate
GFP	Green fluorescent protein
GRB2	Growth factor receptor bound protein 2
GTP	Guanosine triphosphate
HER	Human epidermal growth factor receptor
HMG	High mobility group
ICI	Immune checkpoint inhibitor
IFN	Interferon
ISG	Interferon-stimulated gene
IRES	Internal ribosomal entry site
ITIM	Immunoreceptor tyrosine-based inhibitory motif
MAPK	Mitogen-activated protein kinase
MAPKi	MAPK inhibitor
MEK	Mitogen-activated protein kinase kinase
MITF	Microphthalmia-associated transcription factor
MOI	Multiplicity of infection

NCG	NOD CRISPR Prkdc Il2r gamma
NK	Natural killer
NF1	Neurofibromin 1
NTC	Non-targeting control
PCR	Polymerase chain reaction
PROTAC	Proteolysis targeting chimeras
PRR	Pattern recognition receptor
PTEN	Phosphatase and tensin homolog
PVDF	Polyvinylidene difluoride
qPCR	Quantitative PCR
RAF	Rapidly accelerated fibrosarcoma
RAS	Rat sarcoma virus
RBD	RAS-binding domain
Res	Resistant
RFP	Red fluorescent protein
RIPA	Radioimmunoprecipitation Assay
RNA	Ribonucleic acid
RPM	Revolutions per minute
RTK	Receptor tyrosine kinase
RUXO	Ruxolitinib
SCID	Severe combined immunodeficiency
scRNA-seq	Single-cell RNA sequencing
SgRNA	Single guide RNA

ShRNA	Short hairpin RNA
SiRNA	Small interfering RNA
SNV	Single nucleotide variant
SOS	Son of sevenless
Sox	Sry HMB-box
Sry	Sex-determining region Y
TA	Transactivation domain
TBST	Tris-buffered saline with Tween 20
TCGA	The Cancer Genome Atlas
TIM3	T cell immunoglobulin and mucin domain-containing protein 3
Tyr	Tyrosinase
UV	Ultraviolet
Vemu	Vemurafenib
$Vemu^S$	Vemu sensitive
$Vemu^R$	Vemu resistant
VSV	Vesicular stomatitis virus
VSVΔ51	VSV methionine deletion at 51
YFP	Yellow fluorescent protein
YUMM	Yale University mouse melanoma

Acknowledgements

Firstly, I would like to thank Dr. Luc Sabourin for creating a potential scientist out of me. You were always there to challenge me on everything I did, teaching me to think on my feet and understand that cancer is not static but rather dynamic.

I would next like to thank my parents and siblings for all their love and support. Although most of the time all you heard was a bunch of nonsense, you all still look the time of day to ask me how my research was going and whether I found something cool.

To Marlena, thank you for being that driving force to motivate me to complete my PhD. Whenever something was going a stray, you always knew what to say and kept me focused. I love you for that, and hopefully I could do the same when it is your time.

To the South Wing, I would like to thank all previous and present students, technicians, and PIs for allowing me to learn from all of you. You all created what I like to call my lab family, where coming to school was no longer a pain but rather a family get-together, everyday, through all the good and bad days.

To the Sabourin lab, thank you for making every day an adventure, creating and relieving stress, and always being there to challenge me. Specifically, I would like to thank my mentors, Ben, Cedrik and Khalid. I would not have the dedication to science without any of you. To Brennan and Sam, thank you for making my last couple years in the lab so much fun, you guys made it hard for me to leave.

Finally, I would like to thank Jonathan, who although was not in my lab was the person I went to the most during the good, bad and ugly times throughout my graduate degree. Without you I probably would have not started my PhD, or remained in science.

Chapter 1

General Introduction

1.1 Molecular Subtypes of Melanoma

1.1.1 The four subtypes of melanoma

Melanoma is the most aggressive form of skin cancer. Although accounting for less than 2% of all skin cancer cases in the United States it does account for most skin-related deaths(1,2). Melanoma can be divided into four groups; cutaneous melanoma (CM) (melanoma of the skin), mucosal melanoma (mucous membrane), acral melanoma (located on palms, nail beds and the soles of feet), and uveal melanoma (melanoma of the eye)(3). CM is the most common and is the focus of my work.

CM can be further divided according to the molecular landscape of genes that can modulate the mitogen-activated protein kinase (MAPK) cascade(4). The most common subtype, the B-Rapidly Accelerated Fibrosarcoma (BRAF) mutants account for approximately 40-50% of all CM(4,5). This mutation status is common in melanomas arising from intermittent sun exposure and tend to have less somatic mutations compared to the other subtypes(6,7). The Ras subtype, typically NRAS accounts for about 30% of all melanoma(4,5). Unlike the BRAF subtype, NRAS melanomas occur in older patients following chronic sun exposure(8,9). The third common subtype is associated with a neurofibromatosis type I (NF1) loss of function mutation which causes a lack of negative regulation on RAS proteins, leading to hyper activation of the MAPK cascade(4,5,10). The least common CM subtype is the triple wild type which has no mutations on BRAF, NRAS, or NF1 but tend to have increased mutations and amplifications of genes associated cell cycle progression or receptor tyrosine kinases that signal downstream to the MAPK cascade(4,5,11).

1.1.2 The mitogen-activated protein kinase (MAPK) pathway

The most common MAPK pathway observed to be altered in cancer is the RAS-RAF-MEK-ERK cascade(12). Although many cancer types have an activating mutation within this cascade, others stimulate this pathway through the amplification of receptor tyrosine kinases (RTK) found at the surface of the cell(13,14). Canonical RAS-RAF-MEK-ERK signalling can be initiated by the activation of various RTKs (HER, FGFR, PDGFR) found at the surface of the cell(15). Following activation, RTKs can dimerize and autophosphorylate, allowing various adaptor protein docking such as GRB2(15). GRB2 can then recruit various Ras guanine nucleotide exchange factors such as SOS which facilitates the exchange of GDP to GTP on RAS proteins(15). GTP bound RAS can interact with RAF proteins at the plasma membrane, facilitating the homo, or heterodimerization of RAF proteins and activating their kinase activity(15). RAF dimers can then phosphorylate the serine/threonine kinase MEK, and subsequently ERK(15). ERK, the final kinase of the canonical MAPK pathway, can phosphorylate a plethora of proteins including transcription factors c-Jun and c-Myc, promoting cell growth, proliferation and survival(15)(Figure 1.1A).

1.1.3 BRAF(V600E) subtype

BRAF is a serine/threonine kinase part of a larger family of active RAF proteins including ARAF and CRAF(16). Three conserved regions make up the RAF proteins (CR1, CR2 and CR3)(17). CR1 contains two specific domains: the RAS-binding domain (RBD) and the cysteine-rich domain (CRD), where it functions as the GTP-binding domain used for its interaction with RAS proteins(18,19). CR2 acts as a hinge to allow for conformational changes of RAF proteins and to enter an open/active or closed/inactive state. This region is predominantly serine-rich and allows for 14-3-3 protein binding(20). CR3 is the catalytic domain and allows for the

phosphorylation of RAF specific targets(20–22). Interestingly BRAF is the most commonly mutated RAF protein in various cancer types such as colorectal cancers, thyroid cancers and melanoma(23). Although it is not fully understood why BRAF is a preferential target for mutations, various explanations have been proposed such as tissue specificity and expression level. Since BRAF has the highest basal kinase activity compared to other RAF proteins due to its constitutively negative charge in the kinase domain, it may also be the reason for its oncogenic potential(24–26).

Before an activation signal, BRAF remains as a monomer in the cytosol in its closed conformation(27). It is held in this conformation through autoinhibition by CR1 and CR3 binding and through interaction with a 14-3-3 protein that is mediated through phosphorylation in the CR2 domain(17,20). This stabilizes the closed conformation and blocks kinase activity. BRAF activation begins with GTP bound RAS binding to the RBD on BRAF(28–32). This binding allows for BRAF recruitment to the plasma membrane where the CRD can bind to phosphatidyl-serines in the plasma membrane(28–33). Once both the RBD and CRD are engaged, BRAF loses its autoinhibitory conformation(32,33). At the plasma membrane, interaction with phospholipids allows for the release of 14-3-3 bound to the CR2 region and dephosphorylation of the CR1 domain converting BRAF into its open state(34–36). Once in its active conformation, BRAF can form homo or heterodimers with other RAF proteins, where they can allosterically activate one another in the CR3 region(36). Active BRAF can phosphorylate MEK which in turn can phosphorylate ERK1/2 to complete signal transduction(37)(Figure 1.1A).

Over 80% of all BRAF mutations found in melanoma revolve around the missense mutation at nucleotide 1799 where is a thymine to adenine substitution(23). This mutation converts the amino acid at position 600 from a valine to a glutamic acid. This is important since the V600

position is part of the glycine rich segment that allows for hydrophobic interactions with other segments of BRAF, keeping the DFG motif in its inactive/closed conformation(38,39). Due to the V600E mutation, the hydrophobic valine is now a charged glutamic acid, disrupting the hydrophobic interaction and forcing the DFG motif into its open active conformation, aligning ATP and the peptide recognition, leading to constitutive kinase activity(38,39). Normally ERK phosphorylation is a negative regulator of BRAF activity. ERK phosphorylates BRAF at S705 and T753, disrupting the formation of a dimer, which causes BRAF to enter an inactive conformation(40,41). Valine 600 is located in the activation loop, where it keeps BRAF in an inactive conformation. Following a V600E mutation, BRAF switches to an active confirmation and can signal independently of upstream stimuli or downstream negative feedback regulation(39)(Figure 1.1B).

The oncogenic potential of BRAF(V600E) is dependent on the genetic landscape. $BRAF^{V600E}$ expression in melanocytes leads to a common phenomenon called oncogene-induced senescence(42–44). Following a rapid cell division, melanocytes lose their growth capabilities and begin to stain positive for senescent markers such as $p16^{INK4A}$ and SA-β-gal(45). In mice it was found that $BRAF^{V600E}$ expression in melanocytes gave rise to melanocytic nevi(43,44). These nevi undergo growth arrest following multiple cell cycles and share the expression of senesce-induced genes. Although these nevi are not truly senescent but rather in this quiescent-like state, they can bypass this growth arrest and form melanoma. This is achieved through the loss or inhibition of tumour suppressors like PTEN or CDNK2a which removes the growth arrest signal to induce a malignant tumour(46,47).

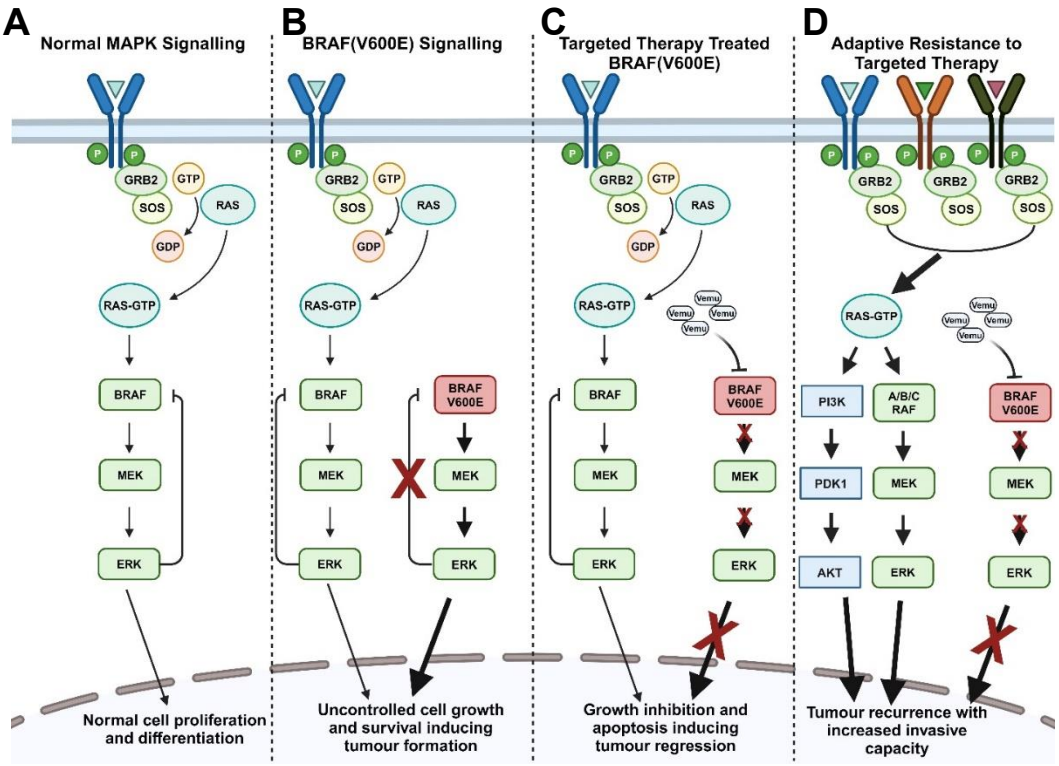

Figure 1.1 Schematic representation of MAPK signalling pre- and post tumour treatment. (A) Representation of MAPK signalling in normal tissue. (B) $BRAF^{V600E}$ induced MAPK signalling is unaltered by ERK negative feedback and does not require upstream cues for activation. (C) $BRAF^{V600E}$ inhibition using vemurafenib blocks downstream signalling, reducing tumour burden and inducing cell death. (D) Chronic MAPK inhibition induces adaptive reactivation of the MAPK cascade and neighbouring signalling pathways to promote tumour regrowth. Figure was generated in BioRender.

1.1.4 Generation of murine models using the V600E mutation

Various murine melanoma models do exist that usually recapitulate various RAS or BRAF-driven melanomas. The most common studies focus on the $NRAS^{Q61R}$ and $BRAF^{V600E}$ mutations which all produce melanocytic nevi in mice(48). Interestingly many models pair these oncogenic mutations with conditional deletions of various tumour suppressors including $p16^{INK4A}$, PTEN and P53(48). These deletions are accomplished using the Cre-lox recombinase system where two loxP sites are flanking critical domains within the gene of interest. Tissue-specific expression of Cre allows critical exons to be excised, resulting in null alleles in organs of interest(49). In melanoma models, two main promoters are typically used: the DCT or Tyrosinase (Tyr) promoter(48). Current melanoma models use an inducible system. For example, the $BRAF^{V600E}$, $PTEN^{fl/fl}$, $Cdkn2^{fl/fl}$ utilizes the CreER that is driven off the Tyr promoter(46). This allows for topical or systemic melanoma induction that is dependent on 4-OHT treatment(46). Interestingly, termed YUMM, various C57 cell lines from $BRAF^{V600E}$ models harboring various genetic mutations have been derived(50). These cell lines have a similar genetic makeup but differ in various properties including in vitro and in vivo growth potential, immune infiltration and resistance to targeted therapies(50).

1.2 Therapeutic approach to treating BRAF(V600E) melanomas

1.2.1 Targeted therapies

Targeted therapies use various forms of agents to target specific proteins to halt and kill cancer cells. This strongly differs from chemotherapies as those target rapidly cycling cells, which is not always the case in some cancers(51). Targeted therapies are aimed at specific mutations, amplifications, or increased enzyme activity that is specific to particular cancers, increasing specificity and decreasing the death of normal neighbouring tissue(51).

Targeted therapies usually come in two forms: monoclonal antibodies (eg. Herceptin), and small molecules (eg. Imatinib)(52–54). One of the first tested targeted therapies used against melanoma consisted of two kinase inhibitors, sorafenib and RAF-265(55). These two molecules are both non-selective inhibitors, targeting multiple proteins due to the similarity of the kinase structure. Although functioning as intended, they lack the specificity leading to increased toxicity in patients(55). The high mutation burden found in melanoma thus allowed for the ability to develop targeted therapies.

The first targeted therapy developed against melanoma was the BRAF inhibitor Zelboraf (further known as vemurafenib)(56). Vemurafenib is a small molecule inhibitor that functions similarly to sorafenib by competing with ATP, but rather than targeting the inactive kinase, vemurafenib primarily inhibits BRAF in its active/open conformation, increasing specificity for the $BRAF^{V600E}$ variant(56,57). Although vemurafenib caused inhibition of $BRAF^{V600E}$ (31nM) it could also inhibit other kinases at various potencies including c-RAF-1 (48nM) and wild-type BRAF (100nM)(56,57). Differences in inhibition were negligible when tested in biochemical assays but this was not the case when vemurafenib was tested in vitro and in vivo(58–61). In clinical trials, vemurafenib was shown to extend overall survival and progression free survival in metastatic $BRAF^{V600E}$ melanoma, making it an important treatment(62–64). Vemurafenib was able to produce great response rates with an increase in clinical response by approximately 50%(62–64)(Figure 1.1C). However, within a year patients no longer responded to vemurafenib treatment and began to relapse(65). This lack of response to vemurafenib was due to the activation of various resistant mechanisms currently being studied in melanoma(65).

1.2.2 Immunotherapies

Like targeted therapies, immunotherapies are one of the best lines of defense for advanced metastatic melanoma. Immunotherapies exist in various forms, with the most common being the immune checkpoint inhibitors (ICI). They utilize monoclonal antibodies to block ligand access to inhibitory receptors on cytotoxic lymphocytes. Ligands such as PDL-1, CD80, LAG3, HVEM and CEACAM1 can bind to their respective receptors on immune cells and impose an immunosuppressive effect(66).

Currently approved ICIs include Ipilimumab and Nivolumab(67–69). These antibodies block CTLA-4 and PD-1, respectively, two inhibitory receptors usually found on cytotoxic T-cells (67–69). These checkpoint blockers function through binding to their respective receptor, no longer allowing ligand-receptor interaction and therefore, blocking the T-cells from entering an exhausted, shutdown state (66). This allows for the reactivation of the host's immune cells, recognition of the cancer and immune-mediated cell death. Although these various checkpoint blockers show great efficacy and are utilized in metastatic melanoma in conjunction with targeted therapies, the patients once again relapse and lose sensitivity(70–72). Combined with the loss of vemurafenib sensitivity, this dual resistance is referred to as “cross resistance”. Following resistance, a vast majority of these ligands become expressed at the cellular surface causing increased immunosuppression (66). Other ICIs blocking LAG-3 and TIM-3 interactions are currently being tested to circumvent this overall resistance observed. Combination therapy of anti-PD-1/LAG-3 has shown approximately a 13% objective response rate in patients previously treated with anti/PD-1 therapy(73,74). Although minuscule these findings provide initial proof for the use of other ligand/receptor blockers to allow for re-sensitization to checkpoint inhibitors.

Although anti-PD-1 and CTLA-4 blocking antibodies are currently used in the clinic, other advancements have been made in various forms of immunotherapy. One therapy that is beginning to gain traction is a form of adoptive cell therapy using host tumour infiltrating lymphocytes (TILs)(75). Briefly, TILs are harvested from the patient, expanded and activated ex vivo, and then subsequently administered back to the patient. Since they were harvested from the host's tumour microenvironment, they harbor an inherent recognition of the tumour-associated antigens, and therefore can recognize and properly clear the tumour. In a phase III clinical trial, the efficacy of TIL therapy was compared to ipilimumab where the overall objective response rate and overall survival was found to be higher in the TIL-treated compared to the ipilimumab-treated group(76). Overall, TIL therapy is a promising avenue which is currently being tested in a co-treatment regimen with ICIs to allow for reactivation of the host's immune system and complete tumour clearance.

1.2.3 Virotherapies

Oncolytic virotherapy functions in two major ways: 1) through the direct lysis of cancer cells and 2) through the recruitment of anti-tumour immune cells to the tumour microenvironment. Although there are various forms of oncolytic viruses, only the herpes simplex virus, T-Vec, has been FDA-approved for medical use in melanoma(77). But with the breakthrough of targeted and ICI therapies, the mode of action of T-VEC has not been fully elucidated as well as for other oncolytic viruses(78).

Vesicular stomatitis virus (VSV) is a single negative strand RNA virus that belongs to the Rhabdoviridae family. Interestingly, VSV tends to infect horses, rodents and cattle but minimally infects humans with only mild/asymptomatic outcomes. VSV harbors an 11kbp genome containing only 5 genes, the Nucleocapsid protein (N), Phosphoprotein (P), Matrix protein (M),

Glycoprotein (G) and the Large polymerase protein (L)(79,80). These 5 proteins make up the bullet shaped envelope virus and allow for its viral entry, replication and spread(79–81).

During viral infection, the cells have a multipurpose defense/sense mechanism that activates the type I IFN response that inhibits viral replication(82). During viral infection, the Type I interferon response can be activated through various pathways known as pattern recognition receptors (PRRs)(82). Although PRRs come in many forms against RNA viruses, two families are mainly involved including Toll like receptors and RIG-I-like receptors. These PRRs sense VSV proteins or genomic RNA that are not familiar to the hosts or have improper localization and can further induce the type I IFN response(82). The type I IFN response signals through its receptors IFNAR1/2 which dimerize following IFN binding(82). This binding promotes the autophosphorylation of JAK1 and TYK2 which phosphorylates STAT1 and STAT2 promoting their dimerization(82). Following STAT1/2 phosphorylation, they can enter the nucleus as a trimer with IRF9 where they can activate various interferon-stimulated genes (ISG)(82). These ISGs play various roles in blocking viral infection and propagation, terminating the viral spread(82).

Although resistance can be observed following oncolytic treatment, understanding the mechanisms behind this resistance can help improve treatments. A majority of studies have looked into VSV treatment and potential mechanisms of resistance to oncolytic infection. Specifically in melanoma, it has been shown that different human melanoma cells have varying susceptibility to VSVΔ51(83). Pre-treatment with IFNβ was able to resolve these differences but at varying concentrations, indicating that certain cells have various levels of defects in the antiviral IFN response (83). Following immune checkpoint inhibitor resistance in melanoma, a proportion of patients show a loss of function mutation within the IFN-JAK-STAT pathway(84). Oncolytic virus treatment post ICI resistance has shown an increase in VSV susceptibility which is due to the loss

of function of JAK2 and an impaired IFN signaling pathway (84), providing a potential alternative treatment for ICI resistance.

1.3 Targeted therapy resistance

1.3.1 Modes of resistance

One major mechanism of targeted therapy resistance in melanoma is the ability of the cells to reactivate the MAPK pathway(65). This is primarily achieved through the upregulation of various receptor tyrosine kinases such as PDGFRβ, EGFR, AXL and IGF1R(85–87)(Figure 1.1D). These kinases perpetuate the downstream signaling of the MAPK cascade independently of the $BRAF^{V600E}$ mutation through the activation of either wild-type BRAF, other RAF proteins and or neighbouring signalling pathways. The administration of MEK inhibitors in conjunction with BRAF inhibitors has been introduced to eliminate MAPK cascade reactivation(88–91). This dual treatment prolonged patient survival compared to single agent use and is the current therapy standard of care for the treatment of metastatic melanoma(88–93). Therapy resistance, although delayed, still occurs following dual treatment and therefore understanding the downstream mechanisms that drive resistance is needed.

Re-activation of the MAPK pathway also occurs due to the genomic instability of various genes in the MAPK cascade. Interestingly, approximately 20% of MAPKi resistant cases have acquired NRAS mutations(94). Patient sequencing data has also confirmed that in about 8% of resistant cases, there is a MEK mutation within exon 3 or 6(94,95). Mutations within these MAPK signalling molecules has allowed for the activation of the MAPK cascade, bypassing the effects of BRAF inhibitors. Surprisingly, there are also $BRAF^{V600E}$ splice variants that occur following targeted therapy resistance(96). These splice variants usually occur within the RBD region allowing for easier dimerization and therefore enhanced downstream signalling(96). BRAF is also

observed to show gene amplification following resistance that can further stimulate MAPK downstream signalling(96,97).

Although the MAPK pathway plays a very important role in tumourgenicity, melanomas sometimes activate MAPK-independent pathways to overcome resistance. One interesting pathway that becomes stimulated through RTKs is the PI-3K/AKT signalling pathway(98,99). This signalling cascade can crosstalk with ERK, skipping BRAF and MEK signalling. Bypassing these key proteins in the cascade has allowed for constitutive activation of ERK, reimplementing the proliferative and pro-tumourigenic cues associated with melanoma(98–101)(Figure 1.1D).

Other pathways have also shown to play a role in MAPKi resistance such as the WNT/Catenin network, various metabolic pathways and other genomic alterations(102,103). Although the molecular cues and phenotypic changes post-treatment are well understood, understanding how the cell acquires these phenotypes is an area of active research.

1.3.2 Heterogeneous populations

Intratumoural heterogeneity is the idea that various cancer cells within the same tumour express various molecular and phenotypical functions and remains an important problem for the treatment of cancers with single agents(104). The notion of intratumoural heterogeneity originated from two key ideas: clonal evolution and the cancer stem cell (CSC) model(104). Clonal evolution focuses on the idea that various mutational signatures allow for epigenetic changes that result in slightly different tumour cells, each potentially having its own distinct phenotype within the tumour microenvironment. Interestingly, with the use of SNV and CNV, melanoma display one of the largest clonal populations when compared to other solid tumours(105,106). The CSC model hypothesizes that the tumour initiates off a specific subset of tumourigenic CSCs, allowing for the

development of phenotypically distinct populations of melanoma cells. These CSCs have tumour initiation activity while the major populations within the tumours do not. The earliest studies on CSC in melanoma focused on sorting CSCs and assessing their tumourigenic potential. Sorted $CD34^{+}p75^{-}$ melanoma cells showed increased tumour formation while the $CD34^{-}p75^{+}$ cells rarely formed tumours in immunocompromised mice(107). There is no unique marker of CSC in melanoma. However, various stem cell markers have been widely used such as CD271, CD133, Sox2, and ALDH1(108–111). Various studies have shown that these markers may exist in a proportion of melanomas but not in others (108–112). These populations when isolated and transplanted into partial immunocompromised mice led to overall tumour growth, where the negative isolates did not(109,110,113). Interestingly, single cell transplants of human melanoma cells in complete immunocompromised mice showed increased uptake and growth of a large proportion of melanoma cells, contradicting the CSC model (114,115). In addition, transplantation of melanoma cells selected for common CSC markers had no increase in tumourigenic potential compared to the negative isolates when implanted into complete immunocompromised mice(114,115). Interestingly, the sorted populations were found to be unstable, where the negative and positive populations reverted back to homeostatic levels, suggesting an alternative mechanism to the CSC model(115).

Although clonal evolution and the CSC model have previously been used to explain drug resistance in cancer, one new concept that focuses on cellular plasticity has been suggested(116). This model focuses on the idea that cancer cells can transition dynamically from a proliferative drug sensitive state to a therapy tolerant and invasive state(116). Non-CSC-like cells can transition to CSC-like cells and these transitions are dependent on various cues that exist within the tumour microenvironment. Indeed, studies have identified two populations within melanoma; a

proliferative (differentiated) and invasive (undifferentiated) phenotype(117–119). With the use of transcriptomics, the proliferative state was shown to express SOX10 and MITF, two major players in melanoma initiation and progression(117–120)(Figure 1.2). The invasive state expressed various EMT-like markers including ZEB1, SNAI1, and EGFR(117–119). Using cohorts of melanoma within the TCGA dataset, tumours appear to transition from one state to the next independently of the mutational status, strengthening the idea of a dynamic epigenetic landscape(119). TEAD/AP-1 were identified as drivers of this invasive state due to their enrichment in open/active regulatory regions found within the invasive cohort whereas SOX10 and MITF sites were enriched within the proliferative state(119). In general, the proliferative state can be identified as a $SOX10^{High}$, $MITF^{High}$ AXL^{Low}, $SOX9^{Low}$ state while the invasive state displays the reverse expression(117–121)(Figure 1.2).

Additional molecular states have now been identified using various markers and shown transition between each other, dependent on cellular cues(122–124). Following gene signature clustering, two new molecular states were identified: the transitory state and neural crest like state, showing varying levels of SOX9, SOX10, MITF, and RTKs(122–124). It was shown that, following treatment with vemurafenib, the transition from the proliferative state followed a linear trajectory. Cells entered a transitory state followed by a neural crest-like phenotype and finally ending at the undifferentiated state(123). The undifferentiated state was shown to be susceptible to ferroptosis-inducing compounds capable of eradicating targeted therapy resistant cells within the cell population(123). Using scRNA-seq, these states were confirmed within patient-derived melanoma cell lines(124). Although in various proportions, not all cells within a cell population transition to any one state. Some cells remain in intermediate states able to transition back and

forth(124). Interestingly, manipulation of SOX10 levels appear to a transition to a more migratory and therapy resistant state (124).

Although the drug resistance and the transition between various states is well documented, no therapeutics have been uncovered that can prevent resistance to the original MAPK inhibitors. Understanding what key markers are driving these resistant states and whether the transition to these states can be blocked or modulated is critical to fully control resistance and restore sensitivity.

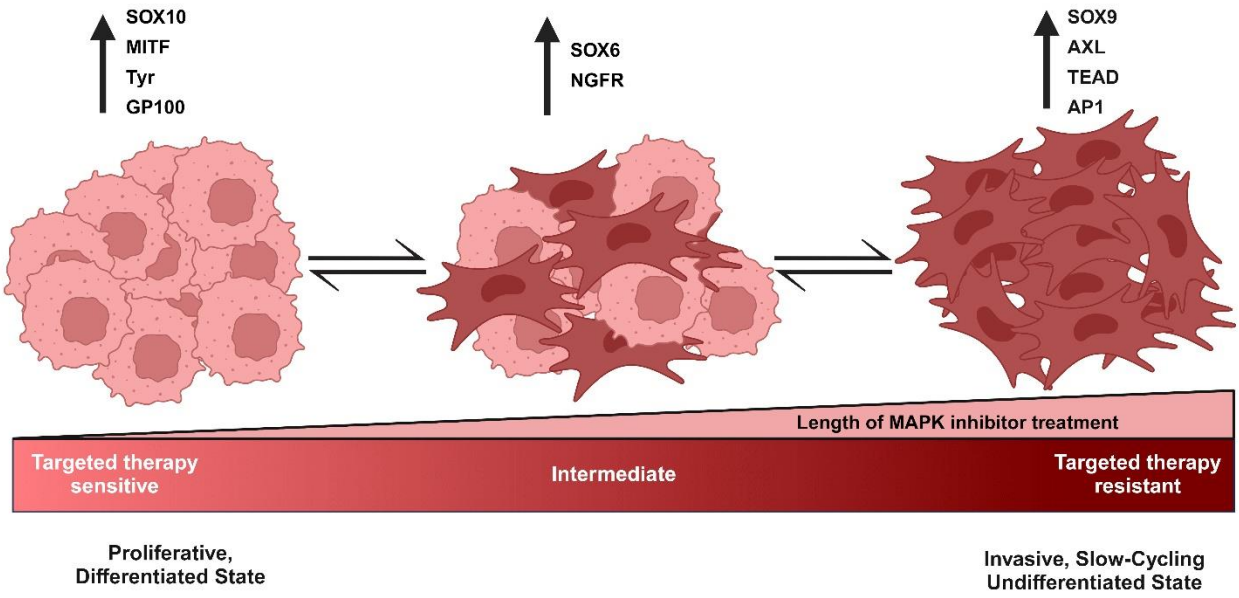

Figure 1.2 Cellular plasticity model in melanoma following treatment with MAPK inhibitors. Naïve melanoma tumour cells transition from a proliferative, Sox10+ differentiated state into an invasive slow-cycling Sox9+ state following chronic treatment with MAPK inhibitors (eg. vemurafenib). This transition is believed to be initiated through the loss of SOX10 and MITF and the induction of AXL, TEAD, and AP1. Figure was generated in BioRender.

1.4 Carcinoembryonic antigen-related adhesion molecules

1.4.1 CEACAM family and structure

Carcinoembryonic antigen-related cell adhesion molecules (CEACAMs) are a group of glycoproteins found on the surface of various cell types(125). The human genome expresses 12 *CEACAM* members, *CEACAM1*, *CEACAM3-8*, *CEACAM16* and *CEACAM18-21*, which all contain various structures with different functions(125). CEACAM1 can be found on a plethora of cell types including cancer and immune cells(126). In humans, there are 12 different isoforms of *CEACAM1* produced through alternative splicing while only 4 exist in mice(126–128). Murine CEACAM1 isoforms consist of one N-terminal IgV immunoglobulin domain that functions as a binding region to CEACAM1's various partners(128). One or three IgC2 immunoglobulin domains follow the IgV immunoglobulin bound to the transmembrane domain and a cytoplasmic tail(128). The two CEACAM1 long isoforms consist of a long cytoplasmic tail containing an immunoreceptor tyrosine-based inhibitory motif (ITIM), while the short isoforms lack this ITIM(128). CEACAM1 functions through cis or trans dimerization with its binding partners to induce downstream signaling within the cells(127,128)(Figure 1.3). It has been shown to bind to itself and CEACAM5 with high specificity(127,128). Although it is also predicted to bind to CEACAM3, 6 and CEACAM8, its affinity to these proteins is lower(128).

1.4.2 CEACAM1 in cancer and immune surveillance

In various cancers, CEACAM1 has been shown to have antitumourigenic effects(129–132). However, in melanoma it appears to promote tumour proliferation, migration and invasion(133,134). Interestingly, using an activating antibody specific to CEACAM1, one study found that it reduced melanoma viability and promoted apoptosis in vitro(135). Whether

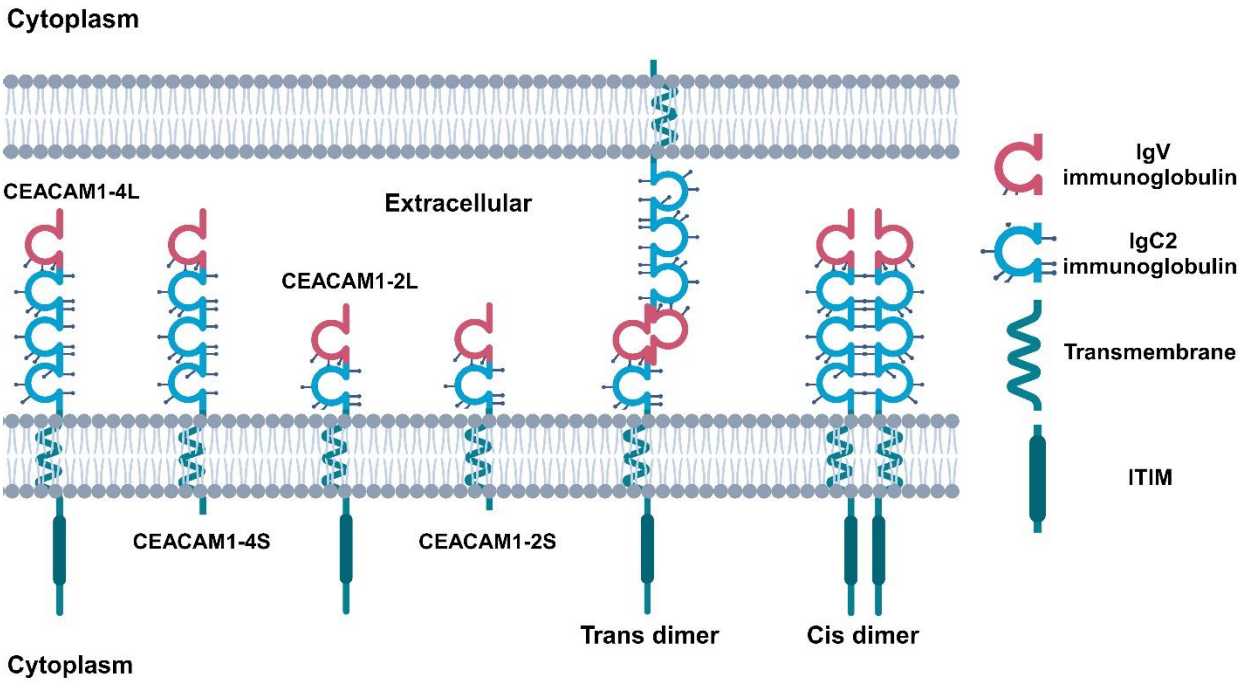

Figure 1.3 Schematic representation of the murine CEACAM1 isoforms. CEACAM1-4L contains all N-terminal immunoglobulins and a complete C-terminal intracellular tail bearing the ITIM domain. CEACAM1-4S contains all N-terminal domains similar to CEACAM1-4L but lacks a complete intracellular tail. CEACAM1-2L has a complete intracellular tail but lacks 2/3 of the IgC2 immunoglobulin domains. CEACAM1-2S is the smallest murine CEACAM1 isoform lacking both a complete N-terminal and C-terminal domain. CEACAM1 isoforms can dimerize in trans where it is facilitated through the IgV immunoglobulin, or in cis where dimerization is facilitated through all immunoglobulins. L; long form, S; short form. Figure was generated in BioRender.

these functions are isoform specific in the context of melanoma has not been fully elucidated. Various studies have highlighted the immunosuppressive capabilities of CEACAM1, primarily on NK cells. In melanoma, CEACAM1 found on the NK cells can bind to CEACAM1/5 on melanoma cells, suppressing the cytotoxic capabilities of the NK cells(136–138). CEACAM1 on melanoma is also hypothesized to regulate the trafficking of NKG2D ligands, suppressing their transport to the plasma membrane and therefore repressing NK-mediated cytolysis(139).

1.5 The *Sry*-related HMG box family of transcription factors

1.5.1 The SOX family

With over 1500 members encoded by the human genome, transcription factors (TF) have been subdivided into various subgroups. The sex determining region Y (**S**ry) high mobility group (HMG)-b**ox** (SOX) family of TFs is comprised of 20 different proteins which are divided into nine subgroups (A, B1, B2 C to H), with each protein within the group displaying a specific characteristic(140,141). These SOX proteins are characterized by their highly conserved HMG box domain which primarily binds the DNA site (A/T)(A/T)CAA(A/T)G (142). The SOX genes are known as architectural TFs due to their ability to bind to the minor groove of DNA, creating distinct bends in the template(143–145). This brings various regulatory regions in close proximity and allows for direct regulation by various factors(143,144). The HMG-box is flanked by two nuclear localization signals and bears one nuclear export signal, allowing for nucleocytoplasmic shuttling of the SOX transcription factors(146–148). Although all the SOX proteins play important roles in development and lineage specification, they have widely different functions within cancer initiation, maintenance and progression(148,149).

1.5.2 The SoxE subgroup

SOX8, SOX9 and SOX10 make up the SoxE family of transcription factors (150). In addition to a C-terminal transactivation domain (TA), the SoxE group is characterized by a unique dimerization (DIM) domain which allows for homo or heterodimerization with other SOX proteins(151,152)(Figure 1.4). SoxE dimerization is facilitated by a DIM-to-HMG box domain interaction, suggesting that only one DIM domain is required for dimerization between SOX proteins(151). This also suggests that SoxE transcription factor binding though the DIM domain is SOX-specific(151). Interaction of SoxE proteins with other TFs is thought to be independent of the DIM domain. For example, SOX10 binds to PAX3 through its HMG domain and that was corroborated using SOX10 protein truncations that lack the HMG domain causing a loss in all protein-protein interaction(153).

While also containing a TA, the SoxE group also shares a K2 domain which acts as a transactivation region primarily in the center of the protein. Although highly homologous, these domains play varying roles depending on the gene. Sox8 has been shown to primarily function from its K2 central domain and to lack any activity from its TAC(154,155). However, Sox9 transactivates primarily from its TA where it contains an extra proline, glutamine and alanine (PQA) rich region that amplifies transcriptional activity that is context-dependent(156,157). Sox10 has been shown to require both the K2 and TA for optimal transcriptional activation. The use of the TA independently of K2 is believed to be also context dependent(158,159). More recently the K2 and TA in all SoxE proteins have been shown to have cooperative and independent functions that are completely context dependent (160)(Figure 1.4).

The SoxE genes were originally studied for their critical roles in the reproductive system and their ability to promote lineage differentiation from neural crest cells to melanocytes,

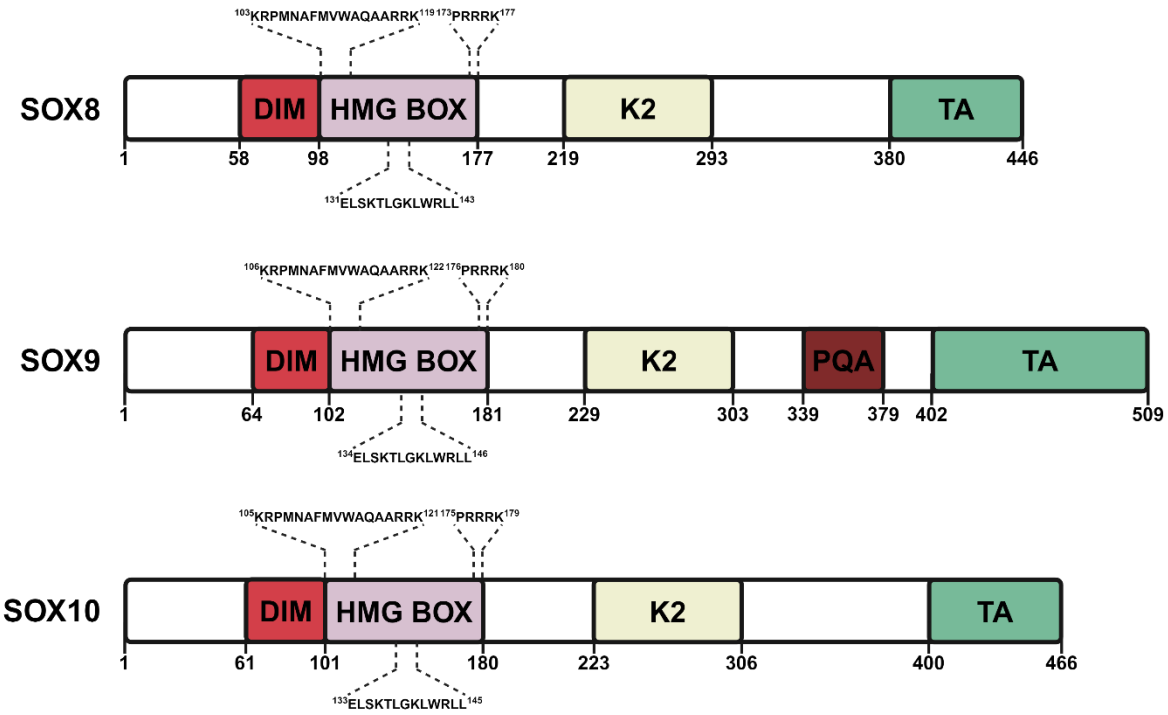

Figure 1.4 Schematic representation of human SOXE proteins. Amino acid numbering provides specific locations of various regions highly conserved throughout the family. Both NLS and the NES sequence are noted with their specific amino acid location. Highly conserved regions include the dimerization (DIM) domain, the high mobility group (HMG), the K2 and transactivation (TA) domain and the proline, glutamine and alanine (PQA) rich domain. Figure was generated in BioRender.

oligodendrocytes and chondrocytes(161,162). Due to the high homology between the SoxE members, many functions are assumed to be redundant or compensated for by other members. One example of this phenomenon is in oligodendrocytes where individual SOX9 or SOX10 knockouts shows no overall phenotypes(163,164). However, deletion of both genes gives rise to localized apoptosis(164). The SOXE proteins have also been shown to have antagonistic functions. For instance, in melanoma SOX10 drives the initiation and proliferation of melanocytic nevi(165). SOX9 induction is believed to induce a pro-apoptotic environment, therefore having the opposite effect(165). Together the functions of SOX9 and SOX10 seem to be context-dependent and can display similar or antagonistic functions in various cancers.

1.5.3 SOX9 in cancer

SOX9 was initially identified in 1993 with another seven new SOX genes (SOX8-14) bringing the total to 14 SOX genes expressed in mouse embryos at 11.5 dpc (150). While SOX9's role in cancer has been well documented, its specific function and target genes are still largely unknown. SOX9 has been shown to promote proliferation and protumourigenic phenotypes in oesophageal squamous cell carcinoma, hepatocarcinoma and pancreatic tumour cells while also being proapoptotic in melanoma cells(166).

Although SOX9 plays multiple roles in cancer, it is generally associated with the epithelial-to-mesenchymal transition (EMT) process(166). Briefly, EMT is the transition of epithelial-like cells to a more mesenchymal state, increasing motility and invasion of the cells. Although it is a non-epithelial cancer, in melanoma, this transition is termed phenotype switching and resembles the EMT by transitioning to a more invasive, de-differentiated state(167). SOX9 has been shown to bind to key regulatory regions altering the expression of mesenchymal TFs markers including SLUG, Vimentin, and ZEB1(168,169). These have been shown to play pivotal roles in the

initiation of EMT in various cancers(167). The loss of SOX9 has also been shown to result in the downregulation of a majority of these markers as well as phenotypically reduce the invasive capacity of various cancers both in vitro and in vivo(166).

In various solid tumours, SOX9 has also been shown to play a pivotal role in maintaining the cancer stem cell population(166). In conjunction with SLUG, SOX9 knockdown reduces the tumour initiating cell population in both breast and lung cancer(170,171). This was accompanied by a reduction in sphere formation as well as a reduction in overall metastatic potential(170,171). SOX9 induced CSC properties, promoted EMT and contributed to drug resistance(166,171). Recent findings in basal-like breast cancer identified SOX9 as a regulator of lineage plasticity(172). Subsequently, SOX9 was identified as an upregulated gene during the transition to a plastic state (172,173). This upregulation was accompanied by a strong positive correlation between SOX9 expression and neoadjuvant hormone therapy-treated patients(173). These findings are not unique as SOX9 expression has been shown to correlate with a resistant state in various cancers such as ER+ breast cancer, lung cancer and renal cell carcinoma(174–176).

1.5.4 SOX9 in melanoma

The role of SOX9 as a pro-or-antitumourigenic factor has been strongly debated over the past two decades. Early melanoma patient data has found that SOX9 is only expressed in approximately 20% of melanoma nevi and that this expression drops further in primary and metastatic melanomas to 4% and 0% respectively(177). Exogenous expression of SOX9 perturbed the proliferative abilities of melanoma in vivo and in-vitro, suggesting a strong antitumourigenic function for SOX9(177). In contrast, others identified SOX9 expression in primary melanoma as well as in subset of invasive human melanoma cell lines (121,178). Interestingly, 5-aza cytidine and bisulphite sequencing showed methylation of the Sox9 gene in proliferative melanomas (121).

When over-expressed, SOX9 induced cell cycle arrest while also mediating a more invasive phenotype in vitro and in vivo(121). Ultimately, a study identified SOX9 expression in human patient samples to be predominantly expressed in metastatic melanoma lesions compared to primary melanoma and nevi(179). It was further determined that SOX9's function in melanoma is threshold dependent where low SOX9 expression seems to mediate an antiproliferative response while elevated levels increase the metastatic potential(179).

1.5.5 SOX10 in cancer

SOX10 expression is observed in various forms of epithelial cancers such as breast and ovarian but most predominantly in melanoma(180). However, its role in modulating the growth, EMT and the CSC state as well as drug resistance has not been fully elucidated.

In bladder cancer, patients with high levels of SOX10 show poor survival. It was also found that the loss of SOX10 reduces the overall proliferative, migratory and invasive capabilities of the cancer cells (181). Similar findings were reported for hepatocellular carcinoma, where the overexpression of SOX10 was able to facilitate the binding of TCF4 and β-catenin, two prominent markers of proliferation (182).

Interestingly in the mammary epithelium, SOX10 functions as a stem cell marker, where the loss of Sox10 in the fetal and adult mammary glands reduces the stem/progenitor activity (183). In HER2-positive breast cancer, the overexpression of SOX10 promoted the CSC properties, while also promoting cell growth in vivo (184). In triple-negative breast cancer, SOX10 has been shown to promote the expansion of a $CD44^{+}/CD24^{-}$ population, common markers of CSC found within breast cancer (185). Whether these SOX10-dependent cancer stem-like phenotypes are also observed in melanoma remains to be elucidated.

1.5.6 SOX10 in melanoma

SOX10 plays a pivotal role in melanoma initiation and progression. Early studies showed that the loss of SOX10 reduced melanoma proliferation in vitro, causing a cell cycle arrest in G1 (186). SOX10 haploinsufficiency reduced nevi formation in vivo while also altering tumour initiation from 2 months in control mice to 5 months in SOX10-LacZ mice (186). A similar study focused on $NRAS^{Q61K}$ driven melanoma where it was found that SOX10 haploinsufficiency reduces the hyperpigmentation found within tumours and increase the time to tumour onset (187). A reduction in SOX10 levels also reduced the proliferative status of melanoma and abolished tumour growth in vivo (187). This loss of tumour growth was also associated with the loss of the NCSC marker CD271, previously associated with melanoma initiation (113,187,188). Interestingly multiple studies have shown that SOX10 plays an important role in regulating melanoma proliferation, migration and invasion (189–191).

Although the importance SOX10 in melanoma initiation and maintenance has been thoroughly documented, its role in therapy resistance remains elusive. One study has found that SOX10 can regulate FOXD3, a stem cell marker that induces targeted therapy resistance in melanoma (192,193). Interestingly, inhibition of ERK with the use of vemurafenib promoted the transcriptional activity of SOX10 on the FOXD3 promoter (193). This in turn promoted overall resistance to MAPK inhibitors (193). In contrast, various studies have marked the SOX10 population as the drug-tolerant state (119,194–197). With the use of CRISPR-Cas9, it was found that the deletion of SOX10 pushes the cells into a dormant/quiescent-like state (197). These slow cycling cells were characterized by an upregulation of ZEB1, PDGFRβ, WNT5, and Sox9, increasing the overall invasiveness and targeted therapy resistance in melanoma (197). With the use of published datasets, one group curated a list of *SOX10*-associated genes(198). This gene

signature was negatively correlated with targeted therapy resistant melanoma samples in both single BRAF inhibition and combination therapy with MEK inhibitors(198). It was also found that the *SOX10* gene signature also negatively correlated with ICI-resistant patient samples, suggesting the loss of SOX10 may drive a cross resistant phenomenon in melanoma (198). This is in contrast to findings showing that SOX10-depleted melanoma cells are more sensitive to cytotoxic T cells and the secreted cytokines TNFα and IFNγ(199). Despite these studies, it is still not clear how SOX10 may be regulating drug resistance and the cross resistant state.

1.5.7 Antagonistic relationship of SOX9 and SOX10 in melanoma

Although SOX9 and SOX10 are key players during the lineage specification of neural crest cells, they appear to have opposing roles in melanoma. Interestingly in melanocytes, removal of Sox9 using the Cre/Lox system did not affect melanocyte maintenance(165). On the contrary, the removal of Sox10 caused the loss of melanocyte pigmentation(165). These different phenotypes were further validated in giant congenital naevi where Sox9 knockout mice did not affect hyperpigmentation lesions while Sox10 removal blocked lesion formation (165). This study further identified that the loss of Sox10 in melanoma activated Sox9 which increased apoptosis in melanoma. Interestingly, Sox9 was shown to suppress Sox10 expression through direct binding to the Sox10 promoter region (165). This antagonistic relationship between SOX9 and SOX10 also appears to exist between the proliferative drug sensitive state (SOX9-/SOX10+) and slow cycling drug resistant state (SOX9+/SOX10-) (119,124,196,197). Surprisingly, little is known about the role of Sox9 in targeted therapy resistance even though it is activated following the loss of SOX10(119,124,197).

1.6 Rational, objectives and chapter overview

1.6.1 Rational and objectives

Numerous transcriptomic studies have linked SOX10 to the proliferative, drug sensitive state and SOX9 to the invasive, therapy resistant state (119,194–197). Some studies have shown that SOX10 can drive this sensitive state and that the loss of SOX10 alters the genomic landscape, switching melanoma to a more invasive, therapy resistant, $SOX9^{high}$ state(119,124,196,197). The loss of SOX10 appears to be a critical step in drug resistance and SOX9 activation. **Therefore, whether it is BRAF-targeted or immune-directed, our global hypothesis was that the SOX10-SOX9 interplay is critical for drug resistance and the phenomenon of cross resistance.** Our prediction was that the loss of SOX10 would trigger a stem-like phenotype switch accompanied with resistance to multiple therapeutics.

1.6.2 Chapter overview

The overall goal of this thesis was to investigate the role of SOX9 and SOX10 in melanoma therapy resistance. In **Chapter 2**, we investigated the potential relationship of SOX9 and SOX10 in melanoma targeted therapy resistance. We found that SOX9 is not activated via demethylation but potentially becomes activated indirectly through the loss of SOX10. We also find that SOX9 does not play a direct role in inducing vemurafenib resistance but rather acts as a gatekeeper, where expression of SOX9 is required to reach and activate a resistant state but is no longer required post-resistance.

In **Chapter 3** we further validate others findings that the loss of SOX10 regulates targeted therapy resistance to vemurafenib. This acquired resistance and resistance induced by the loss of SOX10 further perpetuates the resistant mechanism to OV (VSV) due to the induction of ISGs.

Chapter 4 further divulges into potential reason why SOX10 may cause a decrease in vemurafenib resistance. We find that our SOX10 positive cells have a decreased progenitor-like population where this lack of CSCs can be enriched by sorting for the CEACAM1+ population, driven by SOX10. We also find that SOX10 reduces the infiltration of CD8-positive Tcells promoting tumour growth to an extent until enriched for CEACAM1.

Chapter 2

Sox9 mediates the transition to a targeted therapy resistant state in melanoma

2.1 Preface

Abou-Hamad, J., Cook, D., & Sabourin, L. A. (2024). Loss of Sox9 blocks the transition to a targeted therapy resistant state in melanoma. In preparation.

Author contributions

Abou-Hamad J: Performed all experiments with exception to the RNA-seq and ATAC-seq analysis. I also wrote and proofread the manuscript

Cook D: Performed the alignment and analysis for the RNA-seq and ATAC. Wrote the methods pertaining to the RNA and ATAC-seq analysis.

Sabourin L: Provided general expertise throughout the project. Also proofread and edited the manuscript.

2.2 Title page

This paper is in preparation for submission

Sox9 mediates the transition to a targeted therapy resistant state in melanoma

Authors

John Abou-Hamad [1, 2], David Cook [1, 2], Luc A Sabourin [1, 2]

Affiliations

1. Centre for Cancer Therapeutics, Ottawa Hospital Research Institute, 501 Smyth Road, Ottawa, ON K1H 8L6, Canada.
2. Department of Cellular and Molecular Medicine, University of Ottawa, Ottawa, ON K1H 8L6, Canada.

Funding

This work was supported by grants to L.A.S. from the Canadian Institutes of Health Research, the Canadian Cancer Society, and the Cancer Research Society

2.3 Abstract

SOX9 and SOX10 are key transcription factors that display a mutually exclusive expression pattern in melanoma. Here we find that SOX10 is lost following chronic vemurafenib treatment, a targeted therapy used to treat $BRAF^{V600E}$ positive melanoma. Upon the loss of SOX10, SOX9 is induced post-treatment. Interestingly, overexpression of either SOX9 or SOX10 has no impact on vemurafenib sensitivity. Surprisingly, we show that the loss of SOX9 also does not alter the sensitivity of the cells to vemurafenib in both intrinsically and adaptively resistant murine melanoma cell lines. However, we find that SOX9 is necessary to confer a vemurafenib-resistance memory state. Indeed, SOX9 deletion in pre-treated cells confers the same overall sensitivity as naïve controls, suggesting that SOX9 is required early during the cells transition to the resistant state. We observed that SOX9 activation upon acquired resistance occurs through chromatin remodeling with increased open chromatin along Sox9's promoter regions. Overall, these findings identify SOX9 as a gatekeeper between naive and therapy resistant melanoma.

2.4 Introduction

Melanoma development is typically due to increased activation of the MAP kinase cascade, commonly due to a mutation upstream of the MEK-ERK signaling cascade. The $BRAF^{V600E}$ mutation, which accounts for approximately 50% of melanoma cases was first discovered in 2002(23). This mutation creates a constitutively active kinase no longer affected by inhibitory signals produced from excessive MAPK signaling, inducing an uncontrolled proliferative phenotype(38,39). Vemurafenib, a highly specific $BRAF^{V600E}$ inhibitor, was the first of its kind and showed outstanding clinical activity(56). Tumors shrunk and overall patient survival increased to 84% within 6 months compared to 64% in the dacarbazine group(62–64). Albeit promising, patients relapsed within 12 months(65). This acquired resistance state is believed to be due to the reactivation of the MAPK cascade, independently of the oncogene(200).

The development of intratumoral heterogeneity is a common mode of resistance following drug treatment. Melanoma has one of the largest mutation burdens as well as more clonal populations (through CNV and SNV) than any other cancers, contributing to its tremendous heterogeneity(105,106). Various studies have identified multiple molecular states characterized by differential gene expression(117–120,122–124). These states have specialized functions pertaining to proliferation, invasion, targeted therapy resistance and/or immune modulation(122–124). Although drivers of these states may be well documented, how these drivers become activated and whether the transition to various molecular states can be blocked is currently unknown.

SOX10 is a transcription factor required for neural crest differentiation into melanocytes(201). Following the loss of SOX10, melanoma transitioned into a targeted therapy resistant state that was accompanied by an increase in metastatic potential(194,197). Interestingly, SOX10 loss also induced a dormant-like invasive state that is marked by an increase in invasive

markers such as *Zeb1* and *Sox9*(197). The expression of SOX9, another SOXE protein, was originally found to be mutually exclusive with that of SOX10 in melanoma(165). Various studies have shown that SOX9 acts in an antitumor-like fashion in melanoma where it is silenced due to hypermethylation of its promoter region(121,177). One study found SOX9's function is dependent on its expression level, switching from an antitumor function to a pro-proliferative phenotype(179). Since SOX10 marks the proliferative state in melanoma, while SOX9 is observed in the slow cycling but aggressive state, we tested whether the activation of SOX9 plays a role in promoting the resistant state(119,124,196,197).

Our studies show that the expression of SOX9 and SOX10 is indeed mutually exclusive in a new subset of $BRAF^{V600E}$ positive murine melanoma cell lines (YUMM). We find that SOX9 expression strongly correlates with the vemurafenib resistant population of melanoma cells while SOX10 levels are downregulated. Interestingly, we find that exogenous expression of either SOX9 or SOX10 does not impact vemurafenib (Vemu) sensitivity. However, intrinsically sensitive cells with SOX9 deleted lose the ability of the cells to enter a resistant state following Vemu treatment. When rechallenged, SOX9 knockout cells restores Vemu sensitivity upon drug rechallenge, suggesting that SOX9 activity is required to impart a resistant "memory state" in melanoma cells. Finally, we find that SOX9 activation upon Vemu treatment of SOX9-negative cells is not due to altered methylation but rather to de novo transcriptional activation at the SOX9 locus.

2.5 Materials and Methods:

Cell culture

Yale University Mouse Melanoma (YUMM) cell lines were a kind gift from Dr. William Damsky (Yale University). YUMM cell lines were cultured in 1XDMEM supplemented with 10% FBS,

1X penicillin/streptomycin, 1% L-glutamine, and 1X nonessential amino acids. Cell cultures were grown at 37°C with 5% CO2 in humidified chambers.

Western Blotting

Equivalent amounts of protein were prepared in RIPA Buffer and 1X SDS sample buffer (50mM tris pH 7.4, 100mM DTT, 2% SDS, 10% glycerol, 1.5mM bromophenol blue). Lysates were denatured at 100^{o}C for 5 minutes and electrophoresed on polyacrylamide gels for 45 minutes at 50mA in SDS running buffer (25mM tris base, 250mM glycine, 3.5mM SDS). Polyacrylamide gels were removed and contents within the gels were transferred onto PVDF (Cat: IPFL00010, Millipore Sigma) (polyvinylidene difluoride) membrane for 90 minutes at 100V in transfer buffer (50mM tris base, 40mM glycine). Membranes were probed with primary antibodies in 5% bovine serum albumin (BSA) in 1X TBST (50mM tris base, 2.7mM potassium chloride, 135mM NaCl, 0.1% Tween-20) overnight at 4^{o}C. Following the next day, primary antibody was collected and the membrane was washed three times, 5 minutes each with 1X TBST. HRP-conjugated secondaries (Cat: 1706515 or 1706516, Bio-Rad) were added at a 1:5000 dilution in 5% BSA in 1X TBST on the membrane and incubated at room temperature for one hour. Secondary antibodies were removed, the membrane was once again washed three times for 5 minutes each and incubated with Enhanced chemiluminescence reagent for 30 seconds and exposed to X-ray film (Cat: E3031, Thomas Scientific). For multiple probing, membranes are incubated for 20 minutes for three times with stripping buffer, washed three times with 1X TBST and primary and secondary probing is repeated. Primary antibodies used include SOX10 (Cat: 89356, CellSignaling), SOX9 (Cat: 82630. CellSignaling) and Beta-Actin (Cat: A5316, Sigma-Aldrich).

Resazurin viability assay

Melanoma cells were plated in a 96-well dish and treated with various compounds for 72 hours. At the end of the treatment, supernatants in each well were removed and replaced with 100µL of resazurin solution (55µM resazurin salt (Cat: R7017, Millipore Sigma), 10% FBS, 1XDMEM). Four hours after adding resazurin solution the absorbance of each well was read at 570 and 604nm.

Establishment and isolation of Vemurafenib resistant cell clones

Melanoma cell lines were plated in 60mm dishes at 40% confluencey and allowed to adhere overnight. The next day cells were treated with Vemurafenib (Cat: S1267, Selleckchem) at their respective IC50 for 6 weeks, with fresh media and drug replacement occurring every three days. Following the six weeks cells were taken off the drug treatment and allowed to recover. Recovered cells were retested with a vemurafenib drug curve for three days to confirm the resistant phenotype.

RNA isolation, cDNA synthesis and QPCR

Cell cultures were collected by using 1mL of Trizol (Cat: 15596018, Life Tech) and scraping the contents into a 1.5mL Eppendorf. To the Trizol collected samples, 200µL of chloroform was added, and tubes were mixed for 15 seconds. Samples were left to rest at room temperature for 3 minutes and phase separation was performed by spinning each sample at 12000 x g for 15 minutes at 4^{o}C. The aqueous phase was placed into a clean 1.5mL Eppendorf and 500µL of isopropanol was added and mixed. Samples were incubated for 10minutes to allow for mRNA precipitation and spun at 12000 x g for 10 minutes. Supernatants were removed and the mRNA pellets were washed with 1mL of 75% ethanol. Ethanol was removed by spinning at 7500 x g for 5 minutes and the pellets were allowed to dry at room temperature for 10 minutes. mRNA samples were resuspended in 100µL of RNase free water and was further purified from potential DNA

contamination using the RNeasy Mini Kit (Cat: 74104, Qiagen). Purified mRNA samples were quantified and purity was assessed using a nanodrop.

Purified mRNA samples were used for the generation of cDNA. 250ng of mRNA, 50µL of random primers (Cat: 48190011, LifeTech) , 250ng of oligo$(dT)_{12-18}$ (Cat: 18418012, LifeTech), and 10nM of dNTP were resuspended in a total of 13µL and incubated at 65^{o}C for 5 minutes. Contents within the tubes were collected by pulse centrifugation and 4µL of 5X First Strand Buffer, 1µL of 0.1M DTT, 1µL of RNase OUT (Cat: 10777019, LifeTech) and 1µL of SuperScript III reverse transcriptase (Cat: 18080093, LifeTech) was added. To create cDNA the samples were then incubated at 25^{o}C for 5 minutes, 55^{o}C for 60 minutes and 70^{o}C for 15 minutes. Samples were then diluted 1:200 in nuclease-free water and stored at -20^{o}C.

To run a RT-PCR all samples used were run in technical triplicates, where relative mRNA expression was determined using the $\Delta\Delta C_T$ method with normalization to Actin or ribosomal 18S. Each well in the RT-PCR contained 5µL of 2X iTaq Universal SYBR Green Supermix (Cat: 1725124, Bio-Rad), 0.6µL of 10µM primer, 1µL cDNA and 3.4µL water. Plates were then run on an Applied Biosystems 7500 Real-time Fast PCR thermocycler at 50^{o}C for 5 minutes, 95^{o}C for 10 minutes, and then 40 cycles of 95^{o}C for 15 seconds and 60^{o}C for one minute.

Bisulfite sequencing

Bisulfite conversion was done following the user manual for the kit EpiTect DNA Bisulfite Kit (Cat: 59104, Qiagen). In short, 2µg of DNA was mixed with the DNA protect and bisulfite mix buffer. Samples were vortexed and incubated at 95^{o}C for 5 minutes, 60^{o}C for 25 minutes, 95^{o}C for 5 minutes, 60^{o}C for 85 minutes, 95^{o}C for 5 minutes and 95^{o}C for 175 minutes. Converted DNA was cleaned up and the Sox9 promoter region was amplified using the forward primer:

ATTAGAGATTTTGAGTTGGAAG and reverse: AAAACTCCTCTTCCCTCAACTAC. Amplicons were cloned into CloneJet1.2, and 5 clones were prepped and sequenced to identify methylated cytosines.

Cloning of expression plasmids and guide RNA

For SOX9 and SOX10 expression plasmids, the coding sequence of each gene was amplified and ligated into CloneJet (Cat: K1231, LifeTech) from Origene constructs (Cat: MR227031 & MR207452, Origene). Primers used for the pBABE-SOX10 cloning were flanked by restriction enzymes BamHI and EcoRI. With the use of BamHI and EcoRI SOX10 was removed from the CloneJet plasmid and ligated into pBABE-puro (Cat: 1746, Addgene). Similar processes were used to clone SOX9 and SOX10 into the pMSCV-IRES-GFP II (Cat: 52107, Addgene) plasmid although the restriction enzyme sites were reversed on the primer sequence. To synthesize the guide RNA plasmids complementary oligonucleotides were annealed using a thermocycler at 37°C for 30 min, 95°C for 5 min and temperature was ramped down 5 °C/min to 25°C and ligated into the plasmid pLKO H2B-mRFP-2A puro. For SOX9 guides oligos sgSox9-K1 FWD: CACCGGATGACCGACGAGCAGGAGA, sgSox9-K1 REV: AAACTCTCCTGCTCGTCGGT CATCC, sgSox9-K2 FWD: CACCGGTGTCCGAGCCGGAGCCCGA, and sgSox9-K2 REV: AAACTCGGGCTCCGGCTCGGACACC were used. Generation of the SOX10 guide RNA has been previously described.

Retro/lentivirus production and viral transduction

Viral particles were produced by seeding 5 x 10^6 of 293Ts in a 10cm dish. 293Ts were transfected using lipofectamine 3000 with 10µg of construct, 8µg of pUMVC or pCMV-dR8.2 dvpr (for retrovirus or lentivirus respectively) and 2µg of pCMV-VSV-G. The next day media was changed

with 6mL of fresh media corresponding to the culture cells that were infected. Viral soup was collected 72 hours post media change through a 0.44µm filter. Melanoma cells were infected for 6 hours with 1mL of viral soup diluted in 5mL of cell culture media supplemented with 10µg/mL of polybrene. Post infection media was replaced with full media and melanoma cells were selected with 5µg/mL of blasticidin (Cas9 selection), 5µg/mL of puromycin (pBABE SOX10), sorted for GFP (SOX9-GFP and SOX10-GFP), or sorted for RFP (sgRNA) 48 hours post infection. Expression and knockout cells were confirmed using Western blotting.

RNA-Sequencing

Transcript quantification was executed using Kallisto (v0.45.0) with the GRCh38 build of the transcriptome and the -b 50 bootstrap option. Following alignment, raw abundance counts were analyzed and genes with fewer than 10 counts across samples were filtered out. Differential gene expression was done using the 'results' function of DESeq2, contrasting the relevant control-treatments pairs for each cell line.

Assay for transposase-accessible chromatin sequencing

ATAC-sequencing sample preparation was done following the user manual for the ATAC-Seq kit (Cat: 53150, ActiveMotif). In brief, 50000 cells from each cell line were collected and washed with 1X PBS. Samples were resuspended using the ATAC-Lysis Buffer and spun for 10 minutes at 4^{o}C to isolate nuclei. Nuclei was resuspended with the Tagmentation Master Mix and incubated on a thermomixer at 37^{o}C for 30 minutes, set to 800rpm. Following this incubation, DNA becomes fragmented and is isolated through the use of a column. Isolated DNA undergoes library preparation and multiplexing using PCR amplification at 72^{o}C for 5 minutes, 98^{o}C for 30 seconds, and then 11 cycles of 98^{o}C for 10 seconds, 63^{o}C for 30 seconds, and 72^{o}C for 1 minute. Libraries

are then purified using an SPRI bead solution set to 1.2X of the library volume to allow for the isolation of open chromatin. Samples were prepared and sequencing was performed (Genome Quebec) using the Illumina NovaSeq 6000. Fastq files for each library were then processed with the Nextflow (v22.10.6) nf-core ATAC-seq pipeline (v2.0)(202). Bigwig files were then visualized with IGV and SOX9 and SOX10 regions were analyzed.

Statistical analysis

All statistical analysis was done through GraphPad Prism software and data is represented as the SEM(±SEM). T tests, and nonlinear regressions were used for statistical analysis of various experiments (statistical significance and tests used is specified in figure legends).

2.6 Results

Correlation of *Sox* gene expression and target therapy resistance in YUMM cell lines

To assess any potential correlation between *Sox* gene expression and targeted therapy resistance we used the Yale University murine melanoma (YUMM) cell lines(50). Overall intrinsic resistance to targeted therapies was evaluated with vemurafenib, a small molecule that blocks $BRAF^{V600E}$ signaling. One cell line out of the panel (YUMM1.1) was found to be highly sensitive to vemurafenib while the others showed various degrees of resistance until plateauing at about 10uM (Figure 2.1A). Although similar trends were observed using Trametinib, a MEK inhibitor, a higher sensitivity was observed in all cell lines (Figure 2.1B). To determine potential drivers of vemurafenib resistance between the YUMM lines we performed RNA sequencing analysis on three independent cultures of YUMM1.1 (vemurafenib sensitive; $Vemu^{S}$) and YUMM1.7 (vemurafenib resistant; $Vemu^{R}$) cell lines. We observed over 1300 genes that were upregulated 2-fold in either the YUMM1.1 or YUMM1.7 cell lines (Supplemental Figure 2.1A). Following Go

term analysis, we found that the YUMM1.7 cell line shows enrichment in multiple pathways focused on the cell migration associated processes such as “extracellular matrix organization”, “focal adhesion”, and “regulation of cell migration” (Supplemental Figure 2.1B). A major marker of melanoma is the SoxE gene, *Sox10*. From our RNA sequencing analysis, we found that *Sox10* is highly expressed in the YUMM1.1 cell line while it is undetectable in the YUMM1.7 line (Figure 1C). Mutual exclusivity between *Sox9* and *Sox10* has been previously reported and was found to be the case between the YUMM1.1 and YUMM1.7 cell lines (Figure 2.1C)(165). We further mined all *Sox* genes from our RNA-sequencing analysis and found that seven showed differential expression (Figure 2.1C). It should be noted that many *Sox* genes did not show adequate levels of transcripts, suggesting that they are not expressed (Figure 2.1C). Direct comparison shows that *Sox4*, *Sox6* and *Sox10* are upregulated in the YUMM1.1 cell lines whereas *Sox2*, *Sox12*, *Sox9* and *Sox7* are highly expressed in YUMM1.7 cells (Figure 2.1C). We then validated the expression of SOX9 and SOX10 in our panel of YUMM cell lines. As expected, we did find that the YUMM1.1 cells expressed SOX10 exclusively while the YUMM1.7 and YUMM1.9 cell lines had no expression of SOX10 but high levels of SOX9 (Figure 2.1D). Interestingly, one cell line expressed both and displayed moderate drug resistance, suggesting that SOX9 and SOX10 could be used as key markers of targeted therapy resistance in melanoma (Figure 2.1D).

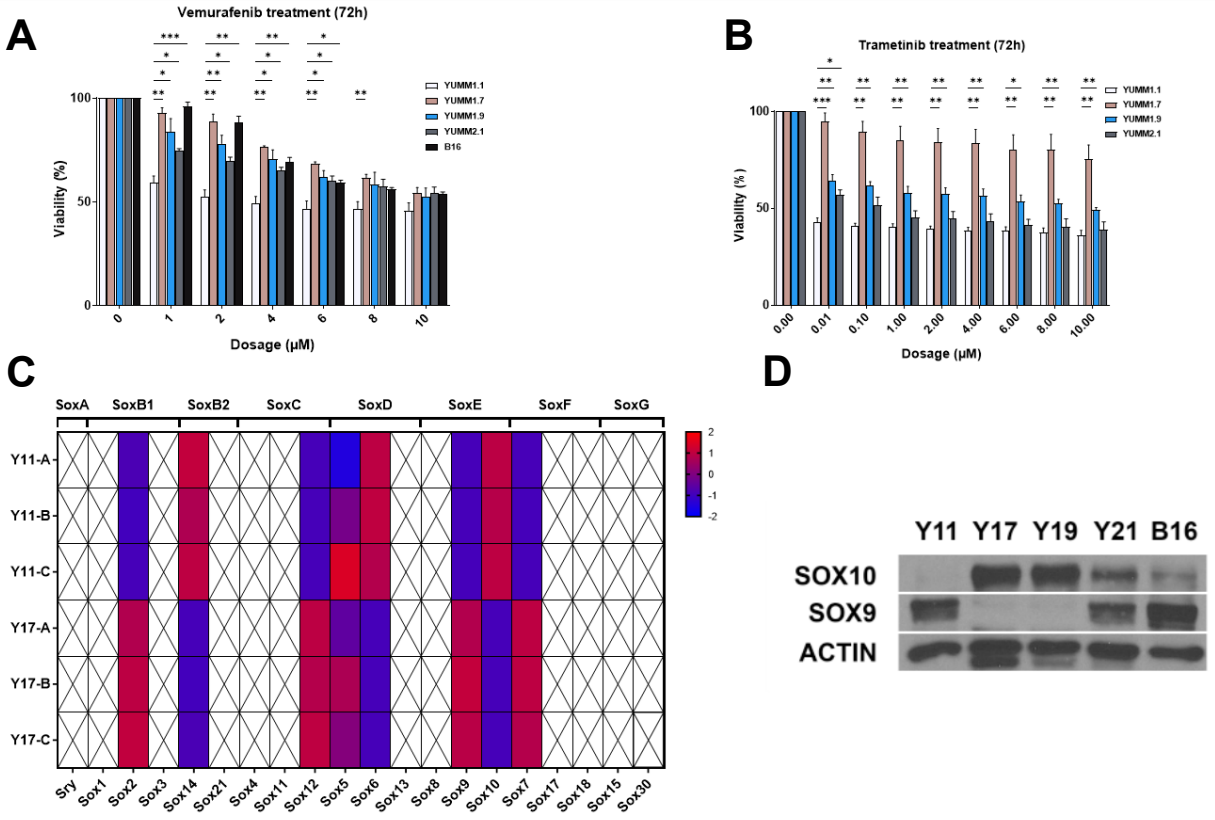
A
Vemurafenib treatment (72h)
Viability (%)
Dosage (μM)
YUMM1.1
YUMM1.7
YUMM1.9
YUMM2.1
B16
B
Trametinib treatment (72h)
Viability (%)
Dosage (μM)
YUMM1.1
YUMM1.7
YUMM1.9
YUMM2.1
C
SoxA
SoxB1
SoxB2
SoxC
SoxD
SoxE
SoxF
SoxG
Y11-A
Y11-B
Y11-C
Y17-A
Y17-B
Y17-C
Sry
Sox1
Sox2
Sox3
Sox14
Sox21
Sox4
Sox11
Sox12
Sox5
Sox6
Sox13
Sox8
Sox9
Sox10
Sox7
Sox17
Sox18
Sox15
Sox30
D
Y11
Y17
Y19
Y21
B16
SOX10
SOX9
ACTIN

Figure 2.1: SOX9 and SOX10 correlate with inherent drug resistance in various murine melanoma cell lines. (A and B) In vitro viability assay between the panel of various YUMM cell lines treated with vemurafenib (A) or trametinib (B) for 72 hours. (C) Heatmap analysis from the RNA-sequencing data of all Sox genes within the YUMM1.1 and YUMM1.7 cell lines. (D) Western blot analysis of SOX9 and SOX10 in the various YUMM cell lines. Data is representative of three independent experiments (A-C). (A & B) Significance was calculated using a two-tailed t-test, where * = $p < 0.05$, ** = $p < 0.01$ and *** = $p < 0.001$.

Chronic vemurafenib treatment alters SOX9 and SOX10 expression

To further assess the role of SOX9 and SOX10 in drug resistance, the YUMM lines were treated with vemurafenib acutely at their approximate IC50 (YUMM1.1 5um, YUMM1.7/9 10uM) and monitored for SOX9 and SOX10 levels. Surprisingly, SOX10 was found to be further upregulated post-treatment in YUMM1.1 cells while SOX9 showed a downregulation in resistant YUMM1.7 cells (Figure 2.2A). Others have also shown that SOX10 can facilitate resistance to vemurafenib through the activation of FOXD3(193). To determine whether this expression was observed chronically we further assessed SOX9 and SOX10 levels following acquired resistance. We treated the YUMM1.1 and YUMM1.9 cells at their approximate IC50 (5, 10um respectively) continuously for 6 weeks. Three separate resistant clones were isolated and vemurafenib resistance was confirmed using an alamar blue viability assay (Figure 2.2B and C). Western blot analysis of all resistant clones was accompanied by an increase in SOX9 expression and a loss of SOX10 (Figure 2.2D and E). Together, our data suggest that acquired and stable BRAF inhibitor resistance is accompanied by concomitant SOX9 induction and SOX10 loss.

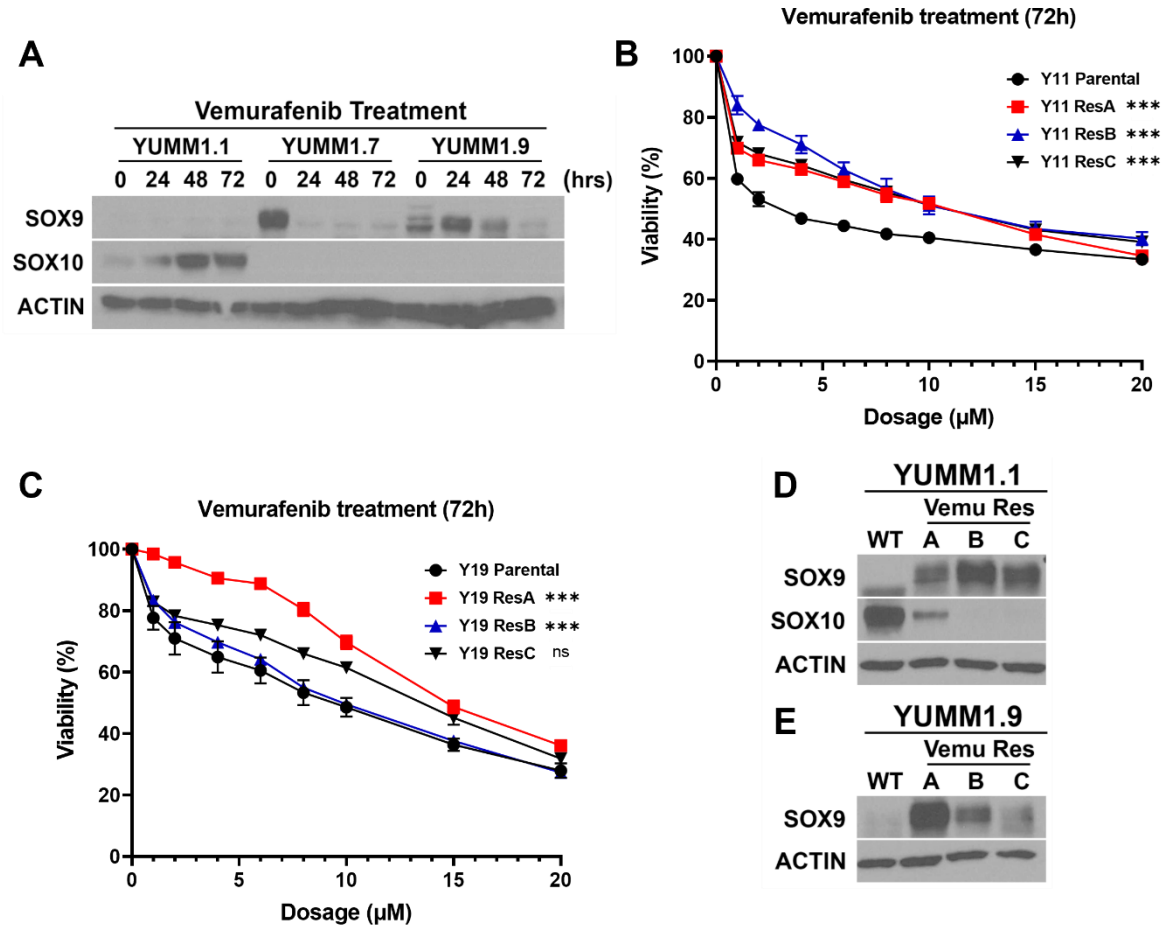
A
Vemurafenib Treatment
YUMM1.1
YUMM1.7
YUMM1.9
0 24 48 72 0 24 48 72 0 24 48 72 (hrs)
SOX9
SOX10
ACTIN
B
Vemurafenib treatment (72h)
Y11 Parental
Y11 ResA ***
Y11 ResB ***
Y11 ResC ***
Viability (%)
Dosage (μM)
C
Vemurafenib treatment (72h)
Y19 Parental
Y19 ResA ***
Y19 ResB ***
Y19 ResC ns
Viability (%)
Dosage (μM)
D
YUMM1.1
Vemu Res
WT A B C
SOX9
SOX10
ACTIN
E
YUMM1.9
Vemu Res
WT A B C
SOX9
ACTIN

Figure 2.2: Vemurafenib resistance induces SOX9 expression in melanoma. (A) Western blot analysis of SOX9 and SOX10 on acute vemurafenib treated YUMM lines. (B and C) In vitro viability assay on three individual vemurafenib resistant YUMM1.1 (B) and YUMM1.9 (C) populations, rechallenged with vemurafenib. (D and E) Western blot analysis of SOX9 and SOX10 in the vemurafenib resistant YUMM1.1 (D) and YUMM1.9 (E) populations. Data is representative of three independent experiments (B and C). (Figure 2.2B has been modified from Figure 3.2B). (B & C) Significance was calculated by first identifying the IC50 of the curves using a non-linear regression. IC50s of the resistant populations was compared to the parental populations where *** = $p < 0.001$ represents two distinct IC50s.

Exogenous SOX9 expression does not alter vemurafenib sensitivity

To further test the role of SOX9 and SOX10 in Vemu resistance, we used lenti/retroviral infection to express SOX9 and SOX10 at high levels. We first stably expressed SOX9 in the YUMM1.1 sensitive cells and validated its expression using Western blotting (Supplemental Figure 2.2A). We next evaluated vemurafenib sensitivity in SOX9-expressing YUMM1.1 cells. Unexpectedly, we found that the expression of SOX9 did not alter Vemu sensitivity in YUMM1.1 cells (Figure 2.3A). We then tested the effect of SOX10 expression on the Vemu resistant SOX10-deficient YUMM1.7 cells (Supplemental Figure 2.2B). Again, the expression of SOX10 in YUMM1.7 cells did not affect their vemurafenib sensitivity (Figure 2.3B). Since both the YUMM1.1 and YUMM1.7 cells express endogenous SOX10 and SOX9, respectively, the *SoxE* binding sites could be already bound or saturated. To test this hypothesis, we used the YUMM5.2 cell line, which still harbors the $BRAF^{V600E}$ mutation but lacks both SOX9 and SOX10 protein expression. We confirmed stable expression of SOX9 and SOX10 using western blotting and tested a vemurafenib dose response over 72 hours (Supplemental Figure 2.2C). No change in vemurafenib sensitivity was observed for either SOX9 or SOX10-expressing YUMM5.2 cells (Figure 2.3C).

We then evaluated whether the loss of SOX9 would affect vemurafenib sensitivity. We used various *shRNAs* targeting *Sox9* to deplete mRNA levels in both the YUMM1.7 (intrinsically resistant) and YUMM1.1 ResA (adaptively resistant) cells (Supplemental Figure 2.2D-F). Two out of the three *shRNAs* targeting *Sox9* showed significant knockdown following Western analysis and Q-PCR. Those *shRNAs* (*shSox9* 6165 and 6167) were then used for further characterization (Supplemental Figure 2.2D-F). Surprisingly, the downregulation of SOX9 in both the YUMM1.1 ResA and YUMM1.7 cell lines had no impact on their overall vemurafenib sensitivity (Figure

2.3D and E). These data suggest that exogenous expression of SOX9 and SOX10 does not alter drug resistance. Furthermore, the loss of SOX9 in Vemu^{R} cells does not confer drug sensitivity and that the loss of SOX10 is sufficient to induce a therapy resistant state.

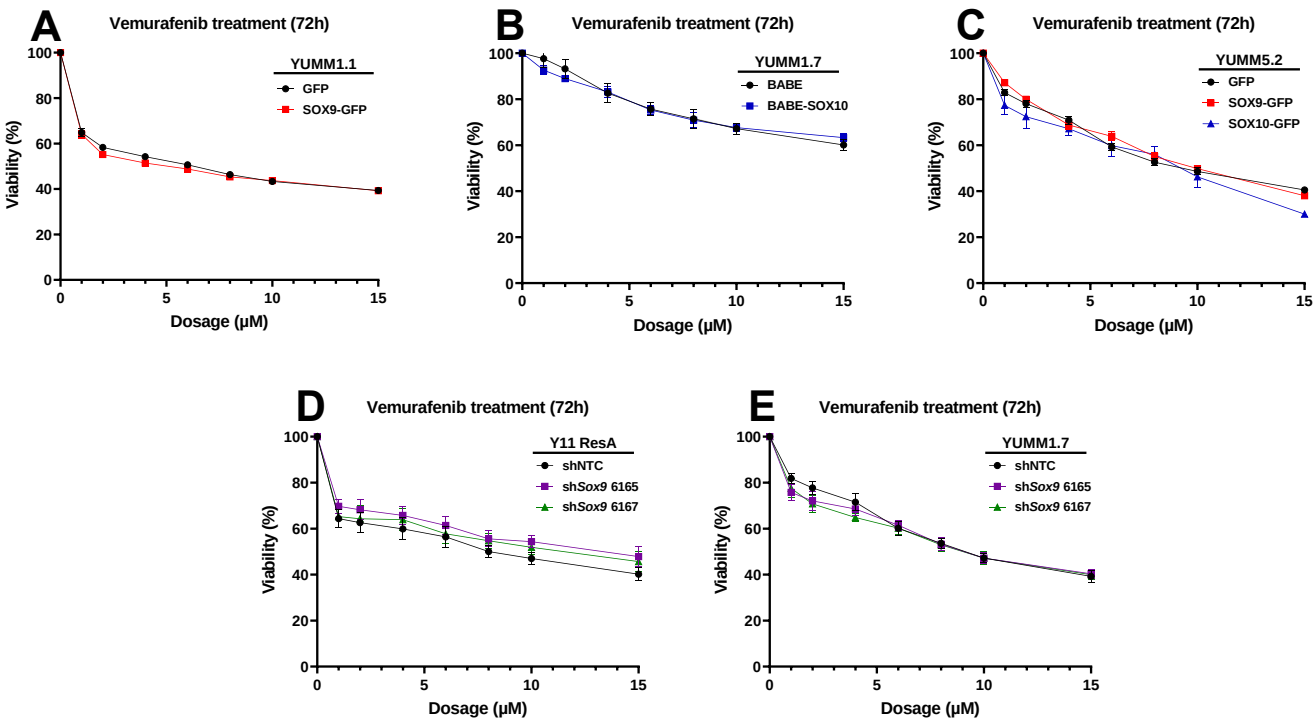
A
Vemurafenib treatment (72h)
YUMM1.1
GFP
SOX9-GFP
Viability (%)
Dosage (μM)
B
Vemurafenib treatment (72h)
YUMM1.7
BABE
BABE-SOX10
Viability (%)
Dosage (μM)
C
Vemurafenib treatment (72h)
YUMM5.2
GFP
SOX9-GFP
SOX10-GFP
Viability (%)
Dosage (μM)
D
Vemurafenib treatment (72h)
Y11 ResA
shNTC
shSox9 6165
shSox9 6167
Viability (%)
Dosage (μM)
E
Vemurafenib treatment (72h)
YUMM1.7
shNTC
shSox9 6165
shSox9 6167
Viability (%)
Dosage (μM)

Figure 2.3: SOX9 and SOX10 can not recapitulate drug resistance/sensitivity in naïve melanoma cell lines. (A-E) In vitro viability assay of manipulated YUMM cell lines treated with varying doses of vemurafenib for 72 hours. (A) SOX9 was transduced into the YUMM1.1 ($SOX9^{Low}/SOX10^{High}$) cell line, (B) SOX10 was transduced into the YUMM1.7 ($SOX9^{High}/SOX10^{Low}$) cell line, and (C) SOX9 and SOX10 was transduced into the YUMM5.2 ($SOX9^{Low}/SOX10^{Low}$) cell line. (D and E) *Sox9* targeting *shRNAs* were transduced into the (D) YUMM1.1 ResA and (E) YUMM1.7 cell lines. Data is representative of three independent experiments (A-E).

SOX9 allows for a transition to a memory state post vemurafenib treatment

Since over-expression or knock down of SOX9 did not alter the acute resistance status of the melanoma cell lines, we hypothesized that SOX9 may drive the transition to an acquired resistant state. To test this, we used the CRISPR/Cas9 system to knockout both *Sox9* and *Sox10* in YUMM1.1 cells prior to vemurafenib treatment. As expected, the loss of SOX10 induces SOX9 expression while also inducing resistance at lower doses of Vemu as previously shown (Figure 2.4A and B). As expected, the knock-out of SOX9 in the YUMM1.1 cells did change their vemurafenib sensitivity (Figure 2.4B). To test whether SOX9 plays a role in the transition to an acquired resistant state, all Sox9-deficient lines and non-targeting controls (NTC) were treated with 5um of vemurafenib for 15 days and allowed to recover for 7 days without Vemu. The SOX9 and SOX10 levels were then evaluated post treatment by western blotting (Figure 2.4C). Interestingly, SOX9 became highly induced in the NTC controls at levels that were comparable to that observed in the SOX10 knockout cells (Figure 2.4C). The NTC cells also had lowered SOX10 levels, suggesting that a transition from a sensitive to a resistant state had occurred (Figure 2.4C). Although the SOX9 knockout cells show some levels of SOX9 (due to bulk knockout) it was found to be markedly lower than the NTC controls (Figure 2.4C). They also retained high SOX10 levels suggesting that they had not proceeded to an acquired resistance state (Figure 2.4C). To test the hypothesis that SOX9 is critical for transition to acquired resistance, we re-exposed our previously DMSO-treated and vemurafenib-treated cells to vemurafenib for 72 hours after a 7 day recovery. Strikingly, during this re-challenge, we observed that the NTC controls pre-treated with vemurafenib for 15 days had acquired a “memory state” showing Vemu resistance comparable to SOX9+ YUMM1.7 cells (Figure 2.4D and E). This “memory state” is defined by the increased viability of the pretreated cells when rechallenged with vemurafenib compared back to the

pretreated DMSO controls. Supporting our hypothesis, the SOX9-deficient cells that were re-challenged with vemurafenib remained sensitive to the drug as the DMSO control pre-treated SOX9 knockout cells (Figure 2.4D, F, G). These findings suggest that SOX9 plays a role as a gatekeeper to an acquired resistant state. Without the activation of SOX9, the cells do not gain a "memory state" to drug treatment, remaining sensitive to targeted therapies.

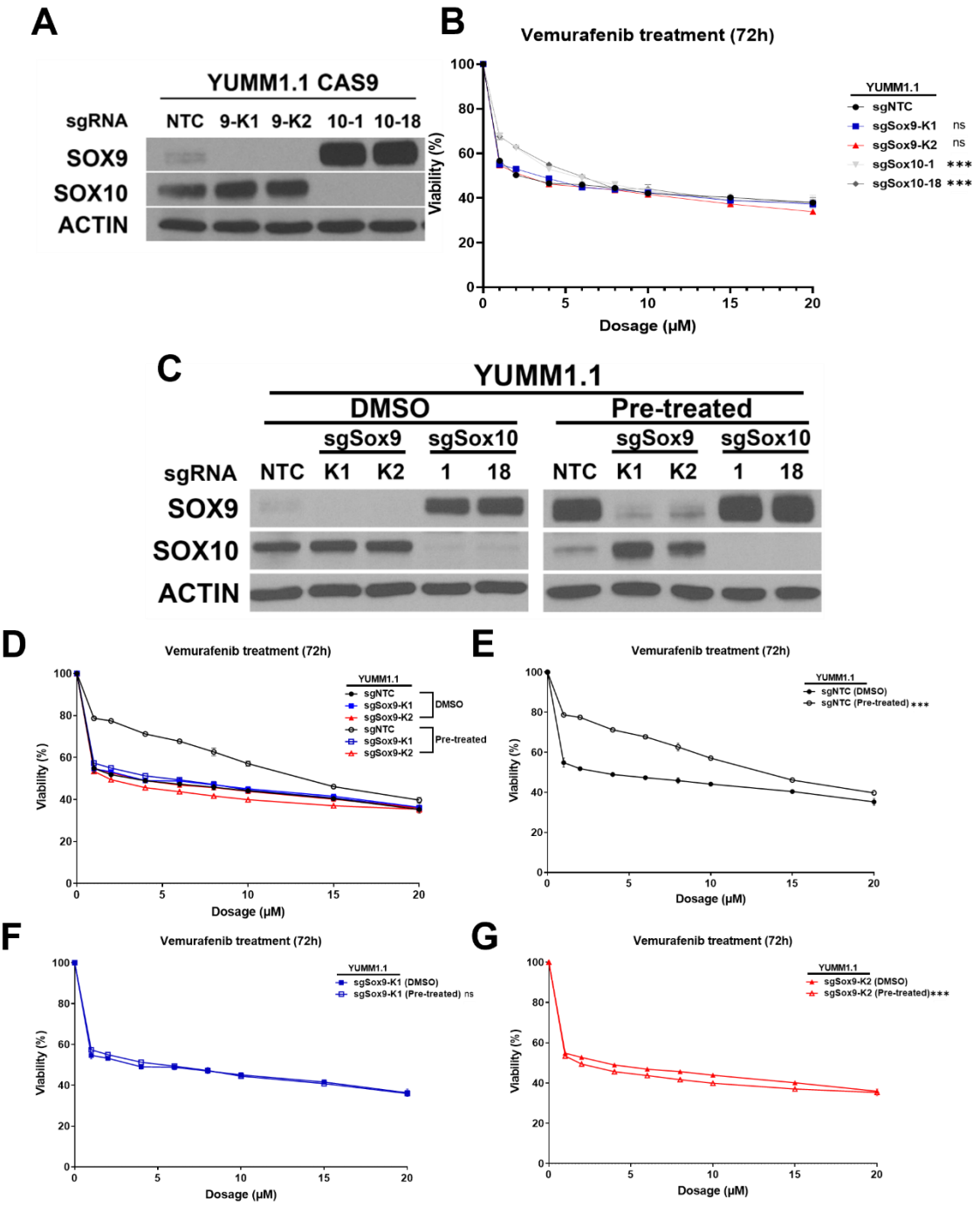
A
YUMM1.1 CAS9
sgRNA
NTC
9-K1
9-K2
10-1
10-18
SOX9
SOX10
ACTIN
B
Vemurafenib treatment (72h)
Viability (%)
Dosage (μM)
YUMM1.1
sgNTC
sgSox9-K1 ns
sgSox9-K2 ns
sgSox10-1 ***
sgSox10-18 ***
C
YUMM1.1
DMSO
Pre-treated
sgSox9
sgSox10
sgRNA
NTC
K1
K2
1
18
SOX9
SOX10
ACTIN
D
Vemurafenib treatment (72h)
YUMM1.1
sgNTC
sgSox9-K1
sgSox9-K2
DMSO
sgNTC
sgSox9-K1
sgSox9-K2
Pre-treated
Viability (%)
Dosage (μM)
E
Vemurafenib treatment (72h)
YUMM1.1
sgNTC (DMSO)
sgNTC (Pre-treated) ***
Viability (%)
Dosage (μM)
F
Vemurafenib treatment (72h)
YUMM1.1
sgSox9-K1 (DMSO)
sgSox9-K1 (Pre-treated) ns
Viability (%)
Dosage (μM)
G
Vemurafenib treatment (72h)
YUMM1.1
sgSox9-K2 (DMSO)
sgSox9-K2 (Pre-treated)***
Viability (%)
Dosage (μM)

Figure 2.4: SOX9 is required for the transition into the resistant state. (A) Western blot analysis of SOX9 and SOX10 expression on SOX9 and SOX10 knockout YUMM1.1 cell lines. (B) In vitro viability assay on two independent SOX9 and SOX10 knockout YUMM1.1 cell lines. (C) YUMM1.1 SOX9 knockout and SOX10 knockout cells were pretreated for 15 days with 5μM vemurafenib or DMSO. The drug was removed for nine days and cells were collected for Western blot analysis of SOX9 and SOX10. (D) SOX9 knockout and control pre-treated or DMSO treated cells were re-exposed to vemurafenib for 72 hours and viability was determined using alamarblue. (E-G) DMSO or vemurafenib pre-treated (E) YUMM1.1 sgNTC, (F) sgSox9-K1, or (G) sgSox9-K2 cells individually plotted from panel D. Data is representative of three independent experiments (B, D-G). (B & E-G) Significance was calculated by first identifying the IC50 of the curves using a non-linear regression. IC50s of the pre-treated populations was compared to the DMSO control populations where ns = not significant and *** = $p < 0.001$ represents two distinct IC50s.

Vemurafenib resistance alters the genomic landscape around Sox9 and Sox10

SOX9 has previously been shown to be methylated in highly proliferative melanomas and this methylation status is lost in the invasive state(121). Since invasion and target therapy resistance usually co-exist, we assessed whether methylation played a role in *Sox9* and *Sox10* expression in the YUMM1.1 ($SOX9^-/SOX10^+$), YUMM1.1 ResA ($SOX9^+/SOX10^-$) and YUMM1.7 ($SOX9^+/SOX10^-$) cell lines. The YUMM cells were treated for three days with 5-azacytidine (5-aza), which inhibits DNA methyltransferases by acting as a cytidine analog. We then assessed mRNA levels for both *Sox9* and *Sox10* following the 5-aza treatment. All cell lines displayed increased levels of *Sox9* transcripts with the YUMM1.1 cell line showing the largest increase relative to basal levels (Figure 2.5A), suggesting that differential methylation can regulate *Sox9* (Figure 2.5A). This was accompanied with an upregulation in SOX9 protein in the YUMM1.1 and YUMM1.1 ResA cells (Figure 2.5C). Although this did not translate into increased protein levels, we observed an upregulation in *Sox10* mRNA in the YUMM1.1 ResA and YUMM1.7 cells, suggesting a tightly regulated post-transcriptional mechanism (Figure 2.5B and C).

To test whether the Sox9 promoter was specifically demethylated, we identified potential CpG islands using of the *Sox9* promoter region using MethPrimer(203). We found five CpG islands 1500 bp up- and downstream from the *Sox9* transcriptional start site (TSS) (Supplemental Figure 2.3A). *SOX9* has previously been shown to be hypermethylated within island 2 and 3 in human melanoma cells therefore, we developed primers to amplify a 330bp stretch within this region (Supplemental Figure 2.3A)(121). Bisulfite sequencing of genomic DNA from YUMM1.1 and YUMM1.7 cells showed no major differences in methylated cytosines, suggesting that *Sox9* expression in YUMM1.7 cells is not due differential promoter methylation (Supplemental Figure

2.3B). To gain further insight into *Sox9* and *Sox10* regulation following the transition to a resistant state, we performed ATAC-sequencing on YUMM1.1 control, ResA and *Sox10* knockout cells. Interestingly, we observed an increase in accessible chromatin at the *Sox9* locus in both the *Sox10* knockout and ResA YUMM1.1 cell lines, both expressing Sox9 (Figure 2.5D). We also find that the upstream region of the *Sox10* locus is less accessible following the loss of *Sox10* and during the transition to the resistant state (Figure 2.5E). Together, these data suggest that both *Sox9* and *Sox10* are regulated through chromatin accessibility of their upstream regions, likely through key histone modifiers during the transition to an acquired resistance state in $BRAF^{V600E}$ driven melanoma.

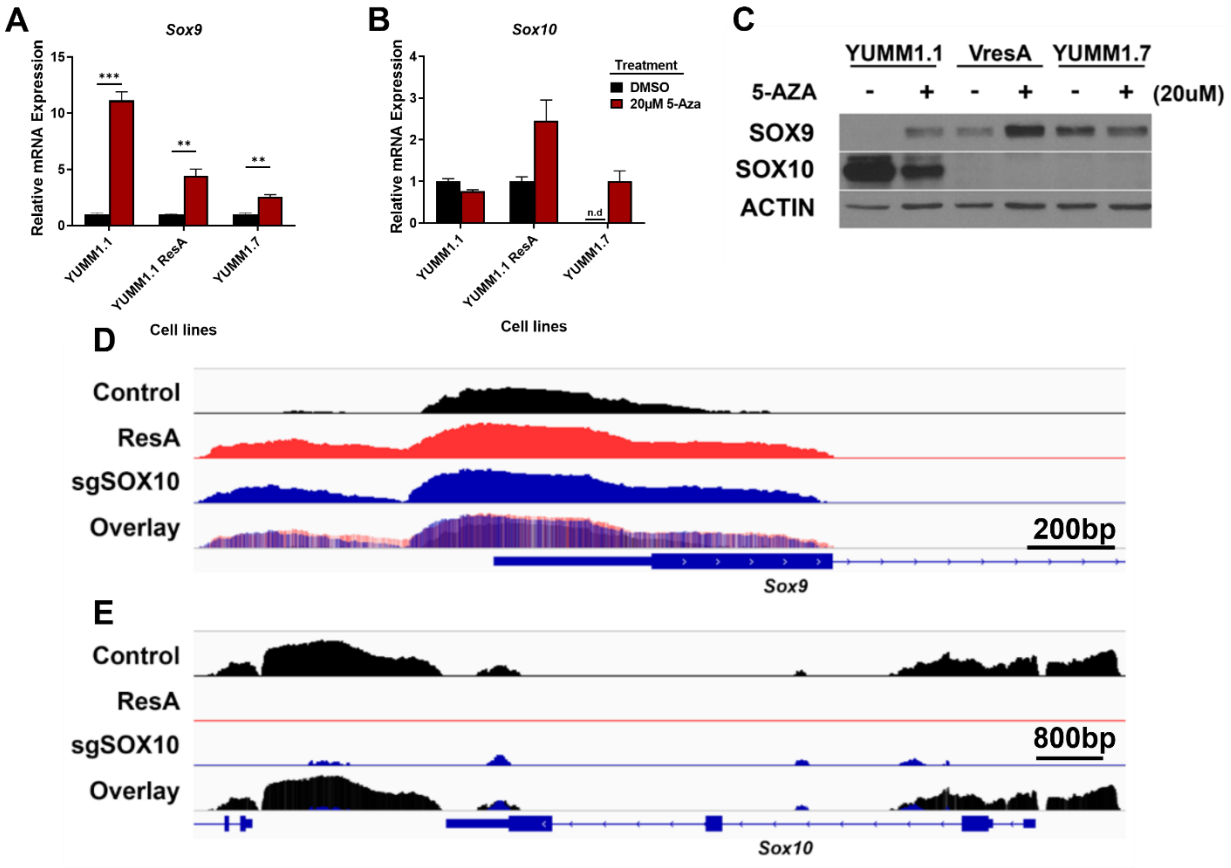
A
Sox9
Relative mRNA Expression
15
10
5
0
***
**
**
YUMM1.1
YUMM1.1 ResA
YUMM1.7
Cell lines
B
Sox10
Relative mRNA Expression
4
3
2
1
0
Treatment
DMSO
20μM 5-Aza
n.d
YUMM1.1
YUMM1.1 ResA
YUMM1.7
Cell lines
C
YUMM1.1
VresA
YUMM1.7
5-AZA
- + - + - + (20uM)
SOX9
SOX10
ACTIN
D
Control
ResA
sgSOX10
Overlay
200bp
Sox9
E
Control
ResA
sgSOX10
Overlay
800bp
Sox10

Figure 2.5: Chromatin remodeling is required to turn on *Sox9* and turn off *Sox10* expression during resistance. (A and B) RNA was collected in triplicate from YUMM1.1, YUMM1.1 ResA and YUMM1.7 cell lines treated with DMSO or 5-AZA for 72 hours. Differential expression of (A) *Sox9* and (B) *Sox10* following 5-AZA treatment was determined using qPCR. (C) YUMM1.1, YUMM1.1 ResA and YUMM1.7 cells were treated with 20μM of 5-aza-2'-deoxycytidine (5-AZA) for 72 hours. Protein was collected from DMSO and 5-AZA treated samples and SOX9 and SOX10 expression was determined using Western blotting. (D and E) ATAC-seq tracks representing biological duplicates comparing overall open chromatin of the (D) Sox9 or (E) Sox10 locus in YUMM1.1, YUMM1.1 ResA and YUMM1.1 sgSOX10 cells. (A) Significance was calculated using a two-tailed t-test, where * = $p < 0.05$, ** = $p < 0.01$ and *** = $p < 0.001$.

2.7 Discussion

Chronic MAPK inhibition in melanoma drives tumours into a therapy resistant state (65,204). *Sox10,* a transcription factor important for melanoma initiation and progression, has previously been shown to mark the proliferative therapy sensitive state in melanoma(119,187,189–191,194,195,197). *Sox9,* another SOXE factor, was found to have an opposing role in melanoma and has previously been identified in the slow cycling, targeted therapy resistant state (119,124,165,196,197). Although markers of both of these states, how *Sox9* and *Sox10* become activated/repressed during this transition and what unique function they play within each state is still unknown. We find that chronic treatment of sensitive and intrinsically resistant melanoma cells with vemurafenib leads to the loss of SOX10 and the induction of SOX9. Surprisingly, expression of SOX9 or SOX10 in different melanoma cell lines did not alter the vemurafenib resistance. Furthermore, the knockdown of *Sox9* did not affect overall resistance in both intrinsically resistant and adaptively resistant melanoma cell lines. It has been previously shown that the knockdown of *Sox10* can shift cells into a resistant state (194,197,205). We find that, although SOX9 knockout cells did not change their acute sensitivity to vemurafenib, they did inhibit the transition to a targeted therapy resistant state following a subacute treatment regimen. ATAC-seq analyses on vemurafenib sensitive, resistant and SOX10 knockout cell lines showed an overall increased, open chromatin region within the *Sox9* locus and a suppressed, closed region at the *Sox10* locus upon therapy resistance. We believe that the change in overall chromatin structure could be due to the switch from SOX10 to SOX9 acquired therapy resistance in melanoma.

SOX9 and SOX10 have both been shown to regulate therapy resistance in various cancer subtypes. In melanoma, the loss of Sox10 drives cells into a slow-cycling/dormant-like state that gains resistance to various MAPK inhibitors (194,197). In gastric cancer, SOX9 has been shown

to alter cisplatin resistance through its ability to regulate the expression of various miRNAs (206,207). Similar findings were also observed in cervical and ovarian cancer (208,209). Since *Sox10* and *Sox9* have previously been shown to mark the MAPK inhibitor-sensitive and resistant state, respectively, we hypothesized that the over-expression of either of these genes would result in a shift in tolerance (119,124,165,196,197). Surprisingly, SOX9 and SOX10 expression in our melanoma cell lines did not affect drug resistance. Although previously identified as a marker of the sensitive state, the ability of SOX10 to induce sensitivity to MAPK inhibitors could be due to its inability to modulate the chromatin landscape (194,197) in resistant cells. If SOX10 binding sites are in a closed conformation during the transition to the resistant state, expression of SOX10 would not have an effect. Similarly, SOX9 expression could not directly induce resistance in sensitive cells. However, its deletion was shown to block the transition to the resistant state. The availability of both $BRAF^{V600E}$ melanoma models and SOX9 conditional mice could provide a genetic model to test the sensitivity of SOX9-null tumours to MAPK inhibitors.

We find that the activation of SOX9 induces a memory state to targeted therapies. Melanoma cells that lack SOX9 cannot undergo the transition to the resistant state following vemurafenib treatment and remain sensitive to targeted therapies. Although it is still not clear how SOX9 elicits this response, we have found an increase and decrease in open chromatin regions around the *Sox9* and *Sox10* locus, respectively. Interestingly, *Sox9* has been shown to act as an epigenetic regulator in various tissue types (172,210–212). In embryonic epidermal stem cells, the activation of SOX9 promotes a switch in lineage differentiation, where it can alter chromatin access by modulating nucleosome binding(211). In brain tumours, *Sox9* has been found to both repress and promote tumour formation of high-grade glioma and ependymoma, respectively, through the regulation of H3K27ac(212). Although these studies have identified a role for *Sox9* in

altering the genomic landscape, what regulates *Sox9* and its downstream targets in drug resistance requires further investigation.

Limitations and future directions

Various limitations could be observed within this study. Since our findings are predominantly tested in syngeneic murine cell models, common somatic mutations or single nucleotide variations observed within human cell cultures are absent. These variations have previously been observed to alter resistance to MAPK inhibition and remain untested in our hands. Although the loss of SOX9 did stop the transition to the vemurafenib resistant state, this was tested *in vitro*, and was never subsequently confirmed to occur *in vivo*. A key experiment that could answer this question is with the use of the $BRAF^{V600E}$, $PTEN^{fl/fl}$, $Cdkn2^{fl/fl}$, $SOX9^{fl/fl}$ melanoma model. With the removal of SOX9 in melanocytes, melanoma tumours can be treated with MAPK inhibitors, following tumour induction. If SOX9-null tumours regress and remain absent following prolonged MAPK inhibition, it would conclude that SOX9 expression is a requirement to allow for this adaptive resistant response. Since melanoma is highly heterogenic, murine models will never recapitulate various populations found within human melanoma biopsies and this will further remain a limitation with this type of study.

2.8 Supplementary figures

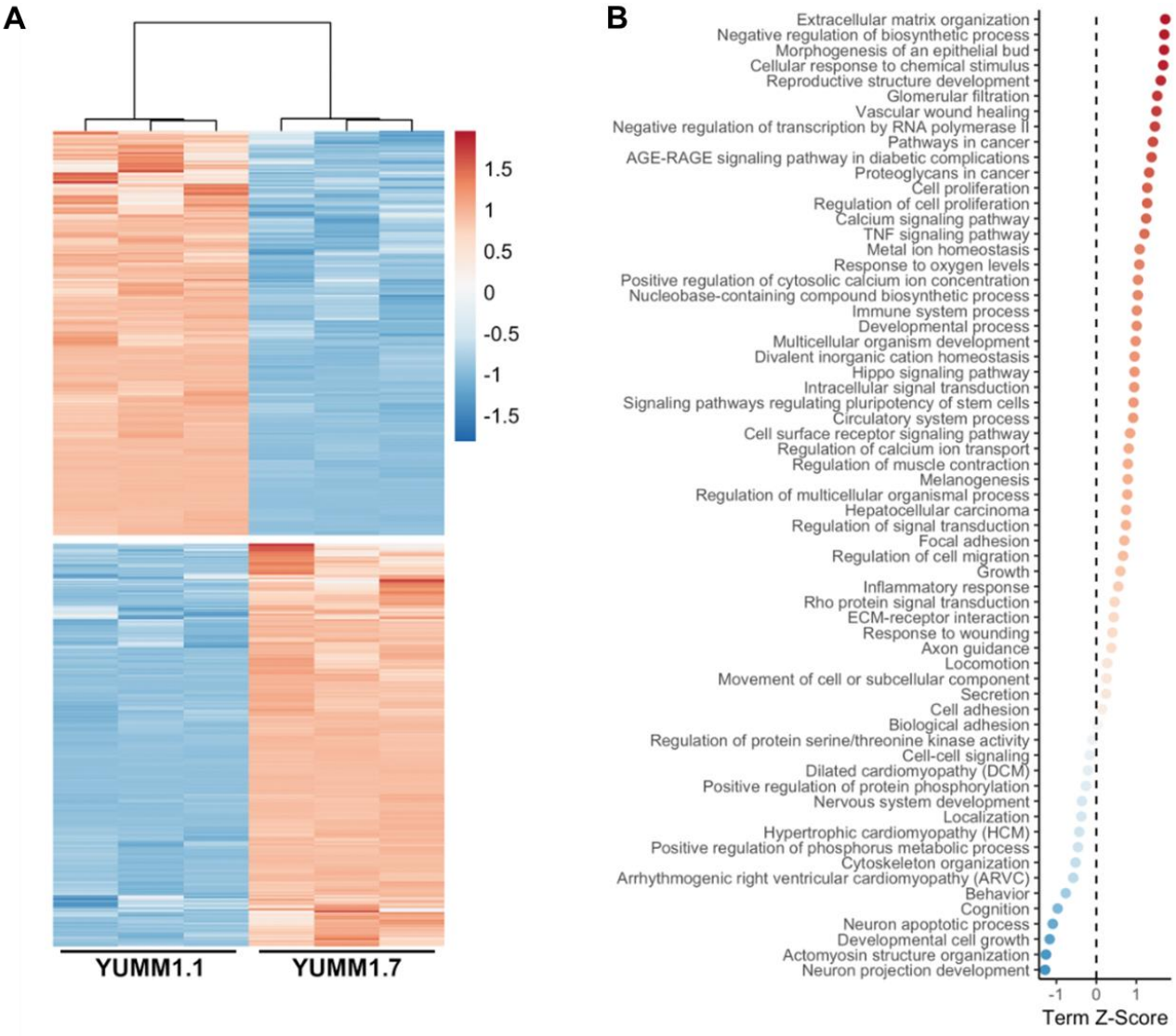

Supplemental Figure 2.1: Gene-ontology (GO) analysis between SOX9^{Low}/SOX10^{high} and SOX9^{High}/SOX10^{Low} YUMM cell lines. (A) RNA was collected in triplicate from YUMM1.1 and YUMM1.7 cell lines. RNA-sequencing was performed and differentially expressed genes were represented in a heatmap where specific colors represent the Z-score of each individual gene. (B) GO terms representing differentially expressed processes between the YUMM1.1 (blue) and YUMM1.7 (red) cell lines.

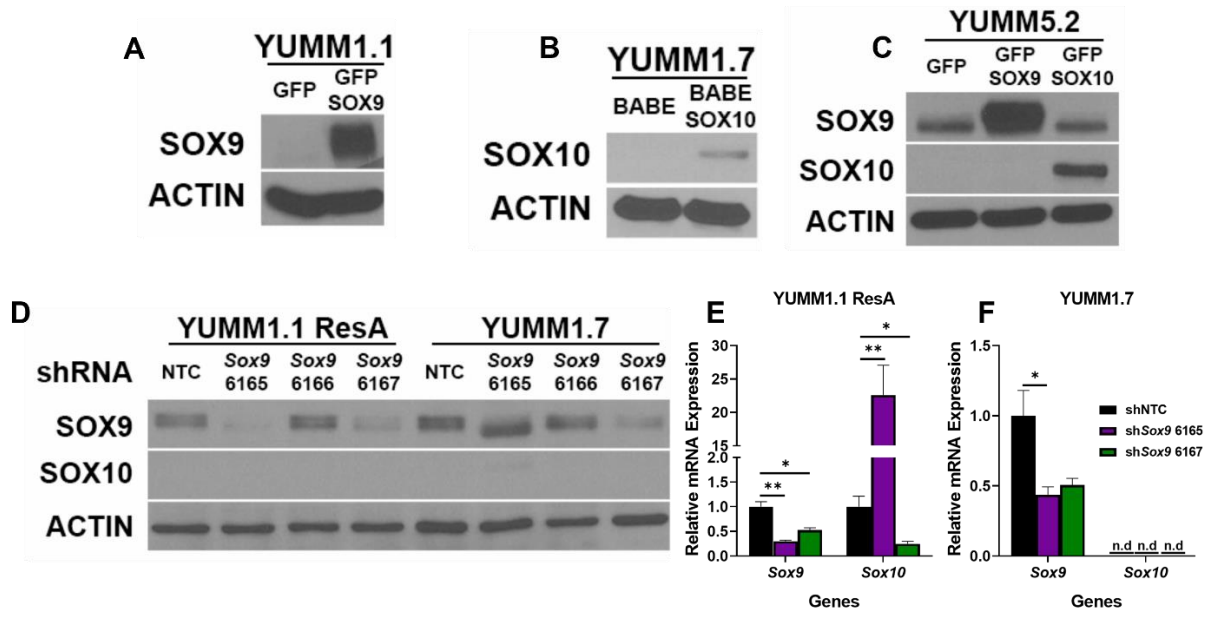

Supplemental Figure 2.2: Validation of SOX9 and SOX10 expression in transduced YUMM lines. (A-D) Western blot analysis of SOX9 and SOX10 in transduced cell lines containing either (A and C) a SOX9, (B and C) a SOX10 expression plasmid or (D) a shRNA targeting Sox9. (E and F) qPCR showing the differential expression of Sox9 treated with shSox9 in the (E) YUMM1.1 ResA or (F) YUMM1.7 cell line. Data is representative of three independent experiments (E and F). (E & F) Significance was calculated using a two-tailed t-test, where * = $p < 0.05$ and ** = $p < 0.01$.

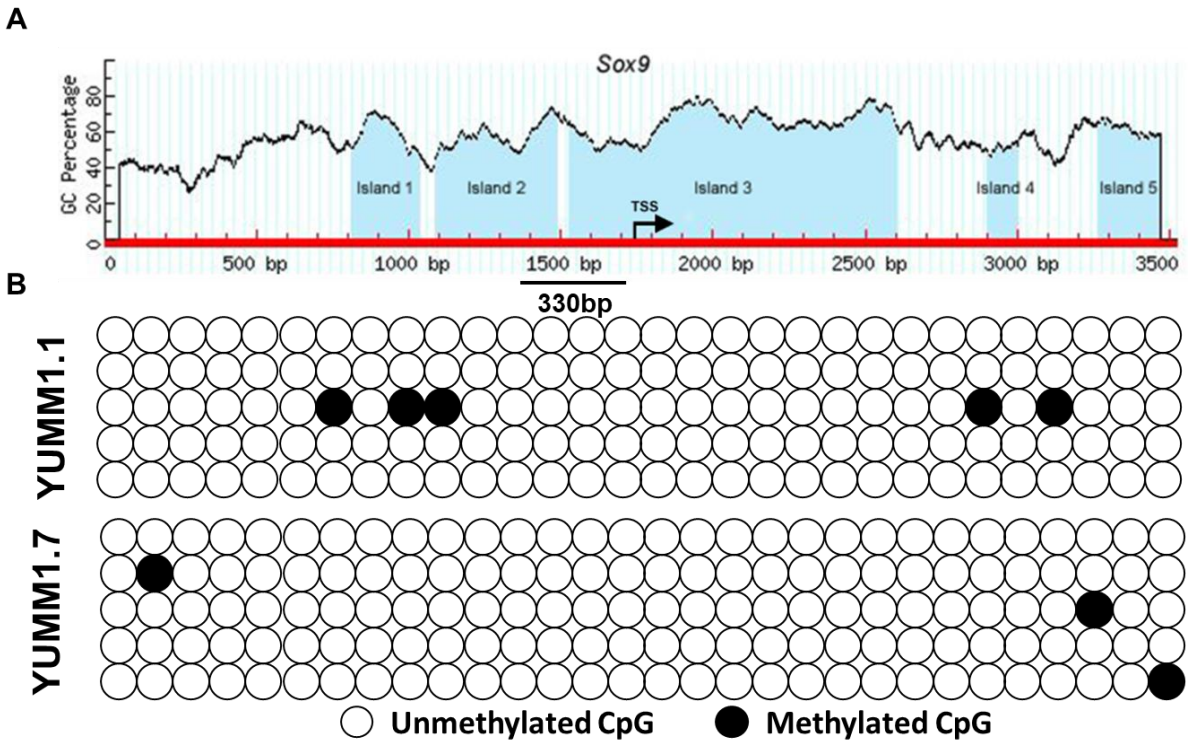

Supplemental Figure 2.3: *Sox9* expression is independent of hypermethylation of the *Sox9* locus in the YUMM cell lines. (A) Representation of the Sox9 locus depicting the 5 CpG islands throughout the 3kbp stretch surrounding the transcription start site (TSS) of Sox9. The 330bp stretch is marked, depicting the amplicon amplified for the bisulfite sequencing. The schematic was created by MethPrimer(203). (B) A representative image depicting each CpG repeat (circle) within the 330bp stretch amplified. White circles represent an unmethylated CpG repeat while black circles represent methylated regions. Five clones were isolated and sequenced for each cell line.

Chapter 3

Sox10-deficient drug resistant melanoma cells are refractory to oncolytic RNA viruses.

3.1 Preface

Abou-Hamad, J., Hodgins, J. J., Yakubovich, E., Vanderhyden, B. C., Ardolino, M., & Sabourin, L. A. (2023). Sox10-Deficient Drug-Resistant Melanoma Cells Are Refractory to Oncolytic RNA Viruses. Cells, 13(1), 73. https://doi.org/10.3390/cells13010073

Author contributions

Abou-Hamad J: Performed all experiments in exception to the RNA-seq analysis. I also wrote and proofread the manuscript

Hodgins JJ: Provided the OVs and the methodology of the experiments.

Yakubovich E: Performed the alignment and analysis for the RNA-seq. Wrote the methods pertaining to the RNA-seq analysis.

Vanderhyden B: Provided ideas and expertise in RNA-seq analysis.

Ardolino M: Provided the ideas and expertise in OV infection

Sabourin L: Provided general expertise throughout the project. Also proofread and edited the manuscript.

3.2 Title page

This paper was submitted to Cells on November 25, 2023

Sox10-deficient drug resistant melanoma cells are refractory to oncolytic RNA viruses.

Authors

John Abou-Hamad [1, 2], Jonathan J Hodgins [1, 3], Edward Yakubovich [1, 2], Barbara C Vanderhyden [1, 2], Michele Ardolino [1, 3], Luc A Sabourin [1, 2,4]

Affiliations

3. Centre for Cancer Therapeutics, Ottawa Hospital Research Institute, 501 Smyth Road, Ottawa, ON K1H 8L6, Canada.
4. Department of Cellular and Molecular Medicine, University of Ottawa, Ottawa, ON K1H 8L6, Canada.
5. Department of Biochemistry, Microbiology and Immunology, University of Ottawa, Ottawa, ON K1H 8L6, Canada.

Disclosures

The authors declare no competing interests.

Funding

This work was supported by grants to L.A.S. from the Canadian Institutes of Health Research, the Canadian Cancer Society, and the Cancer Research Society

Keywords : Melanoma, Sox10, BRAFV600E, oncolytics, vemurafenib, drug resistance

3.3 Abstract

Targeted therapy resistance frequently develops in melanoma due to intratumor heterogeneity and epigenetic reprogramming. This also typically induces cross resistance to immunotherapies. Whether this includes additional modes of therapy has not been fully assessed. We show that co-treatments of MAPKi with VSV-based oncolytics do not function in a synergistic fashion, rather the MAPKis block infection. Melanoma resistance to vemurafenib further perturbs the cells ability to be infected by oncolytic viruses. Resistance to vemurafenib can be induced by the loss of SOX10, a common proliferative marker in melanoma. The loss of SOX10 promotes a cross-resistant state by further inhibiting viral infection and replication. Analysis of RNA-seq datasets we observed an upregulation of ISGs in SOX10 knockout populations and targeted therapy resistant cells. Additionally, the induction of ISGs appears to be independent of type I IFN production. Overall, our data suggests that the pathway mediating oncolytic resistance is due to the loss of SOX10 during acquired drug resistance in melanoma.

3.4 Introduction

Targeted therapies revolutionized melanoma treatment due to their superior efficacy and specificity. Vemurafenib, an ATP analog was the first direct $BRAF^{V600E}$ targeted therapy that showed great specificity and increased overall survival of melanoma patients (213–216). Unfortunately, the effectiveness of these therapies only lasts for about a year when most melanoma patients begin to relapse (217,218). Other MAPK inhibitors (MAPKi) have been used in conjunction with BRAF inhibitors but resistance still occurs (219,220). This is in part due to the large intratumor heterogeneity of melanoma where some cells can undergo epigenetic alterations and shift their gene expression profile during prolonged treatment (221,222).

Interestingly, targeted therapy resistance can be induced through the loss of SOX10, a key player in melanoma initiation and progression (223–227). Studies have also shown that the loss of SOX10 increases the cancer stem cell properties of melanoma, which could be the underlying factor in creating this resistant state (228,229). As more work unravels this concept of cancer stem cells, others have observed that the enrichment of cancer stem cells induces a cross-resistant state to both chemotherapy and immunotherapy (230). Whether targeted therapy induces a cross-resistance environment to all forms of therapy remains to be assessed.

A more recent method of melanoma treatment is an oncolytic virus-derived therapeutic (231). One virus, namely Vesicular Stomatitis Virus (VSV), has been well documented to target and kill proliferative cancers such as melanoma both *in vitro* and *in vivo* (83,232,233). In healthy cells, viral infection induces the type I interferon (IFN) response, which increases the production of IFNα/β (234). This in turn activates specific interferon stimulated genes (ISGs) that are used to repress viral replication and spread (234,235). This response is turned off in cancer cells since the IFN pathway inhibits growth, allowing oncolytic viruses such as VSV to specifically target cancer

cells (236). Although VSV treatment has been shown to readily kill melanoma cells, we tested whether targeted therapy could be used together with oncolytic viruses.

In this study, we find that VSV and MAPKi's do not function synergistically, rather MAPKi's block VSV infection. We further show that melanoma cells that acquire a drug resistant state are less susceptible to viral infection and this cross-resistant state can be recapitulated following the deletion of SOX10. Finally, we find that both the induced resistant state and the loss of SOX10 induces the activation of ISGs independent of IFNα/β, priming the cells for resistance to infection by oncolytic viruses. These data suggest that therapeutic regimen that support a drug sensitive melanocytic state could be enhanced by the addition of oncolytics.

3.5 Material and Methods

Cell culture

The Yale University Mouse Melanoma cell line YUMM1.1 and the human melanoma cell line A375 was a kind gift from Dr. William Damsky and Dr. John Copeland (respectively). Vero cells were a kind gift from Dr. Michele Ardolino and the 293Ts were obtained from ATCC. All cell lines were cultured in DMEM supplemented with 10% FBS, 1% L-glutamine and 1% penicillin/streptomycin. The YUMM1.1 cell line also received a supplement of 1X non-essential amino acids.

Establishment and isolation of Vemurafenib resistant cell populations

Melanoma cell lines were plated in 60mm dishes at 40% confluency and allowed to adhere overnight. The next day, cells were treated with Vemurafenib at their respective IC50 for 6 weeks, with fresh media and drug replacement occurring every three days. The cells were then taken off

the drug treatment and allowed to recover and retested for vemurafenib sensitivity for three days to confirm the resistant phenotype.

Oncolytic infection

Melanoma cells were plated in multiple wells, left to adhere overnight and counted the next day from duplicate wells. The cells were then infected with various viruses at various MOIs (MOI=$\frac{Number\ of\ cells}{amount\ of\ liquid\ added\ per\ well\ (L)} * desired\ MOI * amount\ required$). Viral supernatant was added to each well for 1 hour at 37ºC, removed and replaced with full media for 24 hours. The cells were then collected and quantified for YFP or eGFP by flow cytometry.

Viral titer

Viral supernatant from infected cells were collected 24 hours post infection and overlaid onto confluent Vero cells in multiple serial dilutions and incubated at 37ºC for 90 mins. To allow for virus adherence a 1:1 mix of 1% agar and 2X DMEM with 20% FBS was added to each well and allowed to solidify at room temperature for 10min. Plates were incubated at 37ºC for 24 hours and fixed (3:1 methanol: glacial acetic acid) for one hour. Agar overlays were washed away using water and the wells were stained with Coomassie blue and plaque forming units were counted.

Resazurin viability assay

Melanoma cells were plated in a 96-well plates and treated with various compounds for 48 (any viral infection) or 72 hours (vemurafenib, dabrafenib, and/or trametinib; SelleckChem). Control wells supplemented with PBS, and/or DMSO (viral infection or MAPKi, respectively) were used as a baseline for 100% viability. At the end of the treatment, supernatants in each well were

removed and replaced by 100µL of resazurin solution (55µM resazurin salt, 10% FBS, 1X DMEM). The absorbance of each well was read at 570 and 604nm after four hours.

SiRNA transfection and lentivirus production

All siRNAs used were purchased from Dharmacon. Lipofectamine 3000 (Invitrogen) was used to introduce 200nM of siRNA into the YUMM1.1 cells. Transfected YUMM1.1 cells were seeded into a 96-well dish 24hrs post transfection and subsequently treated with vemurafenib at various concentrations 24hrs post plating.

Viral particles were produced by seeding 293T cells (5×10^6) in a 10cm dish. 293Ts were transfected using lipofectamine 3000 with 10µg of construct, 8µg of pCMV-dR8.2 dvpr and 2µg of pCMV-VSV-G. The next day, medium was changed and viral supernatant was collected 72 hours later and passed through a 0.44µm filter.

Lentiviral-mediated CRISPR/Cas9 knockouts

Melanoma cells were infected for 6 hours with 1mL of viral supernatant diluted in 5mL of cell culture media supplemented with 10µg/mL of polybrene. The medium was replaced with full medium and the cells were selected with 5µg/mL of blasticidin (for Cas9 plasmid) or sorted for RFP (for CRISPR guides) 48 hours post infection. Knockout cells were confirmed using Western blotting. Sequences for mouse sgSOX10 were as previously described (Abou-Hamad et al., 2022).Human guide RNAS have the following sequences; sgSOX10-4: GATGGAGCGCCCGT-CCCGCT and sgSOX10-24: GTGACAAGCGCCCCTTCATC.

Cell lysis and Western Blotting

Melanoma cell lines were lysed using RIPA lysis buffer containing protease and phosphatase inhibitors. Lysates were vortexed at increments of 5 min on ice for a total of 30 minutes or freeze thawed to allow for complete isolation of whole cell protein. Lysates were cleared at 16000 x g for 10 minutes at 4^{o}C. Bradford reagent (BioRad) was used to quantify protein concentration. Equivalent amounts of protein were denatured, electrophoresed on polyacrylamide gels and transferred onto PVDF (polyvinylidene difluoride) membranes. Membranes were probed with primary antibodies in 5% bovine serum albumin (BSA) in 1X TBST overnight at 4^{o}C followed by HRP-conjugated secondary antibodies. Reactive bands were detected with Enhanced chemiluminescence reagent and exposure to X-ray films. Membranes were probed with SOX10 (CellSignaling Technology: Cat:89356), custom pan-VSV (a kind gift from Dr. Jean Simon Diallo) and β-actin (Sigma: Cat:A5316).

RNA-sequencing, EnrichR biological pathway analysis and TPM analysis

Data from A375 control and SOX10-KO-2 was collected from NCBI BioProject PRJNA748713. Transcript quantification was executed using Kallisto (v0.45.0) (237) with the GRCh38 build of the human transcriptome and the -b 50 bootstrap option. Raw counts were imported into DESeq 2 (1.40.2) and analyzed (238). Genes with less than 10 counts were removed. Differential gene expression with adjusted p-value < 0.05 were identified and fold change was determined comparing the A375 sgNTC samples with the SOX10 KO-2 samples.

Genes upregulated in the SOX10 knockout cells were imported into EnrichR to determine the biological processes activated within the SOX10 knockout cells (239,240). Only genes that had a p-value < 0.05 were used during this analysis. Genes found within the gene sets are from MSigDb (241).

To determine whether the correlation observed with the SOX10 KO and the ISGs (Table 2.1) also occurred in targeted therapy resistant cells, we used deposited data from NCBI BioProject PRJNA748714. TPM values for each gene were used and relative expression was calculated using a Z-score.

3.6 Results

MAPKi treatment blocks VSV infection in BRAF^{V600E} melanoma

To determine whether VSV oncolytic therapy could be used in conjunction with current therapies, we tested the combination of VSVΔ51 (242) with MAPK inhibitors. We treated the Sox10-expressing murine YUMM1.1 cells (which harbor a BRAF^{V600E} mutation) with VSVΔ51 and with either vemurafenib (5 μM), dabrafenib (1 μM) or trametinib (0.1 μM) (Fig. 3.1A). Interestingly, we observed a reduction in infection (measured using a viral YFP reporter) when cells were co-treated with BRAF and MEK inhibitors (Fig. 3.1A). When tested in the A375 human melanoma cell line, we observed a similar reduction in viral infection with BRAF/MEK inhibitors (Fig. 3.1A). To confirm these findings, we measured viral replication using plaque assays. In agreement with our viral YFP reporter infection data, we observed approximately a 100-fold decrease in viral titers when YUMM1.1 and A375 melanoma cells were co-treated with MAPKi relative to VSVΔ51 alone (Fig. 3.1B). As expected, there was a significant decrease in viability in cells only infected with VSVΔ51 and cells treated with BRAF/MEK inhibitors only (Fig. 3.1C). However, viability was not significantly altered by co-treatment with BRAF/MEK inhibitors and VSVΔ51 relative to the individual treatments, suggesting that MAPK inhibitors block VSV infection and lytic function (Fig. 3.1C). Therefore, MAPK targeted therapies in melanoma block the *in vitro* efficacy of the oncolytic VSVΔ51.

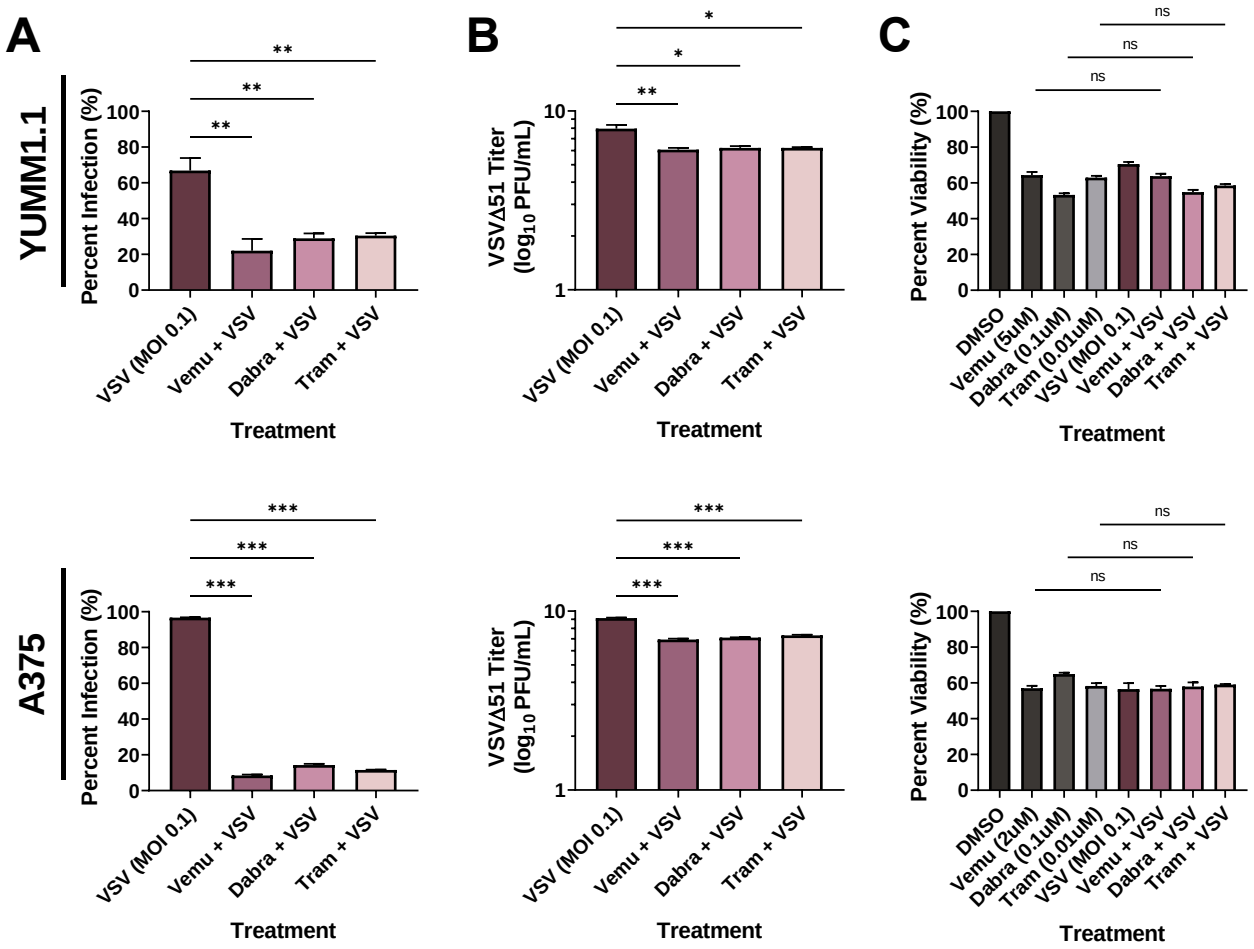
A
B
C
YUMM1.1
A375
Percent Infection (%)
VSVΔ51 Titer (log10 PFU/mL)
Percent Viability (%)
VSV (MOI 0.1)
Vemu + VSV
Dabra + VSV
Tram + VSV
DMSO
Vemu (5uM)
Vemu (2uM)
Dabra (0.1uM)
Tram (0.01uM)
Treatment
**
*
***
ns

Figure 3.1. MAPKi treatment blocks VSV infection in BRAF^{V600E} melanoma. YUMM1.1 and A375 cell lines were co-treated with VSVΔ51 at an MOI of 0.1 and vemurafenib (5μM or 2μM respectively), dabrafenib (0.1μM) or trametinib (0.01μM) for **(A & B)** 24 or **(C)** 48hrs. **(A)** Quantification of YFP positive melanoma cells 24hrs post MAPKi and/or VSVΔ51 treatment. **(B)** Quantification of viral titers by plaque assays 24hrs post infection. **(C)** Cell viability assay (AlamarBlue) 48hrs post single and co-treatments. **(A-C)** All data is represented as a mean ± SEM of biological triplicates. **(A & B)** Significance was calculated using a two-tailed t-test, where * = $p < 0.05$, ** = $p < 0.01$ and *** = $p < 0.001$. **(C)** Significance was calculated using a one-way anova.

Vemurafenib induced targeted therapy resistance promotes a cross-resistant state between other MAPKis and VSV infection

Resistance to targeted therapy is common in clinical settings (217,218). Given that concurrent treatment with MAPKi blocks VSV infection (Fig. 3.1), we determined whether MAPK-resistant melanomas are also resistant to viral infection/lysis. To test this, we generated three independent vemurafenib-resistant populations by chronically treating YUMM1.1 and A375 cell lines for six weeks at their IC_{50} concentrations (5 μM and 2 μM, respectively; Fig. 3.2A). Three independent populations were generated with varying resistance to vemurafenib but also to other MAPKi inhibitors (Fig. 3.2B-D and Fig. S3.1A). Drug-resistant cells were then tested for VSVΔ51 infection. Interestingly, we found that all drug-resistant populations had also acquired resistance to viral infection, with the most dramatic phenotype observed in the YUMM1.1 ResA cells (Fig. 3.2E). This was also observed in human A375 melanoma cells, although not as robust as A375 drug-resistant cells have a tendency to revert back to wild-type tolerance following brief culture in the absence of vemurafenib treatment (Fig. S3.1B). This suggests a tight link between MAPKi-resistance and resistance to viral infection. Plaque assays showed reduced viral titers (Fig. 3.2F) and resistance to virus-induced cell killing (Fig. 3.2G), supporting the notion that MAPKi resistance in melanoma further induces viral therapy resistance against VSVΔ51. This resistance was also assessed in YUMM1.1 cells treated acutely for 3 or 9 days with vemurafenib. After rechallenge with vemurafenib or VSVΔ51 we observed no major differences in VSVΔ51 infection or viability, suggesting that long term transition or reprogramming is required to promote this cross-resistant state (Fig. S3.2A-B). Therefore, resistance to MAPK-targeted therapies in melanoma also promotes cross-resistance to oncolytic virus therapy.

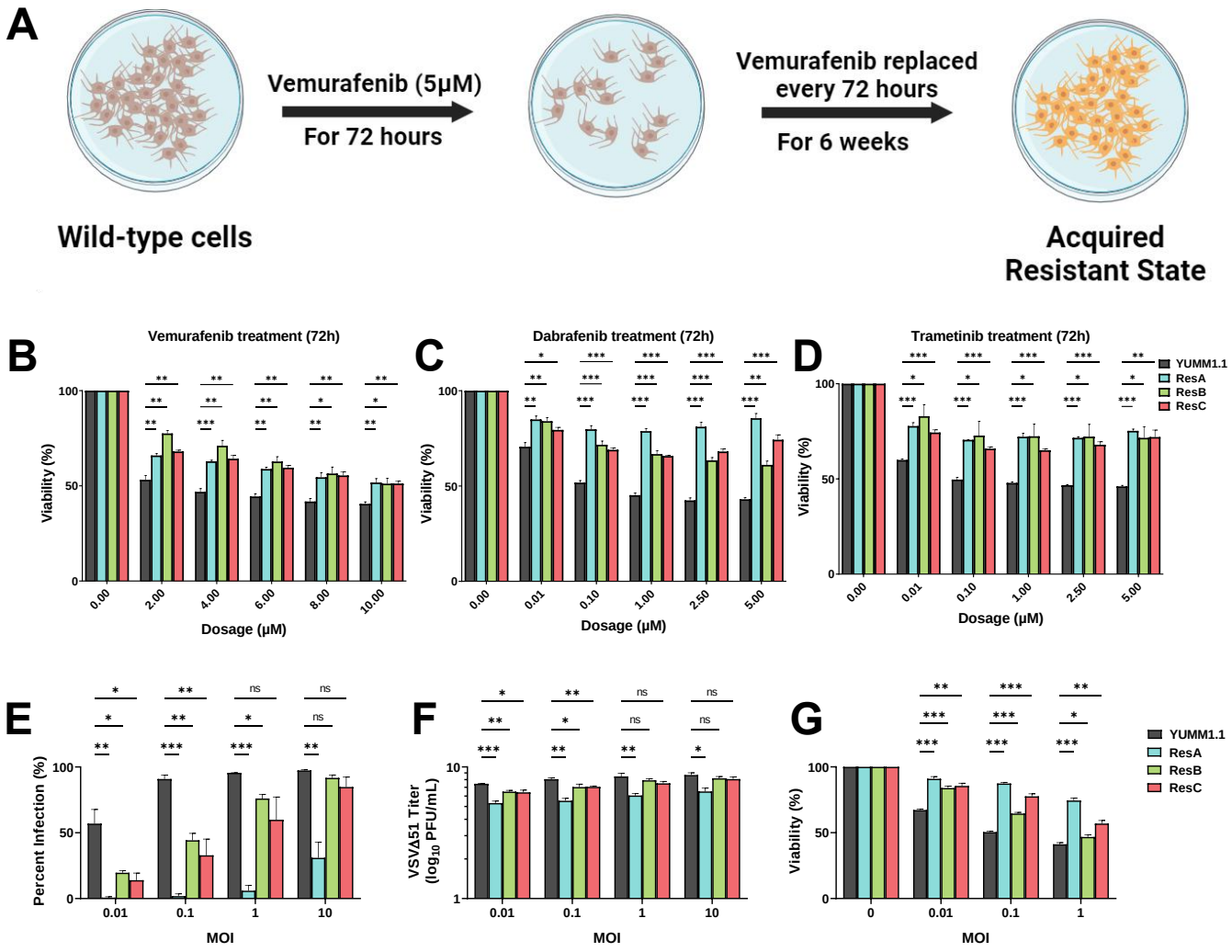
A
Vemurafenib (5μM)
For 72 hours
Vemurafenib replaced every 72 hours
For 6 weeks
Wild-type cells
Acquired Resistant State
B
Vemurafenib treatment (72h)
Viability (%)
Dosage (μM)
C
Dabrafenib treatment (72h)
Viability (%)
Dosage (μM)
D
Trametinib treatment (72h)
Viability (%)
Dosage (μM)
YUMM1.1
ResA
ResB
ResC
E
Percent Infection (%)
MOI
F
VSVΔ51 Titer (log10 PFU/mL)
MOI
G
Viability (%)
MOI

Figure 3.2. Vemurafenib induced targeted therapy resistance promotes a cross-resistant state between other MAPKis and VSV infection. (A) Schematic representing the 6 week treatment regimen to convert the parental YUMM1.1 cell line into a vemurafenib resistant cell state. **(B-D)** YUMM1.1 and Resistant cell lines were seeded in at least technical triplicates and treated at an increasing concentration of vemurafenib **(B)**, dabrafenib **(C)** or trametinib **(D)**. Cell viability was assayed using AlamarBlue 72hrs post treatment. **(E-G)** Quantification of **(E)** YFP positive (E), viral titers (F) and cell viability (G) of YUMM1.1 and Res cells 24 **(E & F)** or 48hrs **(G)** post VSVΔ51 infection. All data is represented as a mean ± SEM of biological triplicates. Significance was calculated using a two-tailed t-test, where * = $p < 0.05$, ** = $p < 0.01$ and *** = $p < 0.001$.

SOX10 is lost during chronic targeted therapy treatment and induces a cross-resistant state to VSVΔ51

Given the prevalence of resistance to MAPK targeted therapies, several genes and pathways potentially implicated in this process have been identified (243,244). We reasoned that these same resistance mechanisms may also play a role in cross-resistance to oncolytic virus therapy. We have previously shown that the transcription factor SOX10, a major marker of primary melanomas and the melanocytic state, reduces the cancer stem cell properties of melanoma cells (228). Others have found that the loss of SOX10 expression induces MAPKi resistance (223–228). Interestingly, SOX10 has been associated with the regulation of immune-related pathways including IRF1, a well-characterized regulator of viral infection (245). Therefore, we hypothesized that the loss of SOX10 in MAPKi-resistant cells could induce resistance to oncolytic virus infection. Chronic vemurafenib treatment lead to the loss of SOX10 in melanoma cells and a marked reduction in VSVΔ51 infection (Fig. 3.3A). Similarly, SOX10 knockdown also promoted resistance to vemurafenib treatment (Fig. 3.3B-C). We further tested VSV infection and replication in stable YUMM1.1 SOX10-null cells (228) and A375 SOX10 knockout cells. In both SOX10-deficient cells, a substantial reduction in VSVΔ51 infection and titers was observed, suggesting that SOX10 plays a key role in resistance to oncolytic virus therapy (Fig. 3.3D&E). In contrast, decreased virus-induced cell death was seen in SOX10 knockout cells (Fig. 3.3F-I). Therefore, SOX10 expression is required for efficient VSVΔ51 infection in melanoma cells and its expression is downregulated following resistance to MAPK inhibitors.

The cellular response to RNA viruses such as VSVΔ51 is notably different from the response to DNA viruses. We then asked if the cross-resistance to oncolytic virus therapy after MAPKi resistance is unique to RNA viruses. To this end, we expanded our panel of viruses to

include another oncolytic RNA virus, Maraba MG1, and the DNA virus vaccinia (VVTT). As expected, our drug-resistant melanoma cells and SOX10 knock out cells were resistant to MG1 but not to vaccinia virus infection (Fig. S3.3A-D), suggesting that this phenotype is conserved among RNA viruses and that these cells become "primed" to RNA virus infection upon acquiring a drug-resistant state.

Although many mechanisms of resistance to viral infection exist, the most prominent arises from the type I interferon pathway (246). Since VSVΔ51 harbors a mutation that sensitizes it to the anti-viral effects of type I IFNs, we examined the role of that pathway in cross-resistance to oncolytic viruses therapy. First, we made use of wildtype VSV, which antagonizes the production of type I IFNs in infected cells. However, wildtype VSV infection was similarly reduced in drug-resistant melanoma cells and SOX10 KO cells, analogous to our data with VSVΔ51 (Fig. S3.4A,B). Next, we treated the cells with the JAK1/2 inhibitor ruxolitinib (RUXO), a blocker of the type I IFN response. Treatment with RUXO restored VSVΔ51-mediated killing and replication to control levels in most drug-resistant cells and the SOX10 KO cells (Fig. S3.4C-D,F). Interestingly, the sensitivity of the highly resistant YUMM1.1 ResA population was restored to wildtype levels following co-treatment with VSV and RUXO (Fig. S3.4E). This suggests that the drug-resistant state acquired through chronic treatment or via the loss of SOX10 alters the type I IFN pathway to block oncolytic RNA viruses.

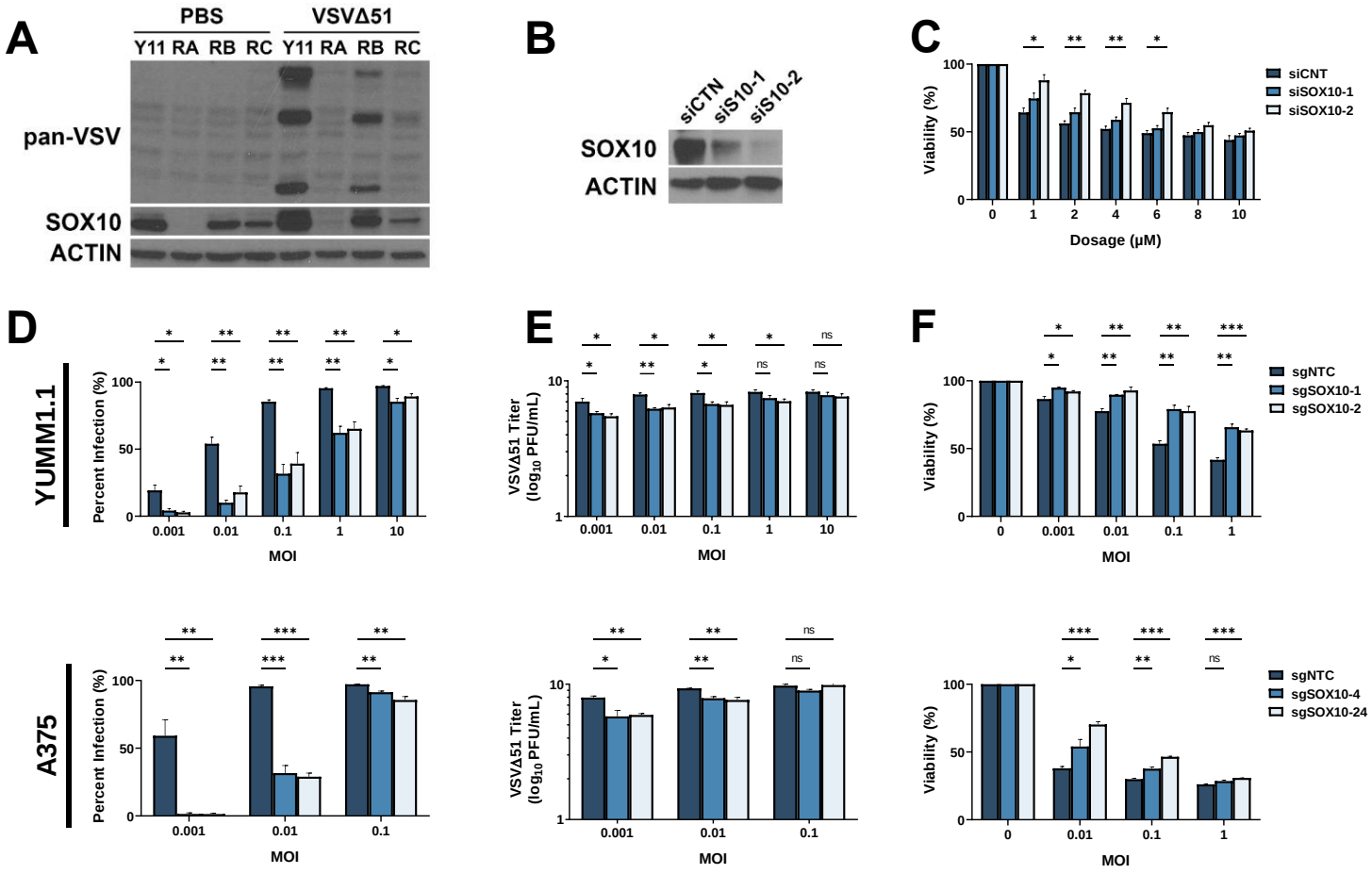
A
PBS
VSVΔ51
Y11 RA RB RC Y11 RA RB RC
pan-VSV
SOX10
ACTIN
B
siCTN
siS10-1
siS10-2
SOX10
ACTIN
C
Viability (%)
Dosage (μM)
siCNT
siSOX10-1
siSOX10-2
D
YUMM1.1
Percent Infection (%)
MOI
A375
E
VSVΔ51 Titer (log10 PFU/mL)
MOI
F
Viability (%)
MOI
sgNTC
sgSOX10-1
sgSOX10-2
sgSOX10-4
sgSOX10-24

Figure 3.3. SOX10 is lost during chronic targeted therapy treatment and induces a cross-resistant state to VSVΔ51. (A) Immunoblot of YUMM1.1 (Y11) and vemurafenib resistant cells ResA (RA), ResB (RB), and ResC (RC) 24hrs post infection with VSVΔ51. **(B)** Immunoblot of YUMM1.1 transfected with siRNA targeting a random sequence (siCTN) or Sox10 (siS10-1 or siS10-2). **(C)** YUMM1.1 cells transfected with siRNAs targeting Sox10 were treated with various concentrations of vemurafenib and viability assays were performed 72hrs post treatment. **(D-F)** YUMM1.1 and A375 cell lines were infected with Cas9 and sgRNA targeting SOX10 to create 2 independent SOX10 knockout populations per cell line. **(D)** Control and SOX10 knockout cells were infected with VSVΔ51 for 24hrs and YFP positive cells were quantified. **(E)** Viral titers were quantified by counting plaques 24hrs post infection. **(F)** Control and SOX10 knockout cells were infected with VSVΔ51 and cell viability was quantified 48hrs post infection with AlamarBlue. All data is represented as a mean ± SEM of biological triplicates. Significance was calculated using a two-tailed t-test, where * = $p < 0.05$, ** = $p < 0.01$ and *** = $p < 0.001$.

RNA-sequencing analysis of A375 SOX10 knockout cells shows enrichment of viral responses gene sets

To gain further insight into the resistant mechanism to VSV infection we re-analyzed RNA-sequencing data from SOX10 knockout A375 cells (227). This dataset shows that there are approximately 3600 upregulated genes in the SOX10 knockouts and 3300 downregulated genes (Fig. 3.4A). By using EnrichR we identified various biological processes that are acquired within the SOX10 knockout populations(239,240). Of the top 14 enriched biological processes in the SOX10-deficient A375, two were associated with the negative regulation of viral infection (Fig. 3.4B). We further mined any significant biological processes that had any impact on viral susceptibility and propagation and identified 14 of them (Fig. 3.4C).

We next evaluated 4 of these viral gene sets (Fig. 3.4C) (defense response to virus, negative regulation of viral process, negative regulation of viral genome, and regulation of viral entry into the host cell) to determine which genes are differentially expressed between SOX10 knockouts and control. In all 4 viral gene sets, we found more viral genes to be upregulated in the knockouts compared to controls (Fig. 3.4D-G). We compared all viral genes from our 4 gene sets that were upregulated in the SOX10 knockout cells and organized them into a venn diagram to determine gene overlap between the gene sets (Fig. 3.4H). Interestingly, IFITM1/2/3, and TRIM6, common to all 4 gene sets, have been shown to repress viral infection (Table 2.1) (247,248). Many of the genes identified within the viral biological processes were ISGs, which become activated post viral infection (Table 2.1). Interestingly we do not observe IFNα/β within our list suggesting that alternative pathways are activating the ISGs (Table 2.1). We also corroborated the activation of those genes in targeted therapy resistant PBRT cells where anti-viral genes are also induced (Table

2.1). This was also correlated with a SOX10 downregulation (Fig. S3.5A). Together, our data suggest that the loss of SOX10 during targeted therapy treatment induces the activation of ISGs genes, allowing for cross-resistance to RNA based oncolytic viruses, in addition to MAPKis.

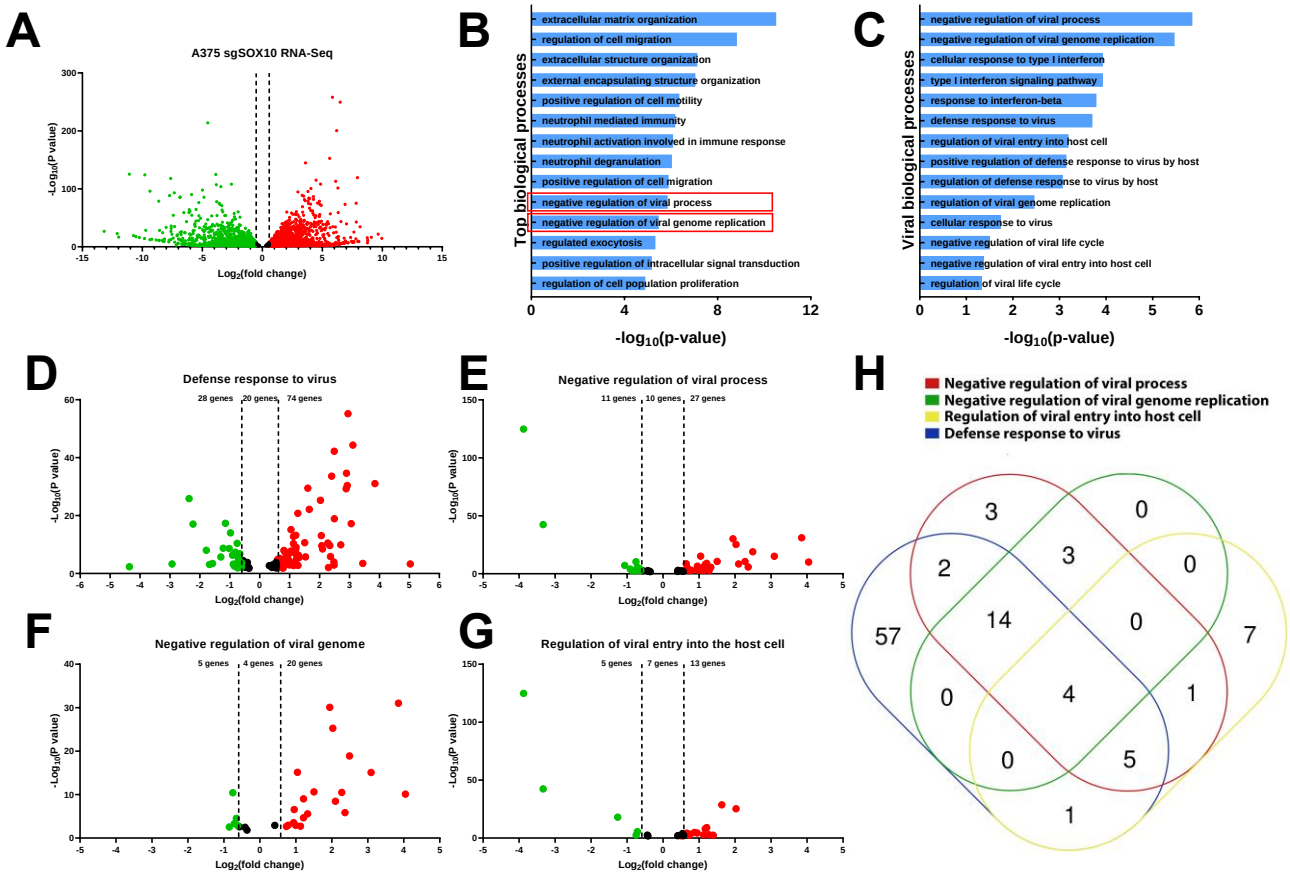
A
A375 sgSOX10 RNA-Seq
-Log10(P value)
Log2(fold change)
B
Top biological processes
extracellular matrix organization
regulation of cell migration
extracellular structure organization
external encapsulating structure organization
positive regulation of cell motility
neutrophil mediated immunity
neutrophil activation involved in immune response
neutrophil degranulation
positive regulation of cell migration
negative regulation of viral process
negative regulation of viral genome replication
regulated exocytosis
positive regulation of intracellular signal transduction
regulation of cell population proliferation
-log10(p-value)
C
Viral biological processes
negative regulation of viral process
negative regulation of viral genome replication
cellular response to type I interferon
type I interferon signaling pathway
response to interferon-beta
defense response to virus
regulation of viral entry into host cell
positive regulation of defense response to virus by host
regulation of defense response to virus by host
regulation of viral genome replication
cellular response to virus
negative regulation of viral life cycle
negative regulation of viral entry into host cell
regulation of viral life cycle
-log10(p-value)
D
Defense response to virus
28 genes
20 genes
74 genes
-Log10(P value)
Log2(fold change)
E
Negative regulation of viral process
11 genes
10 genes
27 genes
-Log10(P value)
Log2(fold change)
F
Negative regulation of viral genome
5 genes
4 genes
20 genes
-Log10(P value)
Log2(fold change)
G
Regulation of viral entry into the host cell
5 genes
7 genes
13 genes
-Log10(P value)
Log2(fold change)
H
Negative regulation of viral process
Negative regulation of viral genome replication
Regulation of viral entry into host cell
Defense response to virus
3
0
2
3
0
57
14
0
7
0
4
1
0
5
1

Figure 3.4. RNA-sequencing analysis of A375 SOX10 knockout cells shows enrichment of viral responses gene sets. (A) The volcano plot illustrating 6900 significantly differentially regulated genes where the red represents upregulation in the A375 SOX10 knockout cells and the green represents the wildtype genes. The black represents the genes that lack an upregulation of more than 1.5-fold. **(B)** GO enrichment analysis of biological processes from the genes upregulated in the SOX10 knockout populations from (A). **(C)** Arrangement of all viral biological processes observed within the A375 Sox10 knockout cells (only viral biological processes $-\log_{10}$(p-value) > 1 is shown). **(D-G)** Volcano plots illustrating the differentially expressed genes within each of the the "defense response to virus" gene set **(D),** "negative regulation of viral process" gene set **(E),** "negative regulation of viral genome" gene set **(F)** and "regulation of viral entry into the host cell" gene set **(G)**. **(H)** Venn diagram illustrating the expression of overlapping genes within each viral gene set **(D-G)** overexpressed in the SOX10 knockout populations.

Table 3.1. Common differentially expressed genes from the A375 SOX10 knockout cells found within each viral gene set.

Process	Number of Genes	Gene List
Defense response to virus, Negative regulation of viral genome replication, Negative regulation of viral process, Regulation of viral entry into host cell	4	IFITM1, IFITM2, IFITM3, TRIM6
Defense response to virus, Negative regulation of viral process, Regulation of viral entry into host cell	5	TRIM31, MID2, TRIM21, TRIM8, TRIM56
Defense response to virus, Negative regulation of viral genome replication, Negative regulation of viral process	14	MAVS, APOBEC3F, ISG20, OASL, APOBEC3G, APOBEC3H, IFIH1, APOBEC3D, OAS2, ISG15, SHFL, RNASEL, APOBEC3C, BST2
Defense response to virus, Negative regulation of viral process	2	STAT1, TRIM32
Defense response to virus, Regulation of viral entry into host cell	1	TRIM38
Negative regulation of viral genome replication, Negative regulation of viral process	3	LTF, SLPI, HMGA2
Negative regulation of viral process, Regulation of viral entry into host cell	1	GSN
Negative regulation of viral process	3	SP100, ZFP36, SRPX2
Regulation of viral entry into host cell	7	TRIM34, NECTIN2, TMPRSS2, SMPD1, FURIN, BSG, LGALS1
Defense response to virus	57	IFI44L, DDX60, F2RL1, PTPN22, PMAIP1, CD86, IFIT1, TBK1, CREB3, DTX3L, ZDHHC12, VAMP8, TNFAIP3, CASP1, ATG7, NMB, TICAM2, KCNJ8, STAT2, UNC93B1, HTRA1, CARD9, IL6, CPTP, MOV10, TICAM1, ZC3H12A, TRIM7, MARCHF2, EXOSC4, IFNE, RIOK3, LYST, NCR1, IFNLR1, STING1, IFNA1, AIM2, PML, NLRX1, IL1B, ITGAX, GPAM, IRF1, IRF3, RNF185, UNC13D, LAMP2, SERTAD3, PARP9, IFIT3, USP20, IL10RB, NLRP3, CXADR, IRF7, ABCC9

3.7 Discussion

We find that acquired resistance to vemurafenib further induces a cross-resistant state to VSV oncolytic treatment (Fig. 3.2). This is also observed within our SOX10 knockout cells (Fig. 3.3). Interestingly, we find a large variation in VSV resistance within our YUMM1.1 Resistant lines (ResA-C) where we observe minimal infection at MOI 10 within our YUMM1.1 ResA cell line (Fig. 3.2E). Surprisingly, this lack of infection could not be enhanced after using ruxolitinib which restored ResB and ResC infection back to wildtype levels (Fig. S3.4C). Although no increase in infection was observed following a 24hr infection, cell viability measurements at 48hrs post-infection restored cell sensitivity to wild type levels during co-treatments (Fig. S3.4E). Although this finding was unexpected it does suggest that the ResA's may express a high baseline level of ISGs that may require a prolonged treatment with Ruxo to completely turn off the JAK-STAT pathway and induce viral sensitivity.

Our data suggest that the transition from wild-type to a targeted therapy resistant state induces an IFN-like response where the cell upregulates the expression of many ISGs that is independent of IFNα/β induction (Fig. 3.4, Table 2.1, Fig. S3.5). Surprisingly, this environment can be recapitulated through the loss of SOX10, suggesting that the loss of SOX10 results in the activation of these ISGs (Fig. 3.4). Although this explanation seems logical, recent findings from our lab (data not shown) and others suggest that SOX10 acts as a gate-keeper to the undifferentiated state (224,227,249). One possibility is that SOX10 is not directly inhibiting these genes but rather acting indirectly by blocking the cells transition to an undifferentiated state. This undifferentiated state is key for cross-resistance and has been identified as a TEAD+/AP-1+/SOX9+ state (224,249). The heterogeneity and complex reprogramming observed in this state

makes it refractory to current therapies, supporting the notion that the maintenance of the SOX10+ differentiated state will be beneficial for different classes of therapeutics.

3.8 Supplementary figures

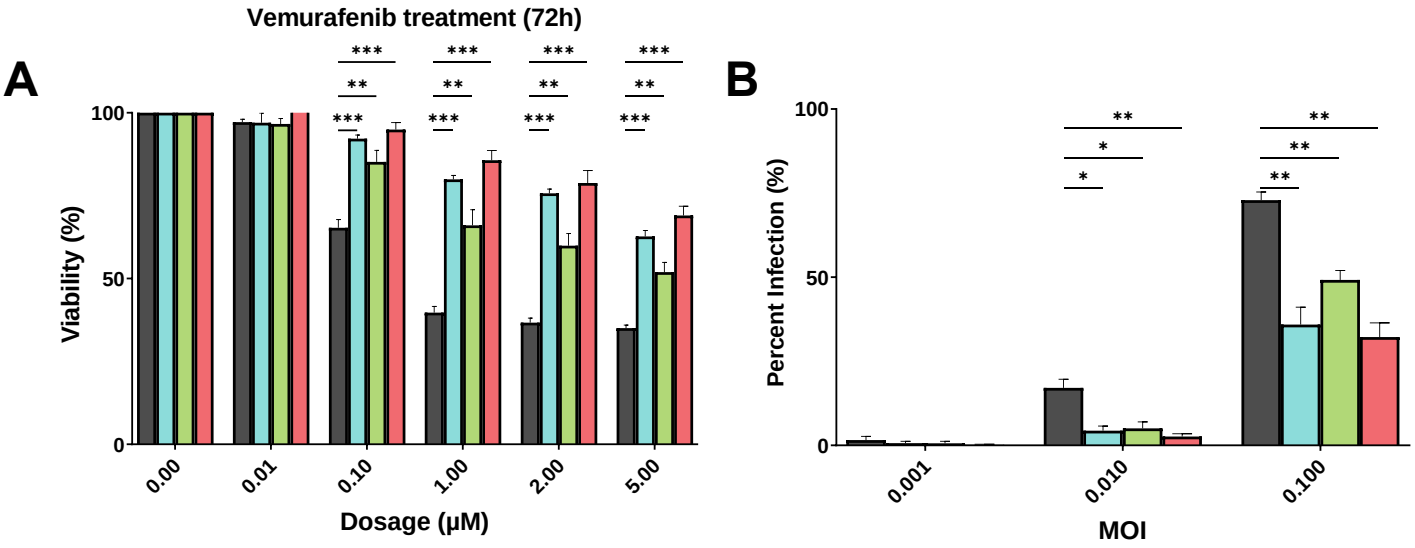

Supplementary Figure 3.1. Vemurafenib resistance also induces cross-resistance to VSVΔ51 in human BRAF^{V600E} melanoma cells. A375 vemurafenib resistant cells were made by treating with vemurafenib at 2μM for 6 weeks. **(A)** A375 and Resistant cell lines were seeded in at least technical triplicates and treated at an increasing concentration of vemurafenib. Cell viability was assayed using AlamarBlue 72hrs post treatment. **(B)** Quantification of YFP positive A375 parental and Res cell lines 24hrs post VSVΔ51 treatment. All data is represented as a mean ± SEM of biological triplicates. Significance was calculated using a two-tailed t-test, where * = $p < 0.05$, ** = $p < 0.01$ and *** = $p < 0.001$.

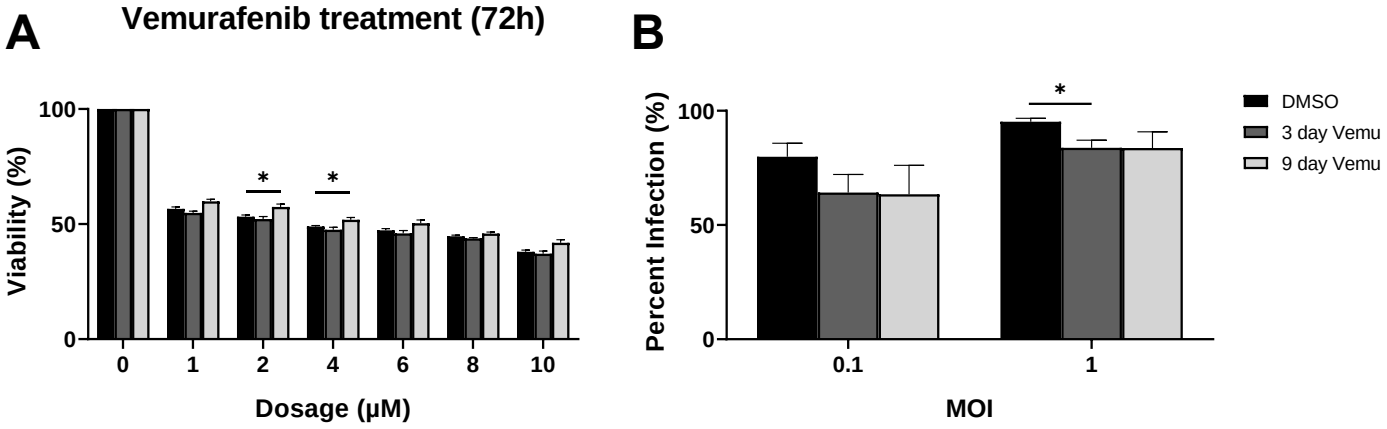

Supplementary Figure 3.2. Acute vemurafenib treatment does not elicit a resistant state upon re-challenge. (A & B) YUMM1.1 cells were treated with 5μM of vemurafenib for 3 or 9 days. **(A)** The treated YUMM1.1 cells were then re-treated with various concentrations of vemurafenib and cell viability was assayed using AlamarBlue 72hrs post treatment. **(B)** The treated YUMM1.1 cells were infected with VSVΔ51 and YFP positive cells were quantified 24hrs post VSVΔ51 treatment. All data is represented as a mean ± SEM of biological triplicates. Significance was calculated using a two-tailed t-test, where * = $p < 0.05$.

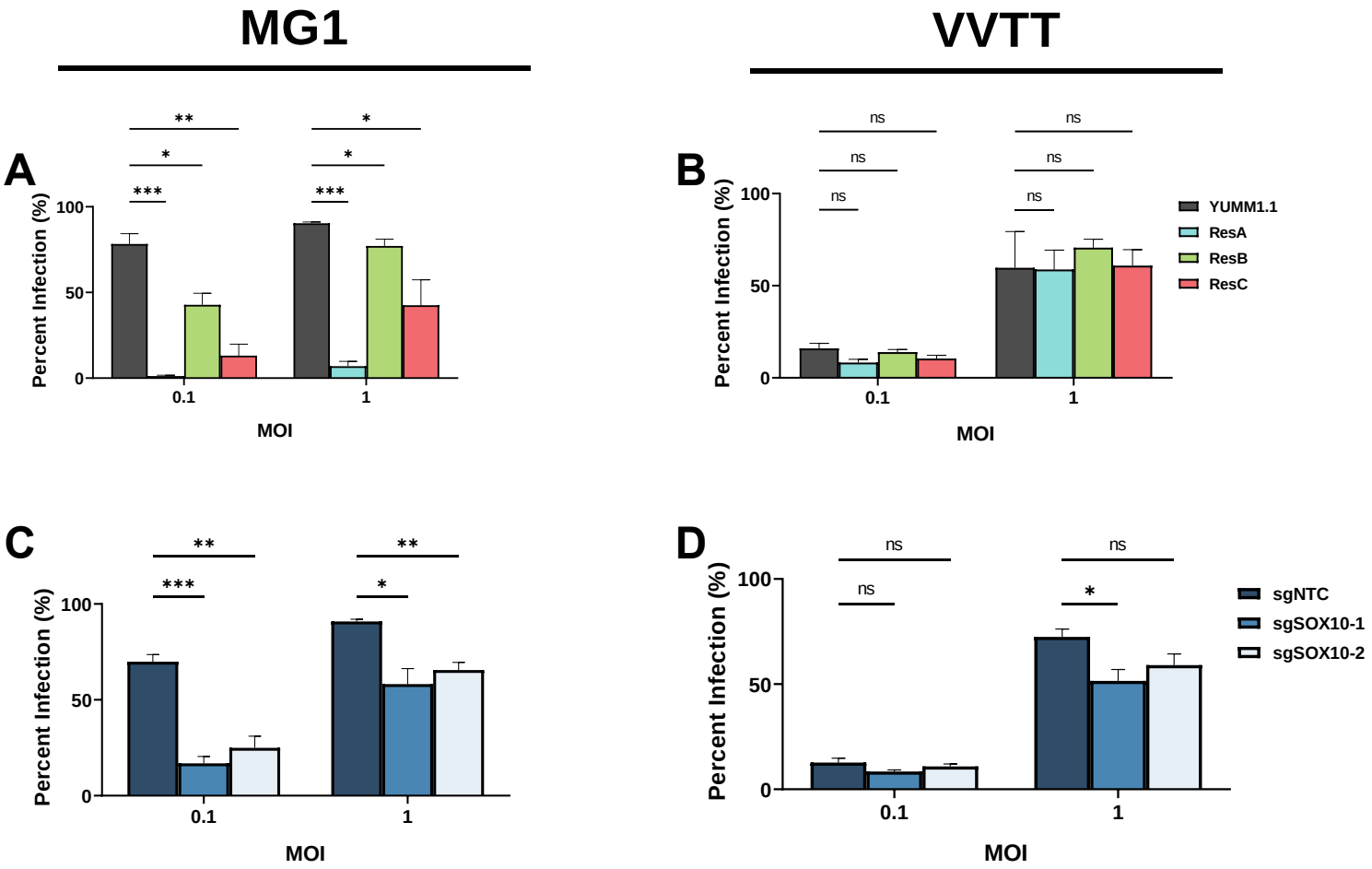

Supplementary Figure 3.3. Vemurafenib resistant YUMM1.1 and SOX10 knockout cells are resistant to ssRNA based oncolytics. (A & B) YUMM1.1 and vemurafenib resistant cells were infected with **(A)** MG1 or **(B)** Vaccinia virus TianTan for 24hrs and GFP positive cells were quantified. **(C & D)** YUMM1.1 SOX10 knockout cells were infected with **(C)** MG1 or **(D)** Vaccinia virus TianTan for 24hrs and GFP positive cells were quantified. All data is represented as a mean ± SEM of biological triplicates. Significance was calculated using a two-tailed t-test, where * = $p < 0.05$, ** = $p < 0.01$ and *** = $p < 0.001$.

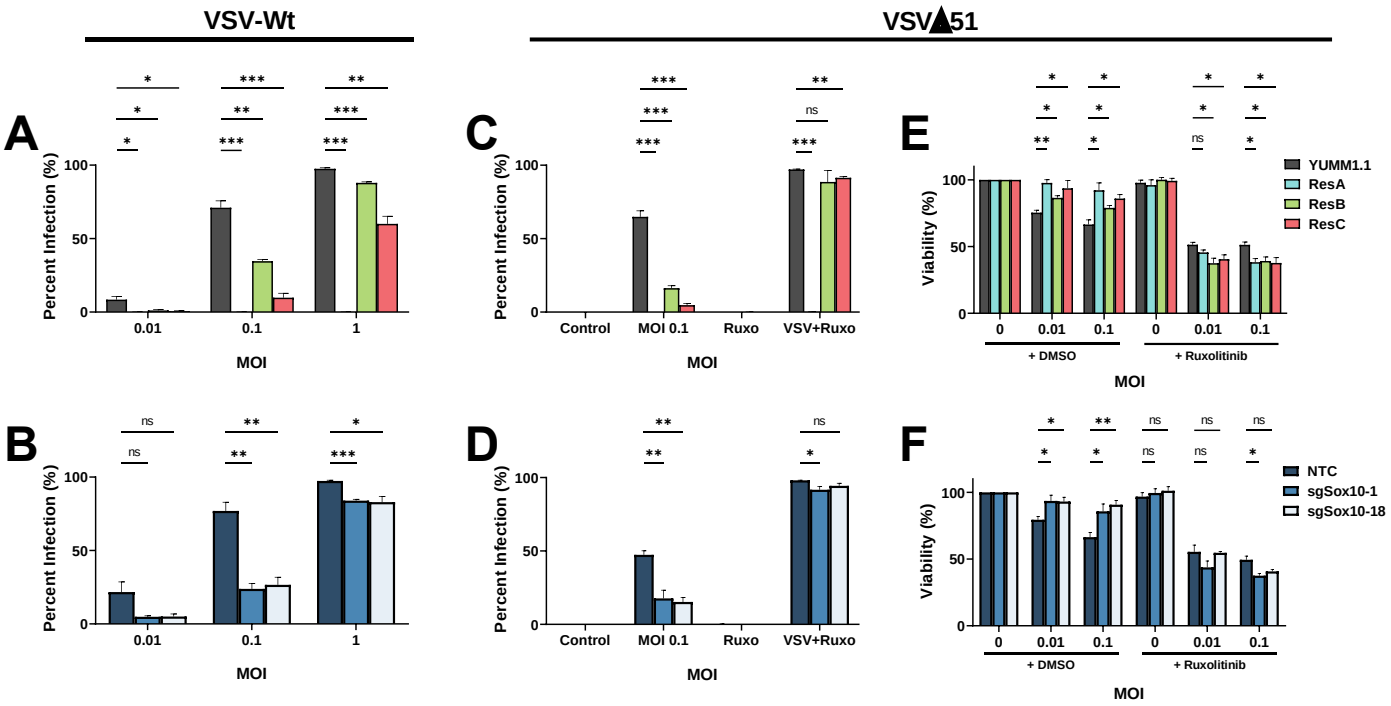

Supplementary figure 3.4. Vemurafenib resistant YUMM1.1 and SOX10 knockout cells are re-sensitized to VSVΔ51 following JAK1/2 inhibition. (A) YUMM1.1 vemurafenib resistant and **(B)** YUMM1.1 SOX10 knockout cells were infected with VSV-Wt for 24hrs and YFP positive cells were quantified. **(C)** YUMM1.1 vemurafenib resistant and **(D)** YUMM1.1 SOX10 knockout cells were co-treated with ruxolitinib (10μM) and various MOIs of VSVΔ51 for 24hrs and YFP positive cells were quantified. **(E)** YUMM1.1 vemurafenib resistant and **(F)** YUMM1.1 SOX10 knockout cells were co-treated with ruxolitinib (10μM) and various MOIs of VSVΔ51 and viability was quantified 48hrs post treatment with AlamarBlue. All data is represented as a mean ± SEM of biological triplicates. Significance was calculated using a two-tailed t-test, where * = $p < 0.05$, ** = $p < 0.01$ and *** = $p < 0.001$.

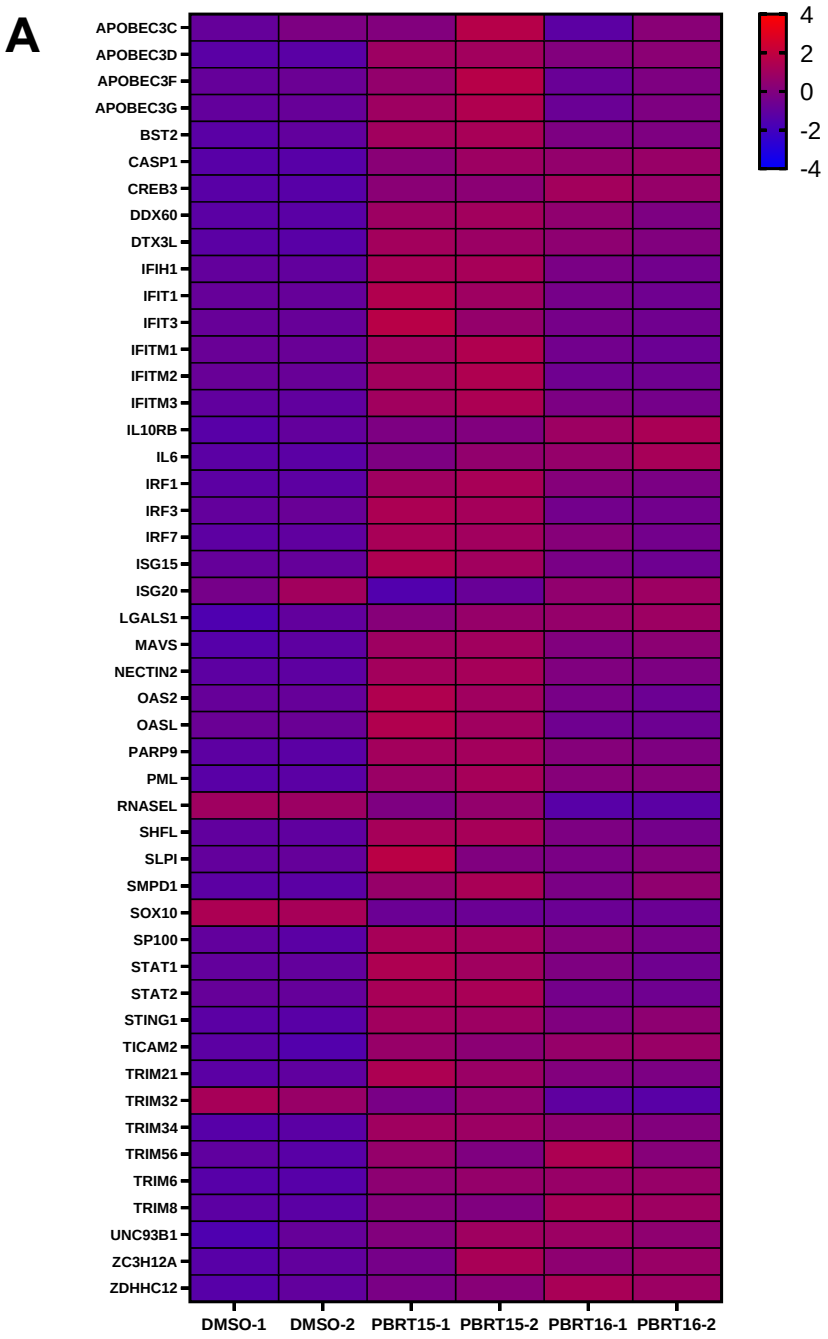

Supplementary Figure 3.5. Correlation between viral gene expression and SOX10 expression in therapy resistant samples. (A) The heatmap represents the relative expression (Z-score) of the genes from Table 2.1 compared to controls and targeted therapy treated 1205Lu tumors. TPM values were extracted from the NCBI BioProject PRJNA748714.

Chapter 4

CEACAM1 is a direct SOX10 target and inhibits melanoma immune infiltration and stemness

4.1 Preface

Abou-Hamad, J., Hodgins, J. J., de Souza, C. T., Garland, B., Labrèche, C., Marotel, M., Gibson, C., Delisle, S., Pascoal, J., Auer, R. C., Ardolino, M., & Sabourin, L. A. (2022). CEACAM1 is a direct SOX10 target and inhibits melanoma immune infiltration and stemness. iScience, 25(12), 105524. https://doi.org/10.1016/j.isci.2022.105524

Author contributions

Abou-Hamad J: Generated all manipulated cell lines, cloned the luciferase fragments, and performed all experiments excluding the subcutaneous injections. Wrote and proofread the manuscript.

Hodgins JJ: Performed the majority of the panel preparation for flow cytometry, and helped collect and process tumours. Proofread the manuscript.

De Souza C: Performed a majority of the melanoma tumour cell injections

Garland B: Performed melanoma tumour cell injections, and helped collect and process tumours.

Labreche C: Helped collect and process a majority of the tumours. Proofread the manuscript.

Marotel M: Performed panel preparation for flow cytometry, and helped process the tumours.

Gibson C: Cloned the CEACAM1 isoform plasmids, and helped collect and process tumours.

Delisle S: Helped collect and process the tumours.

Pascoal J: Helped collect and process the tumours.

Auer R: Provided expertise about tumour injections.

Ardolino M: Provided mouse and flow antibodies.

Sabourin L: Provided expertise throughout the project. Also proofread and edited the manuscript.

4.2 Title page

This paper was published at iScience on December 22, 2022.

CEACAM1 is a direct SOX10 target and inhibits melanoma immune infiltration and stemness

Authors

John Abou-Hamad [1 2], Jonathan J Hodgins [1 3], Christiano T de Souza [1], Brennan Garland [1 2], Cédrik Labrèche [1 2], Marie Marotel [1 3], Cameron Gibson [1], Samuel Delisle [1 2], Julia Pascoal [1], Rebecca C Auer [1 3 4], Michele Ardolino [1 3], Luc A Sabourin [1 2]

Affiliations

1. Centre for Cancer Therapeutics, Ottawa Hospital Research Institute, 501 Smyth Road, Ottawa, ON K1H 8L6, Canada.
2. Department of Cellular and Molecular Medicine, University of Ottawa, Ottawa, ON K1H 8L6, Canada.
3. Department of Biochemistry, Microbiology and Immunology, University of Ottawa, Ottawa, ON K1H 8L6, Canada.
4. Department of Surgery, University of Ottawa, Ottawa, ON K1H 8M5, Canada.

Disclosures

The authors declare no competing interests.

Acknowledgements

We would like to thank Dr. William Damsky (Yale University) for providing us with various mouse melanoma lines (YUMM1.1, 1.7, 1.9, and 2.1). We would also like to thank Dr. John Bell (University of Ottawa) and Dr. Carolina Ilkow (University of Ottawa) for providing us with various human melanoma cell lines. We thank Dr. Daniel Schramek (University of Toronto), specifically Dr. Khalid Al-Zahrani for providing us with pLenti Cas9-Blast and pLKO H2B-mRFP-2A puro. We would finally like to thank the Ottawa Hospital Research Institute Flow Cytometry and Cell Sorting facility (particularly Fernando Ortiz) and the University of Ottawa Flow Cytometry and Virometry facility (particularly Dr. Vera Tang) for assistance with experiments pertaining to flow cytometry.

Funding

This work was supported by grants to L.A.S. from the Canadian Institutes of Health Research, the Canadian Cancer Society, and the Cancer Research Society.

4.3 Abstract

SOX10 is a key regulator of melanoma progression and promotes a melanocytic/ differentiated state. Here we identified melanoma cell lines lacking SOX10 expression which retain their in vivo growth capabilities. More importantly, we find that SOX10 can regulate T-cell infiltration in melanoma while also decreasing common cancer stem cell (CSC) properties. We show that SOX10 regulates CEACAM1, a surface protein with immunomodulatory properties. SOX10 directly binds to a distal CEACAM1 promoter region approximately 3-4kbps from the CEACAM1 transcriptional start site. Furthermore, we show that a SOX10-CEACAM1 axis can suppress CD8+ T-cell infiltration as well as reduce CSC pool within tumors, leading to reduced tumor growth.

Overall, these results identify SOX10 as a direct regulator of CEACAM1, and uncover both a pro- and anti-tumorigenic roles for SOX10 in melanoma.

Highlights

- CEACAM1 is a direct genetic target of SOX10
- Loss of SOX10 and CEACAM1 inhibits tumor growth in immune-competent mice
- CEACAM1 expression inhibits CD8+ T-cell infiltration
- Loss of CEACAM1 and SOX10 enhances cancer stem cell properties in melanoma

4.4 Introduction

The Sox family (SRY-HMG box) of transcription factors plays critical roles in tissue homeostasis, organogenesis, and cell fate decisions in many developmental processes (148,250,251). The SoxE group, including Sox8, 9, and 10, has been extensively studied in the context of reproductive system development, neural crest cell-derived tissues and cell types such as melanocytes. Although the role of the SOX proteins in cancer progression remains elusive and controversial (250), SOX10 has been shown to play an important role in melanoma maintenance and progression in the context of haploinsufficiency (120,187,252). Similarly, studies on SOX9- or SOX10-floxed animals have been performed in the context of the NRASQ61 allele, inducing senescence and nevi formation (165).

BRAF(V600E) and NRAS(Q12,Q13,Q61) accounts for about 80% of melanoma mutations (65,253–256). The design of highly specific BRAFV600E (Vemurafenib), MEK (Trametinib) and immune checkpoint inhibitors (PD-1 and CTLA-4) has produced good response rates in melanoma (65,253,255–261). However, most responses are transient with most patients becoming resistant and progressing within a year due to the reactivation of the MAPK pathway in 70% of cases (65,254). Similarly, immunotherapies to PD-1 and CTLA-4 have improved overall survival in patients with melanoma but with only a subset showing long-term benefits (253,255–261). However, most responses are transient due to the activation of resistance mechanisms. Strikingly, drug resistance is often associated with resistance to immune checkpoint inhibitors, leading to a cross-resistance phenomenon (65,254,259).

A number of studies have identified distinct subpopulations of melanoma cells with variable sensitivity to therapy(118,194,262–264). Genomic studies have revealed the existence of major subpopulations characterized by differential expression of AXL, EGFR, NGFR, SOX9, and

SOX10 in drug-resistant cells. Upon acquired resistance, the sensitive pool (AXL−, EGFR−, NGFR−, SOX9-, SOX10+) undergoes a switch to an AXL+, EGFR+, NGFR+, SOX9+, SOX10- phenotype (119,194,264–266). This phenotype switch involves transcriptional reprogramming rather than mutational evolution or expansion of resistant subpopulations (194,264,267,268). However, the mechanisms of drug resistance are far more complex than initially thought as intermediate populations may exist as well as a neural crest stem cell-like (NCSC) state that can be induced through phenotype switching, regardless of their initial driver mutations(269).

A number of transcription factors have been shown to coordinate phenotype switching (255). Strikingly, SOX10 expression is associated with the highly proliferative and Vemurafenib (Vemu) sensitive cell population (119,264,268). Supporting this, suppression of Sox10 induces EGFR, PDGFRβ and confers resistance to BRAF inhibitors (194). SOX10 typically act in concert with its downstream target MITF, a bHLH transcription factor (120,270). Interestingly, Sox9 was found to be expressed exclusively in the $SOX10^{lo}$ invasive samples together with TEAD and AP-1 (119). A reduction in Sox10 expression was also observed to be associated with increased Sox9 and reduced proliferation, suggesting a negative feedback loop between Sox9 and Sox10. Although numerous other transcription factors have been shown to be important for different aspects of drug resistance and progression, SOX9 and SOX10 appear to be critical to maintain the stem-like and invasive properties of tumors (120,183,263,271–274). Recently the cellular inhibitor of apoptosis protein-1/2 (cIAP1/2) were found to be upregulated in SOX10-deficient cells, contributing to drug resistance in the SOX10- cells (197). Similarly, the expression of CEACAM1 in SOX10 + cells provides a growth advantage in CD8+ T-cell depleted animals (275). These data suggest that SOX10 might regulate aspects of both drug sensitivity and immune surveillance in melanoma cells.

Although a positive correlation between SOX10 and CEACAM1 expression has been previously observed in melanoma (275), we show here that CEACAM1 is a direct target of SOX10. We found that SOX10 regulates CD4+ and CD8+ T-cell infiltration in melanoma while also depleting the CSC properties, primarily the self-renewal capabilities. When SOX10 and CEACAM1 co-exist this perpetuates these effects. In all, we have identified two major contradictory roles of SOX10 not previously known in melanoma.

4.5 Methods

Mice

All mice experiments were approved and in accordance with our Animal care and veterinary committee standard at the University of Ottawa. For our immune competent mouse experiments, C57BL/6J were purchased from Jackson Laboratory and bred in house. For our tumor studies male mice 8–10 weeks old were matched and divided blindly within the different tumor groups. For our various subcutaneous tumor growth models all studies were done at 1×10^5 cells in 100μL of PBS. 12–15 days post-injection mice were palpated and checked for tumor growth using a caliper and tumor size was noted every 3 days until endpoint of $1700mm^3$.

For the immune compromised studies, 1×10^5 YUMM cells in 100μL were administered subcutaneously to the right flank of SCID, RAG1 and NCG mice ranging within the age of 8–12 weeks. For SCID and NCG mice, tumors were checked every 3 days up to 12 days post injection and tumor sizes were measured using a caliper. Mice were euthanized once one animal in the study reached the endpoint set at $1700mm^3$. For RAG1 tumors, mice were all euthanized on day 24 post injection and tumor sizes were compared.

For limiting dilution assays, NCG mice were injected twice, once in each flank with various cell concentrations (1×10^2, 1×10^3, 1×10^4, 1×10^5) (n = 4 per group). 28 days post injection, mice were euthanized and assessed for tumor growths from the various cell concentrations. Images were taken of each respective tumor identified.

Cell lines

All Yale University Mouse Melanoma (YUMM) cell lines were a kind gift from Dr. William Damsky (Yale University). SKMEL-28 and M14 cells were a kind gift from Dr. John Bell (University of Ottawa). SKMEL-2 was obtained from ATCC. A human melanoma cell line OHRI-13 was isolated and provided by Dr. Carolina Ilkow (University of Ottawa). All mouse melanoma cell lines (YUMMs) were maintained in DMEM supplemented with 10% fetal bovine serum, 1X penicillin/streptomycin, 2mM L-glutamine and 1X nonessential amino acids. SKMEL-2, SKMEL-28 and M14 cells were maintained in DMEM supplemented with 10% fetal bovine serum, 1X penicillin/streptomycin, 2mM L-glutamine. The OHRI-13 was maintained in RPMI supplemented with 10% fetal bovine serum, 1X penicillin/streptomycin, 2mM L-glutamine. All cells were grown at 37°C with 5% CO2 in humidified chambers.

Protein collection and western blotting

Cultured cells were all collected within 75–95% confluency and rinsed twice with 4mL of 1X ice-cold DPBS. Cells were scraped and collected at 8000G for 3 min. Cells were than lysed with RIPA lysis buffer (RIPA buffer containing 6μM NaVO3, 10ug/mL pepstatin and 10μM PMSF) and spun down to clear for 10 min at 12000G. For western blots pertaining to tumor lysates, mice were euthanized, tumors were isolated and minced into small pieces and further lysed within RIPA lysis buffer using a hand held homogenizer. Protein lysates were once again cleared for 10 min at

12000G. All lysates were quantified using a Bradford assay. Samples were set to a concentration of 1 μg/μL supplemented with 4X Laemmli buffer and denatured at 95°C for 5 min. Samples were loaded in 8–10% tris-glycine SDS-PAGE gels, transferred to PVDF membranes and analyzed for various protein expression.

qPCR

Total RNA was isolated using TRIzol (ThermoFisher). Cell culture media was removed and 1mL of TRIzol was added to each dish. Dishes were scraped and the TRIzol was transferred to a 1.5mL Eppendorf. 200μL of chloroform was added to each tube and shaken vigorously for 15 s, and left to rest for 3 min. Samples were then spun at 12000 g at 4°C for 15 min and the top clear layer was transferred to a fresh 1.5mL eppendorf. 500μL of isopropanol was added to the new tubes, vortexed and left to rest. After 10 min the samples were spun at 12000 g at 4°C for 10 min and the supernatant was removed, keeping only the white pellet. 1mL of 75% ethanol was added to each tube and spun at 7500G at 4°C for 5 min. Ethanol was removed and the pellet was left to air dry for 10 min before re-suspending in 100μL of water.

RNA was quantified using a nanodrop and 250ng of RNA was moved into PCR tubes. cDNA synthesis was achieved using Superscript III Reverse Transcriptase (ThermoFisher) according to the manufacturer's protocol where 5X First Strand buffer, oligo(dT), random primers, and dNTP mix were all added to the 250ng of RNA. cDNAs were synthesized (25°C at 5 min, 55°C 60 min, 70°C 15 min and finally 37°C at 20 min) and samples were diluted 1/10 for qPCR. qPCRs were run on a 7500 Fast Real-Time PCR system using the standard ΔΔCT program with melt curve.

Tumor sphere assay

For primary spheres, YUMM cells were disaggregated with trypsin, counted and pushed through a 25 gauge needle three times to produce a single cell suspension. 2×10^3 cells were seeded per well into a 24 well ultralow attachment plate in 500μL of 1:1 DMEM/F12 supplemented with 1x B27 supplement and 1x MEGS (ThermoFisher). Each group was seeded in technical duplicates and imaged after 5–7 days s (depending on the cell group). Only spheres greater than or equal to 50μm were counted for total sphere efficiency. To seed secondary spheres, primary spheres were collected, rinsed in 1XPBS, treated with trypsin, ran through a 25 gauge needle three times and counted. 2×10^3 cells were once again seeded in the same process as primary spheres and the quantification process was repeated.

Flow cytometry

Cells were collected and rinsed with 1X DPBS, stained with Zombie NIR viability dye (Biolegend) for 20 min and rinsed with 1X DPBS with 1% BSA (flow buffer). Cells were further stained with FC block (Biolegend) for 20 min and stained for another 20 min with antibodies for ligands found at the surface of cells (antibodies used are found in Table 4.1). For intracellular flow, the Foxp3/Transcription Factor Staining Buffer Set (ThermoFisher) was used following extracellular staining. In short, cells were fixed with Foxp3 Fixation/Permeabilization for 60 min, rinsed with 1X Permeabilization Buffer and stained with anti-rabbit SOX10 (Cell Signaling 1:50) for 60 min. Cells were rinsed once again with 1X Permeabilization Buffer and stained with Goat anti-Rabbit IgG Alexa Fluor 488 secondary for 60 min. Samples were resuspended in flow buffer and stored at 4°C. All tumor samples were minced into small tumor pieces (no larger than 2mm3) homogenized using the GentleMACS Octo Dissociator and incubated with ammonium chloride for 3 min to remove all red blood cells. Samples were then stained for extracellular and/or

intracellular markers using the above methods. Data was collected using FACS DIVA on a BD LSR Fortessa and analyzed using FlowJo.

Cloning, viral production and siRNA transfection

CEACAM1 luciferase fragments were generated using BAC DNA (RP23-404A12 and RP23-64F12). In short various oligonuclotides were synthesized to span 1kbp of the CEACAM1 promoter region and PCR amplicons were cloned into pCloneJet. The CloneJet plasmids were digested with KpnI and XhoI and the inserts were moved over to the luciferase backbone pGL3-P. For pBABE-CEACAM1 Isoform 1 and 4 constructs, cDNAs from origene were amplified and cloned into pCloneJet. Using BamHI and EcoRI, the inserts were subcloned into the pBABE retroviral backbone. Sox10 guides targeting the N-terminal region of Sox10 were created using ChopChop (ChopChop.com), and oligos sgSox10-1 Forward: CACCGGTTGGTACTTGTAGT CCGGA, sgSox10-1 Reverse: AAACTCCGGACTACAAGTACCAACC and sgSox10-18 Forward: CACCGACAAGTACCAACCTCGGCGG, sgSox10-18 Reverse: AAACCCGCCGAG GTTGGTACTTGTC were annealed using a thermocylcer at 37°C for 30 min, 95°C for 5 min and temperature was ramped down 5 °C/min to 25°C. pLKO H2B-mRFP-2A puro (a kind gift from Dr. Daniel Schramek, University of Toronto) was digested with BsmBI and the annealed oligos were subcloned into the digested vector.

For viral transduction 5×10^6 293T cells were transfected with 10μg of plasmid vector, 8μg of pCMV-dR8.2 dVPR (Addgene) or pUMCV (Addgene) packaging plasmid and 2μg of pCMV-VSV-G (Addgene). Media was changed 12 h post transfection and collected 72 h later. The media was filtered and used to infect the various YUMM lines. 48 h post infection, cells were either sorted for RFP (for guide transduction), treated with puromycin for 9 days at 4 μg/mL (pBABE transductions) or blasticidin at 5 μg/mL for 10 days (for Cas9 selection). Specifically for knockout

cells, YUMM cells were first transduced with pLenti-Cas9-Blast and selected for. Following Cas9 selection, cells were then transduced with pLKO H2B-mRFP-2A-Puro encoding the guide RNA targeting Sox10. Cells were sorted for RFP 48 h post infection and knockdown was confirmed by western and qPCR analysis.

Dharmacon-designed siRNA specifically targeting mouse Sox10 was used for short term Sox10 knockdown. Briefly, 200nM of each siRNA was transfected using Lipofectamine 3000 and samples were collected 72 h post transfection.

Luciferase assay

In vitro cell cultures were transfected with 1μg of pGL3P, pGL3P Ceacam1[-1525/+5], pGL3P Ceacam1[-2875/-1435], pGL3P Ceacam1[-4135/-2785] or pGL3P Ceacam1[-5305/-4045] with 0.2μg of pRL-CMV used as the transfection efficiency control. 48hrs post transfection media was aspirated, cells were washed and 200μL 1X passive lysis buffer (provided by vendor) was placed in each well and left for 15 min with vigorous rotation. 20μL of lysed cells were placed in triplicate in a 96-well plate with 100μL of Luciferase assay buffer II and bioluminescence was read using a Biotek Cytation 5 imaging reader. Following the reading 100μL of Stop and Glow buffer was added and the plate was read once gain using Biotek Cytation 5 imaging reader to determine Renilla activity. All individual cell samples were seeded in triplicate and averaged as a single biological replicate. All experiments were done in biological triplicates.

Chromatin immunoprecipitation

For ChIP the SimpleChIP protocol (New England BioLabs) was used. In short, 1×10^6 YUMM1.1 cells were seeded in a 15cm dish and allowed to grow for 48 h. Following 48 h, four 15cm dishes containing the YUMM1.1 cells were cross-linked using formaldehyde, inactivated using glycine

and collected and pooled according to the manufacturer's instructions. Nuclei were isolated and chromatin was digested by treating samples with MNase for 20 min at 37°C followed by sonication on the Misonix sonicator 3000 using 30s pulses at the third setting for a total of three times. Input samples were collected at this point and used downstream in our PCR for normalization. Anti-SOX10 (1:50) was used and mixed with 10µg of digested chromatin while also using total Histone and rabbit IgG as positive and negative controls, respectively. Samples were left on a rotor overnight at 4°C and the next day 30µL of magnetic beads were added to each tube and left on the rotor for an additional 2 h. Beads were rinsed multiple times according to the manufacturer's instructions and chromatin pulled downs were eluted. Chromatin was further cleaned using the DNA spin columns provided and concentration of samples was determined using Qubit 3.0. PCRs were run on various regions of the CEACAM1 promoter while also using RPL30 Intron 2 primers as positive and negative controls. IgG samples were used as our normalization control to assess background noise.

Correlation and immune infiltration analysis

For percent survival between high and low CD4+ and CD8+ T cell infiltration in melanoma, data was processed and analyzed by Timer2.0 (http://timer.cistrome.org/) (276). The top 25% and bottom 25% of T cell infiltrates were used in the Timer2.0 analysis.

The correlation data between SOX10 and CEACAM1 mRNA in melanoma, was retrieved on cBioPortal (https://www.cbioportal.org/) (277,278), and re-plotted using GraphPad Prism software. The Skin Cutaneous Melanoma TCGA Firehose Legacy dataset was used to retrieve the data. Z score threshold of ±2 was used to determine correlation between Sox10 and various genes.

Statistical analysis

All in vitro experiments were performed in three biological replicates while all mice work was done once with animal numbers indicated in the figure legends. All analysis was done through GraphPad Prism software and data is represented as the SEM(±SEM). T tests, one way and two ANOVA were used for statistical analysis of various experiments (statistical significance and tests used is specified in figure legends).

Materials availability

Materials generated in this study can be made available upon request to the Lead Contact.

Data and code availability

This paper did not generate any original code. TCGA data used for correlation analysis is publicly available from https://www.cbioportal.org/. TCGA data used for immune infiltration within skin cutaneous melanoma is publicly available from http://timer.cistrome.org/. Any additional information required to reanalyze the data reported in this paper is available from the lead contact (Luc Sabourin, lsabourin@ohri.ca) upon request.

Table 4.1 Key resources

REAGENT or RESOURCES	**SOURCE**	**IDENTIFIER**
Antibodies		
SOX10	New England BioLabs	Cat# 89356; Clone D5V9L; RRID:AB_2792980
Beta-Actin	Sigma-Aldrich	Cat# A5316; Clone AC-74; RRID:AB_476743
Histone H3	New England BioLabs	Cat# 4620; Clone D2B12; RRID:AB_1904005
Mouse: CEACAM1 BV421	BioLegend	Cat# 134531; Clone Mab-CC1; RRID:AB_2687363
Human: CEACAM1 AF647	R&D Systems	Cat# FAB2244R; Clone 283340

PDL-1 BV786	BD Biosciences	Cat# 741014; Clone MIH5; RRID:AB_2740636
PDL-2 PE	BD Biosciences	Cat# 557796; Clone TY25; RRID:AB_396874
CD80 BV510	BD Biosciences	Cat# 740130; Clone 16-10A1; RRID:AB_2739887
CD86 BV650	BD Biosciences	Cat# 564200; Clone GL1; RRID:AB_2738665
CD45 Pe Texas Red	BioLegend	Cat# 103146; Clone 30-F11; RRID:AB_2564003
CD45 AF700	BioLegend	Cat# 103127; Clone 30-F11; RRID:AB_493714
CD3 PeCy5	BioLegend	Cat# 100310; Clone 145-2C11 RRID:AB_312675
CD4 Fitc	BioLegend	Cat# 100510; Clone RM4-5 RRID:AB_312713
CD8 BV650	BioLegend	Cat# 100742; Clone 53-6.7; RRID:AB_2563056
CD8 BV786	BioLegend	Cat# 100750; Clone 53-6.7; RRID:AB_2562610
Zombie NIR APC Cy7	BioLegend	Cat# 423106
Rat Anti-Mouse CD16/CD32 (Mouse BD Fc Block)	BD Biosciences	Cat# 553142; Clone 2.4G2; AB_394656
Normal Rabbit IgG	New England BioLabs	Cat# 2729; RRID:AB_1031062
BV650 Rat IgG2a Isotype control	BD Biosciences	Cat# 563236; Clone R35-95; AB_2869472
BV510 Hamster IgG2 Isotype control	BD Biosciences	Cat# 563202; Clone B81-3; AB_2869469
PE Rat IgG2a Isotype control	BD Biosciences	Cat# 553930; Clone R35-95; AB_479724
BV786 Rat IgG2a Isotype control	BD Biosciences	Cat# 563335; Clone R35-95; AB_2869486
Alexa Fluor 647 Mouse IgG2b Isotype control	BD Biosciences	Cat# 557903; Clone 27-35; AB_396928
BV421 Mouse IgG1 Isotype control	BD Biosciences	Cat# 562438; Clone X40; AB_11207319
Dnk pAb to Rb IgG AF488	Abcam	Cat# ab150073; RRID:AB_2636877
Goat Anti-Rabbit IgG (H+L)-HRP Conjugate	BIO-RAD	Cat# 1706515; RRID:AB_2617112
Goat Anti-Mouse IgG (H+L)-HRP Conjugate	BIO-RAD	Cat# 1706516; RRID:AB_2921252
Chemicals, Peptides, and Recombinant Proteins		
iTaq Universal SYBR Green Supermix	Bio-Rad	Cat# 1725124;

Lipofectamine 3000 transfection Reagent	ThermoFisher	Cat# L3000008
Mammary Epithelial Growth Supplement (MEGS)	ThermoFisher	Cat# S0155
Critical commercial assays		
eBioscience™ Foxp3 / Transcription Factor Staining Buffer Set	ThermoFisher Scientific	Cat# 00-5523-00;
Dual-Luciferase® Reporter Assay System	Promega	Cat# E1980;
SimpleChIP® Enzymatic Chromatin IP Kit	New England BioLabs	Cat# 9003;
Experimental models: Cell Lines		
Mouse: Yale University Mouse melanoma cell line	Dr. William Damsky; Yale University	YUMM1.1, YUMM1.7, YUMM1.9, YUMM2.1
Human: OHRI-13 melanoma cell line	Dr. Carolina Ilkow; University of Ottawa	OHRI-13
Human: SKMEL2	American Type Culture Collection (ATCC)	Cat# HTB-68
Human: SKMEL28	Dr. John Bell; University of Ottawa	N/A
Human: M14	Dr. John Bell; University of Ottawa	N/A
Human: HEK293T	American Type Culture Collection (ATCC)	Cat# CRL-3216; 293T
Experimental models: Organism/strains		
Mouse: C57BL/6	Jackson Laboratory	Cat# 000664; RRID: IMSR_JAX:000664
Mouse: CB17.Cg-PrkdcscidHrhr/IcrCrl	Charles River	SCID
Mouse: B6.129S7-Rag1tm1Mom/J	Jackson Laboratory (Bred in house; Dr. Michele Ardolino)	Rag1 KO
Mouse: NOD-Prkdcem26Cd52Il2rgem26Cd22/NjuCrl	Charles River (Bred in house; Dr. Michele Ardolino)	NCG
Oligonucleotides		
siRNA SOX10-1	Dharmacon	Cat# J-049957-09
siRNA SOX10-2	Dharmacon	Cat# J-049957-10
siRNA CTN	Dharmacon	Cat# D-001810-01
qPCR Primer: *Sox10* forward: AGGTTGCTGAACGAAAGTGAC		N/A
qPCR Primer: *Sox10* reverse: CCGAGGTTGGTACTTGTAGTCC		N/A
qPCR Primer: *Ceacam1Long* forward: GCGAGATCTCACAGAGCACA		N/A

qPCR Primer: *Ceacam1Long* reverse: GCTGGGAATTGAAGTTCAGG		N/A
qPCR Primer: *Ceacam1Short* forward: CTGGCATCGTGATTGGAGTT		N/A
qPCR Primer: *Ceacam1Short* reverse: CAGAAGGAGCCAGATCCG		N/A
qPCR Primer: *18s* forward: AGTCCCTGCCCTTTGTACACA		N/A
qPCR Primer: 1*8s* reverse: GATCCGAGGCCTCACTAAAC		N/A
ChIP Primer: Ceacam1forward [-4000]: GTAGAACCAACCTAGATCTCCA	This manuscript	N/A
ChIP Primer: Ceacam1 reverse [-3820]: CTGTAAACTTTGTGATTCATCT	This manuscript	N/A
ChIP Primer: Ceacam1 forward [-3820]: GGATGT GGATAGACTTAGAATA	This manuscript	N/A
ChIP Primer: Ceacam1 reverse [-3685]: GTTATATATGTAATTACATGTG	This manuscript	N/A
ChIP Primer: Ceacam1 forward [-2916]: CCTGTACTGGAGCATATAAAGT	This manuscript	N/A
ChIP Primer: Ceacam1 reverse [-2785]: CAACATTATGAACTAACCAGTA	This manuscript	N/A
SimpleChIP Mouse RPL30 Intron 2 Primers	New England BioLabs	Cat# 7015P
Recombinant DNA		
pUMVC	Addgene	Cat# 8449; RRID:Addgene_8449
pCMV-dR8.2 dvpr	Addgene	Cat# 8455; RRID:Addgene_8455
pCMV-VSV-G	Addgene	Cat# 8454; RRID:Addgene_8454
pBABE	Addgene	Cat# 1764; RRID:Addgene_1764
pBABE-SOX10	This manuscript	N/A
pBABE-CEACAM1 Isoform 1	This manuscript	N/A
pBABE-CEACAM1 Isoform 4	This manuscript	N/A
pGL3P	Promega	Cat# E1761
pGL3P Ceacam1[-1525/+5]	This manuscript	N/A
pGL3P Ceacam1[-2875/-1435]	This manuscript	N/A
pGL3P Ceacam1[-4135/-2785]	This manuscript	N/A
pGL3P Ceacam1[-5305/-4045]	This manuscript	N/A
pRL-CMV	Promega	Cat# E2261

pLenti Cas9-Blast	Dr. Daniel Schramek; University of Toronto	N/A
pLKO H2B-mRFP-2A puro	Dr. Daniel Schramek; University of Toronto	N/A
Software and algorithms		
Timer2.0	Li et al., 2020 (276)	http://timer.cistrome.org/
cBioPortal	Cerami et al., 2012; Gao et al, 2013 (277,278)	https://www.cbioportal.org/
Graphpad Prism		
FACSDiva		
FlowJo		
BioRender	Graphical abstract	https://biorender.com/

4.6 Results

SOX10+ cells display a growth advantage in immune-competent mice but reduced self-renewal properties

The role of Sox10 in human melanoma is well established (120,187,252). Interrogation of the Firehose human melanoma dataset shows that high SOX10 expression is correlated with a decrease in survival (Figure 4.1A). To gain further insight into Sox10-driven phenotypes, we set out to identify cells lines with differential SOX10 expression. To achieve this, the YUMM panel of murine congenic melanoma cell lines (50) was assessed for Sox10 expression. Using Western blotting we identified the YUMM1.1 as a SOX10 high cell line, YUMM2.1 showed intermediate levels and YUMM1.7 & YUMM1.9 cells showed little to no expression (Figure 4.1B). This was further validated at the mRNA level, suggesting that Sox10 expression in these cells is likely to be modulated at the transcriptional level (Figure 4.1C). We next tested the in vivo growth potential of the SOX10+ YUMM1.1 and the SOX10- YUMM1.7 cell lines in C57 mice. As expected, the SOX10+ cells reached endpoint significantly faster than the SOX10- cells (Figures 4.1D and 4.1F). Although the SOX10- cells did grow slower, they still formed palpable tumors (Figure 4.1D). Western blot analysis showed that SOX10 was not reactivated in the YUMM1.7 tumors in an immune competent background, confirming that cells lacking SOX10 did not activate it and retained some in vivo growth potential (Figures 4.1D and 4.1F). To test the potential effects of the immune system in this assay, cells were injected in NOD-SCID mice which lack functional T/B cells and have impaired NK cell and macrophage functions. In marked contrast to previously reported results (120,187,252), the SOX10+ cells displayed reduced growth compared to the SOX10- cells (Figure 4.1E and 4.1G) in immuno-compromised hosts. One possibility is that SOX10+ tumors have the ability to negatively modulate the immune system in an immune

competent background. Alternatively, SOX10- cells may have increased cancer stem cell (CSC) potential. Previous findings in our lab and others have identified SOX10 as a CSC marker enhancing tumorsphere forming potential (183,184,274). Using melanosphere assays we tested the CSC potential of both cell lines. Interestingly, the SOX10+ YUMM1.1 melanoma cells displayed low sphere forming potential (Figure 4.1H), suggesting reduced levels of CSCs. This further translated into a decrease in secondary sphere formation, supporting a reduction in self-renewal capabilities. Surprisingly, no secondary spheres could be recovered from the high SOX10 expressing YUMM1.1 cells, whereas the YUMM2.1 cells, expressing intermediate SOX10 levels, generated a low level of secondary spheres (Figure 4.1H and 4.1I). Together, these data suggest that high SOX10 populations have reduced stem cell-like content and that SOX10 may play a different role in epithelial-like cancers.

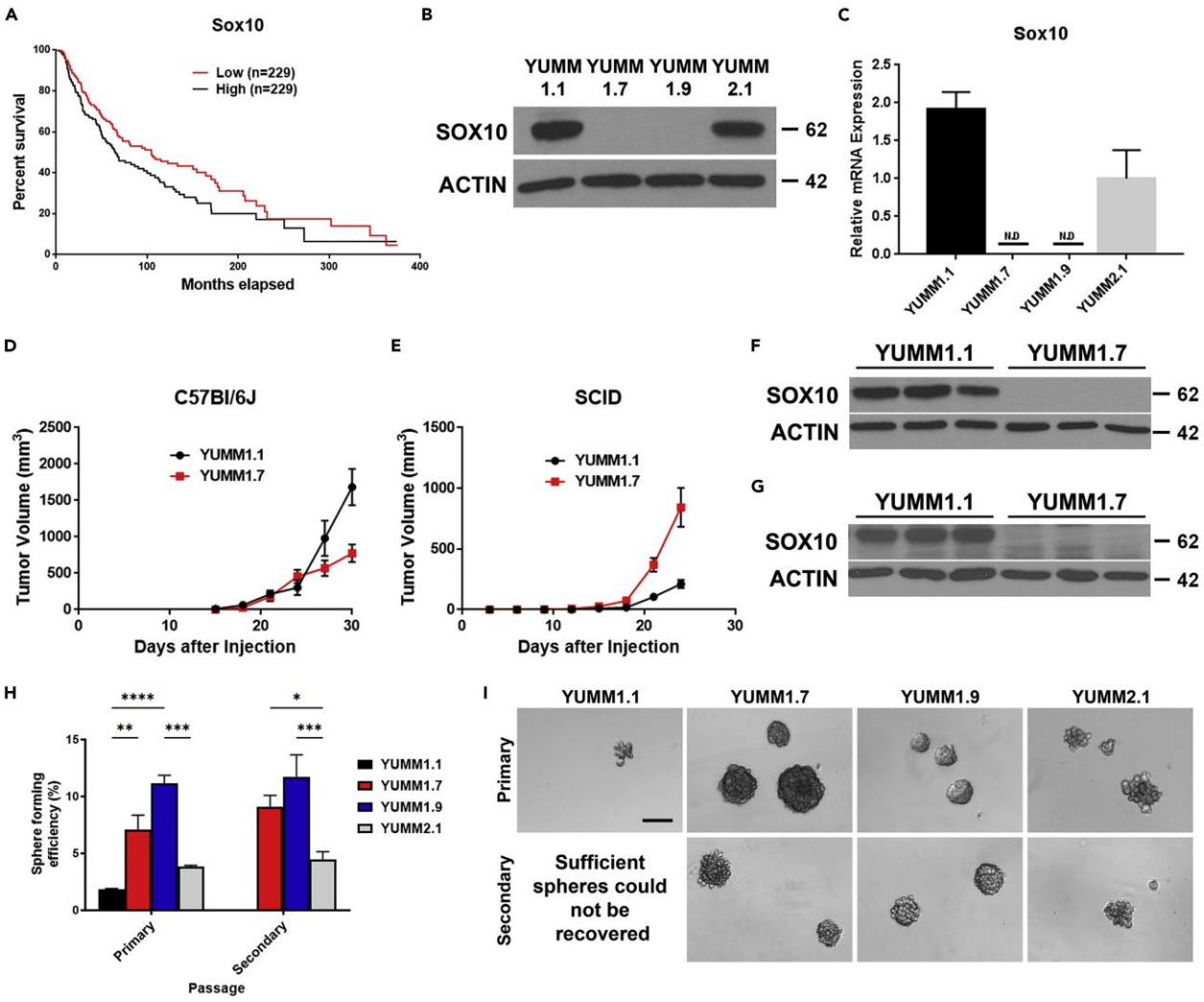
A
Sox10
Low (n=229)
High (n=229)
Percent survival
Months elapsed
B
YUMM 1.1
YUMM 1.7
YUMM 1.9
YUMM 2.1
SOX10
ACTIN
62
42
C
Sox10
Relative mRNA Expression
N.D
N.D
YUMM1.1
YUMM1.7
YUMM1.9
YUMM2.1
D
C57Bl/6J
Tumor Volume (mm3)
YUMM1.1
YUMM1.7
Days after Injection
E
SCID
Tumor Volume (mm3)
YUMM1.1
YUMM1.7
Days after Injection
F
YUMM1.1
YUMM1.7
SOX10
ACTIN
62
42
G
YUMM1.1
YUMM1.7
SOX10
ACTIN
62
42
H
Sphere forming efficiency (%)
YUMM1.1
YUMM1.7
YUMM1.9
YUMM2.1
Primary
Secondary
Passage
I
YUMM1.1
YUMM1.7
YUMM1.9
YUMM2.1
Primary
Secondary
Sufficient spheres could not be recovered

Figure 4.1: SOX10^{+} cells display a growth advantage in an immune competent background but reduced self- renewal properties (**A**) Kaplan Meier curve comparing overall survival in *SOX10*-high and low melanomas patients from the Firehose Legacy dataset. (**B** and **C**) qPCR and Western blots of various YUMM cell lines showing differential *Sox10* expression. (**D** and **E)** *In vivo* growth comparison of high and low SOX10 expressing melanoma cells in immune competent C57 (n=5 and n=4 respectively) (**D**) and immune compromised SCID (n=6 and n=6 respectively) (**E**) mice. Tumor size was measured at each indicated point. (**F** and **G**) Tumors from panels **D** and **E** were collected and protein was harvested. Samples were analysed for SOX10 levels in the YUMM1.1 and YUMM1.7 tumors from the immune competent (**F**) and immune compromised mice (**G**). Three tumors from each cohort were used to allow for representative protein expression found within the various tumors. (**H**) Quantitation of primary and secondary sphere formation for various YUMM lines expressing different levels of SOX10. (**I**) Representative images of both primary and secondary spheres enumerated in (**H**) are shown (scale bar = 100µM). Data is representative of three independent experiments (**C**, **H**). Graphs show the mean ±SEM. *p<0.05, **p<0.005, ***p<0.001, ****p<0.0001 by one-way anova (**H**).

SOX10 modulates the CSC properties of BRAF+ melanomas

To test whether SOX10 expression was sufficient to modulate the CSC potential of melanoma cells, the SOX10- YUMM1.7 cells were transduced with a retrovirus expressing Sox10. Expression was confirmed by Western Blot analysis (Figure 4.2A) and the self-renewal capabilities of the SOX10+ and SOX10- YUMM1.7 cells were tested using sphere forming assays in vitro. Interestingly, expression of SOX10 in the YUMM1.7 cells had no effect on primary sphere formation but slightly decreased the CSC self-renewal capabilities (2^o spheres; Figure 4.2B and 4.2C). To further test the role of SOX10 in self renewal, we knocked out Sox10 in YUMM1.1 cells using CRISPR-Cas9 and guide RNAs targeting the HMG domain in exon two. Western blotting showed a significant SOX10 knock out using two independent guides (Figure 4.2D). In vitro sphere forming assays with both Sox10 knock out cell lines showed that Sox10 deletion enhanced the number of primary and secondary spheres (Figure 4.2E and 4.2F), suggesting that Sox10 expression negatively modulates CSC content. Similarly, Sox10 ablation in YUMM2.1 expressing intermediate levels of SOX10 led to an increase in the sphere forming potential, further suggesting that SOX10 decreases the CSC properties of melanoma (Figure S4.1A and S4.1B). Together our data show that SOX10 expression reduces the CSC potential of BRAF+ melanomas.

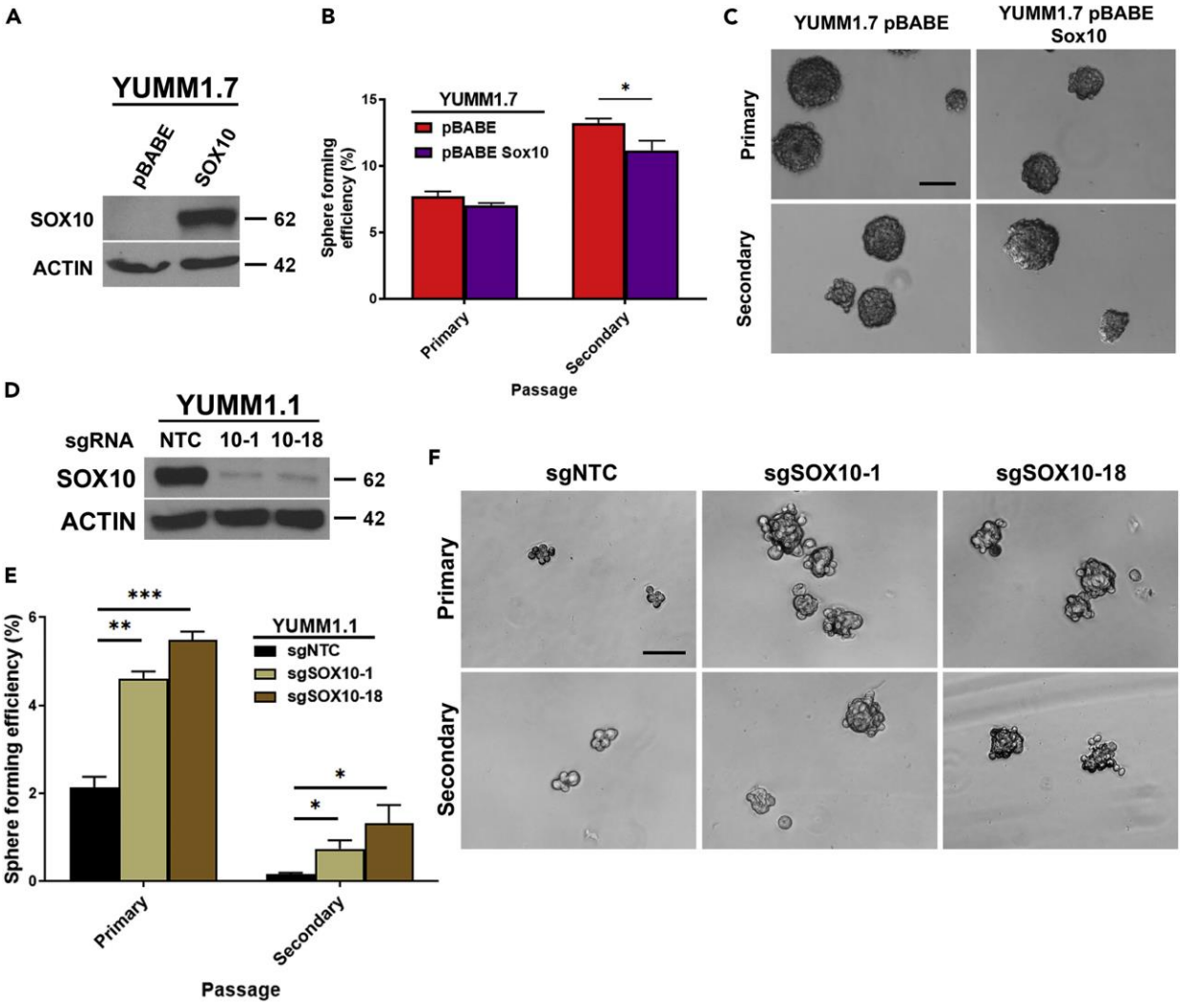
A
YUMM1.7
pBABE
SOX10
SOX10
ACTIN
62
42
B
YUMM1.7
pBABE
pBABE Sox10
Sphere forming efficiency (%)
15
10
5
0
*
Primary
Secondary
Passage
C
YUMM1.7 pBABE
YUMM1.7 pBABE Sox10
Primary
Secondary
D
YUMM1.1
sgRNA
NTC
10-1
10-18
SOX10
ACTIN
62
42
E
Sphere forming efficiency (%)
6
4
2
0
***
**
*
*
YUMM1.1
sgNTC
sgSOX10-1
sgSOX10-18
Primary
Secondary
Passage
F
sgNTC
sgSOX10-1
sgSOX10-18
Primary
Secondary

Figure 4.2: SOX10 modulates the CSC properties of BRAF+ melanomas. (**A**) Immunoblot of YUMM1.7 cells stably expressing SOX10. (**B**) Quantitation of primary and secondary sphere formation of stably expressing SOX10 YUMM1.7 cell line and control. (**C**) Representative images of both primary and secondary spheres enumerated in (**B**). Scale bar = 100μM. (**D**) Immunoblot of SOX10 knockout YUMM1.1 cells. (**E**) Quantitation of primary and secondary sphere formation of our *Sox10* knockout YUMM1.1 cells and control. (**F**) Representative images of both primary and secondary spheres are shown for the YUMM1.1 control and *Sox10* knockout cells (scale bar = 100μM). Data is representative of three independent experiments (**B**, **E**). Graphs show the mean ±SEM. *p<0.05, **p<0.005, ***p<0.001 by two-tailed t test (**B)** or one way anova (**E**).

SOX10 affects CD8+ T-cell infiltration and is co-expressed with the immune modulator CEACAM1

To further assess the role of SOX10 on tumor growth in vivo, the YUMM1.7 cells expressing SOX10 were injected subcutaneously into immune competent mice. As expected, SOX10-expressing YUMM1.7 cells showed an increase in tumor growth compared to controls (Figure 4.3A). One of the hallmarks of melanoma phenotype switching is the ability to evade the immune system (279). Therefore, one possibility is that the observed in vivo enhanced growth by the SOX10+ cells is due to immune suppression. Following tumor growth, we performed flow cytometry on endpoint tumors. Our analyses show equal levels of CD3+ immune cell infiltration in the tumor microenvironment (Figure S4.2A). However, flow analysis showed that the SOX10+ tumors had increased CD4+ T-cell infiltration with a decrease in CD8+ T-cell (Figure 4.3B), suggesting that SOX10-driven melanoma tumors can regulate T-cell infiltration or immune escape. To test this, we repeated the injections using RAG1 mice which lack T/B cells. Interestingly, we found that the SOX10-expressing YUMM1.7 cells grew at the same rate as controls, supporting the notion that SOX10+ melanoma can negatively regulate the immune response (Figure 4.3C and S4.2B). This finding was further corroborated by injecting the SOX10-deficient YUMM1.1 cells (Figure 4.2D) in NCG mice which lack T and B cells while also having an extreme impairment in innate immune function (Figure S4.2C). As SOX10 expression regulated T cell infiltration in tumors, we analysed TCGA data for evidence of correlation between immune infiltration and overall survival in melanomas using TIMER2.0. Interestingly, the extent of CD4+ T cell infiltration within melanomas did not affect overall survival (Figure S4.2D). However, supporting our data, patients with increased levels of CD8+ T cell infiltrates displayed better survival outcomes (Figure S4.2E).

Our previous work in breast cancer identified a number of potential SOX10 targets (184). CEACAM1, a glycoprotein found on the surface of various cell types, was found to be highly expressed in SOX10+ breast cancer cells. Strikingly, CEACAM1 is believed to play multiple roles in inhibiting cytotoxic lymphocyte function (280). To assess whether SOX10 could be driving the expression of ligands inhibiting CD8+ T cell function, we tested a panel of common T cell modulators including CEACAM1, PDL1, PDL2, CD80 and CD86. Conventional ligands such as PDL1, PDL2, CD80, and CD86 had no correlation with SOX10 expression in our various YUMM lines as determined by flow cytometry (Figure S4.3A). However, CEACAM1 expression was only observed in SOX10 expressing YUMM lines with YUMM1.1 displaying the highest CEACAM1 and SOX10 levels (Figure 4.3D). Supporting this, using TCGA data on CBioPortal we found that CEACAM1 and SOX10 mRNA levels are positively correlated in melanoma (Figure S4.3B). This significant correlation between SOX10 and CEACAM1 in melanoma prompted us to test whether CEACAM1 expression was SOX10-dependent. Using flow cytometry, we identified multiple human melanoma cell lines with both SOX10high/CEACAM1high and SOX10high/CEACAM1med levels (Figure 4.3E and S4.3C). This was also observed in the YUMM lines, suggesting that this correlation is conserved in murine cell lines. We found that the YUMM1.7 cells expressed little to no SOX10 or CEACAM1 protein (Q2; Figure 4.3F). In contrast, in both the YUMM1.1 and YUMM2.1, a large proportion of CEACAM1 positive cells are also SOX10 positive (Q2; Figure 4.3F). Although a large proportion of cells are double-positive, a CEACAM1-/SOX10+ population is also present (Q3), suggesting that CEACAM1 expression may also be dependent on additional factors or it is expressed in distinct SOX10+ subpopulations (Figure 4.3E and 4.3F). Furthermore, it suggests that SOX10 expression is independent of CEACAM1.

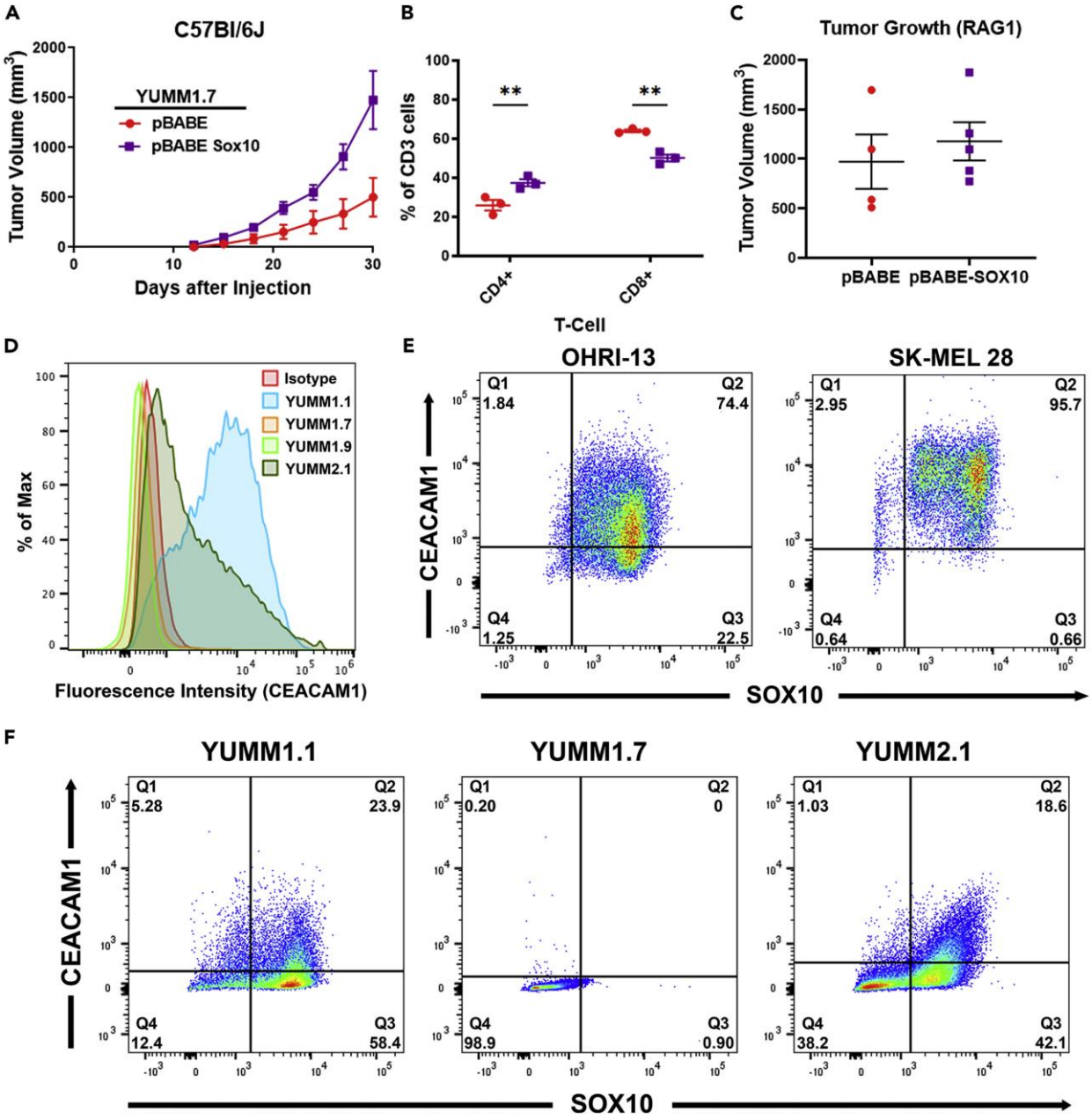
A
C57Bl/6J
YUMM1.7
pBABE
pBABE Sox10
Tumor Volume (mm3)
Days after Injection
B
% of CD3 cells
**
**
CD4+
CD8+
T-Cell
C
Tumor Growth (RAG1)
Tumor Volume (mm3)
pBABE
pBABE-SOX10
D
Isotype
YUMM1.1
YUMM1.7
YUMM1.9
YUMM2.1
% of Max
Fluorescence Intensity (CEACAM1)
E
OHRI-13
SK-MEL 28
CEACAM1
SOX10
Q1 1.84
Q2 74.4
Q4 1.25
Q3 22.5
Q1 2.95
Q2 95.7
Q4 0.64
Q3 0.66
F
YUMM1.1
YUMM1.7
YUMM2.1
CEACAM1
SOX10
Q1 5.28
Q2 23.9
Q4 12.4
Q3 58.4
Q1 0.20
Q2 0
Q4 98.9
Q3 0.90
Q1 1.03
Q2 18.6
Q4 38.2
Q3 42.1

Figure 4.3: SOX10 expression is correlated with CD8+ T-cell infiltration and CEACAM1 levels. (**A**) *In vivo* growth comparison between the pBABE control (n=5) and the pBABE-SOX10 overexpressing (n=5) YUMM1.7 cell lines in C57 immune competent mice. (**B**) Flow cytometry analysis of the CD4+ and CD8+ T-cell populations within the pBABE and pBABE-SOX10 tumors at endpoint. (**C**) Comparison of tumor size 24 days post injection between pBABE control (n=4) and the pBABE-SOX10 overexpressing (n=5) YUMM1.7 cell lines in RAG1 mice. (**D**) Flow analysis showing the proportion of CEACAM1 positive cells in various YUMM cell lines compared to isotype control. (**E**) Flow cytometric staining of SOX10 and CEACAM1 in OHRI-13 and SK-MEL28 human melanoma cell lines. Percentage of each group is indicated within their quadrant. (**F**) Flow cytometric staining of SOX10 and CEACAM1 in the YUMM1.1, YUMM1.7 and YUMM2.1 murine cell lines. Percentage of each group is indicated within their quadrant. Graphs show the mean ±SEM. **p<0.005 by two-tailed t test (**B**).

SOX10 directly activates Ceacam1 on a distal promoter region

To determine whether SOX10 can modulate the expression of CEACAM1, we transfected two siRNAs targeting SOX10 into the YUMM1.1 and YUMM2.1 melanoma cell lines and confirmed knockdown by western blotting (Figure 4.4A and S4.4A). Transfection of the siRNAs resulted in a marked downregulation of CEACAM1 (Figure 4.4B and S4.4B). Interestingly, CEACAM1 levels were higher in YUMM1.1 and YUMM2.1 cells with residual SOX10 expression (Figure 4.4A-B and S4.4A-B). Flow cytometry also revealed that CEACAM1 expression was not re-activated following the long term CRISPR/Cas9-mediated SOX10 knock out protocol (Figure S4.4C).

CEACAM1 is expressed as multiple isoforms generated through alternative splicing (126,281). Most of these isoforms can be grouped as long (full intracellular domain) or short (lacking the complete ITIM domain) with different functions. Although the specific roles of these isoforms have yet to be fully elucidated, CEACAM1-L isoforms seem to be predominantly expressed and have been found to alter CD8 T-cell activation and regulate metastatic potential of various cancers (282,283). To test whether Sox10 preferentially regulates specific CEACAM1 isoforms, we assessed the levels of both long and short isoform groups by qPCR. Sox10 knockdown in the YUMM1.1 decreased both Ceacam1 isoform groups equally, suggesting that Sox10 expression does not affect the splicing mechanisms but overall Ceacam1 expression (Figure 4.4C). To ultimately test whether SOX10 can activate CEACAM1 expression in melanoma, we assessed CEACAM1 levels in SOX10-deficient YUMM1.7 cells following transduction with pBABE-Sox10. Following qPCR, exogenous SOX10 expression induced both Ceacam1 isoform groups in YUMM1.7 cells (Figure 4.4D). Total CEACAM1 upregulation was further confirmed via flow cytometry (Figure 4.4E). To determine whether SOX10 directly activates Ceacam1, we

cloned multiple 1kb fragments of the Ceacam1 promoter region in pGL3-P, a luciferase backbone. The overlapping fragments allowed for coverage of up to -5kb from the Ceacam1 transcriptional start site. Interestingly, we identified two negative regulatory regions (-1525/+5 and -5305/-4045) that showed decreased luciferase activity only in the YUMM1.7 cell lines lacking both CEACAM1 and SOX10 (Figure S4.4D). As expected, we identified one major fragment at approximately -3kbps from the transcriptional start site (-4135/-2785) that displayed a 5-fold increase in luciferase activity in SOX10+ YUMM1.1 cells (Figure 4.4F). Scanning of the -4135/-2785 fragment revealed only one potential SOXE binding site containing the (A/T)(A/T)CAA(A/T)G binding consensus sequence. Previous studies have shown that SOX10 can bind to distal promoter and/or enhancer regions through a variant site with a requirement for a CAA(A/T) sequence. Using the CAA(A/T) motif, we identified eight potential regions with four bearing a single nucleotide mismatch of the conventional SoxE consensus region. To determine whether SOX10 is bound to these consensus regions we used YUMM1.1 cells for ChIP analysis. Chromatin pull downs with anti-SOX10 antibodies showed significant enrichment above IgG in 3 of the 8 regions within the -4135/-2785 fragment bound by SOX10, suggesting that it is a direct regulator of CEACAM1 (Figure 4.4G).

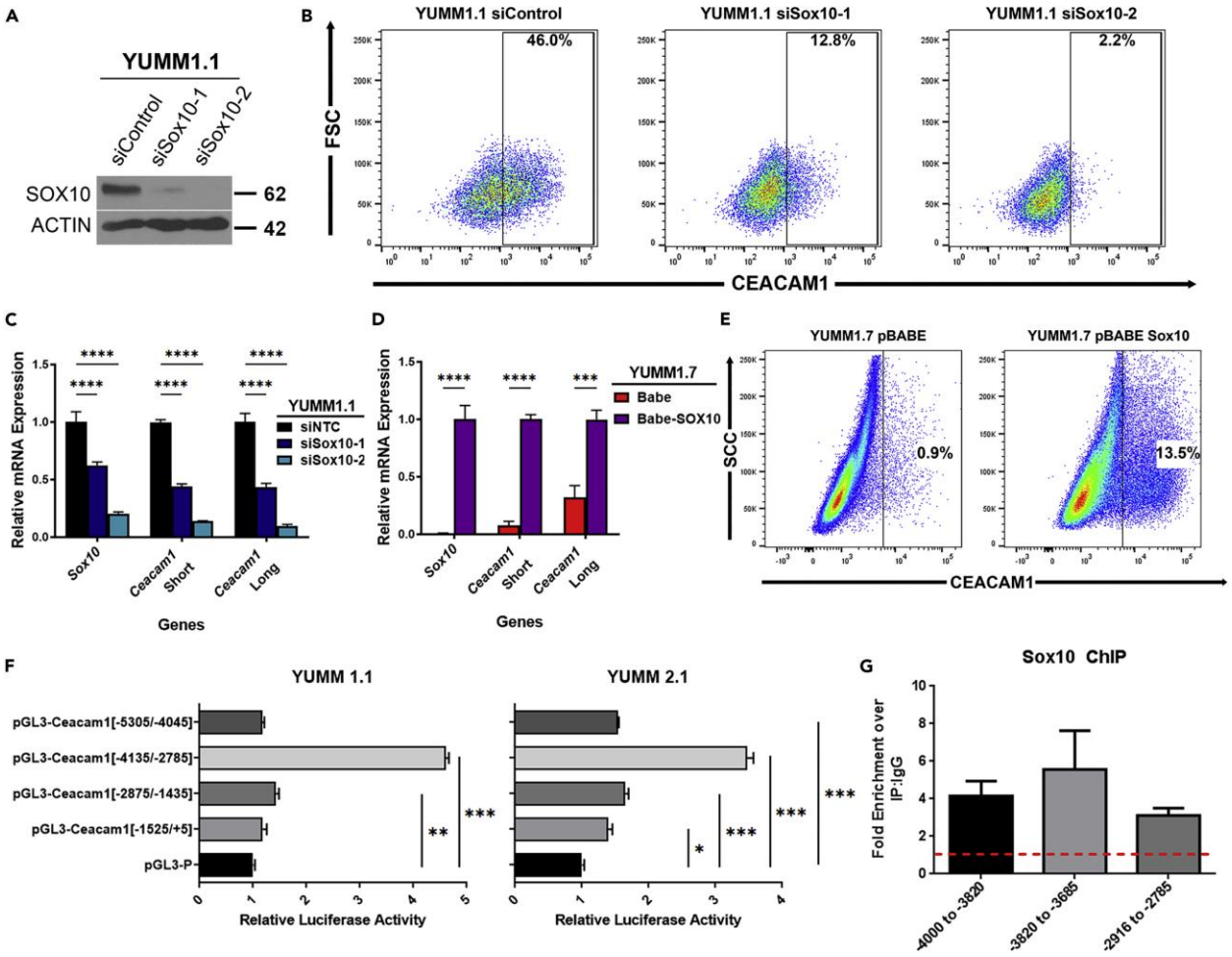
A
YUMM1.1
siControl
siSox10-1
siSox10-2
SOX10
ACTIN
62
42
B
YUMM1.1 siControl
YUMM1.1 siSox10-1
YUMM1.1 siSox10-2
46.0%
12.8%
2.2%
FSC
CEACAM1
C
Relative mRNA Expression
YUMM1.1
siNTC
siSox10-1
siSox10-2
Sox10
Ceacam1 Short
Ceacam1 Long
Genes
D
Relative mRNA Expression
YUMM1.7
Babe
Babe-SOX10
Sox10
Ceacam1 Short
Ceacam1 Long
Genes
E
YUMM1.7 pBABE
YUMM1.7 pBABE Sox10
0.9%
13.5%
SCC
CEACAM1
F
YUMM 1.1
YUMM 2.1
pGL3-Ceacam1[-5305/-4045]
pGL3-Ceacam1[-4135/-2785]
pGL3-Ceacam1[-2875/-1435]
pGL3-Ceacam1[-1525/+5]
pGL3-P
Relative Luciferase Activity
Relative Luciferase Activity
G
Sox10 ChIP
Fold Enrichment over IP:IgG
-4000 to -3820
-3820 to -3685
-2916 to -2785

Figure 4.4: SOX10 directly activates Ceacam1 on a distal enhancer region. (A) YUMM1.1 cells were treated with siRNA at 200nM targeting *Sox10* or a non-targeting control for 72 hours and *Sox10* knockdown was assessed by Immunoblot. (**B**) 72 hours post siRNA transfection cells were isolated and stained for CEACAM1. Representative flow plots were generated with indicated percent CEACAM1+ cells. (**C**) qPCR was used to compare *Sox10* knockdown efficiency with *Ceacam1* isoform levels of the cells in (**A**). (**D**) YUMM1.7 pBABE and YUMM1.7 pBABE-SOX10 cells were collected and analysed by qPCR for *Sox10* and *Ceacam1* isoforms. (**E**) YUMM1.7 pBABE and YUMM1.7 pBABE-SOX10 cells were isolated and stained for CEACAM1. Representative flow plots were generated with indicated percent CEACAM1+ cells. (**F**) Luciferase activity measurements from various Ceacam1 promoter fragments in YUMM1.1 and 2.1 cells. (**G**) RT-PCR of SOX10 ChIP in YUMM1.1 cells from various regions within the CEACAM1 -4135/-2785 fragment showing the fold enrichment over IgG. The red line represents the IgG control set to one. Data is representative of three independent experiments (**C**, **D**, **F**, **G**). Graphs show the mean ±SEM. *p<0.05, **p<0.005, ***p<0.001, ****p<0.0001 by one-way anova (**C**, **D**) or by two-tailed t test (**F**).

CEACAM1 decreases CD8+ T-Cell infiltration and promotes tumor growth

Since CEACAM1 has been shown to be expressed as multiple isoforms we tested whether the longest or shortest isoforms had any effect on tumor growth and CSC properties. Isoform 1 contains the complete extra and intra cellular domains of CEACAM1 whereas isoform 4 has a truncated extracellular and intracellular domain while still allowing for ligand binding (284). These two isoforms were cloned into a retroviral backbone and transduced into YUMM1.7 cells. Expression was confirmed using flow cytometry (Figure 4.5A). We then tested the CSC properties of these cells using tumor sphere assays as above. Similar to SOX10, CEACAM1 expression decreased the secondary sphere formation of these cells (Figure 4.5B). Although both isoforms showed a downward trend, only isoform 4 showed a significant reduction (Figure 4.5B and 4.5C). To test whether this decrease in CSC properties correlated with overall growth, we injected YUMM1.7 cells expressing the different isoforms subcutaneously into NCG mice. Surprisingly, although isoform 4 expression decreased CSC properties, we found that it conferred a marked growth advantage in vivo as previously reported (285) (Figure 4.5D). Interestingly, isoform 1 expression had no effect on tumor growth in vivo (Figure 4.5D). To test the effect of CEACAM1 on immune infiltration we injected the cells in immune competent C57 mice. Although isoform 4 conferred a similar growth advantage, flow cytometry showed that both CEACAM1 isoforms increased CD4+ T-cell and decreased CD8+ T-cell infiltration compared to controls (Figure 4.5E and 4.5F). Together these data show a direct functional correlation between CEACAM1 and SOX10 at repressing CD8+ T-cell infiltration and decreasing CSC properties in BRAF+ melanomas.

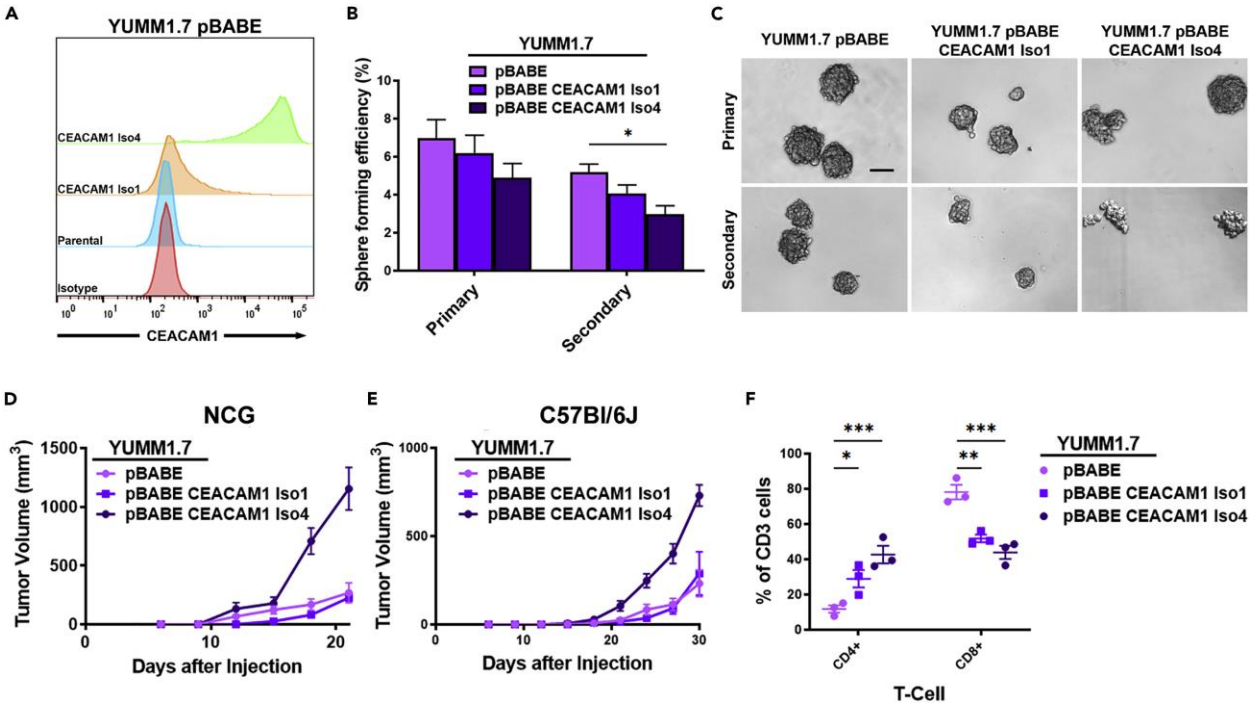
A
YUMM1.7 pBABE
CEACAM1 Iso4
CEACAM1 Iso1
Parental
Isotype
CEACAM1
B
YUMM1.7
pBABE
pBABE CEACAM1 Iso1
pBABE CEACAM1 Iso4
Sphere forming efficiency (%)
Primary
Secondary
C
YUMM1.7 pBABE
YUMM1.7 pBABE CEACAM1 Iso1
YUMM1.7 pBABE CEACAM1 Iso4
Primary
Secondary
D
NCG
YUMM1.7
pBABE
pBABE CEACAM1 Iso1
pBABE CEACAM1 Iso4
Tumor Volume (mm3)
Days after Injection
E
C57Bl/6J
YUMM1.7
pBABE
pBABE CEACAM1 Iso1
pBABE CEACAM1 Iso4
Tumor Volume (mm3)
Days after Injection
F
% of CD3 cells
CD4+
CD8+
T-Cell
YUMM1.7
pBABE
pBABE CEACAM1 Iso1
pBABE CEACAM1 Iso4

Figure 4.5: CEACAM1 decreases CD8+ T-Cell infiltration and promotes tumor growth. (**A**) Overlaid flow profiles representing the YUMM1.7 cells stably expressing CEACAM1 Isoform 1 or 4. (**B**) Quantitation of primary and secondary sphere formation in SOX10-deficient YUMM1.7 cells stably expressing CEACAM1 and controls. (**C**) Representative images of both primary and secondary spheres from the assays in **B** (Scale bar = 100μM). (**D** and **E**) *In vivo* growth comparison between the pBABE controls (n=5), the CEACAM1 iso1 (n=5) and iso4 (n=4) expressing YUMM1.7 cell lines in NCG immune compromised mice (**D**) and C57 immune competent mice (**E)**. (**F**) Flow cytometry analysis of the CD4+ and CD8+ T-cell populations within the pBABE and pBABE-CEACAM1 tumors at endpoint. Data is representative of three independent experiments (**B**). Graphs show the mean ±SEM. *p<0.05, **p<0.005, ***p<0.001 by one-way anova (**B**, **F**).

Co-expression of SOX10-CEACAM1 markedly decreases the CSC pool and CD8+ T-cell infiltration in melanoma

CEACAM1 has been shown to play contradictory roles within different cancer types (134,286,287). To gain insight into the SOX10-CEACAM1-driven phenotypes in melanoma, we sorted our YUMM1.7 pBABE-Sox10 cells into their CEACAM1- and CEACAM1+ populations (Figure5. 6A). These populations remained stable using flow cytometry for up to 17 days post sorting (Figure S4.5A). The YUMM1.7 CEACAM1+ cells were found to be enriched for both the short and long isoforms (Figure 4.6B) and displayed a significant increase in both Sox10 mRNA and protein levels, supporting the observation that Ceacam1 is a SOX10 target (Figure 4.6B and S4.5B). In agreement with this, the CEACAM1- population had lower levels of SOX10 compared to the pBABE-Sox10 and CEACAM1+ cells (Figure S4.5B). To test whether SOX10-CEACAM1 expression could enhance tumor growth, we injected our YUMM1.7 CEACAM+, CEACAM1-, and parental pBABE-Sox10 cells subcutaneously into immune competent mice. Unexpectedly, we found that the CEACAM1+ cells grew the slowest while the pBABE-Sox10 parental line grew significantly faster (Figure 4.6C). Following flow cytometry, we found no major differences in CD4+ T cell content between all groups but an increase in CD8+ T cell infiltration in the CEACAM1-, suggesting that SOX10-driven CEACAM1 expression suppresses CD8+ T cell recruitment (Figure 4.6D).

One possibility for the observed reduced tumor growth in vivo is the potential depletion of the CSC pool within both the YUMM1.7 SOX10-CEACAM1+ and SOX10-CEACAM1- populations. To test this, we performed primary and secondary sphere assays in vitro. Supporting our hypothesis, we found that the CEACAM1+ cells had significantly reduced primary and secondary sphere forming potential, suggesting a reduction in CSC content and self-renewal capacity (Figure

4.6E and 4.6F). Interestingly, both SOX10+ populations showed a reduction in self-renewal capacity compared to the parental YUMM1.7 cells (Figure 4.2B), suggesting that SOX10 expression is sufficient to reduce the CSC content of those cells.

We retested the CSC potential of those cells using limiting dilution assays in vivo. We injected ten-fold dilutions of each group into the flanks of NCG mice and allowed tumors to develop for 4 weeks. Supporting the melanosphere data, CEACAM1+ populations showed a markedly reduced tumor size and take rate upon dilution (Figure. 4.6G and 4.6H). The CSC frequency in CEACAM1- cells was estimated to be approximately 11-fold higher than the CEACAM1+ population (Figure 4.6I). These data suggest that SOX10-driven CEACAM1 expression can negatively modulate the CSC pool but enhance immune evasion by suppressing CD8+ T cell infiltration.

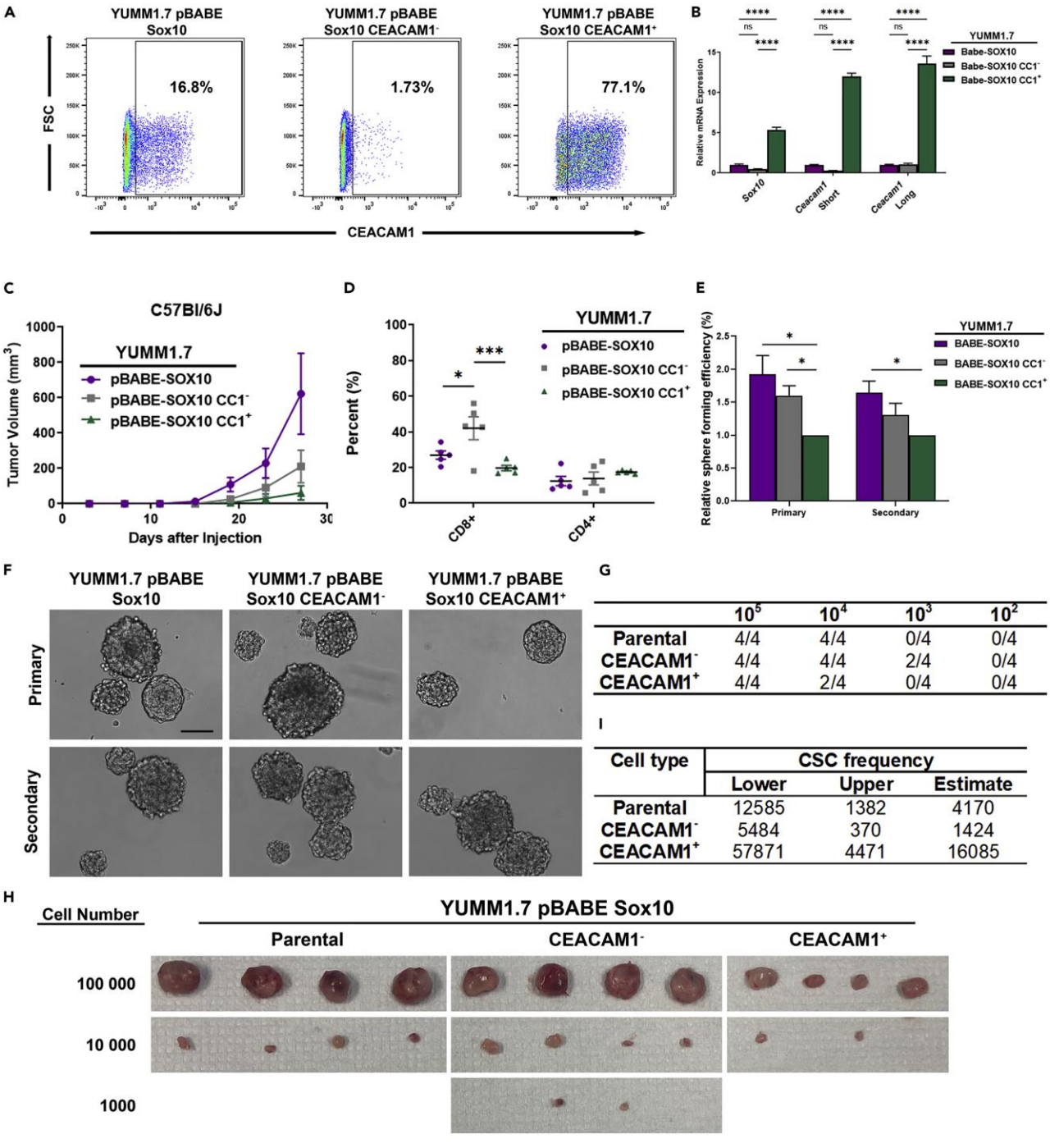

G

	10^5	10^4	10^3	10^2
Parental	4/4	4/4	0/4	0/4
CEACAM1$^-$	4/4	4/4	2/4	0/4
CEACAM1$^+$	4/4	2/4	0/4	0/4

I

Cell type	CSC frequency		
	Lower	Upper	Estimate
Parental	12585	1382	4170
CEACAM1$^-$	5484	370	1424
CEACAM1$^+$	57871	4471	16085

Figure 4.6: SOX10hi/CEACAM1+ cells show decreased CSC pool and CD8+ T-cell infiltration in tumors. (**A**) Representative flow sorts showing the proportion of CEACAM1+ and CEACAM1- cells obtained following SOX10 expression in YUMM1.7 cells. (**B**) qPCR analysis for *Sox10* and the *Ceacam1* isoforms in sorted YUMM1.7 pBABE-SOX10 cells shown in **A**. (**C**) *In vivo* growth comparison between the pBABE-SOX10 (n=5), CEACAM1^{-} (n=5) and CEACAM1^{+} (n=5) YUMM1.7 cell lines in C57 immune competent mice. (**D**) Flow cytometry analysis of the CD4+ and CD8+ T-cell populations within the pBABE-SOX10, CEACAM1^{-} and CEACAM1^{+} tumors at endpoint. (**E**) Quantitation of primary and secondary sphere formation in the YUMM1.7 pBABE-SOX10, CEACAM1^{-} and CEACAM1^{+} cells. (**F**) Representative images of both primary and secondary sphere assays from **E** (scale bar = 100μM). (**G**) 1x10^{5} YUMM1.7 pBABE-SOX10, CEACAM1^{-} and CEACAM1^{+} cells were injected into NCG mice. The mice were euthanized 28 days post injection and the number of palpable tumors per group was recorded. (**H**) Representative images of tumors removed following the 28 day endpoint. (**I**) Estimated frequencies of CSC within the solid tumors isolated from the three groups using ELDA (288). Data is representative of three independent experiments (**B**, **E**). Graphs show the mean ±SEM. *p<0.05, ***p<0.001, ****p<0.0001 by one-way anova (**B, D, E**).

4.7 Discussion

The role of SOX10 in melanoma is well documented. To gain further insight into the role of SOX10 in melanoma progression, we screened a panel of YUMM lines (50) for SOX10 expression. Western blot analysis showed high SOX10 expression in YUMM1.1 cells with moderate and very low levels in YUMM2.1 and 1.7, respectively (Figure 4.1B). Our data show that high SOX10 expression in melanoma confers a tumor growth advantage in immune competent mice (Figure 4.3A). Surprisingly this growth advantage was lost in immune compromised mice, suggesting a role for SOX10 in immunomodulation (Figure 4.3C and S4.2C). Due to the high intra-tumor heterogeneity in melanomas, we tested the CSC potential of SOX10+ YUMM1.1 cells. Unexpectedly, we found that SOX10 decreased the self renewal capacity in those cells (Figure 4.2E and S4.1A). To further investigate the mechanisms underlying these phenotypes, we tested a panel of immune ligands expressed by tumor cells. Those studies revealed that CEACAM1 is a direct gene target of SOX10 (Figure 4.4G). When co-expressed, we also find that the SOX10-CEACAM1 axis is detrimental to tumor growth by depleting the CSC pool (Figure 4.6G-H).

Our data finds that SOX10-null cells have increased CSC properties (Figure 4.2E and S4.1A). This observation is in stark contrast to a large number of reports identifying the SoxE family as CSC-inducing. For example, SOX10 has been shown to induce stem/progenitor activity in mammary epithelial cells (183) while also increasing the CSC pool in HER2+ breast cancer (184). One reason for this opposing function of SOX10 in epithelial cells when compared to melanoma could be due to the mutual exclusivity of SOX10 and SOX9 expression in melanoma (165). Interestingly, SOX9 regulates SOX10 expression by direct binding to SOX10 upstream sequences and reducing transcription (165). Furthermore, SOX9 is believed to be a major marker for CSCs where it has been shown to confer multiple CSC properties in various cancer subtypes,

including glioma, lung and breast cancer (170–172,289–291). Similarly, SOX9 can directly activate SOX10 gene expression in breast cancer to induce a more stem cell-like phenotype (292). As SOX9 is usually not expressed in SOX10+ melanoma populations (165), SOX9 deficiency may lead to a decrease in potential CSC properties. Although SOX9 and SOX10 expression is mutually exclusive in melanoma, understanding the specific phenotypic changes imparted by these factors will shed light into potential SoxE-specific therapeutic strategies.

Here, we have shown that CEACAM1 expression in melanoma is dependent on SOX10 (Figure 4.3E and 4.3F). Furthermore, we find that SOX10 can directly bind to a CEACAM1 distal enhancer region and induce its expression in melanoma (Figure 4.4G). Surprisingly, SOX9 has been shown to repress CEACAM1 in melanoma, further supporting an antagonistic function between SOX9 and SOX10 (293). Although SOX9 and SOX10 share very similar binding sites, SOX9 seems to function more on a CEACAM1 proximal promoter element with no evidence of SOX10 binding within the same region (293,294) (Figure 4.4F). Interestingly, we find that not all SOX10+ cells express CEACAM1, suggesting that SOX10 may require additional co-factor(s) to fully activate CEACAM1 (Figure 4.3E and 4.3F). This has been previously observed for SOX10. Indeed, SOX10-dependent activation of MITF requires Pax3 expression and TYPR1 induction has been shown to be mediated through direct interaction between SOX10 and BRG1 (295,296). Interestingly, we do observe that SOX10 activates both subsets of CEACAM1 isoforms (long and short), suggesting that it does not affect isoform selectivity (Figure 4.4C and 4.4D). The regulation of the SOX10-CEACAM1 axis is still not fully understood and in-depth studies should identify potential SOX10 co-factors critical in the activation of CEACAM1 gene expression.

Although SOX10 promotes tumor formation and was identified as a regulator of the proliferative state in melanoma, the mechanistic details about how it regulates this are not fully

understood (119,120,187,252). We show that SOX10 has the ability to regulate T-cell infiltration, primarily CD8+ T cells (Figure 4.3B). This is in agreement with previous work showing that SOX10 can confer tumor growth partially through blocking CD8+ T-cells infiltration (275). Although various immune subtypes can infiltrate the tumor microenvironment, we find that patients with high CD8+ T-cell infiltration have a better outcome (Figure S4.2E). For this reason, CD8+ T cells have been the primary target of current immunotherapies. Immune checkpoint inhibition, the most common form of immunotherapy, blocks inhibitory receptor interaction on cytotoxic lymphocytes such as CD8+ T-cells, thereby activating the immune response. Current ligands/receptors targets include PDL1/PD1, CTLA4 and TIM3 blockers, currently in clinical trials. Whether SOX10high melanomas can be halted by single checkpoint blockers or in combination is still unclear. Nevertheless, our studies and others (275) have identified SOX10 as a potential biomarker of tumor immunity.

CEACAM1 can be found on both tumor and immune cells where it can participate in homophilic or heterophilic interactions. CEACAM1 is alternatively spliced and is expressed as 12 human and 4 murine isoforms (280,297). Interestingly, blocking CEACAM1 homophillic interactions in melanoma sensitized the cells to CD8+ T-cell cytotoxicity (298). Here we have shown that isoform 4 had a significantly bigger effect on reducing CSC properties as well as CD8+ T-cell infiltration in melanoma (Figure 4.5B and 4.5E). Albeit missing the ITIM domains, the shorter isoform 4 can still activate downstream signaling (299). It has been shown that, although truncated at the N-terminus, the shorter isoforms such as 3S and 2S (human and mouse respectively) still retain their homophilic and heterophilic interactions (284). It is then likely that the differential expression between the various CEACAM1 isoforms or the isoform ratio (Figure 4.5A) plays a critical role in the penetrance of the immune phenotype.

CEACAM1 can also interact with TIM3, a receptor found on CD8+ T-cells usually during exhaustion (300). Current TIM3 blocking antibodies have shown great potential at reactivating immune function and inhibiting tumor immunity (301). It will be of great interest to determine whether CEACAM1 on tumors can induce CD8+ T-cell exhaustion by promoting TIM3-dependent responses. In addition, a greater understanding of the role of the various CEACAM1 isoforms on melanoma progression is required.

Melanomas typically present as heterogeneous populations with gene expression that is non-uniform throughout the tumor (302). Our data show that co-expression of SOX10 and CEACAM1 imparts a marked growth advantage to melanoma tumors (Figure 4.6C). As it was shown that CEACAM1 expression in melanoma was strongest at invading fronts (303), it is possible that the co-expression of SOX10/CEACAM1 occurs at the periphery of tumors This would suggest that CEACAM1 may be expressed primarily on the outer edge of the tumor or areas of vascularization. Overall, our data identifies SOX10 is a direct regulator of CEACAM1. This SOX10-CEACAM1 axis functions in both a pro- and anti-tumorigenic fashion by decreasing CD8-T-cell infiltration but by also modulating the CSC properties in melanoma (Figure 4.6D and 4.6E-I respectively). We believe future studies will identify other potential immune cellular subtypes regulated by this pathway as well as potential immune markers for the development of specific melanoma therapies.

4.8 Supplementary figures

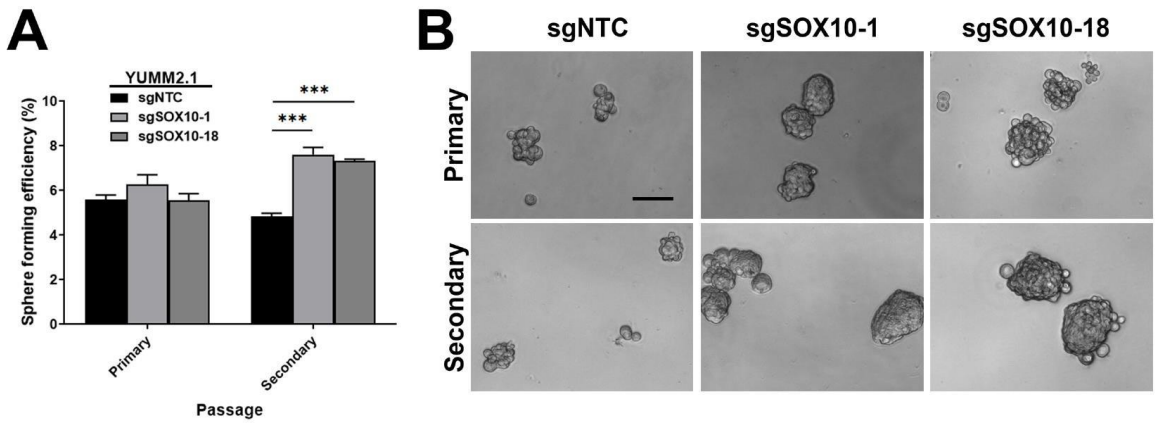

Supplementary Figure 4.1: Increased tumor sphere self-renewal in *Sox10* knockout melanoma. (**A**) Quantitation of primary and secondary sphere formation in *Sox10* knockout YUMM2.1 cells and control. (**B**) Representative images of both primary and secondary spheres enumerated in **A (s**cale bar = 100µM). Data is representative of three independent experiments (**A**). Graphs show the mean ±SEM. ***p<0.001 by one-way anova (**A**).

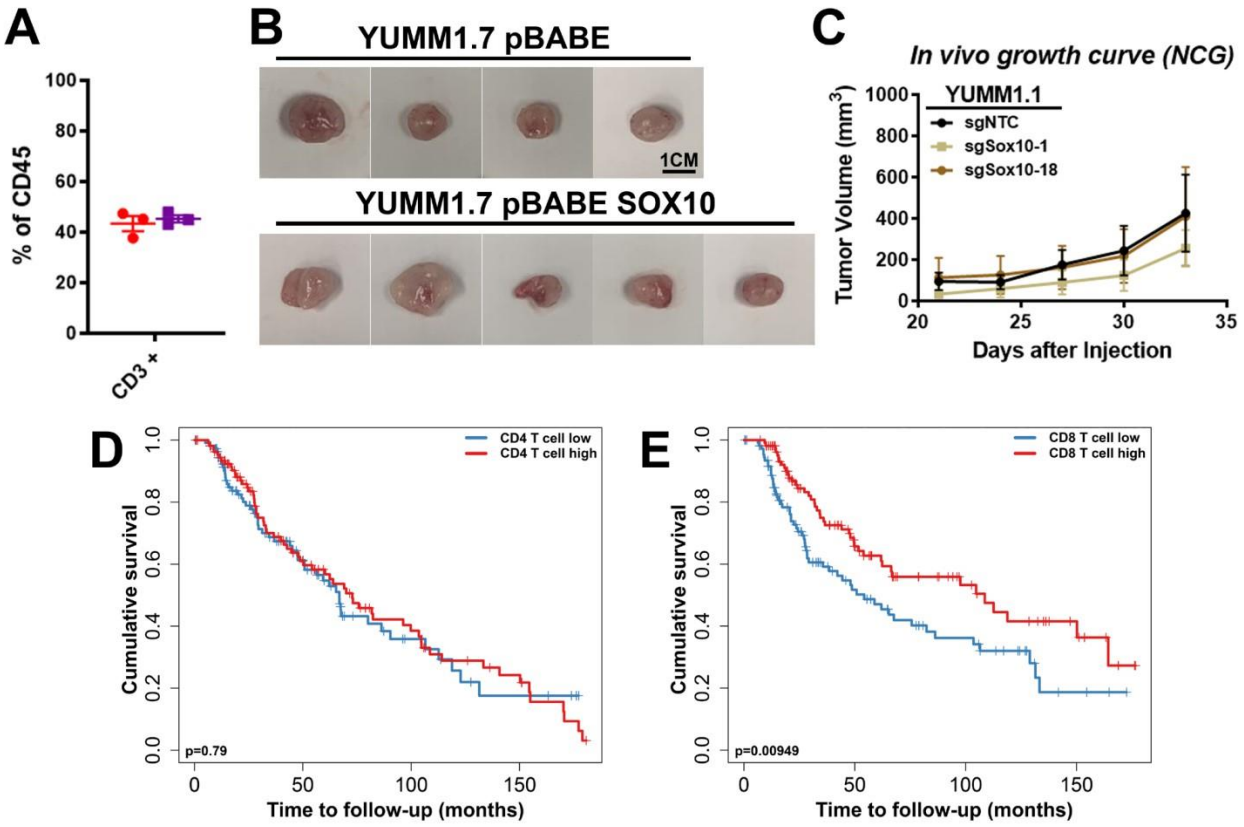

Supplementary Figure 4.2: SOX10 does not affect tumor growth in immune compromised mice. (**A**) Flow cytometry analysis of the CD3+ T-cell populations within the pBABE (red) and pBABE-SOX10 (purple) tumors at endpoint. (**B**) Representative images of tumors removed from RAG1 mice (**Figure 4.3C**) following the 24 day endpoint (scale bar = 1cm). (**C**) *In vivo* growth potential between the YUMM1.1 control (n=5) and two independent *Sox10* knockout (Sg10-1 n=4 and Sg10-18 n=4) cell lines in an immune compromised NCG background. (**D**) Kaplan Meier curve comparing overall survival in CD4+ T-cell-high and low melanoma patients. (**E**) Kaplan Meier curve comparing overall survival in CD8+ T-cell-high and low melanomas patients. Kaplan Meier curve (**D** & **E**) was processed and graphed by Timer2.0 (http://timer.cistrome.org/).

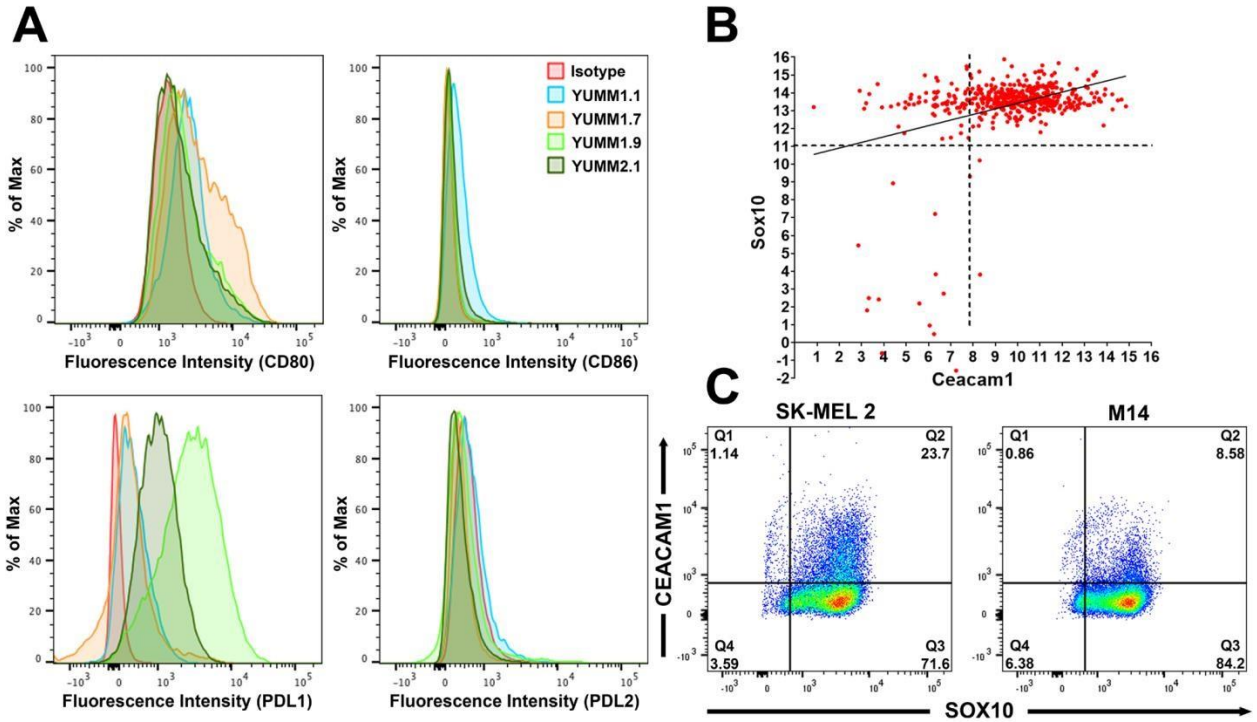

Supplementary Figure 4.3: *Sox10* expression is correlated with *Ceacam1* in melanoma. (**A**) Flow analysis showing the proportion of CD80, CD86, PD-L1 or PD-L2 positive cells in various YUMM cell lines compared to isotype control. (**B**) Correlation analysis between *SOX10* and *CEACAM1* expression using the Skin Cutaneous Melanoma TCGA Firehose legacy dataset on cBioPortal (https://www.cbioportal.org/) (Spearman: 0.13, p = 0.0243; Pearson: 0.32, p = 4.8 x 10^{-8}) (**C**) Flow cytometric staining of SOX10 and CEACAM1 in SK-MEL2 and M14 human melanoma cell lines. Percentage of each group is indicated within their quadrant.

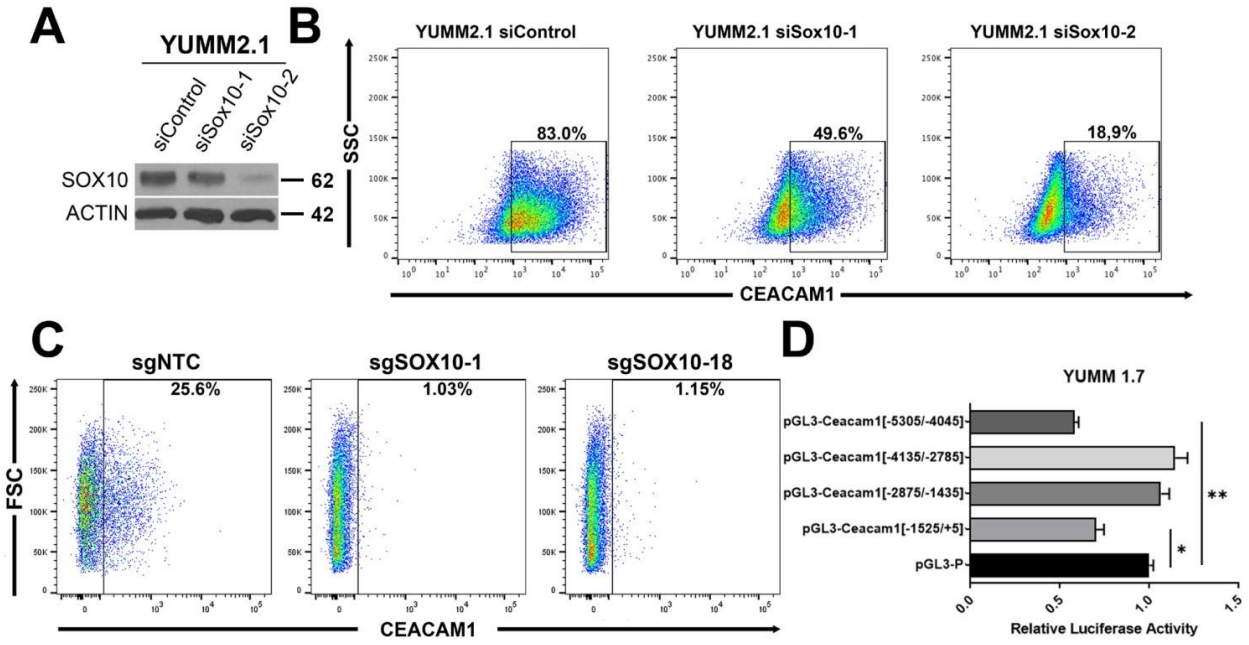

Supplementary Figure 4.4: SOX10 downregulation reduces CEACAM1 expression. (**A, B**) YUMM2.1 cells were treated with siRNA at 200nM targeting *Sox10* or a non-targeting control for 72 hours and *Sox10* knockdown and SOX10 expression was assessed by immunoblot (**A**) and CEACAM1 levels were measured by flow cytometry (**B**). (**C**) Flow analysis for CEACAM1 in YUMM1.1 *Sox10* knockout cells. (**D**) Luciferase activity measurements from various Ceacam1 promoter fragments in YUMM1.7. Data is representative of three independent experiments (**D**). Graphs show the mean ±SEM. *p<0.05, **p<0.005 by two-tailed t test (**D**).

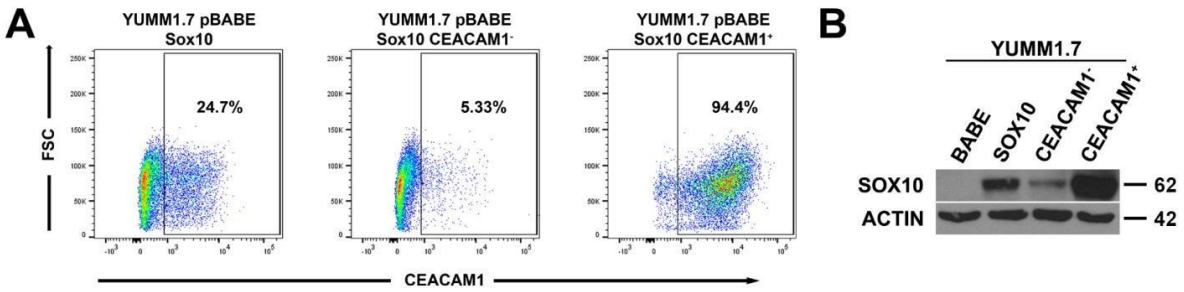

Supplementary Figure 4.5: CEACAM1+ sort enriches for the SOX10 positive population. (**A**) Flow plots showing the proportion of CEACAM1+ and CEACAM1- cells 17 days post flow sort in SOX10-expressing YUMM1.7 cells and controls. (**B**) Immunoblot of YUMM1.7 cells stably expressing SOX10 following sorting for the CEACAM1+ and CEACAM1- populations.

Chapter 5

General Discussion

5.1 Summary

The importance of SOX9 and SOX10 in cancer maintenance and progression is well documented. However, the relationship between these two proteins has not been thoroughly investigated. To dissect the various functions of SOX9 and SOX10, we utilized a panel of murine melanoma cell lines (YUMM) that express SOX9 or SOX10. Interestingly, we find that SOX9 expression is associated with a targeted therapy resistant state in melanoma, while SOX10 expression is observed in drug sensitive cells. Moreover, the loss of SOX10 promotes entry into a therapy resistant state and loss of sensitivity to both targeted therapy and oncolytic virus treatment. On the other hand, we have shown that SOX9 can act as a gatekeeper between states. SOX9-deficient melanoma cells lose the ability to transition into a drug resistant state and remain sensitive during prolonged treatments with MAPK inhibitors. Therapy resistance has previously been linked to the enrichment of CSC within the tumour population. We have shown that SOX10 directly regulates CEACAM1 and that this SOX10-CEACAM1 axis regulates the CSC-like properties in melanoma. This signaling pathway proved to be both pro-and-anti-tumourigenic. For example, tumours enriched for both SOX10 and CEACAM1 had reduced CD8+ T cell infiltration within the tumour microenvironment but also showed reduced overall tumour burden. Overall, we have uncovered novel roles for both SOX9 and SOX10 in melanoma therapy resistance that could lay the foundation for the identification of new pathways driving the transition between therapy sensitive and resistant states.

5.2 The relationship between SOX9 and SOX10

The characterization of SOX9 and SOX10 function has mainly focused on healthy cells. In general, the primary functions of SOX9 and SOX10 are related to development and neural crest lineage specification(161,162). Surprisingly, few studies have simultaneously investigated both

proteins. Therefore, the extent of their co-expression in various tissue types is still unknown. In the mammary epithelium, SOX9 marks the luminal progenitor population and the loss of *Sox9* inhibits mammary gland development (304). Similarly, Mertelmeyer et al., have shown that *Sox10* haploinsufficiency delays early mammary gland development (305). In agreement with these findings Dravis et al., have shown that SOX10 is a marker of fetal mammary stem cells, driving mammary gland development (183,274). Although these studies all examined SOX9 and SOX10 independently, it is not clear if they are co-expressed or whether they have redundant functions. We have shown the co-expression of SOX9 and SOX10 in HER2+ breast cancers (Appendix A)(292). Our data show that Sox10 expression is driven by AKT which can phosphorylate SOX9 and promote Sox10 activation on an upstream enhancer element (Appendix A)(292).

In contrast, SOX9 and SOX10 have been shown to have opposing roles in melanoma. The overexpression of SOX9 in human melanoma cells represses SOX10 (165). We have validated this finding in murine melanoma cell lines where we observe exclusive expression of either SOX9 or SOX10 (Figure 2.1). This unique expression pattern can be used to characterize two distinct states adopted by melanoma cells(119). The $SOX10^{High}$ population represents the proliferative, therapy sensitive state while the $SOX9^{High}$ population represents the slow cycling, therapy resistant state (Figure 2.2)(119). It remains unclear why SOX9 and SOX10 may work in conjunction in breast cancer but antagonistically in melanoma. Yang et al., have reported that SOX9 functions depend on its expression level(179). Therefore, if a certain threshold of SOX9 expression is not achieved, this could explain its different roles between cancer types (179). One study found that certain *Sox9* regulatory elements are buffered to changes in SOX9 expression while others are highly sensitive(306). If the sensitive regulatory elements of *Sox9* are more accessible in one cancer type versus the other, this could lead to activation/repression of different downstream

targets eliciting diverse phenotypes (306). There is also the possibility that SOX9 function is regulated by co-factors and post-translational modifications only present in certain cancer types. We found that SOX9 is bound to various regulatory elements in breast cancer cells without promoting transcriptional activity (Appendix A)(292). Following phosphorylation at S181, SOX9 becomes transcriptionally active at SOXE regulatory elements, driving transcription (Appendix A)(292). However, it is still unclear as to what drives these paradoxical functions of SOX9 and SOX10 in different cancer types and further work is required to address this.

5.3 Targeted therapy resistance in melanoma is regulated by SOX9 and SOX10

Surprisingly, SOX9 expression in melanoma has been shown to be both absent and present in various metastatic human patient tumors(177). Our findings show that SOX9 is only present in cell lines that have intrinsic resistance to targeted therapies or have been chronically treated with vemurafenib to induce a resistant state (Chapter 2). Others have found SOX9 expression primarily in slow-cycling, invasive melanoma(119,121). Although resistance and invasion represent two distinct phenotypes, they are commonly observed together. This begs the question of whether SOX9 is potentially driving both of these states. If SOX9 is the sole driver of this invasive/resistant state, one would predict that manipulation of SOX9 would alter these phenotypes. In our hands, the constitutive expression of SOX9 had no impact on inducing vemurafenib resistance *in vitro* (Figure 2.3). Interestingly, expression of SOX9 has been shown to promote proliferative, migratory and invasive capabilities in many other cancer types(166). One group showed that low to medium SOX9 expression acts in an antiproliferative fashion whereas high levels promote tumor cell growth in melanoma(179). Others have identified the presence of SOX9 in a slow cycling melanoma state, while SOX10 promotes a proliferative state(119,121). In our panel of parental YUMM cell lines, the SOX9-expressing cells have an increased proliferative capacity in

vitro when compared to the SOX10 positive cells (Figure 2.1 and 4.1). This increase in proliferation was also observed in vivo, only in an immune compromised background (Figure 4.1). One possibility is that a threshold of SOX9 expression causing a phenotypic change has not been achieved. Future experiments using an inducible system to study a SOX9-induced phenotype could address this issue.

While SOX10 function has been less scrutinized in the context of melanoma, it has been shown to mediate opposing phenotypes. One group identified SOX10 as a major regulator of FOXD3, a transcription factor shown to promote targeted therapy resistance in melanoma (192,193). The loss of SOX10 reduced FOXD3 expression following MAPK inhibition and in turn sensitized the cells to BRAF inhibition (193). This is stark contrast to other studies, including our own. One potential reason for this discrepancy could be due to the use of knockdown and not knockout melanoma cells in Han et al. study(193). In Han et al, they also did not test cell viability using Resazurin but rather AnnexinV staining(193). When looking at untreated controls vs *Sox10* knockdown cells, the *Sox10* knockdown melanoma cells have inherently higher AnnexinV staining and therefore start off "less viable". Therefore, a true test on increased sensitivity should be looking at total fold change rather than overall AnnexinV positive cells(193). Indeed, we show that the removal of SOX10 perpetuates a therapy resistant state, allowing for the activation of SOX9 (Figure 2.2 and 3.3). Transcriptomic data finds that the loss of SOX10 induces markers of invasion, proliferation, and metabolism in melanoma(197). A loss in SOX10 also increases the migratory and invasive capabilities of melanoma in both 2-D and 3-D cultures(197). Multiple studies also find that SOX10 loss increases MAPK inhibitor resistance in melanoma, further supporting our findings (119,194–197). The loss of SOX10 creates a dormant/quiescent like state, where the cells further gain increased migratory and invasive capabilities(197). The different role of SOX10 in

therapy resistance could be due to multiple factors, including acute vs chronic treatment, low vs high expression and the specific cell lines used. Some critical questions still remain: 1) why is SOX10 expression lost over time in chronically treated samples? and 2) how can SOX10-deficient melanomas be effectively treated?

5.4 SOX9 and SOX10 as gatekeepers of the targeted therapy resistant state

Here, we showed that both SOX9 and SOX10 act as gatekeepers to the resistant state (Chapter 2). We find that the loss of SOX10 following chronic treatment with vemurafenib is due to chromatin remodeling at the *Sox10* locus (Figure 2.5). We also observed that, following the transition to the resistant state, *Sox9* activation is in part due to the opening of chromatin along the *Sox9* promoter region (Figure 2.5). This transitionary period has been documented in various studies, marking these two states as proliferative (SOX10+) and invasive (SOX9+) (119,124,196,197). Interestingly, we find that the knockout of *Sox10* not only reduces the expression of SOX10, but also reduces the open chromatin surrounding the *Sox10* locus (Figure 2.5). In general, CRISPR/Cas9 inactivation shifts the ORF of the targeted region and therefore should not impact the overall genomic landscape of the gene of interest. Our data suggest that the modulation of SOX10 protein expression is sufficient to shift the cells into the previously observed MAPK inhibitor resistant, quiescent state(119,197). To verify this, we constitutively expressed SOX10 in two melanoma cell lines inherently lacking SOX10. Surprisingly, the production of exogenous SOX10 had no impact on vemurafenib resistance, suggesting that SOX10 alone is not sufficient to trigger chromatin remodeling and that the activation of SOX10-independent targets are also required. It would be of interest to modulate SOX10 protein through the use of PROteolysis TArgeting Chimeras (PROTACs). PROTACS is a small molecule that contains two binding moieties, one targeting the protein of interest and the other encodes an E3 ligase. This

allows for the ubiquitination of the protein of interest and promotes its degradation. If targeting SOX10 induces this transition, this would suggest that the loss of SOX10 protein is required to promote chromatin remodelling and modification of *Sox10*'s genomic landscape.

Another possibility is that the loss of genomic accessibility at the *Sox10* locus drives the loss of SOX10 protein and promotes the transition to the resistant state. Since exogenous expression did not affect vemurafenib sensitivity, reversing this resistant state may require genomic manipulation of *Sox10*. The use of CrisprA could revert overall resistance by reopening the chromatin landscape around the *Sox10* locus. This would drive endogenous SOX10 expression, potentially reverting cells to their tolerant state. However, this would not address the mechanisms by which SOX10 expression is lost.

Although SOX9 expression appears to always be correlated with the resistant state, its function and regulation have never been clearly documented(119,197). As the *Sox9* locus opens following resistance to vemurafenib, we speculated that SOX9 was driving this resistant phenotype. Like SOX10, over-expression of SOX9 did not alter resistance to vemurafenib. Surprisingly, unlike the knockdown of *Sox10*, knockdown of *Sox9* did not sensitize intrinsically resistant or adaptively resistant melanoma cells to vemurafenib. This suggests that SOX9 is required for the initial activation of a transcriptional network but not necessary thereafter during the transition to this slow-cycling, MAPK inhibitor resistant state. Sox9 CrisprA could be used to test this idea.

Based on our initial findings, we hypothesized that, although SOX9 does not alter tolerance to MAPK inhibitors, endogenous *Sox9* may be required for the programming of this resistant state. Once achieved, Sox9 will no longer be required due to the activation of a positive feedback loop, perpetuating the resistant state. Here, we have reported that the knockout of Sox9 prior to MAPK

inhibition blocks the cells from entering a resistant state. What was peculiar was that SOX10 expression remained unchanged during our subacute treatment regimen in the Sox9 knockout cells. This finding further supports the hypothesis that SOX9, but not SOX10, may be the major regulator promoting the transition to the resistant state. However, one limitation to our study was the time course of the experiment. A subacute treatment regimen was used to test the importance of SOX9 on melanoma transitioning. Whether SOX9 promotes a delay or a complete block of the transition is still unknown. One important experiment that could shed light on this phenomenon would be the dual knockout of SOX9 and SOX10. This might address whether the inability to turn on SOX9 following SOX10 knockout could still drive cells to a therapy resistant state. Extensive genetic manipulations in vivo and in vitro will be required to address this.

5.5 The role of SOX9 and SOX10 as immunomodulators

Some reports have identified SOX9 as a major regulator of CEACAM1 gene expression. In the colon epithelium, SOX9 has been shown to promote CEACAM1 expression directly together with p300(294). On the contrary, another group has found that SOX9 represses CEACAM1 indirectly in human melanoma cell lines(293). This repression of *Sox9* elicited a resistance to cytotoxic lymphocyte killing in melanoma cells, connecting both CEACAM1 and SOX9 as modulators of immune-mediated cytotoxicity in melanoma(293). Our group and others have found that SOX10 can regulate both CEACAM1 and HVEM in melanoma (Chapter 4)(275). In addition, we have identified SOX10 as a direct regulator of CEACAM1. Furthermore, we find that not all SOX10 positive melanoma cells express CEACAM1 but all CEACAM1-positive melanoma cells express SOX10, in agreement with our findings. Interestingly, we find that the expression of SOX10 affects the ratio of CD3 positive T-cells in the tumour microenvironment. More specifically, it can promote CD4 T-cell infiltration over CD8, promoting overall tumour

growth in immunocompetent mice. Others have also shown that the knockout of SOX10 greatly reduces the tumour burden in immunocompetent mice versus immunocompromised, suggesting an immune suppression mechanism being solicited by SOX10 and potentially CEACAM1(275). Although it is believed that SOX10 marks a therapy sensitive state, these data suggest that it can also enhance immune suppression through a non canonical pathway.

T-cell infiltration varied depending on SOX10 expression, but the activity of these infiltrating T-cells and their subset is still unknown. We do observe decreased CD8 T-cell infiltration following overexpression of SOX10 with a decrease in CD4 T-cells. CD4 T-cells can be grouped into two major classes, the helper T-cells and regulatory T-cells (Tregs)(307). Tregs function in an immunosuppressive fashion where they can inhibit CD8 T-cell requirement and activity(307). Since we observe differing levels of CD4/CD8 T-cell infiltration dependent on SOX10 levels, Tregs could be playing a major role at inducing this T-cell switch within the tumour microenvironment and therefore should be a potential focus in future studies.

CEACAM1 knockout in SOX10-positive melanoma reduced overall tumour burden and prolonged survival in vivo(275). CEACAM1 can bind both in cis and trans with other isoforms of CEACAM1 eliciting different responses. Although we find that both long and short isoforms of CEACAM1 regulate T-cell infiltration in melanoma tumors, the short isoform has a more pronounced effect. Over-expression of the short isoform reduces CD8 T-cell infiltration, and CSC properties but enhances overall tumour burden. It is unknown why the shorter isoform induces more pronounced phenotypes but this could be due to 1) augmented dimerization with binding partners, 2) a shorter, more simplified intracellular tail, and/or 3) the overall levels of the CEACAM1 short isoform are higher. Surprisingly, expression of the CEACAM1 long isoform in our cell lines was found to be lethal. Therefore, we were unable to enrich for populations

expressing the CEACAM1 long isoform. It would be of interest to perform depletion experiments of various immune cells and assess CEACAM1-driven melanoma tumour growth, or whether a blocking antibody targeting CEACAM1 could potentially be used as a checkpoint blockade.

5.6 Cross-resistance phenomenon

Currently, the best treatment regimen for late-stage metastatic melanoma is dual therapy using MAPK inhibitors with ICIs. Various groups have shown that prior treatment with MAPK inhibitors reduces the overall response rate to immunotherapies (308–310). This was further validated using transcriptomics where tumours that were previously treated with MAPK inhibitors had a gene signature related to PD-1 therapy resistance (311). An in vivo study utilizing melanoma mouse tumours found that relapsed tumours post-MAPK inhibitor treatment had intrinsic resistance to both PD-1 and CTLA4 ICI treatment (312). This resistance was due to an immunosuppressive tumour microenvironment, inhibiting cytotoxic T cell function (312). Interestingly, one study correlated a SOX10 gene signature with the MAPK and ICI resistant state (198). Since targeted therapy resistance induces a cross resistance to ICI, we asked whether it could induce resistance to other therapies. We found that adaptively resistant melanoma cell lines also have a cross-resistant response to OVs, specifically VSVΔ51 (Figure 3.2). In agreement with previous findings, the loss of SOX10 recapitulates both MAPK inhibitor resistance and resistance to OVs (Figure 3.3). This transition to the resistant state through chronic MAPK inhibition or the loss of SOX10 both lead to an upregulation in ISGs, typically induced through the activation of the type I IFN response (Figure 3.4). The activation of the type I IFN response and the induction of ISGs has previously been shown to modulate the CSC pool in various cancer types. Our group and others have shown that the loss of SOX10 induces a more quiescent/dormant-like phenotype with enhanced progenitor-like properties(197). However, the ability of SOX10 to regulate these

ISGs has not been thoroughly characterized(313). One study focused on SOX10's ability to activate IRF4 (314). IRF4 represses IRF1, which becomes activated through the JAK1/2 pathway, allowing for the activation of various immunogenic receptors such as MHC class I, PD-L1 and PD-L2(314). Although IRF4 was not part of the various ISGs observed to be induced (Table 4.1), it does suggest that SOX10 plays a specific role in modulating an IFN response. It would be interesting to determine whether SOX10 re-expression in either the SOX10 knockout cells, or the targeted therapy resistant cells could re-sensitize the cells to OVs. Could the re-sensitization of one therapy indirectly lead to an increase in the efficacy other therapies? This could be further addressed using MAPK inhibitors.

5.7 Therapeutic strategies to treat SOX9 or SOX10 melanoma

Overall, we find that melanomas expressing SOX10 remain susceptible to MAPK inhibition and viral infection while the SOX9-positive melanoma cells tend to present with a resistant, more cancer stem-like state. Few studies have attempted to interfere with the MAPK resistant state. Capparelli et al. have found that cIAP is induced in SOX10-deficient melanoma cells (197). These SOX10-deficient cells have increased tolerance to the cIAP inhibitor, Birinapant (197). They also found that a treatment regimen that included BRAF, MEK, and cIAP inhibitors prolonged overall mouse survival and reduced tumour burden in comparison to MAPK inhibitors alone(315). When Birinapant was used following a treatment with MAPK inhibitors, the overall survival was not as favourable compared to when it was used in conjunction(315). We believe the proper course of action is to block what drives the loss of SOX10 or activation of SOX9 during the transition to the resistant state. Although counterintuitive, since SOX10 promotes the proliferative state, it will block the ability of the tumour to transition to a cross resistant state, allowing for prolonged sensitivity to the current standard of care.

5.8 Significance and Concluding Remarks

The ability of cancer cells to transition between a proliferative to invasive state has affected the efficacy of various forms of therapies in melanoma. Multiple studies have identified various markers depicting either a therapy resistant or sensitive state. Currently lacking, is our ability to identify which of these markers, if any, could drive cells to a more proliferative, therapy sensitive state. Here we have shown that SOX9, a key transcription factor found in most epithelial-like cancers, can block the intermediate transition of melanoma cells to a targeted therapy resistant condition. SOX10, another key marker shown to be lost during therapy resistance, remains expressed during this "failed" transition to the resistant state following the knockout of SOX9, supporting antagonistic regulation between these two proteins. However, it is still unclear how and why SOX9 and SOX10 become activated and lost, respectively, during this transition. Our Sox9-deficient model provides a system for the identification of regulators of this transition for therapeutic manipulation.

As melanomas transition to a targeted therapy resistant state, they undergo a genetic shift, activating and repressing different genes. This shift not only induces resistance to standard of care treatments but also causes cross resistance to other types of therapies. We have demonstrated that the transition following chronic vemurafenib treatment results in resistance to OVs, in particular, VSVΔ51. Interestingly, the loss of SOX10 alone can recapitulate this cross resistant state, decreasing sensitivity to MAPK inhibitors as well as VSV infection and propagation.

Lastly, we have linked the loss of SOX10 with the ability to increase the CSC properties of melanoma. It has been previously reported that SOX10 promotes progenitor-like activity during the initiation and propagation of melanoma. Here we show that SOX10 diminishes the CSC pool in already established melanoma cell lines, suggesting an early progenitor-like role for SOX10 that

is lost as melanoma is established. This loss in CSC properties is also driven through the expression of CEACAM1. SOX10 can drive CEACAM1 expression, where enrichment of CEACAM1 can diminish the CSC-like properties in vitro and in vivo. Finally, we have shown that modest SOX10/CEACAM1 expression represses CD8 T cell tumour infiltration increasing overall tumour burden. Enrichment for SOX10/CEACAM1, diminishes the tumour's CSC properties resulting in a loss of proliferation.

Overall, our data show an important role for SOX9 in a memory state imparted by chronic vemurafenib treatment. However, SOX10-expression is associated with cross sensitivity and melanoma self renewal. The ultimate therapeutic approach could involve blocking the induction of the Sox9-dependent network, maintaining SOX10 expression, drug sensitivity and reduced stem cell-like properties. Due to the elusive function of these proteins and the difficulty of targeting transcription factors, understanding their upstream regulators and downstream targets should be the primary focus of future work. Once uncovered, these novel pathways could allow for the development of new therapeutic approaches that could be used to halt or revert resistance in melanoma.

References

1. Grossman DC, Curry SJ, Owens DK, Barry MJ, Caughey AB, Davidson KW, et al. Behavioral Counseling to Prevent Skin Cancer: US Preventive Services Task Force Recommendation Statement. JAMA [Internet]. 2018 Mar 20 [cited 2024 Feb 9];319(11):1134–42. Available from: https://jamanetwork.com/journals/jama/fullarticle/2675556

2. Siegel RL, Miller KD, Jemal A. Cancer statistics, 2017. CA Cancer J Clin [Internet]. 2017 Jan [cited 2024 Feb 9];67(1):7–30. Available from: https://www.cancer.org/research/cancer-facts-statistics/all-cancer-facts-figures/cancer-facts-figures-2017.html

3. Rabbie R, Ferguson P, Molina-Aguilar C, Adams DJ, Robles-Espinoza CD. Melanoma subtypes: genomic profiles, prognostic molecular markers and therapeutic possibilities. J Pathol [Internet]. 2019 Apr 1 [cited 2024 Feb 9];247(5):539. Available from: /pmc/articles/PMC6492003/

4. Akbani R, Akdemir KC, Aksoy BA, Albert M, Ally A, Amin SB, et al. Genomic Classification of Cutaneous Melanoma. Cell [Internet]. 2015 Jun 6 [cited 2024 Feb 9];161(7):1681. Available from: /pmc/articles/PMC4580370/

5. Hayward NK, Wilmott JS, Waddell N, Johansson PA, Field MA, Nones K, et al. Whole-genome landscapes of major melanoma subtypes. Nature 2017 545:7653 [Internet]. 2017 May 3 [cited 2024 Feb 9];545(7653):175–80. Available from: https://www.nature.com/articles/nature22071

6. Kim SY, Kim SN, Hahn HJ, Lee YW, Choe YB, Ahn KJ. Metaanalysis of BRAF mutations and clinicopathologic characteristics in primary melanoma. J Am Acad Dermatol [Internet]. 2015 Jun 1 [cited 2024 Feb 9];72(6):1036-1046.e2. Available from: http://www.jaad.org/article/S0190962215013535/fulltext

7. Shain AH, Bastian BC. From melanocytes to melanomas. Nat Rev Cancer [Internet]. 2016 May 25 [cited 2024 Feb 9];16(6):345–58. Available from: https://pubmed.ncbi.nlm.nih.gov/27125352/

8. Lee JH, Choi JW, Kim YS. Frequencies of BRAF and NRAS mutations are different in histological types and sites of origin of cutaneous melanoma: a meta-analysis. British Journal of Dermatology [Internet]. 2011 Apr 1 [cited 2024 Feb 9];164(4):776–84. Available from: https://dx.doi.org/10.1111/j.1365-2133.2010.10185.x

9. Jakob JA, Bassett RL, Ng CS, Curry JL, Joseph RW, Alvarado GC, et al. NRAS Mutation Status is an Independent Prognostic Factor in Metastatic Melanoma. Cancer [Internet]. 2012 Aug 8 [cited 2024 Feb 9];118(16):4014. Available from: /pmc/articles/PMC3310961/

10. Klose A, Ahmadian MR, Schuelke M, Scheffzek K, Hoffmeyer S, Gewies A, et al. Selective disactivation of neurofibromin GAP activity in neurofibromatosis type 1. Hum Mol Genet [Internet]. 1998 Aug [cited 2024 Feb 9];7(8):1261–8. Available from: https://pubmed.ncbi.nlm.nih.gov/9668168/

11. Xia J, Jia P, Hutchinson KE, Dahlman KB, Johnson D, Sosman J, et al. A meta-analysis of somatic mutations from next generation sequencing of 241 melanomas: a road map for the study of

genes with potential clinical relevance. Mol Cancer Ther [Internet]. 2014 [cited 2024 Feb 9];13(7):1918. Available from: /pmc/articles/PMC4090262/

12. García-Gómez R, Bustelo XR, Crespo P. Protein-Protein Interactions: Emerging Oncotargets in the RAS-ERK Pathway. Trends Cancer [Internet]. 2018 Sep 1 [cited 2024 Feb 9];4(9):616–33. Available from: https://pubmed-ncbi-nlm-nih-gov.proxy.bib.uottawa.ca/30149880/

13. Guo YJ, Pan WW, Liu SB, Shen ZF, Xu Y, Hu LL. ERK/MAPK signalling pathway and tumorigenesis. Exp Ther Med [Internet]. 2020 Jan 15 [cited 2024 Feb 9];19(3):1997. Available from: /pmc/articles/PMC7027163/

14. Burotto M, Chiou VL, Lee JM, Kohn EC. The MAPK pathway across different malignancies: A new perspective. Cancer [Internet]. 2014 Nov 15 [cited 2024 Feb 9];120(22):3446–56. Available from: https://onlinelibrary.wiley.com/doi/full/10.1002/cncr.28864

15. Braicu C, Buse M, Busuioc C, Drula R, Gulei D, Raduly L, et al. A Comprehensive Review on MAPK: A Promising Therapeutic Target in Cancer. Cancers (Basel) [Internet]. 2019 Oct 1 [cited 2024 Feb 9];11(10):1618. Available from: /pmc/articles/PMC6827047/

16. Leicht DT, Balan V, Kaplun A, Singh-Gupta V, Kaplun L, Dobson M, et al. Raf Kinases: Function, Regulation and Role in Human Cancer. Biochim Biophys Acta [Internet]. 2007 Aug [cited 2024 Feb 9];1773(8):1196. Available from: /pmc/articles/PMC1986673/

17. Cook FA, Cook SJ. Inhibition of RAF dimers: it takes two to tango. Biochem Soc Trans [Internet]. 2021 Feb 2 [cited 2024 Feb 9];49(1):237. Available from: /pmc/articles/PMC7924995/

18. Herrmann C, Martin GA, Wittinghofer A. Quantitative analysis of the complex between p21ras and the Ras-binding domain of the human Raf-1 protein kinase. J Biol Chem [Internet]. 1995 Feb 17 [cited 2024 Feb 9];270(7):2901–5. Available from: https://pubmed.ncbi.nlm.nih.gov/7852367/

19. Li S, Jang H, Zhang J, Nussinov R. Raf-1 Cysteine-Rich Domain Increases the Affinity of K-Ras/Raf at the Membrane, Promoting MAPK Signaling. Structure [Internet]. 2018 Mar 6 [cited 2024 Feb 9];26(3):513-525.e2. Available from: https://pubmed.ncbi.nlm.nih.gov/29429878/

20. Fischer A, Baljuls A, Reinders J, Nekhoroshkova E, Sibilski C, Metz R, et al. Regulation of RAF activity by 14-3-3 proteins: RAF kinases associate functionally with both homo- and heterodimeric forms of 14-3-3 proteins. J Biol Chem [Internet]. 2009 Jan 30 [cited 2024 Feb 9];284(5):3183–94. Available from: https://pubmed.ncbi.nlm.nih.gov/19049963/

21. Avruch't J, &iokhlatchev A, Kyriakis JM, Luol Z, Tziviont G, Vavvas~ D, et al. Ras Activation of the Raf Kinase: Tyrosine Kinase Recruitment of the MAP Kinase Cascade. 2001;

22. Chong H, Lee J, Guan KL. Positive and negative regulation of Raf kinase activity and function by phosphorylation. EMBO J [Internet]. 2001 Jul 7 [cited 2024 Feb 9];20(14):3716. Available from: /pmc/articles/PMC125532/

23. Davies H, Bignell GR, Cox C, Stephens P, Edkins S, Clegg S, et al. Mutations of the BRAF gene in human cancer. Nature [Internet]. 2002 Jun 27 [cited 2024 Feb 9];417(6892):949–54. Available from: https://pubmed.ncbi.nlm.nih.gov/12068308/

24. Emuss V, Garnett M, Mason C, Marais R. Mutations of C-RAF are rare in human cancer because C-RAF has a low basal kinase activity compared with B-RAF. Cancer Res [Internet]. 2005 Nov 1 [cited 2024 Feb 9];65(21):9719–26. Available from: https://pubmed.ncbi.nlm.nih.gov/16266992/

25. Mason CS, Springer CJ, Cooper RG, Superti-Furga G, Marshall CJ, Marais R. Serine and tyrosine phosphorylations cooperate in Raf-1, but not B-Raf activation. EMBO J [Internet]. 1999 Apr 15 [cited 2024 Feb 9];18(8):2137–48. Available from: https://pubmed.ncbi.nlm.nih.gov/10205168/

26. Marais R, Light Y, Paterson HF, Mason CS, Marshall CJ. Differential regulation of Raf-1, A-Raf, and B-Raf by oncogenic ras and tyrosine kinases. J Biol Chem [Internet]. 1997 [cited 2024 Feb 9];272(7):4378–83. Available from: https://pubmed.ncbi.nlm.nih.gov/9020159/

27. Nan X, Collisson EA, Lewis S, Huang J, Tamgüney TM, Liphardt JT, et al. Single-molecule superresolution imaging allows quantitative analysis of RAF multimer formation and signaling. Proc Natl Acad Sci U S A [Internet]. 2013 Nov 12 [cited 2024 Feb 9];110(46):18519–24. Available from: /pmc/articles/PMC3831949/

28. Nassar N, Horn G, Herrmann CA, Scherer A, McCormick F, Wittinghofer A. The 2.2 A crystal structure of the Ras-binding domain of the serine/threonine kinase c-Raf1 in complex with Rap1A and a GTP analogue. Nature [Internet]. 1995 [cited 2024 Feb 9];375(6532):554–60. Available from: https://pubmed.ncbi.nlm.nih.gov/7791872/

29. Ghosh S, Strum JC, Sciorra VA, Daniel L, Bell RM. Raf-1 kinase possesses distinct binding domains for phosphatidylserine and phosphatidic acid. Phosphatidic acid regulates the translocation of Raf-1 in 12-O-tetradecanoylphorbol-13-acetate-stimulated Madin-Darby canine kidney cells. J Biol Chem [Internet]. 1996 Apr 5 [cited 2024 Feb 9];271(14):8472–80. Available from: https://pubmed.ncbi.nlm.nih.gov/8626548/

30. Roy S, Lane A, Yan J, McPherson R, Hancock JF. Activity of plasma membrane-recruited Raf-1 is regulated by Ras via the Raf zinc finger. J Biol Chem [Internet]. 1997 Aug 8 [cited 2024 Feb 9];272(32):20139–45. Available from: https://pubmed.ncbi.nlm.nih.gov/9242688/

31. Cutler RE, Stephens RM, Saracino MR, Morrison DK. Autoregulation of the Raf-1 serine/threonine kinase. Proc Natl Acad Sci U S A [Internet]. 1998 Aug 8 [cited 2024 Feb 9];95(16):9214. Available from: /pmc/articles/PMC21318/

32. Zhang M, Maloney R, Jang H, Nussinov R. The mechanism of Raf activation through dimerization. Chem Sci [Internet]. 2021 Dec 12 [cited 2024 Feb 9];12(47):15609. Available from: /pmc/articles/PMC8654025/

33. Cook FA, Cook SJ. Inhibition of RAF dimers: it takes two to tango. Biochem Soc Trans [Internet]. 2021 Feb 2 [cited 2024 Feb 9];49(1):237. Available from: /pmc/articles/PMC7924995/

34. Rommel C, Radziwill G, Lovrić J, Noeldeke J, Heinicke T, Jones D, et al. Activated Ras displaces 14-3-3 protein from the amino terminus of c-Raf-1. Oncogene [Internet]. 1996 Feb 1 [cited 2024 Feb 9];12(3):609–19. Available from: https://europepmc.org/article/med/8637718

35. McPherson RA, Harding A, Sandrine R, Lane A, Hancock JF. Interactions of c-Raf-1 with phosphatidylserine and 14-3-3. Oncogene [Internet]. 1999 Jul 1 [cited 2024 Feb 9];18(26):3862–9. Available from: https://pubmed.ncbi.nlm.nih.gov/10445849/

36. Terrell EM, Morrison DK. Ras-Mediated Activation of the Raf Family Kinases. Cold Spring Harb Perspect Med [Internet]. 2019 Jan 1 [cited 2024 Feb 9];9(1). Available from: /pmc/articles/PMC6311149/

37. Matallanas D, Birtwistle M, Romano D, Zebisch A, Rauch J, von Kriegsheim A, et al. Raf Family Kinases: Old Dogs Have Learned New Tricks. Genes Cancer [Internet]. 2011 Mar 1 [cited 2024 Feb 9];2(3):232. Available from: /pmc/articles/PMC3128629/

38. Garnett MJ, Marais R. Guilty as charged: B-RAF is a human oncogene. Cancer Cell [Internet]. 2004 [cited 2024 Feb 9];6(4):313–9. Available from: https://pubmed.ncbi.nlm.nih.gov/15488754/

39. Wan PTC, Garnett MJ, Roe SM, Lee S, Niculescu-Duvaz D, Good VM, et al. Mechanism of activation of the RAF-ERK signaling pathway by oncogenic mutations of B-RAF. Cell [Internet]. 2004 Mar 19 [cited 2024 Feb 9];116(6):855–67. Available from: https://pubmed.ncbi.nlm.nih.gov/15035987/

40. Brummer T, Naegele H, Reth M, Misawa Y. Identification of novel ERK-mediated feedback phosphorylation sites at the C-terminus of B-Raf. Oncogene [Internet]. 2003 Dec 4 [cited 2024 Feb 11];22(55):8823–34. Available from: https://pubmed.ncbi.nlm.nih.gov/14654779/

41. Yao Z, Torres NM, Tao A, Gao Y, Luo L, Li Q, et al. BRAF Mutants Evade ERK-Dependent Feedback by Different Mechanisms that Determine Their Sensitivity to Pharmacologic Inhibition. Cancer Cell [Internet]. 2015 Sep 14 [cited 2024 Feb 11];28(3):370–83. Available from: https://pubmed.ncbi.nlm.nih.gov/26343582/

42. Patton EE, Widlund HR, Kutok JL, Kopani KR, Amatruda JF, Murphey RD, et al. BRAF mutations are sufficient to promote nevi formation and cooperate with p53 in the genesis of melanoma. Curr Biol [Internet]. 2005 Feb 8 [cited 2024 Feb 9];15(3):249–54. Available from: https://pubmed.ncbi.nlm.nih.gov/15694309/

43. Dhomen N, Reis-Filho JS, da Rocha Dias S, Hayward R, Savage K, Delmas V, et al. Oncogenic Braf induces melanocyte senescence and melanoma in mice. Cancer Cell [Internet]. 2009 Apr 7 [cited 2024 Feb 9];15(4):294–303. Available from: https://pubmed.ncbi.nlm.nih.gov/19345328/

44. Goel VK, Ibrahim N, Jiang G, Singhal M, Fee S, Flotte T, et al. Melanocytic nevus-like hyperplasia and melanoma in transgenic BRAFV600E mice. Oncogene [Internet]. 2009 Jun 6 [cited 2024 Feb 9];28(23):2289. Available from: /pmc/articles/PMC3125533/

45. Michaloglou C, Vredeveld LCW, Soengas MS, Denoyelle C, Kuilman T, Van Der Horst CMAM, et al. BRAFE600-associated senescence-like cell cycle arrest of human naevi. Nature [Internet]. 2005 Aug 4 [cited 2024 Feb 9];436(7051):720–4. Available from: https://pubmed.ncbi.nlm.nih.gov/16079850/

46. Dankort D, Curley DP, Cartlidge RA, Nelson B, Karnezis AN, Damsky WE, et al. BRafV600E cooperates with Pten silencing to elicit metastatic melanoma. Nat Genet [Internet]. 2009 May [cited 2024 Feb 9];41(5):544. Available from: /pmc/articles/PMC2705918/

47. Damsky W, Micevic G, Meeth K, Muthusamy V, Curley DP, Santhanakrishnan M, et al. mTORC1 activation blocks BrafV600E-induced growth arrest but is insufficient for melanoma formation. Cancer Cell [Internet]. 2015 [cited 2024 Feb 9];27(1):41–56. Available from: https://pubmed.ncbi.nlm.nih.gov/25584893/

48. Kuzu OF, Nguyen FD, Noory MA, Sharma A. Current State of Animal (Mouse) Modeling in Melanoma Research. Cancer Growth Metastasis [Internet]. 2015 Jan [cited 2024 Feb 9];8(Suppl 1):81. Available from: /pmc/articles/PMC4597587/

49. Kim H, Kim M, Im SK, Fang S. Mouse Cre-LoxP system: general principles to determine tissue-specific roles of target genes. Lab Anim Res [Internet]. 2018 Oct 1 [cited 2024 Feb 9];34(4):147. Available from: /pmc/articles/PMC6333611/

50. Meeth K, Wang JX, Micevic G, Damsky W, Bosenberg MW. The YUMM lines: a series of congenic mouse melanoma cell lines with defined genetic alterations. Pigment Cell Melanoma Res. 2016 Sep 1;29(5):590–7.

51. Padma VV. An overview of targeted cancer therapy. Biomedicine (Taipei) [Internet]. 2015 Dec 1 [cited 2024 Feb 9];5(4):1–6. Available from: /pmc/articles/PMC4662664/

52. Carter P, Presta L, Gorman CM, Ridgway JBB, Henner D, Wong WLT, et al. Humanization of an anti-p185HER2 antibody for human cancer therapy. Proceedings of the National Academy of Sciences [Internet]. 1992 May 15 [cited 2024 Feb 9];89(10):4285–9. Available from: https://www.pnas.org/doi/abs/10.1073/pnas.89.10.4285

53. Druker BJ, Tamura S, Buchdunger E, Ohno S, Segal GM, Fanning S, et al. Effects of a selective inhibitor of the Abl tyrosine kinase on the growth of Bcr-Abl positive cells. Nat Med [Internet]. 1996 [cited 2024 Feb 9];2(5):561–6. Available from: https://pubmed.ncbi.nlm.nih.gov/8616716/

54. Zimmermann J, Buchdunger E, Mett H, Meyer T, Lydon NB. Potent and selective inhibitors of the Abl-kinase: phenylamino-pyrimidine (PAP) derivatives. Bioorg Med Chem Lett. 1997 Jan 21;7(2):187–92.

55. Khattak M, Fisher R, Turajlic S, Larkin J. Targeted therapy and immunotherapy in advanced melanoma: an evolving paradigm. Ther Adv Med Oncol [Internet]. 2013 [cited 2024 Feb 9];5(2):105. Available from: /pmc/articles/PMC3556874/

56. Tsai J, Lee JT, Wang W, Zhang J, Cho H, Mamo S, et al. From the Cover: Discovery of a selective inhibitor of oncogenic B-Raf kinase with potent antimelanoma activity. Proc Natl Acad Sci U S A [Internet]. 2008 Feb 2 [cited 2024 Feb 9];105(8):3041. Available from: /pmc/articles/PMC2268581/

57. Bollag G, Hirth P, Tsai J, Zhang J, Ibrahim PN, Cho H, et al. Clinical efficacy of a RAF inhibitor needs broad target blockade in BRAF-mutant melanoma. Nature [Internet]. 2010 Sep 9 [cited 2024 Feb 9];467(7315):596. Available from: /pmc/articles/PMC2948082/

58. Yang H, Higgins B, Kolinsky K, Packman K, Go Z, Iyer R, et al. RG7204 (PLX4032), a selective BRAFV600E inhibitor, displays potent antitumor activity in preclinical melanoma models. Cancer Res [Internet]. 2010 Jul 1 [cited 2024 Feb 9];70(13):5518–27. Available from: https://pubmed-ncbi-nlm-nih-gov.proxy.bib.uottawa.ca/20551065/

59. Søndergaard JN, Nazarian R, Wang Q, Guo D, Hsueh T, Mok S, et al. Differential sensitivity of melanoma cell lines with BRAFV600Emutation to the specific Raf inhibitor PLX4032. J Transl Med [Internet]. 2010 Apr 20 [cited 2024 Feb 9];8(1):1–11. Available from: https://translational-medicine-biomedcentral-com.proxy.bib.uottawa.ca/articles/10.1186/1479-5876-8-39

60. Lee JT, Li L, Brafford PA, Van Den Eijnden M, Halloran MB, Sproesser K, et al. PLX4032, a potent inhibitor of the B-Raf V600E oncogene, selectively inhibits V600E-positive melanomas. Pigment Cell Melanoma Res [Internet]. 2010 Dec 1 [cited 2024 Feb 9];23(6):820–7. Available from: https://onlinelibrary-wiley-com.proxy.bib.uottawa.ca/doi/full/10.1111/j.1755-148X.2010.00763.x

61. Joseph EW, Pratilas CA, Poulikakos PI, Tadi M, Wang W, Taylor BS, et al. The RAF inhibitor PLX4032 inhibits ERK signaling and tumor cell proliferation in a V600E BRAF-selective manner. Proc Natl Acad Sci U S A [Internet]. 2010 Aug 17 [cited 2024 Feb 9];107(33):14903–8. Available from: https://www-pnas-org.proxy.bib.uottawa.ca/doi/abs/10.1073/pnas.1008990107

62. Flaherty KT, Puzanov I, Kim KB, Ribas A, McArthur GA, Sosman JA, et al. Inhibition of Mutated, Activated BRAF in Metastatic Melanoma. N Engl J Med [Internet]. 2010 Aug 8 [cited 2024 Feb 9];363(9):809. Available from: /pmc/articles/PMC3724529/

63. Sosman JA, Kim KB, Schuchter L, Gonzalez R, Pavlick AC, Weber JS, et al. Survival in BRAF V600-mutant advanced melanoma treated with vemurafenib. N Engl J Med [Internet]. 2012 Feb 23 [cited 2024 Feb 9];366(8):707–14. Available from: https://pubmed.ncbi.nlm.nih.gov/22356324/

64. Chapman PB, Hauschild A, Robert C, Haanen JB, Ascierto P, Larkin J, et al. Improved survival with vemurafenib in melanoma with BRAF V600E mutation. N Engl J Med [Internet]. 2011 Jun 30 [cited 2024 Feb 9];364(26):2507–16. Available from: https://pubmed.ncbi.nlm.nih.gov/21639808/

65. Arozarena I, Wellbrock C. Overcoming resistance to BRAF inhibitors. Ann Transl Med. 2017 Oct 1;5(19):1–12.

66. Qin S, Xu L, Yi M, Yu S, Wu K, Luo S. Novel immune checkpoint targets: moving beyond PD-1 and CTLA-4. Mol Cancer [Internet]. 2019 Nov 6 [cited 2024 Feb 9];18(1). Available from: /pmc/articles/PMC6833286/

67. Hodi FS, O'Day SJ, McDermott DF, Weber RW, Sosman JA, Haanen JB, et al. Improved survival with ipilimumab in patients with metastatic melanoma. N Engl J Med [Internet]. 2010 Aug 19 [cited 2024 Feb 9];363(8):711–23. Available from: https://pubmed.ncbi.nlm.nih.gov/20525992/

68. Robert C, Long G V., Brady B, Dutriaux C, Maio M, Mortier L, et al. Nivolumab in previously untreated melanoma without BRAF mutation. N Engl J Med [Internet]. 2015 Jan 22 [cited 2024 Feb 9];372(4):320–30. Available from: https://pubmed.ncbi.nlm.nih.gov/25399552/

69. Ascierto PA, Long G V., Robert C, Brady B, Dutriaux C, Di Giacomo AM, et al. Survival Outcomes in Patients With Previously Untreated BRAF Wild-Type Advanced Melanoma Treated With Nivolumab Therapy: Three-Year Follow-up of a Randomized Phase 3 Trial. JAMA Oncol [Internet]. 2019 Feb 1 [cited 2024 Feb 9];5(2):187–94. Available from: https://pubmed.ncbi.nlm.nih.gov/30422243/

70. Cooper ZA, Juneja VR, Sage PT, Frederick DT, Piris A, Mitra D, et al. Response to BRAF inhibition in melanoma is enhanced when combined with immune checkpoint blockade. Cancer Immunol Res [Internet]. 2014 Jul 1 [cited 2024 Feb 9];2(7):643–54. Available from: https://pubmed.ncbi.nlm.nih.gov/24903021/

71. Gutzmer R, Stroyakovskiy D, Gogas H, Robert C, Lewis K, Protsenko S, et al. Atezolizumab, vemurafenib, and cobimetinib as first-line treatment for unresectable advanced BRAFV600 mutation-positive melanoma (IMspire150): primary analysis of the randomised, double-blind, placebo-controlled, phase 3 trial. Lancet [Internet]. 2020 Jun 13 [cited 2024 Feb 9];395(10240):1835–44. Available from: https://pubmed.ncbi.nlm.nih.gov/32534646/

72. Thornton J, Chhabra G, Singh CK, Guzmán-Pérez G, Shirley CA, Ahmad N. Mechanisms of Immunotherapy Resistance in Cutaneous Melanoma: Recognizing a Shapeshifter. Front Oncol [Internet]. 2022 Apr 19 [cited 2024 Feb 9];12:880876. Available from: www.frontiersin.org

73. Hamid O, Weise A, Kim TM, Mckean M, Lakhani N, Crown J, et al. 400P Phase I study of fianlimab, a human lymphocyte activation gene-3 (LAG-3) monoclonal antibody, in combination with cemiplimab in advanced melanoma (mel). Annals of Oncology [Internet]. 2022 Nov 1 [cited 2024 Apr 14];33:S1598. Available from: http://www.annalsofoncology.org/article/S0923753422046221/fulltext

74. Hamid O, Lewis KD, Weise AM, McKean M, Papadopoulos KP, Crown J, et al. Significant durable response with fianlimab (anti-LAG-3) and cemiplimab (anti-PD-1) in advanced melanoma: Post adjuvant PD-1 analysis. https://doi.org/101200/JCO20234116_suppl9501 [Internet]. 2023 May 31 [cited 2024 Apr 14];41(16_suppl):9501–9501. Available from: https://ascopubs.org/doi/10.1200/JCO.2023.41.16_suppl.9501

75. Mooradian MJ, Sullivan RJ. Immunotherapy in Melanoma: Recent Advancements and Future Directions. Cancers (Basel) [Internet]. 2023 Aug 1 [cited 2024 Apr 14];15(16). Available from: /pmc/articles/PMC10452647/

76. Rohaan MW, Borch TH, van den Berg JH, Met Ö, Kessels R, Geukes Foppen MH, et al. Tumor-Infiltrating Lymphocyte Therapy or Ipilimumab in Advanced Melanoma. N Engl J Med [Internet]. 2022 Dec 8 [cited 2024 Apr 14];387(23):2113–25. Available from: https://pubmed.ncbi.nlm.nih.gov/36477031/

77. Bommareddy PK, Patel A, Hossain S, Kaufman HL. Talimogene Laherparepvec (T-VEC) and Other Oncolytic Viruses for the Treatment of Melanoma. Am J Clin Dermatol [Internet]. 2017 Feb 1 [cited 2024 Feb 7];18(1):1. Available from: /pmc/articles/PMC8977104/

78. Kohlhapp FJ, Kaufman HL. Molecular pathways: Mechanism of action for talimogene laherparepvec, a new oncolytic virus immunotherapy. Clinical Cancer Research [Internet]. 2016

Mar 1 [cited 2024 Feb 7];22(5):1048–54. Available from: /clincancerres/article/22/5/1048/79756/Molecular-Pathways-Mechanism-of-Action-for

79. Knipe D, Rose JK, Lodish HF. Translation of individual species of vesicular stomatitis viral mRNA. J Virol [Internet]. 1975 Apr [cited 2024 Feb 7];15(4):1004. Available from: /pmc/articles/PMC354545/?report=abstract

80. Knipe DM, Baltimore D, Lodish HF. Separate pathways of maturation of the major structural proteins of vesicular stomatitis virus. J Virol [Internet]. 1977 Mar [cited 2024 Feb 7];21(3):1128. Available from: /pmc/articles/PMC515654/?report=abstract

81. Cartwright B, Brown F. Serological relationships between different strains of vesicular stomatis virus. J Gen Virol [Internet]. 1972 Sep 1 [cited 2024 Feb 7];16(3):391–8. Available from: https://www.microbiologyresearch.org/content/journal/jgv/10.1099/0022-1317-16-3-391

82. McNab F, Mayer-Barber K, Sher A, Wack A, O'Garra A. Type I interferons in infectious disease. Nat Rev Immunol [Internet]. 2015 Jan 23 [cited 2024 Feb 9];15(2):87–103. Available from: https://pubmed.ncbi.nlm.nih.gov/25614319/

83. Blackham AU, Northrup SA, Willingham M, D'Agostino RB, Lyles DS, Stewart JH. Variation in susceptibility of human malignant melanomas to oncolytic vesicular stomatitis virus. Surgery [Internet]. 2013 Mar [cited 2023 Aug 23];153(3):333–43. Available from: https://pubmed.ncbi.nlm.nih.gov/23102637/

84. Nguyen TT, Ramsay LA, Ahanfeshar-Adams M, Lajoie M, Schadendorf D, Alain T, et al. Mutations in the IFNγ-JAK-STAT pathway causing resistance to immune checkpoint inhibitors in melanoma increase sensitivity to oncolytic virus treatment. Clinical Cancer Research [Internet]. 2021 Jun 1 [cited 2023 Aug 30];27(12):3432–42. Available from: https://dx.doi.org/10.1158/1078-0432.CCR-20-3365

85. Nazarian R, Shi H, Wang Q, Kong X, Koya RC, Lee H, et al. Melanomas acquire resistance to B-RAF(V600E) inhibition by RTK or N-RAS upregulation. Nature [Internet]. 2010 Dec 16 [cited 2024 Feb 9];468(7326):973–7. Available from: https://pubmed.ncbi.nlm.nih.gov/21107323/

86. Villanueva J, Vultur A, Lee JT, Somasundaram R, Fukunaga-Kalabis M, Cipolla AK, et al. Acquired resistance to BRAF inhibitors mediated by a RAF kinase switch in melanoma can be overcome by co-targeting MEK and IGF-1R/PI3K. Cancer Cell [Internet]. 2010 Dec 12 [cited 2024 Feb 9];18(6):683. Available from: /pmc/articles/PMC3026446/

87. Girotti MR, Pedersen M, Sanchez-Laorden B, Viros A, Turajlic S, Niculescu-Duvaz D, et al. Inhibiting EGF receptor or SRC family kinase signaling overcomes BRAF inhibitor resistance in melanoma. Cancer Discov [Internet]. 2013 [cited 2024 Feb 9];3(2):158. Available from: /pmc/articles/PMC5321574/

88. Long G V., Weber JS, Infante JR, Kim KB, Daud A, Gonzalez R, et al. Overall Survival and Durable Responses in Patients With BRAF V600-Mutant Metastatic Melanoma Receiving Dabrafenib Combined With Trametinib. J Clin Oncol [Internet]. 2016 Mar 10 [cited 2024 Feb 9];34(8):871–8. Available from: https://pubmed.ncbi.nlm.nih.gov/26811525/

89. Johnson DB, Flaherty KT, Weber JS, Infante JR, Kim KB, Kefford RF, et al. Combined BRAF (Dabrafenib) and MEK inhibition (Trametinib) in patients with BRAFV600-mutant melanoma experiencing progression with single-agent BRAF inhibitor. J Clin Oncol [Internet]. 2014 Nov 20 [cited 2024 Feb 9];32(33):3697–704. Available from: https://pubmed.ncbi.nlm.nih.gov/25287827/

90. Ribas A, Gonzalez R, Pavlick A, Hamid O, Gajewski TF, Daud A, et al. Combination of vemurafenib and cobimetinib in patients with advanced BRAF(V600)-mutated melanoma: a phase 1b study. Lancet Oncol [Internet]. 2014 [cited 2024 Feb 9];15(9):954–65. Available from: https://pubmed.ncbi.nlm.nih.gov/25037139/

91. Ascierto PA, McArthur GA, Dréno B, Atkinson V, Liszkay G, Di Giacomo AM, et al. Cobimetinib combined with vemurafenib in advanced BRAF(V600)-mutant melanoma (coBRIM): updated efficacy results from a randomised, double-blind, phase 3 trial. Lancet Oncol [Internet]. 2016 Sep 1 [cited 2024 Feb 9];17(9):1248–60. Available from: https://pubmed.ncbi.nlm.nih.gov/27480103/

92. Grob JJ, Amonkar MM, Karaszewska B, Schachter J, Dummer R, Mackiewicz A, et al. Comparison of dabrafenib and trametinib combination therapy with vemurafenib monotherapy on health-related quality of life in patients with unresectable or metastatic cutaneous BRAF Val600-mutation-positive melanoma (COMBI-v): results of a phase 3, open-label, randomised trial. Lancet Oncol [Internet]. 2015 [cited 2024 Feb 9];16(13):1389–98. Available from: https://pubmed.ncbi.nlm.nih.gov/26433819/

93. Schadendorf D, Amonkar MM, Stroyakovskiy D, Levchenko E, Gogas H, De Braud F, et al. Health-related quality of life impact in a randomised phase III study of the combination of dabrafenib and trametinib versus dabrafenib monotherapy in patients with BRAF V600 metastatic melanoma. Eur J Cancer [Internet]. 2015 May 1 [cited 2024 Feb 9];51(7):833–40. Available from: https://pubmed.ncbi.nlm.nih.gov/25794603/

94. Van Allen EM, Wagle N, Sucker A, Treacy DJ, Johannessen CM, Goetz EM, et al. The genetic landscape of clinical resistance to RAF inhibition in metastatic melanoma. Cancer Discov [Internet]. 2014 Jan [cited 2024 Feb 9];4(1):94. Available from: /pmc/articles/PMC3947264/

95. Wagle N, Emery C, Berger MF, Davis MJ, Sawyer A, Pochanard P, et al. Dissecting Therapeutic Resistance to RAF Inhibition in Melanoma by Tumor Genomic Profiling. Journal of Clinical Oncology [Internet]. 2011 Aug 8 [cited 2024 Feb 9];29(22):3085. Available from: /pmc/articles/PMC3157968/

96. Poulikakos PI, Persaud Y, Janakiraman M, Kong X, Ng C, Moriceau G, et al. RAF inhibitor resistance is mediated by dimerization of aberrantly spliced BRAF(V600E). Nature [Internet]. 2011 Dec 15 [cited 2024 Feb 9];480(7377):387–90. Available from: https://pubmed.ncbi.nlm.nih.gov/22113612/

97. Shi H, Moriceau G, Kong X, Lee MK, Lee H, Koya RC, et al. Melanoma whole exome sequencing identifies V600EB-RAF amplification-mediated acquired B-RAF inhibitor resistance. Nat Commun [Internet]. 2012 Mar 6 [cited 2024 Feb 9];3:724. Available from: /pmc/articles/PMC3530385/

98. Paraiso KHT, Xiang Y, Rebecca VW, Abel E V., Chen YA, Munko AC, et al. PTEN loss confers BRAF inhibitor resistance to melanoma cells through the suppression of BIM expression. Cancer Res [Internet]. 2011 Apr 4 [cited 2024 Feb 9];71(7):2750. Available from: /pmc/articles/PMC3070772/

99. Shi H, Hong A, Kong X, Koya RC, Song C, Moriceau G, et al. A novel AKT1 mutant amplifies an adaptive melanoma response to BRAF inhibition. Cancer Discov [Internet]. 2014 Jan [cited 2024 Feb 9];4(1):69. Available from: /pmc/articles/PMC3893054/

100. Jain A, Tripathi R, Turpin CP, Wang C, Plattner R. Abl kinase regulation by BRAF/ERK and cooperation with Akt in melanoma. Oncogene [Internet]. 2017 Aug 10 [cited 2024 Feb 9];36(32):4585–96. Available from: https://pubmed.ncbi.nlm.nih.gov/28368422/

101. Perna D, Karreth FA, Rust AG, Perez-Mancera PA, Rashid M, Iorioc F, et al. BRAF inhibitor resistance mediated by the AKT pathway in an oncogenic BRAF mouse melanoma model. Proc Natl Acad Sci U S A [Internet]. 2015 Feb 10 [cited 2024 Feb 9];112(6):E536–45. Available from: https://pubmed.ncbi.nlm.nih.gov/25624498/

102. Hartsough E, Shao Y, Aplin AE. Resistance to RAF inhibitors revisited. J Invest Dermatol [Internet]. 2014 [cited 2024 Feb 9];134(2):319. Available from: /pmc/articles/PMC3947111/

103. Proietti I, Skroza N, Bernardini N, Tolino E, Balduzzi V, Marchesiello A, et al. Mechanisms of Acquired BRAF Inhibitor Resistance in Melanoma: A Systematic Review. Cancers (Basel) [Internet]. 2020 Oct 1 [cited 2024 Feb 9];12(10):1–29. Available from: /pmc/articles/PMC7600801/

104. Prasetyanti PR, Medema JP. Intra-tumor heterogeneity from a cancer stem cell perspective. Mol Cancer [Internet]. 2017 Feb 16 [cited 2024 Feb 9];16(1). Available from: /pmc/articles/PMC5314464/

105. Andor N, Graham TA, Jansen M, Xia LC, Aktipis CA, Petritsch C, et al. Pan-cancer analysis of the extent and consequences of intra-tumor heterogeneity. Nat Med [Internet]. 2016 Jan 1 [cited 2024 Feb 9];22(1):105. Available from: /pmc/articles/PMC4830693/

106. Ding L, Kim M, Kanchi KL, Dees ND, Lu C, Griffith M, et al. Clonal Architectures and Driver Mutations in Metastatic Melanomas. PLoS One [Internet]. 2014 Nov 13 [cited 2024 Feb 9];9(11):111153. Available from: /pmc/articles/PMC4230926/

107. Held MA, Curley DP, Dankort D, McMahon M, Muthusamy V, Bosenberg MW. Characterization of Melanoma Cells Capable of Propagating Tumors from a Single Cell. Cancer Res [Internet]. 2010 Jan 1 [cited 2024 Jan 28];70(1):388. Available from: /pmc/articles/PMC4026296/

108. Gedye C, Quirk J, Browning J, Svobodová S, John T, Sluka P, et al. Cancer/testis antigens can be immunological targets in clonogenic CD133+ melanoma cells. Cancer Immunology, Immunotherapy [Internet]. 2009 Oct 17 [cited 2024 Jan 28];58(10):1635–46. Available from: https://link.springer.com/article/10.1007/s00262-009-0672-0

109. Santini R, Vinci MC, Pandolfi S, Penachioni JY, Montagnani V, Olivito B, et al. Hedgehog-GLI signaling drives self-renewal and tumorigenicity of human melanoma-initiating cells. Stem Cells

[Internet]. 2012 Sep [cited 2024 Jan 28];30(9):1808–18. Available from: https://pubmed.ncbi.nlm.nih.gov/22730244/

110. Santini R, Pietrobono S, Pandolfi S, Montagnani V, D'Amico M, Penachioni JY, et al. SOX2 regulates self-renewal and tumorigenicity of human melanoma-initiating cells. Oncogene. 2014 Sep 18;33(38):4697–708.

111. Civenni G, Walter A, Kobert N, Mihic-Probst D, Zipser M, Belloni B, et al. Human CD271-positive melanoma stem cells associated with metastasis establish tumor heterogeneity and long-term growth. Cancer Res [Internet]. 2011 Apr 15 [cited 2024 Jan 28];71(8):3098–109. Available from: https://pubmed.ncbi.nlm.nih.gov/21393506/

112. Speigl L, Janssen N, Weide B, Sinnberg T, Pawelec G, Shipp C. Putative Cancer Stem Cell Markers are Frequently Expressed by Melanoma Cells in Vitro and in Situ but are also Present in Benign Differentiated Cells. Front Biosci (Landmark Ed) [Internet]. 2023 [cited 2024 Feb 9];28(9). Available from: https://pubmed.ncbi.nlm.nih.gov/37796710/

113. Civenni G, Walter A, Kobert N, Mihic-Probst D, Zipser M, Belloni B, et al. Human CD271-positive melanoma stem cells associated with metastasis establish tumor heterogeneity and long-term growth. Cancer Res [Internet]. 2011 Apr 15 [cited 2024 Feb 3];71(8):3098–109. Available from: https://pubmed.ncbi.nlm.nih.gov/21393506/

114. Quintana E, Shackleton M, Sabel MS, Fullen DR, Johnson TM, Morrison SJ. Efficient tumor formation by single human melanoma cells. Nature [Internet]. 2008 Dec 12 [cited 2024 Jan 28];456(7222):593. Available from: /pmc/articles/PMC2597380/

115. Quintana E, Shackleton M, Foster HR, Fullen DR, Sabel MS, Johnson TM, et al. Phenotypic heterogeneity among tumorigenic melanoma cells from patients that is reversible and not hierarchically organized. Cancer Cell [Internet]. 2010 Nov 11 [cited 2024 Jan 28];18(5):510. Available from: /pmc/articles/PMC3031091/

116. Diazzi S, Tartare-Deckert S, Deckert M. The mechanical phenotypic plasticity of melanoma cell: an emerging driver of therapy cross-resistance. Oncogenesis 2023 12:1 [Internet]. 2023 Feb 11 [cited 2024 Feb 9];12(1):1–7. Available from: https://www.nature.com/articles/s41389-023-00452-8

117. Restivo G, Diener J, Cheng PF, Kiowski G, Bonalli M, Biedermann T, et al. low neurotrophin receptor CD271 regulates phenotype switching in melanoma. Nat Commun [Internet]. 2017 Dec 1 [cited 2024 Feb 9];8(1). Available from: https://pubmed.ncbi.nlm.nih.gov/29215016/

118. Hoek KS, Eichhoff OM, Schlegel NC, Döbbeling U, Kobert N, Schaerer L, et al. In vivo switching of human melanoma cells between proliferative and invasive states. Cancer Res. 2008 Feb 1;68(3):650–6.

119. Verfaillie A, Imrichova H, Atak ZK, Dewaele M, Rambow F, Hulselmans G, et al. Decoding the regulatory landscape of melanoma reveals TEADS as regulators of the invasive cell state. Nat Commun. 2015 Apr 9;6.

120. Tudrej KB, Czepielewska E, Kozlowska-Wojciechowska M. SOX10-MITF pathway activity in melanoma cells. Archives of Medical Science. 2017;13(6):1493–503.

121. Cheng PF, Shakhova O, Widmer DS, Eichhoff OM, Zingg D, Frommel SC, et al. Methylation-dependent SOX9 expression mediates invasion in human melanoma cells and is a negative prognostic factor in advanced melanoma. Genome Biol [Internet]. 2015 Feb 22 [cited 2023 Oct 28];16(1). Available from: /pmc/articles/PMC4378455/

122. Rambow F, Rogiers A, Marin-Bejar O, Aerts S, Lund AW, Marine JC. Toward Minimal Residual Disease-Directed Therapy in Melanoma. Cell [Internet]. 2018 [cited 2024 Jan 28];174:843–55. Available from: https://doi.org/10.1016/j.cell.2018.06.025

123. Tsoi J, Robert L, Paraiso K, Galvan C, Sheu KM, Lay J, et al. Multi-stage differentiation defines melanoma subtypes with differential vulnerability to drug-induced iron-dependent oxidative stress. Cancer Cell [Internet]. 2018 May 5 [cited 2024 Jan 28];33(5):890. Available from: /pmc/articles/PMC5953834/

124. Wouters J, Kalender-Atak Z, Minnoye L, Spanier KI, De Waegeneer M, Bravo González-Blas C, et al. Robust gene expression programs underlie recurrent cell states and phenotype switching in melanoma. Nature Cell Biology 2020 22:8 [Internet]. 2020 Aug 3 [cited 2024 Jan 28];22(8):986–98. Available from: https://www.nature.com/articles/s41556-020-0547-3

125. Kuespert K, Pils S, Hauck CR. CEACAMs: their role in physiology and pathophysiology. Curr Opin Cell Biol [Internet]. 2006 Oct [cited 2024 Feb 9];18(5):565. Available from: /pmc/articles/PMC7127089/

126. Helfrich I, Singer BB. Size matters: The functional role of the CEACAM1 isoform signature and its impact for NK cell-mediated killing in melanoma. Cancers (Basel). 2019 Mar 1;11(3).

127. Nagaishi T, Chen Z, Chen L, Iijima H, Nakajima A, Blumberg RS. CEACAM1 and the regulation of mucosal inflammation. Mucosal Immunology 2008 1:1 [Internet]. 2008 Oct 15 [cited 2024 Feb 9];1(1):S39–42. Available from: https://www.nature.com/articles/mi200850

128. Kim WM, Huang YH, Gandhi A, Blumberg RS. CEACAM1 structure and function in immunity and its therapeutic implications. Semin Immunol [Internet]. 2019 Apr 1 [cited 2024 Feb 9];42:101296. Available from: /pmc/articles/PMC6814268/

129. Abou-Rjaily GA, Lee SJ, May D, Al-Share QY, DeAngelis AM, Ruch RJ, et al. CEACAM1 modulates epidermal growth factor receptor–mediated cell proliferation. J Clin Invest [Internet]. 2004 Oct 1 [cited 2024 Feb 4];114(7):944–52. Available from: http://www.jci.org

130. Leung N, Turbide C, Olson M, Marcus V, Jothy S, Beauchemin N. Deletion of the carcinoembryonic antigen-related cell adhesion molecule 1 (Ceacam1) gene contributes to colon tumor progression in a murine model of carcinogenesis. Oncogene 2006 25:40 [Internet]. 2006 Apr 17 [cited 2024 Feb 4];25(40):5527–36. Available from: https://www.nature.com/articles/1209541

131. Florian W, Lenfert E, Gerstel D, Ehrenstein L von, Einhoff J, Schmidt G, et al. CEACAM1 controls the EMT switch in murine mammary carcinoma in vitro and in vivo. Oncotarget [Internet]. 2016

Aug 27 [cited 2024 Feb 4];7(39):63730–46. Available from: https://www.oncotarget.com/article/11650/text/

132. Xu J, Liu B, Ma S, Zhang J, Ji Y, Xu L, et al. Characterizing the Tumor Suppressor Role of CEACAM1 in Multiple Myeloma. Cellular Physiology and Biochemistry [Internet]. 2018 Mar 6 [cited 2024 Feb 4];45(4):1631–40. Available from: https://dx.doi.org/10.1159/000487730

133. Ortenberg R, Galore-Haskel G, Greenberg I, Zamlin B, Sapoznik S, Greenberg E, et al. CEACAM1 Promotes Melanoma Cell Growth through Sox-2. Neoplasia. 2014 May 1;16(5):451–60.

134. Wicklein D, Otto B, Suling A, Elies E, Lüers G, Lange T, et al. CEACAM1 promotes melanoma metastasis and is involved in the regulation of the EMT associated gene network in melanoma cells. Sci Rep. 2018 Dec 1;8(1).

135. Zaffran I, Landolina N, Gaur P, Rovis TL, Stipan J, Mandelboim O, et al. Activation of CEACAM1 with an agonistic monoclonal antibody results in inhibition of melanoma cells. Cancer Gene Therapy 2022 29:11 [Internet]. 2022 Jun 9 [cited 2024 Feb 4];29(11):1676–85. Available from: https://www-nature-com.proxy.bib.uottawa.ca/articles/s41417-022-00486-x

136. Markel G, Gruda R, Achdout H, Katz G, Nechama M, Blumberg RS, et al. The critical role of residues 43R and 44Q of carcinoembryonic antigen cell adhesion molecules-1 in the protection from killing by human NK cells. J Immunol [Internet]. 2004 Sep 15 [cited 2024 Jan 30];173(6):3732–9. Available from: https://pubmed.ncbi.nlm.nih.gov/15356119/

137. Stern N, Markel G, Arnon TI, Gruda R, Wong H, Gray-Owen SD, et al. Carcinoembryonic Antigen (CEA) Inhibits NK Killing via Interaction with CEA-Related Cell Adhesion Molecule 1. The Journal of Immunology [Internet]. 2005 Jun 1 [cited 2024 Jan 30];174(11):6692–701. Available from: https://dx.doi.org/10.4049/jimmunol.174.11.6692

138. Hosomi S, Chen Z, Baker K, Chen L, Huang YH, Olszak T, et al. CEACAM1 on activated NK cells inhibits NKG2D-mediated cytolytic function and signaling. Eur J Immunol [Internet]. 2013 Sep [cited 2024 Jan 30];43(9):2473–83. Available from: https://pubmed.ncbi.nlm.nih.gov/23696226/

139. Chen Z, Chen L, Baker K, Olszak T, Zeissig S, Huang YH, et al. CEACAM1 dampens antitumor immunity by down-regulating NKG2D ligand expression on tumor cells. J Exp Med [Internet]. 2011 Dec 12 [cited 2024 Jan 30];208(13):2633. Available from: /pmc/articles/PMC3244030/

140. Bowles J, Schepers G, Koopman P. Phylogeny of the SOX Family of Developmental Transcription Factors Based on Sequence and Structural Indicators. Dev Biol. 2000 Nov 15;227(2):239–55.

141. Schepers GE, Teasdale RD, Koopman P. Twenty pairs of Sox: Extent, homology, and nomenclature of the mouse and human Sox transcription factor gene families. Dev Cell [Internet]. 2002 Aug 1 [cited 2023 Aug 27];3(2):167–70. Available from: http://www.cell.com/article/S153458070200223X/fulltext

142. Harley VR, Lovell-Badge1 R, Goodfellow PN. Definition of a consensus DNA binding site for SRY. Nucleic Acids Res. 1994;22(8):1500–1.

143. Werner MH, Burley SK. Architectural transcription factors: Proteins that remodel DNA. Cell [Internet]. 1997 Mar 21 [cited 2024 Feb 7];88(6):733–6. Available from: http://www.cell.com/article/S0092867400819170/fulltext

144. Wegner M. Secrets to a healthy Sox life: lessons for melanocytes. Pigment Cell Res [Internet]. 2005 Apr 1 [cited 2024 Feb 7];18(2):74–85. Available from: https://onlinelibrary.wiley.com/doi/full/10.1111/j.1600-0749.2005.00218.x

145. Ferrari1 S, Harley2 VR, Pontiggia3 A, Goodfellow2 PN, Lovell-Badge4 R, Bianchi1l5 ME. SRY, like HMG1, recognizes sharp angles in DNA. EMBO J [Internet]. 1992 Dec 1 [cited 2024 Feb 9];11(12):4497–506. Available from: https://www.embopress.org/doi/10.1002/j.1460-2075.1992.tb05551.x

146. Südbeck P, Scherer G. Two Independent Nuclear Localization Signals Are Present in the DNA-binding High-mobility Group Domains of SRY and SOX9. Journal of Biological Chemistry. 1997 Oct 31;272(44):27848–52.

147. Gasca S, Cañizares J, De Santa Barbara P, Méjean C, Poulat F, Berta P, et al. A nuclear export signal within the high mobility group domain regulates the nucleocytoplasmic translocation of SOX9 during sexual determination. Proc Natl Acad Sci U S A [Internet]. 2002 Aug 20 [cited 2024 Feb 9];99(17):11199–204. Available from: https://www.pnas.org/doi/abs/10.1073/pnas.172383099

148. She ZY, Yang WX. SOX family transcription factors involved in diverse cellular events during development. Eur J Cell Biol. 2015 Dec 1;94(12):547–63.

149. Grimm D, Bauer J, Wise P, Krüger M, Simonsen U, Wehland M, et al. The role of SOX family members in solid tumours and metastasis. Semin Cancer Biol. 2020 Dec 1;67:122–53.

150. Wright EM, Snopek B, Koopman P. Seven new members of the Sox gene family expressed during mouse development. Vol. 21, Nucleic Acids Research. 1993.

151. Huang YH, Jankowski A, Cheah KSE, Prabhakar S, Jauch R. SOXE transcription factors form selective dimers on non-compact DNA motifs through multifaceted interactions between dimerization and high-mobility group domains. Sci Rep. 2015 May 27;5.

152. Peirano RI, Wegner M. The glial transcription factor Sox10 binds to DNA both as monomer and dimer with different functional consequences. Nucleic Acids Res [Internet]. 2000 Aug 15 [cited 2024 Feb 9];28(16):3047–55. Available from: https://pubmed.ncbi.nlm.nih.gov/10931919/

153. Lang D, Epstein JA. Sox10 and Pax3 physically interact to mediate activation of a conserved c-RET enhancer. Hum Mol Genet [Internet]. 2003 Apr 15 [cited 2024 Feb 9];12(8):937–45. Available from: https://pubmed.ncbi.nlm.nih.gov/12668617/

154. Pfeifer D, Poulat F, Holinski-Feder E, Kooy F, Scherer G. The SOX8 Gene Is Located within 700 kb of the Tip of Chromosome 16p and Is Deleted in a Patient with ATR-16 Syndrome. Genomics. 2000 Jan 1;63(1):108–16.

155. Schepers GE, Bullejos M, Hosking BM, Koopman P. Cloning and characterisation of the Sry-related transcription factor gene Sox8. Nucleic Acids Res [Internet]. 2000 Mar 3 [cited 2023 Aug 27];28(6):1473. Available from: /pmc/articles/PMC111037/

156. Südbeck P, Schmitz ML, Baeuerle PA, Scherer G. Sex reversal by loss of the C-terminal transactivation domain of human SOX9. Nat Genet [Internet]. 1996 Jun [cited 2023 Aug 27];13(2):230–2. Available from: https://pubmed.ncbi.nlm.nih.gov/8640233/

157. Ng LJ, Wheatley S, Muscat GEO, Conway-Campbell J, Bowles J, Wright E, et al. SOX9 Binds DNA, Activates Transcription, and Coexpresses with Type II Collagen during Chondrogenesis in the Mouse. Dev Biol. 1997 Mar 1;183(1):108–21.

158. Pusch C, Hustert E, Pfeifer D, Südbeck P, Kist R, Roe B, et al. The SOX10/Sox10 gene from human and mouse: Sequence, expression, and transactivation by the encoded HMG domain transcription factor. Hum Genet [Internet]. 1998 [cited 2023 Aug 27];103(2):115–23. Available from: https://link.springer.com/article/10.1007/s004390050793

159. Schreiner S, Cossais F, Fischer K, Scholz S, Bösl MR, Holtmann B, et al. Hypomorphic Sox10 alleles reveal novel protein functions and unravel developmental differences in glial lineages. Development [Internet]. 2007 Sep 15 [cited 2023 Aug 27];134(18):3271–81. Available from: https://dx.doi.org/10.1242/dev.003350

160. Haseeb A, Lefebvre V. The SOXE transcription factors—SOX8, SOX9 and SOX10—share a bi-partite transactivation mechanism. Nucleic Acids Res [Internet]. 2019 Jul 7 [cited 2023 Aug 27];47(13):6917. Available from: /pmc/articles/PMC6649842/

161. She ZY, Yang WX. Sry and SoxE genes: How they participate in mammalian sex determination and gonadal development? Semin Cell Dev Biol. 2017 Mar 1;63:13–22.

162. Sox Genes - Transcriptional Control of Neural Crest Development - NCBI Bookshelf [Internet]. [cited 2024 Feb 9]. Available from: https://www.ncbi.nlm.nih.gov/books/NBK53136/

163. Claus Stolt C, Rehberg S, Ader M, Lommes P, Riethmacher D, Schachner M, et al. Terminal differentiation of myelin-forming oligodendrocytes depends on the transcription factor Sox10. Genes Dev [Internet]. 2002 Jan 15 [cited 2024 Feb 9];16(2):165–70. Available from: https://pubmed.ncbi.nlm.nih.gov/11799060/

164. Finzsch M, Stolt CC, Lommes P, Wegner M. Sox9 and Sox10 influence survival and migration of oligodendrocyte precursors in the spinal cord by regulating PDGF receptor αexpression. Development [Internet]. 2008 Feb 15 [cited 2024 Feb 9];135(4):637–46. Available from: https://dx.doi.org/10.1242/dev.010454

165. Shakhova O, Cheng P, Mishra PJ, Zingg D, Schaefer SM, Debbache J, et al. Antagonistic Cross-Regulation between Sox9 and Sox10 Controls an Anti-tumorigenic Program in Melanoma. PLoS Genet. 2015;11(1).

166. Aguilar-Medina M, Avendaño-Félix M, Lizárraga-Verdugo E, Bermúdez M, Romero-Quintana JG, Ramos-Payan R, et al. SOX9 Stem-Cell Factor: Clinical and Functional Relevance in Cancer. J Oncol [Internet]. 2019 [cited 2024 Feb 9];2019. Available from: /pmc/articles/PMC6463569/

167. Li FZ, Dhillon AS, Anderson RL, McArthur G, Ferrao PT. Phenotype Switching in Melanoma: Implications for Progression and Therapy. Front Oncol [Internet]. 2015 [cited 2024 Feb 9];5(FEB). Available from: /pmc/articles/PMC4327420/

168. Lin S, Chou Y, Jiang S, Chang J, research CCC, 2016 undefined. Epigenetic Switch between SOX2 and SOX9 Regulates Cancer Cell Plasticity. AACRSC Lin, YT Chou, SS Jiang, JL Chang, CH Chung, YR Kao, IS Chang, CW WuCancer research, 2016•AACR [Internet]. 2016 [cited 2024 Feb 9]; Available from: https://aacrjournals.org/cancerres/article-abstract/76/23/7036/613967

169. Ma Y, Shepherd J, Zhao D, Bollu LR, Tahaney WM, Hill J, et al. SOX9 is essential for triple-negative breast cancer cell survival and metastasis. Molecular Cancer Research [Internet]. 2020 Dec 1 [cited 2024 Feb 9];18(12):1825–38. Available from: /mcr/article/18/12/1825/270873/SOX9-Is-Essential-for-Triple-Negative-Breast

170. Guo W, Keckesova Z, Donaher JL, Shibue T, Tischler V, Reinhardt F, et al. Slug and Sox9 cooperatively determine the mammary stem cell state. Cell. 2012 Mar 2;148(5):1015–28.

171. Luanpitpong S, Li J, Manke A, Brundage K, Ellis E, McLaughlin SL, et al. SLUG is required for SOX9 stabilization and functions to promote cancer stem cells and metastasis in human lung carcinoma. Oncogene. 2016 Jun 2;35(22):2824–33.

172. Christin JR, Wang C, Chung CY, Liu Y, Dravis C, Tang W, et al. Stem Cell Determinant SOX9 Promotes Lineage Plasticity and Progression in Basal-like Breast Cancer. Cell Rep. 2020 Jun 9;31(10).

173. Nouri M, Massah S, Caradec J, Lubik AA, Li N, Truong S, et al. Transient SOX9 expression facilitates resistance to androgen-targeted therapy in prostate cancer. Clinical Cancer Research [Internet]. 2020 Apr 1 [cited 2024 Feb 9];26(7):1678–89. Available from: /clincancerres/article/26/7/1678/83072/Transient-Sox9-Expression-Facilitates-Resistance

174. Li XL, Chen XQ, Zhang MN, Chen N, Nie L, Xu M, et al. SOX9 was involved in TKIs resistance in renal cell carcinoma via Raf/MEK/ERK signaling pathway. Int J Clin Exp Pathol [Internet]. 2015 [cited 2024 Jan 20];8(4):3871. Available from: /pmc/articles/PMC4466958/

175. Voronkova MA, Rojanasakul LW, Kiratipaiboon C, Rojanasakul Y. The SOX9-Aldehyde Dehydrogenase Axis Determines Resistance to Chemotherapy in Non-Small-Cell Lung Cancer. Mol Cell Biol [Internet]. 2020 Jan 3 [cited 2024 Jan 20];40(2). Available from: https://pubmed.ncbi.nlm.nih.gov/31658996/

176. Jeselsohn R, Cornwell M, Pun M, Buchwalter G, Nguyen M, Bango C, et al. Embryonic transcription factor SOX9 drives breast cancer endocrine resistance. Proc Natl Acad Sci U S A [Internet]. 2017 May 30 [cited 2024 Jan 20];114(22):E4482–91. Available from: https://pubmed.ncbi.nlm.nih.gov/28507152/

177. Passeron T, Valencia JC, Namiki T, Vieira WD, Passeron H, Miyamura Y, et al. Upregulation of SOX9 inhibits the growth of human and mouse melanomas and restores their sensitivity to retinoic acid. J Clin Invest [Internet]. 2009 Apr 4 [cited 2023 Oct 28];119(4):954. Available from: /pmc/articles/PMC2662541/

178. Flammiger A, Besch R, Cook AL, Maier T, Sturm RA, Berking C. SOX9 and SOX10 but not BRN2 are required for nestin expression in human melanoma cells. Journal of Investigative Dermatology [Internet]. 2009 Apr 1 [cited 2023 Oct 28];129(4):945–53. Available from: http://www.jidonline.org/article/S0022202X15342810/fulltext

179. Yang X, Liang R, Liu C, Liu JA, Cheung MPL, Liu X, et al. SOX9 is a dose-dependent metastatic fate determinant in melanoma. J Exp Clin Cancer Res [Internet]. 2019 Jan 14 [cited 2023 Oct 28];38(1). Available from: /pmc/articles/PMC6330758/

180. Bahmad HF, Thiravialingam A, Sriganeshan K, Gonzalez J, Alvarez V, Ocejo S, et al. Clinical Significance of SOX10 Expression in Human Pathology. Curr Issues Mol Biol [Internet]. 2023 Dec 1 [cited 2024 Feb 9];45(12):10131. Available from: /pmc/articles/PMC10742133/

181. Yin H, Qin C, Zhao Y, Du Y, Sheng Z, Wang Q, et al. SOX10 is over-expressed in bladder cancer and contributes to the malignant bladder cancer cell behaviors. Clinical and Translational Oncology [Internet]. 2017 Aug 1 [cited 2024 Jan 30];19(8):1035–44. Available from: https://link-springer-com.proxy.bib.uottawa.ca/article/10.1007/s12094-017-1641-2

182. Zhou D, Bai F, Zhang X, Hu M, Zhao G, Zhao Z, et al. SOX10 is a novel oncogene in hepatocellular carcinoma through Wnt/β-catenin/TCF4 cascade. Tumor Biology [Internet]. 2014 Oct 1 [cited 2024 Jan 30];35(10):9935–40. Available from: https://link-springer-com.proxy.bib.uottawa.ca/article/10.1007/s13277-014-1893-1

183. Dravis C, Spike BT, Harrell JC, Johns C, Trejo CL, Southard-Smith EM, et al. Sox10 Regulates Stem/Progenitor and Mesenchymal Cell States in Mammary Epithelial Cells. Cell Rep. 2015 Sep 29;12(12):2035–48.

184. Al-Zahrani KN, Abou-Hamad J, Cook DP, Pryce BR, Hodgins JJ, Labrèche C, et al. Loss of the Ste20-like kinase induces a basal/stem-like phenotype in HER2-positive breast cancers. Oncogene. 2020 Jun 4;39(23):4592–602.

185. Feng W, Liu S, Zhu R, Li B, Zhu Z, Yang J, et al. SOX10 induced Nestin expression regulates cancer stem cell properties of TNBC cells. Biochem Biophys Res Commun. 2017 Apr 1;485(2):522–8.

186. Cronin JC, Watkins-Chow DE, Incao A, Hasskamp JH, Schonewolf N, Aoude LG, et al. SOX10 ablation arrests the cell cycle, induces senescence and suppresses melanomagenesis. Cancer Res [Internet]. 2013 Sep 9 [cited 2024 Jan 20];73(18):5709. Available from: /pmc/articles/PMC3803156/

187. Shakhova O, Zingg D, Schaefer SM, Hari L, Civenni G, Blunschi J, et al. Sox10 promotes the formation and maintenance of giant congenital naevi and melanoma. Nat Cell Biol. 2012 Aug;14(8):882–9.

188. Boiko AD, Razorenova O V., Van De Rijn M, Swetter SM, Johnson DL, Ly DP, et al. Human melanoma-initiating cells express neural crest nerve growth factor receptor CD271. Nature [Internet]. 2010 Jul 1 [cited 2024 Feb 3];466(7302):133–7. Available from: https://pubmed.ncbi.nlm.nih.gov/20596026/

189. Graf SA, Busch C, Bosserhoff AK, Besch R, Berking C. SOX10 promotes melanoma cell invasion by regulating melanoma inhibitory activity. J Invest Dermatol [Internet]. 2014 [cited 2024 Jan 30];134(8):2212–20. Available from: https://pubmed.ncbi.nlm.nih.gov/24608986/

190. Lv X Bin, Wu W, Tang X, Wu Y, Zhu Y, Liu Y, et al. Regulation of SOX10 stability via ubiquitination-mediated degradation by Fbxw7α modulates melanoma cell migration. Oncotarget [Internet]. 2015 [cited 2024 Jan 30];6(34):36370–82. Available from: https://pubmed.ncbi.nlm.nih.gov/26461473/

191. Seong I, Min HJ, Lee JH, Yeo CY, Kang DM, Oh ES, et al. Sox10 controls migration of B16F10 melanoma cells through multiple regulatory target genes. PLoS One [Internet]. 2012 Feb 21 [cited 2024 Jan 30];7(2). Available from: https://pubmed.ncbi.nlm.nih.gov/22363655/

192. Basile KJ, Abel E V., Aplin AE. Adaptive up-regulation of FOXD3 and resistance to PLX4032/4720-induced cell death in mutant B-RAF melanoma cells. Oncogene [Internet]. 2012 May 5 [cited 2024 Jan 30];31(19):2471. Available from: /pmc/articles/PMC3262107/

193. Han S, Ren Y, He W, Liu H, Zhi Z, Zhu X, et al. ERK-mediated phosphorylation regulates SOX10 sumoylation and targets expression in mutant BRAF melanoma. Nat Commun [Internet]. 2018 Dec 1 [cited 2024 Jan 30];9(1). Available from: /pmc/articles/PMC5750221/

194. Sun C, Wang L, Huang S, Heynen GJJE, Prahallad A, Robert C, et al. Reversible and adaptive resistance to BRAF(V600E) inhibition in melanoma. Nature. 2014;508(1):118–22.

195. Shaffer SM, Dunagin MC, Torborg SR, Torre EA, Emert B, Krepler C, et al. Rare cell variability and drug-induced reprogramming as a mode of cancer drug resistance. Nature 2017 546:7658 [Internet]. 2017 Jun 15 [cited 2024 Jan 30];546(7658):431–5. Available from: https://www-nature-com.proxy.bib.uottawa.ca/articles/nature22794

196. Berico P, Cigrang M, Davidson G, Braun C, Sandoz J, Legras S, et al. CDK7 and MITF repress a transcription program involved in survival and drug tolerance in melanoma. EMBO Rep [Internet]. 2021 Sep 9 [cited 2024 Jan 30];22(9). Available from: /pmc/articles/PMC8419699/

197. Capparelli C, Purwin TJ, Glasheen MK, Caksa S, Tiago M, Wilski N, et al. Targeting SOX10-deficient cells to reduce the dormant-invasive phenotype state in melanoma. Nat Commun. 2022 Dec 1;13(1).

198. Purwin TJ, Caksa S, Sacan A, Capparelli C, Aplin AE. Gene signature reveals decreased SOX10-dependent transcripts in malignant cells from immune checkpoint inhibitor-resistant cutaneous melanomas. iScience [Internet]. 2023 Sep 9 [cited 2024 Feb 3];26(9). Available from: /pmc/articles/PMC10450419/

199. Rosenbaum SR, Caksa S, Stefanski CD, Trachtenberg I V., Wilson HP, Wilski NA, et al. SOX10 Loss Sensitizes Melanoma Cells to Cytokine-Mediated Inflammatory Cell Death. Molecular Cancer Research [Internet]. 2024 Feb 1 [cited 2024 Feb 3];22(2):209–20. Available from: /mcr/article/22/2/209/733691/SOX10-Loss-Sensitizes-Melanoma-Cells-to-Cytokine

200. Swaika A, Crozier JA, Joseph RW. Vemurafenib: an evidence-based review of its clinical utility in the treatment of metastatic melanoma. Drug Des Devel Ther [Internet]. 2014 Jun 16 [cited 2024 Feb 9];8:775. Available from: /pmc/articles/PMC4064951/

201. Wegner M. Melanocytes and the transcription factor Sox10. From Melanocytes to Melanoma: The Progression to Malignancy [Internet]. 2006 [cited 2024 Feb 9];71–80. Available from: https://link.springer.com/chapter/10.1007/978-1-59259-994-3_4

202. nf-core/atacseq: [2.1.2] - 2022-08-07. [cited 2024 Feb 9]; Available from: https://zenodo.org/records/8222875

203. Li LC, Dahiya R. MethPrimer: Designing primers for methylation PCRs. Bioinformatics. 2002 Nov 1;18(11):1427–31.

204. Jandova J, Wondrak GT. Vemurafenib Drives Epithelial-to-Mesenchymal Transition Gene Expression in BRAF Inhibitor–Resistant BRAFV600E/NRASQ61K Melanoma Enhancing Tumor Growth and Metastasis in a Bioluminescent Murine Model. Journal of Investigative Dermatology. 2022 May 1;142(5):1456-1465.e1.

205. Abou-Hamad J, Hodgins JJ, Yakubovich E, Vanderhyden BC, Ardolino M, Sabourin LA. Sox10-Deficient Drug-Resistant Melanoma Cells Are Refractory to Oncolytic RNA Viruses. Cells [Internet]. 2023 Dec 29 [cited 2024 Feb 10];13(1):73. Available from: https://pubmed.ncbi.nlm.nih.gov/38201278/

206. Wang J, Xue X, Hong H, Qin M, Zhou J, Sun Q, et al. Upregulation of microRNA-524-5p enhances the cisplatin sensitivity of gastric cancer cells by modulating proliferation and metastasis via targeting SOX9. Oncotarget. 2017;8(1):574–82.

207. Xue M, Li G, Sun P, Zhang D, Fang X, Li W. MicroRNA-613 induces the sensitivity of gastric cancer cells to cisplatin through targeting SOX9 expression. Am J Transl Res [Internet]. 2019 [cited 2024 Feb 10];11(2):885. Available from: /pmc/articles/PMC6413272/

208. Feng C, Ma F, Hu C, Ma J an, Wang J, Zhang Y, et al. SOX9/miR-130a/CTR1 axis modulates DDP-resistance of cervical cancer cell. Cell Cycle [Internet]. 2018 Feb 16 [cited 2024 Feb 10];17(4):448–58. Available from: https://www.tandfonline.com/doi/abs/10.1080/15384101.2017.1395533

209. Xiao S, Li Y, Pan Q, Ye M, He S, Tian Q, et al. MiR-34c/SOX9 axis regulates the chemoresistance of ovarian cancer cell to cisplatin-based chemotherapy. J Cell Biochem [Internet]. 2019 Mar 1 [cited 2024 Feb 10];120(3):2940–53. Available from: https://onlinelibrary.wiley.com/doi/full/10.1002/jcb.26865

210. Fuglerud BM, Drissler S, Lotto J, Stephan TL, Thakur A, Cullum R, et al. SOX9 reprograms endothelial cells by altering the chromatin landscape. Nucleic Acids Res [Internet]. 2022 [cited 2024 Feb 10];50(15):8547–65. Available from: https://doi.org/10.1093/nar/gkac652

211. Yang Y, Gomez N, Infarinato N, Adam RC, Sribour M, Baek I, et al. The pioneer factor SOX9 competes for epigenetic factors to switch stem cell fates. Nature Cell Biology 2023 25:8

[Internet]. 2023 Jul 24 [cited 2024 Feb 10];25(8):1185–95. Available from: https://www.nature.com/articles/s41556-023-01184-y

212. Sardar D, Chen HC, Reyes A, Varadharajan S, Jain A, Mohila C, et al. Sox9 directs divergent epigenomic states in brain tumor subtypes. 2022 [cited 2024 Feb 10]; Available from: https://doi.org/10.1073/pnas.2202015119

213. Yang H, Higgins B, Kolinsky K, Packman K, Go Z, Iyer R, et al. RG7204 (PLX4032), a selective BRAFV600E inhibitor, displays potent antitumor activity in preclinical melanoma models. Cancer Res [Internet]. 2010 Jul 1 [cited 2023 Aug 23];70(13):5518–27. Available from: https://pubmed.ncbi.nlm.nih.gov/20551065/

214. Flaherty KT, Puzanov I, Kim KB, Ribas A, McArthur GA, Sosman JA, et al. Inhibition of Mutated, Activated BRAF in Metastatic Melanoma. New England Journal of Medicine [Internet]. 2010 Aug 26 [cited 2023 Aug 23];363(9):809–19. Available from: https://www.nejm.org/doi/10.1056/NEJMoa1002011

215. Chapman PB, Hauschild A, Robert C, Haanen JB, Ascierto P, Larkin J, et al. Improved Survival with Vemurafenib in Melanoma with BRAF V600E Mutation. N Engl J Med [Internet]. 2011 Jun 6 [cited 2023 Aug 23];364(26):2507. Available from: /pmc/articles/PMC3549296/

216. Sosman JA, Kim KB, Schuchter L, Gonzalez R, Pavlick AC, Weber JS, et al. Survival in BRAF V600–Mutant Advanced Melanoma Treated with Vemurafenib. N Engl J Med [Internet]. 2012 Feb 2 [cited 2023 Aug 23];366(8):707. Available from: /pmc/articles/PMC3724515/

217. Hauschild A, Grob JJ, Demidov L V., Jouary T, Gutzmer R, Millward M, et al. An update on BREAK-3, a phase III, randomized trial: Dabrafenib (DAB) versus dacarbazine (DTIC) in patients with BRAF V600E-positive mutation metastatic melanoma (MM). https://doi.org/101200/jco20133115_suppl9013. 2013 May 20;31(15_suppl):9013–9013.

218. Long G V., Stroyakovskiy D, Gogas H, Levchenko E, de Braud F, Larkin J, et al. Combined BRAF and MEK inhibition versus BRAF inhibition alone in melanoma. N Engl J Med [Internet]. 2014 Nov 13 [cited 2023 Aug 23];371(20):1877–88. Available from: https://pubmed.ncbi.nlm.nih.gov/25265492/

219. Larkin J, Ascierto PA, Dréno B, Atkinson V, Liszkay G, Maio M, et al. Combined vemurafenib and cobimetinib in BRAF-mutated melanoma. N Engl J Med [Internet]. 2014 Nov 13 [cited 2023 Aug 23];371(20):1867–76. Available from: https://pubmed.ncbi.nlm.nih.gov/25265494/

220. Robert C, Karaszewska B, Schachter J, Rutkowski P, Mackiewicz A, Stroiakovski D, et al. Improved overall survival in melanoma with combined dabrafenib and trametinib. N Engl J Med [Internet]. 2015 Jan 1 [cited 2023 Aug 23];372(1):30–9. Available from: https://pubmed.ncbi.nlm.nih.gov/25399551/

221. Shaffer SM, Dunagin MC, Torborg SR, Torre EA, Emert B, Krepler C, et al. Rare cell variability and drug-induced reprogramming as a mode of cancer drug resistance. Nature [Internet]. 2017 Jun 15 [cited 2023 Aug 23];546(7658):431–5. Available from: https://pubmed.ncbi.nlm.nih.gov/28607484/

222. Giunta EF, Arrichiello G, Curvietto M, Pappalardo A, Bosso D, Rosanova M, et al. Epigenetic Regulation in Melanoma: Facts and Hopes. Cells [Internet]. 2021 Aug 1 [cited 2023 Aug 23];10(8). Available from: https://pubmed.ncbi.nlm.nih.gov/34440824/

223. Graf SA, Busch C, Bosserhoff AK, Besch R, Berking C. SOX10 promotes melanoma cell invasion by regulating melanoma inhibitory activity. J Invest Dermatol [Internet]. 2014 [cited 2023 Aug 23];134(8):2212–20. Available from: https://pubmed.ncbi.nlm.nih.gov/24608986/

224. Sun C, Wang L, Huang S, Heynen GJJE, Prahallad A, Robert C, et al. Reversible and adaptive resistance to BRAF(V600E) inhibition in melanoma. Nature 2014 508:7494 [Internet]. 2014 Mar 26 [cited 2023 Aug 23];508(7494):118–22. Available from: https://www.nature.com/articles/nature13121

225. Kaufman CK, Mosimann C, Fan ZP, Yang S, Thomas AJ, Ablain J, et al. A zebrafish melanoma model reveals emergence of neural crest identity during melanoma initiation. Science [Internet]. 2016 Jan 29 [cited 2023 Aug 23];351(6272). Available from: https://pubmed.ncbi.nlm.nih.gov/26823433/

226. Han S, Ren Y, He W, Liu H, Zhi Z, Zhu X, et al. ERK-mediated phosphorylation regulates SOX10 sumoylation and targets expression in mutant BRAF melanoma. Nature Communications 2017 9:1 [Internet]. 2018 Jan 2 [cited 2023 Aug 23];9(1):1–14. Available from: https://www.nature.com/articles/s41467-017-02354-x

227. Capparelli C, Purwin TJ, Glasheen MK, Caksa S, Tiago M, Wilski N, et al. Targeting SOX10-deficient cells to reduce the dormant-invasive phenotype state in melanoma. Nature Communications 2022 13:1 [Internet]. 2022 Mar 16 [cited 2023 Aug 23];13(1):1–16. Available from: https://www.nature.com/articles/s41467-022-28801-y

228. Abou-Hamad J, Hodgins JJ, de Souza CT, Garland B, Labrèche C, Marotel M, et al. CEACAM1 is a direct SOX10 target and inhibits melanoma immune infiltration and stemness. iScience [Internet]. 2022 Dec 22 [cited 2023 Aug 23];25(12). Available from: https://pubmed.ncbi.nlm.nih.gov/36437876/

229. Phi LTH, Sari IN, Yang YG, Lee SH, Jun N, Kim KS, et al. Cancer Stem Cells (CSCs) in Drug Resistance and their Therapeutic Implications in Cancer Treatment. Stem Cells Int [Internet]. 2018 [cited 2023 Aug 23];2018. Available from: /pmc/articles/PMC5850899/

230. Makena MR, Ranjan A, Thirumala V, Reddy AP. Cancer stem cells: Road to therapeutic resistance and strategies to overcome resistance. Biochimica et Biophysica Acta (BBA) - Molecular Basis of Disease. 2020 Apr 1;1866(4):165339.

231. Robinson C, Xu MM, Nair SK, Beasley GM, Rhodin KE. Oncolytic viruses in melanoma. Front Biosci (Landmark Ed) [Internet]. 2022 Feb 2 [cited 2023 Aug 23];27(2):63. Available from: /pmc/articles/PMC9888358/

232. Wollmann G, Drokhlyansky E, Davis JN, Cepko C, van den Pol AN. Lassa-vesicular stomatitis chimeric virus safely destroys brain tumors. J Virol [Internet]. 2015 Jul [cited 2023 Aug 23];89(13):6711–24. Available from: https://pubmed.ncbi.nlm.nih.gov/25878115/

233. Kimpel J, Urbiola C, Koske I, Tober R, Banki Z, Wollmann G, et al. The Oncolytic Virus VSV-GP Is Effective against Malignant Melanoma. Viruses [Internet]. 2018 Mar 2 [cited 2023 Aug 23];10(3). Available from: /pmc/articles/PMC5869501/

234. Katze MG, He Y, Gale M. Viruses and interferon: a fight for supremacy. Nature Reviews Immunology 2002 2:9 [Internet]. 2002 Sep [cited 2023 Aug 23];2(9):675–87. Available from: https://www.nature.com/articles/nri888

235. Schneider WM, Chevillotte MD, Rice CM. Interferon-Stimulated Genes: A Complex Web of Host Defenses. Annu Rev Immunol [Internet]. 2014 [cited 2023 Aug 23];32:513. Available from: /pmc/articles/PMC4313732/

236. Matveeva O V., Chumakov PM. Defects in interferon pathways as potential biomarkers of sensitivity to oncolytic viruses. Rev Med Virol [Internet]. 2018 Nov 1 [cited 2023 Aug 23];28(6). Available from: /pmc/articles/PMC6906582/

237. Bray NL, Pimentel H, Melsted P, Pachter L. Near-optimal probabilistic RNA-seq quantification. Nat Biotechnol [Internet]. 2016 May 1 [cited 2023 Sep 3];34(5):525–7. Available from: https://pubmed.ncbi.nlm.nih.gov/27043002/

238. Love MI, Huber W, Anders S. Moderated estimation of fold change and dispersion for RNA-seq data with DESeq2. Genome Biol [Internet]. 2014 Dec 5 [cited 2023 Sep 3];15(12):1–21. Available from: https://genomebiology.biomedcentral.com/articles/10.1186/s13059-014-0550-8

239. Kuleshov M V., Jones MR, Rouillard AD, Fernandez NF, Duan Q, Wang Z, et al. Enrichr: a comprehensive gene set enrichment analysis web server 2016 update. Nucleic Acids Res [Internet]. 2016 Jul 8 [cited 2023 Aug 23];44(W1):W90–7. Available from: https://pubmed.ncbi.nlm.nih.gov/27141961/

240. Xie Z, Bailey A, Kuleshov M V., Clarke DJB, Evangelista JE, Jenkins SL, et al. Gene Set Knowledge Discovery with Enrichr. Curr Protoc [Internet]. 2021 Mar 1 [cited 2023 Aug 23];1(3):e90. Available from: https://onlinelibrary.wiley.com/doi/full/10.1002/cpz1.90

241. Liberzon A, Birger C, Thorvaldsdóttir H, Ghandi M, Mesirov JP, Tamayo P. The Molecular Signatures Database (MSigDB) hallmark gene set collection. Cell Syst [Internet]. 2015 Dec 12 [cited 2023 Sep 3];1(6):417. Available from: /pmc/articles/PMC4707969/

242. Stojdl DF, Lichty BD, TenOever BR, Paterson JM, Power AT, Knowles S, et al. VSV strains with defects in their ability to shutdown innate immunity are potent systemic anti-cancer agents. Cancer Cell [Internet]. 2003 Oct 1 [cited 2023 Sep 19];4(4):263–75. Available from: http://www.cell.com/article/S1535610803002411/fulltext

243. Tian Y, Guo W. A Review of the Molecular Pathways Involved in Resistance to BRAF Inhibitors in Patients with Advanced-Stage Melanoma. Med Sci Monit [Internet]. 2020 Apr 10 [cited 2023 Aug 23];26:e920957-1. Available from: /pmc/articles/PMC7169438/

244. Tangella LP, Clark ME, Gray ES. Resistance mechanisms to targeted therapy in BRAF-mutant melanoma - A mini review. Biochimica et Biophysica Acta (BBA) - General Subjects. 2021 Jan 1;1865(1):129736.

245. Yokoyama S, Takahashi A, Kikuchi R, Nishibu S, Lo JA, Hejna M, et al. SOX10 Regulates Melanoma Immunogenicity through an IRF4-IRF1 Axis. Cancer Res [Internet]. 2021 Dec 15 [cited 2023 Aug 23];81(24):6131–41. Available from: https://pubmed.ncbi.nlm.nih.gov/34728538/

246. Murira A, Lamarre A. Type-I interferon responses: From friend to foe in the battle against chronic viral infection. Front Immunol. 2016 Dec 19;7(DEC):233563.

247. Gómez-Herranz M, Taylor J, Sloan RD. IFITM proteins: Understanding their diverse roles in viral infection, cancer, and immunity. Journal of Biological Chemistry [Internet]. 2023 Jan 1 [cited 2023 Aug 23];299(1). Available from: http://www.jbc.org/article/S002192582201184X/fulltext

248. Giraldo MI, Hage A, van Tol S, Rajsbaum R. TRIM Proteins in Host Defense and Viral Pathogenesis. Curr Clin Microbiol Rep [Internet]. 2020 Dec 1 [cited 2023 Aug 23];7(4):101. Available from: /pmc/articles/PMC7414267/

249. Verfaillie A, Imrichova H, Atak ZK, Dewaele M, Rambow F, Hulselmans G, et al. Decoding the regulatory landscape of melanoma reveals TEADS as regulators of the invasive cell state. Nature Communications 2015 6:1 [Internet]. 2015 Apr 9 [cited 2023 Sep 3];6(1):1–16. Available from: https://www.nature.com/articles/ncomms7683

250. Xu YR, Yang WX. SOX-mediated molecular crosstalk during the progression of tumorigenesis. Semin Cell Dev Biol. 2017 Mar 1;63:23–34.

251. Bondurand N, Sham MH. The role of SOX10 during enteric nervous system development. Dev Biol. 2013 Oct 1;382(1):330–43.

252. Cronin JC, Watkins-Chow DE, Incao A, Hasskamp JH, Schonewolf N, Aoude LG, et al. SOX10 ablation arrests cell cycle, induces senescence, and suppresses melanomagenesis. Cancer Res. 2013 Sep 15;73(18):5709–18.

253. Merlino G, Herlyn M, Fisher DE, Bastian BC, Flaherty KT, Davies MA, et al. The state of melanoma: challenges and opportunities. Pigment Cell Melanoma Res. 2016 Jul 1;29(4):404–16.

254. Manzano JL, Layos L, Bugés C, De los Llanos Gil M, Vila L, Martínez-Balibrea E, et al. Resistant mechanisms to BRAF inhibitors in melanoma. Ann Transl Med. 2016 Jun 1;4(12):1–9.

255. Damsky WE, Bosenberg M. Melanocytic nevi and melanoma: Unraveling a complex relationship. Oncogene. 2017 Oct 19;36(42):5771–92.

256. Ilieva KM, Correa I, Josephs DH, Karagiannis P, Egbuniwe IU, Cafferkey MJ, et al. Effects of BRAF mutations and BRAF inhibition on immune responses to melanoma. Mol Cancer Ther. 2014 Dec 1;13(12):2769–83.

257. Damsky WE, Theodosakis N, Bosenberg M. Melanoma metastasis: New concepts and evolving paradigms. Oncogene. 2014 May 8;33(19):2413–22.

258. Evans MS, Madhunapantula SR V., Robertson GP, Drabick JJ. Current and future trials of targeted therapies in cutaneous melanoma. Adv Exp Med Biol. 2013;779:223–55.

259. Seidel JA, Otsuka A, Kabashima K. Anti-PD-1 and anti-CTLA-4 therapies in cancer: Mechanisms of action, efficacy, and limitations. Front Oncol. 2018 Mar 28;8(MAR).

260. Koppolu V, Rekha Vasigala V. Checkpoint immunotherapy by nivolumab for treatment of metastatic melanoma. J Cancer Res Ther. 2018 Oct 1;14(6):1167–75.

261. Greene MH, Elder DE, Guerry D, Epstein MN, Greene MH, Van Horn M. A study of tumor progression: The precursor lesions of superficial spreading and nodular melanoma. Hum Pathol. 1984;15(12):1147–65.

262. Kaur A, Webster MR, Marchbank K, Behera R, Ndoye A, Kugel CH, et al. SFRP2 in the aged microenvironment drives melanoma metastasis and therapy resistance. Nature. 2016 Apr 14;532(7598):250–4.

263. Smith MP, Brunton H, Rowling EJ, Ferguson J, Arozarena I, Miskolczi Z, et al. Inhibiting Drivers of Non-mutational Drug Tolerance Is a Salvage Strategy for Targeted Melanoma Therapy. Cancer Cell. 2016 Mar 14;29(3):270–84.

264. Corrigendum: Rare cell variability and drug-induced reprogramming as a mode of cancer drug resistance (Nature (2017) 546 (431-435) DOI: 10.1038/nature22794). Nature. 2018 Mar 8;555(7695):274.

265. Müller J, Krijgsman O, Tsoi J, Robert L, Hugo W, Song C, et al. Low MITF/AXL ratio predicts early resistance to multiple targeted drugs in melanoma. Nat Commun. 2014;5.

266. Perego M, Maurer M, Wang JX, Shaffer S, Müller AC, Parapatics K, et al. A slow-cycling subpopulation of melanoma cells with highly invasive properties. Oncogene. 2018 Jan 18;37(3):302–12.

267. Hugo W, Shi H, Sun L, Piva M, Song C, Kong X, et al. Non-genomic and Immune Evolution of Melanoma Acquiring MAPKi Resistance. Cell. 2015 Sep 10;162(6):1271–85.

268. Zingg D, Sommer L. Rare, yet relevant tumor cells – A new twist to melanoma cell plasticity. Pigment Cell Melanoma Res. 2018 Jan 1;31(1):7–9.

269. Rambow F, Rogiers A, Marin-Bejar O, Aibar S, Femel J, Dewaele M, et al. Toward Minimal Residual Disease-Directed Therapy in Melanoma. Cell. 2018 Aug 9;174(4):843-855.e19.

270. Fufa TD, Harris ML, Watkins-Chow DE, Levy D, Gorkin DU, Gildea DE, et al. Genomic analysis reveals distinct mechanisms and functional classes of SOX10-regulated genes in melanocytes. Hum Mol Genet. 2015 Oct 1;24(19):5433–50.

271. Cohen-Solal KA, Kaufman HL, Lasfar A. Transcription factors as critical players in melanoma invasiveness, drug resistance, and opportunities for therapeutic drug development. Pigment Cell Melanoma Res. 2018 Mar 1;31(2):241–52.

272. Mascarenhas JB, Littlejohn EL, Wolsky RJ, Young KP, Nelson M, Salgia R, et al. PAX3 and SOX10 activate MET receptor expression in melanoma. Pigment Cell Melanoma Res. 2010 Apr;23(2):225–37.

273. Malladi S, MacAlinao DG, Jin X, He L, Basnet H, Zou Y, et al. Metastatic Latency and Immune Evasion through Autocrine Inhibition of WNT. Cell. 2016 Mar 24;165(1):45–60.

274. Dravis C, Chung CY, Lytle NK, Herrera-Valdez J, Luna G, Trejo CL, et al. Epigenetic and transcriptomic profiling of mammary gland development and tumor models disclose regulators of cell state plasticity. Cancer Cell [Internet]. 2018 Sep 9 [cited 2023 Aug 24];34(3):466. Available from: /pmc/articles/PMC6152943/

275. Rosenbaum SR, Tiago M, Caksa S, Capparelli C, Purwin TJ, Kumar G, et al. SOX10 requirement for melanoma tumor growth is due, in part, to immune-mediated effects. Cell Rep. 2021 Dec 7;37(10).

276. Li T, Fu J, Zeng Z, Cohen D, Li J, Chen Q, et al. TIMER2.0 for analysis of tumor-infiltrating immune cells. Nucleic Acids Res. 2020 Jul 2;48(W1):W509–14.

277. Cerami E, Gao J, Dogrusoz U, Gross BE, Sumer SO, Aksoy BA, et al. The cBio Cancer Genomics Portal: An open platform for exploring multidimensional cancer genomics data. Cancer Discov. 2012 May;2(5):401–4.

278. Gao J, Aksoy BA, Dogrusoz U, Dresdner G, Gross B, Sumer SO, et al. Integrative analysis of complex cancer genomics and clinical profiles using the cBioPortal. Sci Signal. 2013 Apr 2;6(269).

279. Tucci M, Passarelli A, Mannavola F, Felici C, Stucci LS, Cives M, et al. Immune System Evasion as Hallmark of Melanoma Progression: The Role of Dendritic Cells. Front Oncol. 2019 Nov 5;9.

280. Dankner M, Gray-Owen SD, Huang YH, Blumberg RS, Beauchemin N. CEACAM1 as a multi-purpose target for cancer immunotherapy. Oncoimmunology. 2017 Jul 3;6(7).

281. Öbrink B. CEA adhesion molecules: Multifunctional proteins with signal-regulatory properties. Curr Opin Cell Biol. 1997;9(5):616–26.

282. Chen Z, Chen L, Qiao SW, Nagaishi T, Blumberg RS. Carcinoembryonic Antigen-Related Cell Adhesion Molecule 1 Inhibits Proximal TCR Signaling by Targeting ZAP-70. The Journal of Immunology. 2008 May 1;180(9):6085–93.

283. Ieda J, Yokoyama S, Tamura K, Takifuji K, Hotta T, Matsuda K, et al. Re-expression of CEACAM1 long cytoplasmic domain isoform is associated with invasion and migration of colorectal cancer. Int J Cancer. 2011 Sep 15;129(6):1351–61.

284. Gray-Owen SD, Blumberg RS. CEACAM1: Contact-dependent control of immunity. Nat Rev Immunol. 2006 Jun;6(6):433–46.

285. Ullrich N, Heinemann A, Nilewski E, Scheffrahn I, Klode J, Scherag A, et al. CEACAM1-3S drives melanoma cells into NK cell-mediated cytolysis and enhances patient survival. Cancer Res. 2015 May 1;75(9):1897–907.

286. Oliveira-Ferrer L, Tilki D, Ziegeler G, Hauschild J, Loges S, Irmak S, et al. Dual role of carcinoembryonic antigen-related cell adhesion molecule 1 in angiogenesis and invasion of human urinary bladder cancer. Cancer Res. 2004 Dec 15;64(24):8932–8.

287. Xu J, Liu B, Ma S, Zhang J, Ji Y, Xu L, et al. Characterizing the Tumor Suppressor Role of CEACAM1 in Multiple Myeloma. Cellular Physiology and Biochemistry. 2018 Mar 1;45(4):1631–40.

288. Hu Y, Smyth GK. ELDA: Extreme limiting dilution analysis for comparing depleted and enriched populations in stem cell and other assays. J Immunol Methods. 2009 Aug 15;347(1–2):70–8.

289. Kawai T, Yasuchika K, Ishii T, Miyauchi Y, Kojima H, Yamaoka R, et al. SOX9 is a novel cancer stem cell marker surrogated by osteopontin in human hepatocellular carcinoma. Sci Rep. 2016 Jul 26;6.

290. Wang Z, Xu X, Nan-Liu, Cheng Y, Jin W, Zhang P, et al. SOX9-PDK1 axis is essential for glioma stem cell self-renewal and temozolomide resistance. Oncotarget. 2018;9(1):192–204.

291. Xue Y, Lai L, Lian W, Tu X, Zhou J, Dong P, et al. SOX9/FXYD3/Src axis is critical for ER þ breast cancer stem cell function. Molecular Cancer Research. 2019 Jan 1;17(1):238–49.

292. AKT-mediated phosphorylation of Sox9 induces Sox10 transcription in a murine model of HER2-positive breast cancer - PMC [Internet]. [cited 2023 Aug 24]. Available from: https://www.ncbi.nlm.nih.gov/pmc/articles/PMC8120776/

293. Ashkenazi S, Ortenberg R, Besser M, Schachter J, Markel G. SOX9 indirectly regulates CEACAM1 expression and immune resistance in melanoma cells. Oncotarget. 2016 May 24;7(21):30166–77.

294. Zalzali H, Naudin C, Bastide P, Quittau-Prévostel C, Yaghi C, Poulat F, et al. CEACAM1, a SOX9 direct transcriptional target identified in the colon epithelium. Oncogene. 2008 Nov 27;27(56):7131–8.

295. Bondurand N, Pingault V, Goerich DE, Lemort N, Sock E, Le Caignec C, et al. Interaction among SOX10, PAX3 and MITF, three genes altered in Waardenburg syndrome. Hum Mol Genet. 2000 Aug 12;9(13):1907–17.

296. Marathe HG, Watkins-Chow DE, Weider M, Hoffmann A, Mehta G, Trivedi A, et al. BRG1 interacts with SOX10 to establish the melanocyte lineage and to promote differentiation. Nucleic Acids Res. 2017 Jun 1;45(11):6442–58.

297. Beauchemin N, Draber P, Dveksler G, Gold P, Gray-Owen S, Grunert F, et al. Redefined nomenclature for members of the carcinoembryonic antigen family. Exp Cell Res. 1999 Nov 1;252(2):243–9.

298. Ortenberg R, Sapir Y, Raz L, Hershkovitz L, Arav A Ben, Sapoznik S, et al. Novel immunotherapy for malignant melanoma with a monoclonal antibody that blocks CEACAM1 homophilic interactions. Mol Cancer Ther. 2012 Jun;11(6):1300–10.

299. Edlund M, Blikstad I, Öbrink B. Calmodulin binds to specific sequences in the cytoplasmic domain of C-CAM and down-regulates C-CAM self-association. Journal of Biological Chemistry. 1996 Jan 19;271(3):1393–9.

300. Erratum: CEACAM1 regulates TIM-3-mediated tolerance and exhaustion (Nature (2015) 517 (386-390) DOI: 10.1038/nature13848). Nature. 2016 Mar 16;536(7616):359.

301. Acharya N, Acharya N, Sabatos-Peyton C, Anderson AC, Anderson AC. Tim-3 finds its place in the cancer immunotherapy landscape. J Immunother Cancer. 2020 Jun 29;8(1).

302. Grzywa TM, Paskal W, Włodarski PK. Intratumor and Intertumor Heterogeneity in Melanoma. Transl Oncol. 2017 Dec 1;10(6):956–75.

303. Thies A, Moll I, Berger J, Wagener C, Brümmer J, Schulze HJ, et al. CEACAM1 expression in cutaneous malignant melanoma predicts the development of metastatic disease. Journal of Clinical Oncology. 2002 May 15;20(10):2530–6.

304. Malhotra GK, Zhao X, Edwards E, Kopp JL, Naramura M, Sander M, et al. The role of Sox9 in mouse mammary gland development and maintenance of mammary stem and luminal progenitor cells. BMC Dev Biol [Internet]. 2014 Dec 20 [cited 2024 Feb 6];14(1):1–11. Available from: https://bmcdevbiol.biomedcentral.com/articles/10.1186/s12861-014-0047-4

305. Mertelmeyer S, Weider M, Baroti T, Reiprich S, Fröb F, Stolt CC, et al. The transcription factor Sox10 is an essential determinant of branching morphogenesis and involution in the mouse mammary gland. Scientific Reports 2020 10:1 [Internet]. 2020 Oct 20 [cited 2024 Feb 6];10(1):1–16. Available from: https://www.nature.com/articles/s41598-020-74664-y

306. Naqvi S, Kim S, Hoskens H, Matthews HS, Spritz RA, Klein OD, et al. Precise modulation of transcription factor levels identifies features underlying dosage sensitivity. Nature Genetics 2023 55:5 [Internet]. 2023 Apr 6 [cited 2024 Feb 7];55(5):841–51. Available from: https://www.nature.com/articles/s41588-023-01366-2

307. Kondělková K, Vokurková D, Krejsek J, Borská L, Fiala Z, Ctirad A. Regulatory T cells (TREG) and their roles in immune system with respect to immunopathological disorders. Acta Medica (Hradec Kralove) [Internet]. 2010 [cited 2024 Apr 13];53(2):73–7. Available from: https://pubmed.ncbi.nlm.nih.gov/20672742/

308. Ackerman A, Klein O, McDermott DF, Wang W, Ibrahim N, Lawrence DP, et al. Outcomes of patients with metastatic melanoma treated with immunotherapy prior to or after BRAF inhibitors. Cancer. 2014 Jun 1;120(11):1695–701.

309. Tétu P, Mangana J, Dummer R, Dutriaux C, Beneton N, Dalle S, et al. Benefit of the nivolumab and ipilimumab combination in pretreated advanced melanoma. Eur J Cancer. 2018 Apr 1;93:147–9.

310. Mason R, Dearden HC, Nguyen B, Soon JA, Smith JL, Randhawa M, et al. Combined ipilimumab and nivolumab first-line and after BRAF-targeted therapy in advanced melanoma. Pigment Cell Melanoma Res. 2019 Mar 1;33(2):358–65.

311. Hugo W, Zaretsky JM, Sun L, Song C, Moreno BH, Hu-Lieskovan S, et al. Genomic and Transcriptomic Features of Response to Anti-PD-1 Therapy in Metastatic Melanoma. Cell [Internet]. 2016 Mar 3 [cited 2024 Feb 5];165(1):35. Available from: /pmc/articles/PMC4808437/

312. Haas L, Elewaut A, Gerard CL, Umkehrer C, Leiendecker L, Pedersen M, et al. Acquired resistance to anti-MAPK targeted therapy confers an immune-evasive tumor microenvironment and cross-resistance to immunotherapy in melanoma. Nature Cancer 2021 2:7 [Internet]. 2021 Jul 15 [cited 2024 Feb 5];2(7):693–708. Available from: https://www.nature.com/articles/s43018-021-00221-9

313. Martin-Hijano L, Sainz B. The Interactions Between Cancer Stem Cells and the Innate Interferon Signaling Pathway. Front Immunol [Internet]. 2020 Mar 31 [cited 2024 Feb 9];11:526. Available from: /pmc/articles/PMC7136464/

314. Yokoyama S, Takahashi A, Kikuchi R, Nishibu S, Lo JA, Hejna M, et al. SOX10 regulates melanoma immunogenicity through an IRF4-IRF1 axis. Cancer Res [Internet]. 2021 Dec 12 [cited 2024 Feb 5];81(24):6131. Available from: /pmc/articles/PMC8678351/

315. Glasheen MQ, Caksa S, Young AG, Wilski NA, Ott CA, Chervoneva I, et al. Targeting up-regulated cIAP2 in SOX10-deficient drug tolerant melanoma. Mol Cancer Ther [Internet]. 2023 Sep 1 [cited 2024 Feb 9];22(9):1087–99. Available from: /mct/article/22/9/1087/728673/Targeting-Upregulated-cIAP2-in-SOX10-Deficient

Appendix A

AKT-mediated phosphorylation of Sox9 induces Sox10 transcription in a murine model of HER2-positive breast cancer

Al-Zahrani, K. N., Abou-Hamad, J., Pascoal, J., Labrèche, C., Garland, B., & Sabourin, L. A. (2021). AKT-mediated phosphorylation of Sox9 induces Sox10 transcription in a murine model of HER2-positive breast cancer. Breast cancer research: BCR, 23(1), 55. https://doi.org/10.1186/s13058-021-01435-6

Author contributions

Al-Zahrani K: Performed and conceptualized most experiments. Wrote, proofread, and edited the manuscript.

Abou-Hamad J: Conceptualized experiments, cloned a majority of the luciferase plasmids, and performed a majority of the luciferase assays. Proofread the manuscript.

Pascoal J: Performed most experiments during the review process.

Labrèche C: Performed experiments during the review process.

Garland G: Performed experiments during the review process.

Sabourin L: Provided expertise throughout the project. Wrote, proofread, and edited the manuscript.

This paper was published in Breast Cancer Research on May 13, 2021.

AKT-mediated phosphorylation of Sox9 induces Sox10 transcription in a murine model of HER2-positive breast cancer

Authors

Khalid N Al-Zahrani 1 2, John Abou-Hamad 1 2, Julia Pascoal 1, Cédrik Labrèche 1 2, Brennan Garland 1 2, Luc A Sabourin 3 4

Affiliations

1. Centre for Cancer Therapeutics, Ottawa Hospital Research Institute, 501 Smyth Road, Ottawa, ON, K1H 8L6, Canada.
2. Department of Cellular and Molecular Medicine, University of Ottawa, Ottawa, ON, K1H 8M5, Canada.
3. Centre for Cancer Therapeutics, Ottawa Hospital Research Institute, 501 Smyth Road, Ottawa, ON, K1H 8L6, Canada. lsabourin@ohri.ca.
4. Department of Cellular and Molecular Medicine, University of Ottawa, Ottawa, ON, K1H 8M5, Canada. lsabourin@ohri.ca.

Disclosures

The authors declare no competing interests.

Funding

K.N.A. is funded by and would like to thank the Canadian Breast Cancer Foundation. J.A. is funded by scholarships from the Canadian Institutes of Health Research. This study was supported

by grants from the Canadian Breast Cancer Foundation, the Canadian Cancer Society Research Institute, and the Canadian Institutes of Health Research.

ABSTRACT

Background

Approximately 5–10% of HER2-positive breast cancers can be defined by low expression of the Ste20-like kinase, SLK, and high expression of SOX10. Our lab has observed that genetic deletion of SLK results in the induction of Sox10 and significantly accelerates tumor initiation in a HER2-induced mammary tumor model. However, the mechanism responsible for the induction of SOX10 gene expression in this context remains unknown.

Methods

Using tumor-derived cell lines from MMTV-Neu mice lacking SLK and biochemical approaches, we have characterized the signaling mechanisms and relevant DNA elements driving Sox10 expression.

Results

Biochemical and genetic analyses of the SOX10 regulatory region in SLK-deficient mammary tumor cells show that Sox10 expression is dependent on a novel −7kb enhancer that harbors three SoxE binding sites. ChIP analyses demonstrate that Sox9 is bound to those elements in vivo. Our data show that AKT can directly phosphorylate Sox9 in vitro at serine 181 and that AKT inhibition blocks Sox9 phosphorylation and Sox10 expression in SLK(-/-) tumor cells. AKT-mediated Sox9 phosphorylation increases its transcriptional activity on the Sox10 −7kb enhancer without altering

its DNA-binding activity. Interestingly, analysis of murine and human mammary tumors reveals a direct correlation between the levels of active phospho-Sox9 S181 and Sox10 expression.

Conclusions

Our results have identified a novel Sox10 enhancer and validated Sox9 as a direct target for AKT. As Sox10 is a biomarker for triple-negative breast cancers (TNBC), these findings might have major implications in the targeting and treatment of those cancers.

INTRODUCTION

Approximately, 12% of all new cancers yearly are reported as breast carcinomas. However, extensive heterogeneity and the complex biology and etiology for the various breast cancer subtypes make treatment difficult. Breast cancer subtypes are generally classified based on the expression of the estrogen receptor (ESR1), progesterone receptor (PGR), or the human epidermal growth factor receptor 2 (HER2) (1,2). The HER2-positive subtype, characterized by overexpression and amplification of HER2, accounts for 20–30% of all breast cancers and is associated with poor prognosis and aggressive cancers(3,4). The activation of the HER2 receptor through tyrosine phosphorylation (5,6) results in the upregulation of proliferative and survival pathways (7,8). Although HER2 amplification is a critical event in the etiology of HER2+ breast cancers, the molecular mechanisms regulating its progression are not fully understood.

The Ste20-like kinase (SLK) has been shown to regulate multiple biological responses(9). In addition to cell migration (10,11), SLK has been observed to play an important role in the breakdown of E-cadherin and ZO-1-positive junctions following TGFβ stimulation(12). The loss of SLK delayed EMT, suggesting that it regulates the cytoskeletal changes associated with this process (12,13). We have previously shown that SLK is activated downstream of Neu (rat homolog

of HER2) and requires PI3K or PLCγ activity for maximal activation(14). Supporting a role for SLK in HER2-driven signaling, expression of a dominant negative SLK K63R reduced HER2-dependent chemotaxis in human breast cancer cell lines.

The Akt/PKB literature is constantly growing since the cloning of v-Akt in 1987 (extensively reviewed in (15)). It is now well established that Akt activation occurs downstream of phosphoinositide-3-kinase (PI3K), a lipid kinase implicated in tumorigenesis and the insulin response. The PI3K-dependent generation of PtdIns-3,4-P3 (PIP3) recruits and activates Akt at the membrane in concert with PDK1 and mTORC2. There are well over 100 reported Akt substrates implicated cell survival, proliferation, metabolism, neuronal functions, and angiogenesis. To date, the only transcription factors reported to be Akt targets are the Forkhead Box O proteins (FoxO1, 3, 4, and 6), regulating multiple transcription programs. Their phosphorylation induces their cytosolic retention through interactions with 14-3-3 proteins, blocking their access to target genes. The importance of turning off the PI3K-Akt pathway is underscored by the sheer number of negative feedback and cross-talk pathways. The most critical signal terminator is the phosphatase tumor suppressor PTEN, capable of converting the activator PIP3 to PIP2. Obviously, perturbations in AKT signaling lead to numerous pathological conditions such as overgrowth syndromes, autoimmune diseases, and cancer.

The Sry-HMG-box (Sox) family of transcription (reviewed in (16–18)) plays critical roles in many developmental processes. The SoxE group proteins, including Sox8, 9, and 10, have been extensively studied in the context of reproductive system development, neural crest cell-derived tissues, and cell types such as melanocytes. Although Sox9 and Sox10 have been widely studied during development, little is known about the mechanisms that regulate their activities other than their nucleocytoplasmic shuttling. The role of the Sox proteins in cancer progression remains

elusive and controversial (reviewed in (18)). Different members have been shown to play a role both as tumor promoters and tumor suppressors in various types of cancers through the regulation of oncogenic pathways. Supporting this, Sox2 and Sox9 have been shown to be critical for the persistence of quiescent stem-like cancer cells through immune evasion(19). We and others have recently identified Sox10 as a marker of triple-negative breast cancers (TNBC) (20) and secretory carcinomas, often triple negative and basal-like. Recently, Sox10 was found to be specifically expressed in mammary progenitor cells, including fetal and adult mammary cells in vivo (21) and be critical to maintain the stem cell state and reprogramming in breast cancer (22). Strikingly, Sox10 deletion impairs mammary gland reconstitution whereas its overexpression increases it (21).

We have recently demonstrated that conditional SLK deletion in a MMTV-Neu background activates the PDK1-Akt system and accelerates breast tumor onset (23). Although they are HER2/Neu+, those tumors display a basal-like phenotype. Strikingly, early lesions and tumor-derived cell lines express high levels of Sox10, a marker of TNBC(20). This is accompanied by increased tumor stem cell activity in vitro and enhanced tumor growth in xenograft models. Interestingly, this phenotype is dependent on AKT activity and Sox10 expression. To gain insights into the molecular mechanisms regulating Sox10 expression, we have further assessed the role of the PI3K-PDK1-AKT pathway on Sox10 regulation. Our data show that AKT-driven Sox10 expression is dependent on Sox9 activation. Furthermore, this activation requires direct Sox9 phosphorylation by AKT. Our studies have uncovered Sox9 as a novel substrate for AKT, providing a novel link between AKT and tumor progression.

METHODS

Plasmids and cloning

Fragments of the Sox10 promoter were amplified by PCR (see Supp. Table 1) from the bacterial artificial chromosome (BAC) RP23-424P8 which contains up to 12 kb of the Sox10 promoter and was purchased from the Centre of Applied Genomics (SickKids, Toronto, Canada). Each fragment of the Sox10 promoter was amplified using the indicated primers in Supplementary Table 1, digested with KpnI and XhoI (which were included in the forward or reverse primer, respectively) and ligated into pGL3P which was linearized with KpnI and XhoI.

pGEX-Sox9 was generated by PCR amplifying Sox9 cDNA from pCMV6-myc-DDK-Sox9 with the indicated primers in Supplementary Table 1, digested with BamHI and XhoI (which were included in the forward or reverse primer, respectively) and ligated into pGEX-4T2 which was linearized with BamHI and XhoI.

pGEX-Sox91-223 was generated by linearizing and purifying pGEX-Sox9 with SmaI and NotI. The linear fragment was then blunted with Klenow (New England Biolabs) and purified from a 0.8% agarose gel using the QIAGEN Gel Extraction Kit (28704). The linearized vector was then incubated with T4 DNA ligase (New England Biolabs) to generate the circular plasmid.

Sox9 S181A mutants were generated using either pGEX-Sox91-223 or pCMV6-myc-DDK-Sox9 as template. The point mutation was generated using the QuickChange XL Site-directed Mutagenesis Kit according to the manufacturer's protocol. The primers used to generate the point mutations are listed in Supplementary Table 1.

Cell culture

All mammary tumor cell lines were maintained in DMEM/F12 containing 10% FBS, 1% mammary epithelial growth supplement (Life Technologies), 1% penicillin/streptomycin, and 1% l-glutamine. Mammary tumor cell lines were isolated as described from individual tumors at

endpoint (23). All experiments were performed on three independent isolates and representative data are shown. All mammary tumor cell lines were used within 30 passages of initial isolation. All other cell lines used were maintained in DMEM containing 10% FBS, 1% penicillin/streptomycin, and 1% l-glutamine. Cells were cultured at 37°C in a humidified incubator set at 5% CO2. Cells were routinely passaged at a one in ten dilution every 2–3 days.

For plasmid and siRNA (Supplementary Table 3) transfections, cells were seeded such that they would reach approximately 75% confluency the day of the transfection. Lipofectamine 3000 was used for all transfections according to the manufacturer's protocol using 8 μg of plasmid DNA or 200 nM of each siRNAs. Transfections were performed for 48–72 h prior to cell harvest.

Immunohistochemistry

The tissues were harvested and fixed in 10% buffered formalin phosphate for 24 h and then transferred to 70% ethanol for storage. The tissues were formalin fixed, paraffin-embedded, and sectioned at a 5-μm thickness. Tissue sections were deparaffinized and subjected to antigen retrieval in 10 mM citrate buffer (pH 6.0) and quenched with 3% hydrogen peroxide. Sections were blocked in 5% donkey serum and incubated overnight with the indicated primary antibody (Supplementary Table 2) at 4°C. Sections were washed followed by incubation with the appropriate HRP-conjugated secondary antibody. For mouse monoclonal antibodies on mouse tissues, mouse-on-mouse blocking solution (Vector Laboratories) was added to the blocking step. All IHC staining were carefully controlled with no primary antibody controls. Staining was developed using DAB substrate (Sigma Aldrich), and sections were counterstained with hematoxylin. Sections were dehydrated in ethanol then xylene and mounted. Sections were imaged using the Aperio Scanscope (Leica Biosystems), and images were processed and/or analyzed using Imagescope or ImageJ. For quantification, stained and scanned sections were opened in

ImageScope and the percentage of DAB-positive (brown) pixels for each core was quantified using the built-in Aperio positive pixel count algorithm. Only pixels that fell into the "strong positive" default setting were counted. For the murine hyperplastic lesions, a total of 10 mammary glands were surveyed for each genotype.

Western blotting

Tissues and cell lines were homogenized in RIPA lysis buffer containing protease inhibitors (0.05% SDS, 1% Triton X-100, 1% NP-40, 50 mM Tris-HCl, pH 7.5, 150 mM NaCl, 2 mM EDTA, pH 8.0, 12 mM Na-Deoxycholate, 10 mM NaF, 1 mM DTT, 10 mM β-glycerophosphate, 0.6 mM NaVO3, 1 mM PMSF, 10 μg/mL leupeptin, 10 μg/mL aprotinin, 10 μg/mL pepstatin, and 100 μM benzamide). Lysate was cleared by centrifugation and protein concentrations were determined using Bradford reagent (Bio-Rad). Equal amounts of protein lysate were denatured and subject to SDS-PAGE. Samples were then transferred to a PVDF membrane and probed with the indicated primary antibody (Supplementary Table 2) overnight at 4°C in 5% BSA. The membranes were washed and incubated with the appropriate HRP-conjugated secondary antibody. Reactive proteins were detected by chemiluminescence (Perkin Elmer) and exposure to X-ray film.

GST-fusion protein production and kinase assay

RP bacteria were transformed with the indicated GST or GST-fusion plasmids and glycerol stocks were stored at −80°C. Glycerol stocks were used to inoculate 3 mL of LB broth containing the appropriate antibiotic, and cultures were left to grow overnight at 37°C with shaking at 225 rpm. The 3-mL cultures were then expanded to 30 mL and left to shake at 225 rpm for 1 h at 37°C. GST-fusion protein production was then induced with 1 mM IPTG for 2 h at 37°C with shaking at 225 rpm. The bacterial cultures were then pelleted at 3000 rpm for 15 min at 4°C. Bacterial pellets

were lysed in 500 μL of RIPA lysis buffer containing protease inhibitors and incubated on ice for 15 min with occasional vortexing. Lysates were then sonicated with three 15-s pulses and cleared by centrifugation at 14000 rpm for 30 min at 4°C. GST-fusion proteins were then purified with 20 μL of GST-sepharose beads (GE Healthcare) using the immunoprecipitation protocol.

In vitro kinase assays were performed as previously described (11). Briefly, GST samples were pulled down and washed beads were resuspended in 1x kinase buffer (20-mM Tris-HCl, pH 7.4, 0.25-mM NaVO3, 1-mM NaF, 10-mM β-glycerophosphate, 1-mM DTT, and 15-mM MgCl2). The kinase assay was initiated by the addition of 1 μL of [32P]γATP (5 μCi/μL, Perkin Elmer) and incubated for 30 min at 30°C. Recombinant human GST-AKT fusion protein (200ng; Sigma Aldrich, SRP-5001) was added to the kinase assay master mix. The reactions were terminated with the addition of 4x SDS sample buffer (200-mM Tris-HCl, 400-mM DTT, 8% SDS, 0.4% bromophenol blue, and 40% glycerol) and subject to SDS-PAGE. The incorporation of the radiolabeled phosphate was detected by autoradiography and the efficiency of immunoprecipitation was determined by Western blot.

Quantitative real-time PCR and microarray analysis

The total RNA was isolated using Trizol (Invitrogen). cDNA synthesis was performed using the Superscript III Reverse Transcriptase (Life Technologies) according to the manufacturer's protocol. qRT-PCR was performed using an Applied Biosystems 7500 Real-Time Fast PCR thermocycler. Relative mRNA expression was calculated using the ΔΔCT method and normalizing to total levels of ribosomal 18S. For microarray analysis, total RNA was hybridized to the Mouse Gene 2.0 ST Array (Affymetrix). Microarray data analysis was carried out in the r statistical programming environment with Bioconductor (GSE128514). Primers used for qRT-PCR are listed in Supplementary Table 1.

Bisulfite sequencing

Genomic DNA for bisulfite conversion was isolated using the DNeasy Blood and Tissue Kit following the manufacturer's protocol (QIAGEN). Bisulfite conversion of genomic DNA was performed using the EpiTect Plus DNA Bisulfite Kit (QIAGEN) following the manufacturer's protocol. Promoter regions of control and bisulfite converted DNA were amplified using the primers indicated in Supplementary Table 1 using Taq polymerase (Invitrogen). Amplicons were subcloned into pGEM-T (Promega) according to the manufacturer's protocol. Five clones for each conversion reaction were picked, miniprepped, and sequenced to identify methylated cytosine residues.

Luciferase assay

For luciferase assays, 1.5 × 105 cells were seeded in triplicate wells of a 6-well plate. The following day, the cells were transfected using lipofectamine 3000 with 1.25 μg of the appropriate pGL3P reporter construct and 1.25 μg of pRL-CMV (encoding Renilla luciferase) for 48 h. Luciferase assays were performed using the Dual Luciferase Assay Reporter System (Promega). Cells were collected in 1.5 mL Eppendorf tubes and lysed in 100 μL of 1X passive lysis buffer with rotation at room temperature for 30 min. Lysates were cleared by centrifugation at 13000 rpm for 10 min at room temperature. 20 μL of each sample was transferred in triplicate into a black-sided 96-well plate with a clear bottom. 100 μL of resuspended Luciferase Assay Substrate was added to each well and read using a luminometer with a read time of 10 s and a 2-s delay per well. 100 μL of Stop and Glo solution was then added to each well and read using a luminometer with a read time of 10 s and a 2-s delay per well. Luciferase counts were normalized to the pRL-CMV counts to account for differences in transfection efficiency between wells.

Chromatin immunoprecipitation

For chromatin immunoprecipitation, 5×106 cells from each condition were seeded in two 15-cm plates and cultured for 48 h. Cells were then cross-linked in 1% formaldehyde for 10 min at room temperature. The formaldehyde was then quenched with the addition of glycine to a final concentration of 125 mM. Nuclear extraction, chromatin digestion, and immunoprecipitation and DNA elution were all performed using the SimpleChip Kit (Cell Signaling Technologies) according to the manufacturer's protocol with the addition of a pre-clearing step with beads alone prior to the immunoprecipitation. 10 μg of chromatin was used per immunoprecipitation with 1 μg of the indicated antibody. Following chromatin IP and DNA cleanup, 6.5 μL of chromatin was mixed with 35 μL of iTaq Universal SYBR Green Supermix (BioRad), 6.5 μL of the indicated primers (5μM), and 21 μL of nuclease-free water. The PCR reaction was started with an initial hold and denaturation at 50°C for 5 min and 95°C for 10 min, respectively, followed by 40 cycles of denaturation at 95°C for 15 s and Annealing and Extension at 60°C for 60 s. The percent input was then calculated as follows: percent input = 2% × 2(C[T] 2% input sample – C[T] IP sample). The antibodies used for chromatin immunoprecipitation can be found in Supplementary Table 2. The primers used for ChIP-qPCR can be found in Supplementary Table 1.

RESULTS

Sox10 expression is regulated by several upstream promoter elements in SLK-deficient Neu-induced mammary tumor cells

We have previously shown that deletion of the Ste20-like kinase SLK induces Sox10 expression, enhancing tumorigenesis in vivo (23). This is also accompanied by AKT upregulation and increased tumor stem/progenitor cell activity (23). To gain further insights into the molecular

mechanisms regulating Sox10 expression, we first assessed any potential epigenetic changes at the SOX10 locus. The SOX10 promoter has previously been shown to be epigenetically silenced in human gastric cancers and metastatic melanoma (24–26), the basal level of Sox10 expression is low in vitro, we hypothesized that Sox10 gene induction could be due to gene demethylation in SLK-/- NDL cells. We identified two putative CpG islands immediately upstream of the Sox10 transcription start site using the MethPrimer CpG island prediction software (Supp. Figure 1A) (26). To assess whether the Sox10 gene was methylated, we treated SLKfl/fl and SLK-/- NDL cells with 5-aza-2'-deoxycytidine for 5 days to effectively eliminate any methylation marks within the genome. Following treatment, only a modest increase in Sox10 mRNA was observed in the SLK-/- NDL cells with no significant differences observed in SLK expressing controls (Supp. Figure 1B). The lack of a robust Sox10 induction following 5-aza-2'-deoxycytidine treatment suggests that these putative CpG islands are not heavily methylated in either cell line. To validate this, we isolated genomic DNA and performed bisulfite sequencing on both putative CpG islands and compared the methylation pattern in SLKfl/fl and SLK-/- NDL cells. Using this approach, we found that only approximately 20% of cytosines within these CpG islands are methylated in either cell line with no significant differences observed following SLK deletion (Suppl. Figure 1C). Together, these results indicate that demethylation of the Sox10 promoter is not the main mechanism of Sox10 induction following SLK deletion.

As epigenetic silencing is not responsible for the differential expression of Sox10 in SLKfl/fl and SLK-/- NDL cells, we sought to identify potential signaling systems regulating Sox10 expression. As we have shown that AKT activity is required for maintenance of Sox10 expression in SLK knockout mammary tumor cells (23), we first assessed the levels and nuclear localization of known transcription factors that are AKT-responsive. Direct AKT targets implicated in transcription

control include CREB and Forkhead box factors (FoxA1 and FoxO family (15)). Cellular fractionation and Western blot analysis (Fig 1a) showed no difference in the levels and localization of those factors, suggesting that Sox10 is likely activated through other AKT-dependent mechanisms. To bootstrap our way back to transcriptional regulators controlling Sox10 expression in SLK-null cells, we analyzed potential regulatory regions around the Sox10 gene. Comparative sequence analyses have previously identified multiple-species conserved sequences (MCS) that control Sox10 expression (27). As two of these MCS (4 and 7) have been shown to regulate Sox10 expression in mammary epithelial cells (Fig 1b for schematic), we tested whether these enhancer elements were differentially regulated in SLKfl/fl and SLK-/- NDL cells. Both enhancer elements drove luciferase activity above the levels of the control vector; however, no significant differences between cell lines was observed (Fig. 1c), suggesting that these enhancer sequences do not mediate the differential Sox10 expression observed in the SLK-/- NDL cells but perhaps mediate basal expression of Sox10. Since little is known about the mechanisms regulating Sox10 transcription other than the MCS sequences, we generated luciferase constructs driven by five independent Sox10 promoter elements within −7 kb of the transcription start site. Interestingly, the −3484/−2495 fragment of the promoter contains a repressive element which decreased luciferase activity by approximately 75% in both SLKfl/fl and SLK-/- NDL cell lines and may account for the lower basal expression of Sox10 in cultured mammary epithelial tumor cell lines (Fig 1d). Differential regulation of luciferase activity was observed in the two most distal promoter fragments between SLKfl/fl and SLK-/- NDL cells (Fig 1d). The −6904/−5995 fragment showed a three-fold increase in luciferase activity in the SLK knockout cells, whereas that same element was inactive in the control cell line (Fig 1d), suggesting that it harbors a differentially regulated enhancer region within the Sox10 promoter.

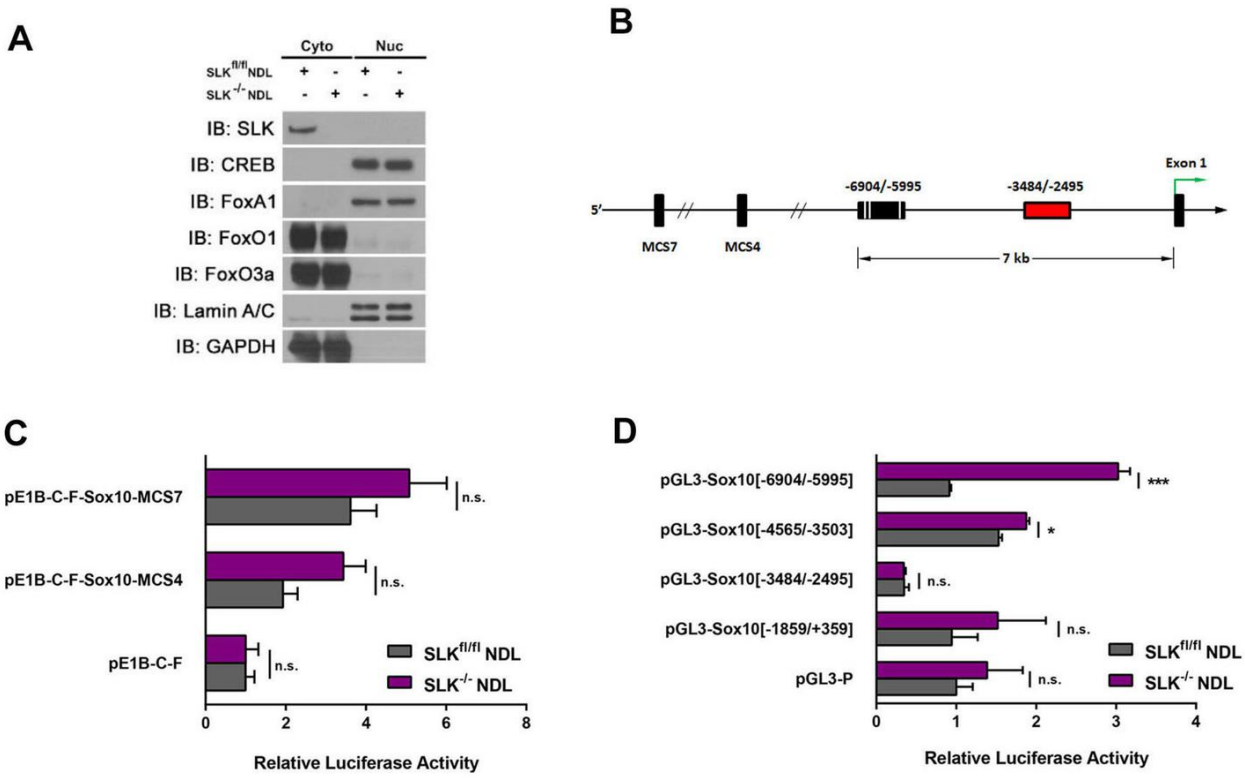
A
Cyto
Nuc
SLK fl/fl NDL
SLK -/- NDL
IB: SLK
IB: CREB
IB: FoxA1
IB: FoxO1
IB: FoxO3a
IB: Lamin A/C
IB: GAPDH
B
Exon 1
-6904/-5995
-3484/-2495
5′
MCS7
MCS4
7 kb
C
pE1B-C-F-Sox10-MCS7
pE1B-C-F-Sox10-MCS4
pE1B-C-F
n.s.
SLK fl/fl NDL
SLK -/- NDL
0
2
4
6
8
Relative Luciferase Activity
D
pGL3-Sox10[-6904/-5995]
pGL3-Sox10[-4565/-3503]
pGL3-Sox10[-3484/-2495]
pGL3-Sox10[-1859/+359]
pGL3-P
***
*
n.s.
SLK fl/fl NDL
SLK -/- NDL
0
1
2
3
4
Relative Luciferase Activity

Figure 1. Identification of a differentially regulated fragment of the Sox10 promoter following Slk deletion. **a** SLK-null tumor cells do not differentially express known transcription factors that are AKT targets. Cytosolic (cyto) and nuclear (nuc) fractions were subjected to Western blot analysis for the indicated proteins. No changes were observed in levels or distribution of the AKT targets surveyed. **b** Schematic representation of putative SoxE binding sites within the Sox10 promoter. Luciferase assays from two multiple-species conserved enhancer sequences (MCS4 and 7) that have been shown to control Sox10 expression (**c**) and approximately 1 kb fragments of the Sox10 promoter (**d**) assessed for their ability to drive luciferase activity in SLKfl/fl and SLK-/- NDL cells. Raw light units from the luciferase constructs were normalized to Renilla for each technical sample. Data is represented as the mean luciferase activity from three independent biological replicates +/− SEM. ns: no statistical difference, *$p < 0.05$, ***$p < 0.0005$

The Sox10 promoter contains putative SoxE binding sites which are bound by Sox9

Interestingly, sequence analysis of the −6904/−5995 enhancer element revealed three consensus SoxE (Sox8, 9, and 10) binding sites (27)within this 909 base pair (bp) region (see Fig. 1c). However, Q-PCR analysis revealed no detectable expression of Sox8 and no differences in Sox9 expression in either cell lines grown in culture (Fig. 2a). As Sox10 is highly expressed in the SLK-deficient cells, we investigated the possibility that Sox10 could control its own expression by assessing the levels of endogenous Sox10 in stable pBABE-Sox10 overexpressing SLKfl/fl NDL cells. Using primers located in the 3′UTR, we found that exogenous Sox10 was unable to induce endogenous gene expression (Fig. 2b).

One possibility is that the locus is in an inactive topology or, alternatively, the Sox10 target sites are bound by another SoxE transcription factor. Interestingly, the Sox9 transcription factor has been shown to induce Sox10 gene expression through SoxE binding sites (16,28–32), As Sox8 is not expressed in NDL cells, we performed chromatin immunoprecipitation (ChIP) for Sox9 at the consensus SoxE binding sites within the active −6904/−5995 element in SLK-deficient NDL cells (Fig. 2c). Although we observed a significant enrichment for Sox9 above IgG pull down in both control and SLK knockout cells, no significant differences between the two cell lines were observed (Fig 2c). Similar results were observed when using an anti-K27 acetylated histone H3 antibody, suggesting an open chromatin conformation around those enhancers (Suppl. Figure 2A). As a negative control, we also performed anti-Sox9 ChIP on a putative SoxE binding site within exon 1 that was unresponsive in our luciferase assay (Fig. 1d). This element was not bound by Sox9 in either cell line (Fig 2c), suggesting that the enrichment observed within the −6904/−5995 element is not due to non-specific chromatin pull down by the Sox9 antibody. Importantly, these

data show that the SoxE sites within the −6904/−5995 Sox10 genomic region are bound by Sox9, suggesting that it plays a role in Sox10 gene expression.

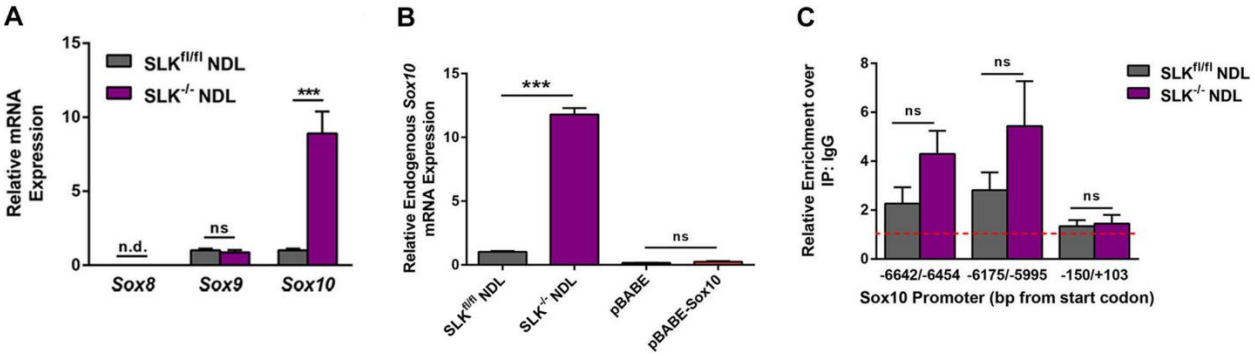
A
Relative mRNA Expression
SLK^fl/fl NDL
SLK^-/- NDL
n.d.
ns
***
Sox8
Sox9
Sox10
B
Relative Endogenous Sox10 mRNA Expression
***
ns
SLK^fl/fl NDL
SLK^-/- NDL
pBABE
pBABE-Sox10
C
Relative Enrichment over IP: IgG
SLK^fl/fl NDL
SLK^-/- NDL
ns
ns
ns
-6642/-6454
-6175/-5995
-150/+103
Sox10 Promoter (bp from start codon)

Figure 2. Sox9 binds directly to the SoxE binding sites within the Sox10 promoter. **a** The expression level of the SoxE family of transcription factors was assessed in SLKfl/fl and SLK-/- NDL cells by qRT-PCR analysis. **b** The levels of endogenous Sox10 were assessed in the indicated cell lines using qRT-PCR primers located within the 3′UTR of Sox10. Note that the retroviral pBABE-Sox10 plasmid only contains the coding cDNA and not the 3′UTR. **c** Chromatin immunoprecipitation (ChIP) was performed on SLKfl/fl and SLK-/- NDL cells to assess Sox9 binding to the Sox10 promoter. Following Sox9 ChIP, qPCR analysis was performed across two putative SoxE binding sites within the −6904/−5995 fragment of the Sox10 promoter. qRT-PCR data was normalized to an IgG ChIP (dashed red line) or a negative control element within exon one (−150/+103). N=3, nd: no detectable expression, ns: no statistical difference, ***$p < 0.0005$

Slk deletion increases Sox9 S181 phosphorylation

As Sox9 is bound to the Sox10 promoter in both wildtype and SLK knockout cell lines, we reasoned that the activity of Sox9 may be enhanced in the absence of SLK, through post-translational modifications, without affecting its DNA binding capacity. Interestingly, Sox9 has been shown to be phosphorylated at S64, S181, and S211 to regulate its nuclear import, stability, and DNA-binding/transcriptional activity(33–36). Using phospho-serine 181 (pSox9 S181) as an indicator of Sox9 activity, we assessed the levels of pSox9 S181 in both cell lines. Western blot analysis showed a marked increase in the levels of Sox9 S181 phosphorylation in SLK knockout tumor cell lines that was correlated with elevated Sox10 levels in these cells (Fig. 3a), suggesting increased Sox9 activity in SLK-null tumor cells compared to the control. This was also correlated with higher levels of active AKT (pAKT S473; Fig. 3a). We have previously reported a two-fold increase in the number of Sox10+ nuclei from SLK-null mammary hyperplasia at 16 weeks of age (23). Supporting this, immunohistochemical analysis for pSox9 S181 on hyperplastic lesions from SLK expressing and knockout hyperplastic lesions shows a similar increase (18 ± 4% vs 35 ± 7%) in the number of pSox9 S181-positive nuclei following SLK deletion in vivo (Fig 3b). We did not observe any differences in the proportion of Sox10+ or pSox9 S181+ nuclei at endpoint, suggesting that SLK deletion affects tumor initiation as previously described (23). Our previous analyses showed that SLK deletion results in a basal-like phenotype in MMTV-Neu mice (23). Furthermore, as high as 13% of HER2+ patients fall within the SLK-low/SOX10-high subtype (23) and that Sox10 is a biomarker of the TNBC subtype (20). Corroborating recent findings (37), analysis of those TCGA datasets reveals a strong correlation between high levels of Sox9 and Sox10 in TNBC samples (Fig. 3c, blue dots). To establish a potential link with active Sox9 in Sox10+ human samples, we assessed the levels of pSox9 S181 and Sox10 by immunohistochemistry across

HER2-positive, luminal, and TNBC tumor cores. Consistent with our TCGA analysis (also see (23,37)and murine data, we observed that 43% of TNBC cores were Sox10hi and that all Sox10hi nuclei in those cores also showed a pSox9 S181hi signal (Fig. 3d), suggesting that the activation of Sox9 and Sox10 induction is also observed in human breast cancer samples. Together, these studies suggest that the loss of SLK results in the activation of Sox9 that can directly induce Sox10 expression in murine tumors as well as human breast cancers.

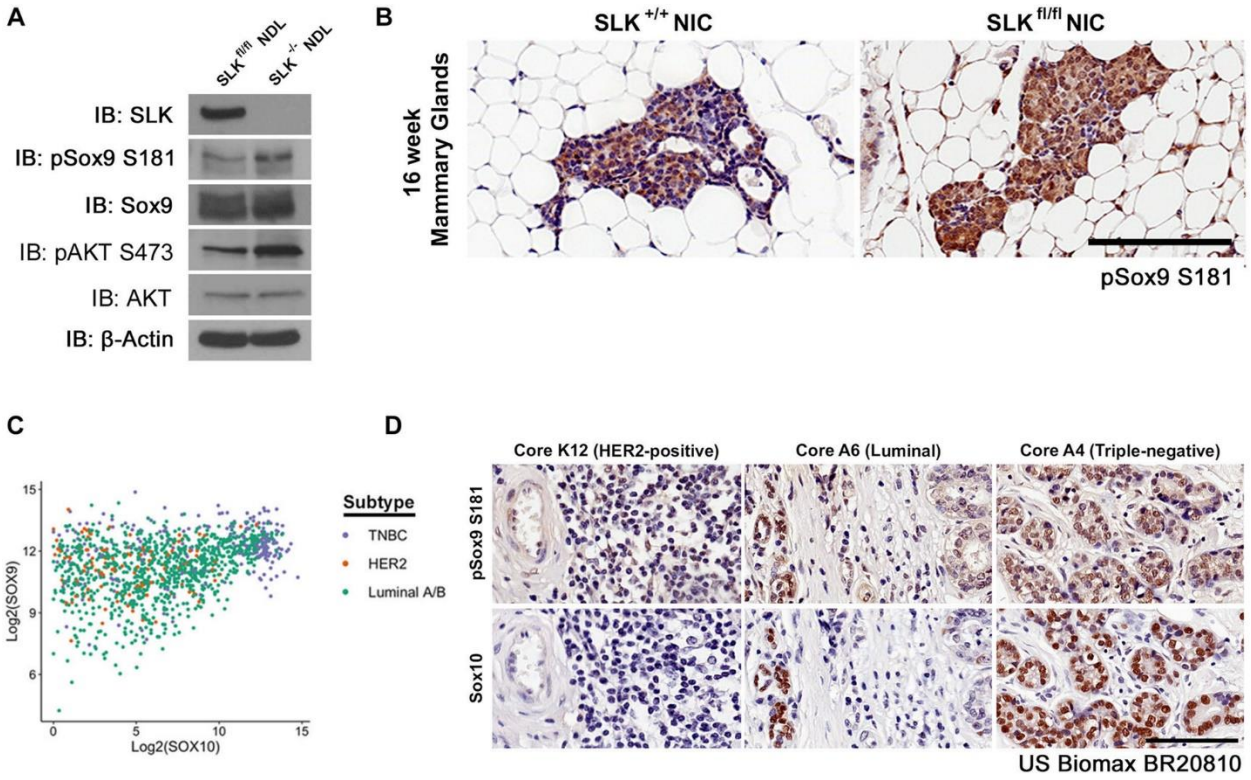
A
SLK fl/fl NDL
SLK -/- NDL
IB: SLK
IB: pSox9 S181
IB: Sox9
IB: pAKT S473
IB: AKT
IB: β-Actin
B
SLK +/+ NIC
SLK fl/fl NIC
16 week Mammary Glands
pSox9 S181
C
Log2(SOX9)
Log2(SOX10)
Subtype
TNBC
HER2
Luminal A/B
D
Core K12 (HER2-positive)
Core A6 (Luminal)
Core A4 (Triple-negative)
pSox9 S181
Sox10
US Biomax BR20810

Figure 3. Slk deletion increases phosphorylated Sox9 which is correlated with higher Sox10 expression in human breast cancer samples. a Activity of Sox9 was assessed by Western blot analysis using a pS181-specific antibody in SLKfl/fl and SLK-/- NDL cells. Active AKT was assessed using a pS473 antibody. **b** pSox9 S181 histochemistry was performed on hyperplastic lesions from mammary glands of SLK+/+ and SLKfl/fl NIC mice (n=10 glands/genotype) and representative images are shown for each genotype. Quantitation showed that SLK-null hyperplasia have a two-fold increase in pSox9 S181-positive nuclei (18 ± 4% vs 35 ± 7%; $p<0.05$). Scale bar = 100 μm. **c** The TCGA dataset was interrogated for expression of SOX9 and SOX10 across all breast cancer subtypes. Co-expression of both genes was observed in these patient samples with a Pearson correlation coefficient of 0.351 for all subtypes combined. **d** Serial sections of a human breast cancer TMA, BR20810, containing 104 breast cancer cases were stained with pSox9 S181 and Sox10 antibodies. Representative cores from each major molecular subtype, as defined by staining intensity of HER2, ESR1, and PGR, are shown. Scale bar = 200 μm

Sox9 is directly phosphorylated by AKT at serine 181

We have previously shown that Slk deletion results in enhanced mammary tumorigenesis with the activation of PDK1 and AKT (23). Therefore, we tested the possibility that Sox9 could be activated downstream of that pathway. Interestingly, amino acid sequence alignment and analysis of Sox9 revealed a putative AKT consensus phosphorylation site at serine 181, resembling several bona fide AKT targets (Fig. 4a). To assess whether Sox9 was a direct target of AKT, we performed in vitro kinase assays using recombinant proteins and monitored direct phosphorylation. As the full-length GST-Sox9 fusion protein is unstable and readily broken down in bacteria (not shown), we tested whether Sox9 was directly phosphorylated at serine 181 by AKT using a GST-Sox91-223 truncation. Recombinant AKT was able to efficiently phosphorylate the GST-Sox91-223 fusion protein, which contained the serine 181 residue (Fig. 4b, c). Mutation of serine 181 to alanine (S181A) in the GST-Sox91-223 truncation completely abolished AKT-dependent phosphorylation of Sox9 (Fig. 4c), suggesting that Sox9 is a novel substrate for AKT at the serine 181 consensus site.Supporting our in vitro kinase assays, treatment of SLK knockout cells with the AKT inhibitor MK-2206 significantly reduced the expression of Sox10 and the phosphorylation of AKT and Sox9 (Fig. 4d). Furthermore, MK-2206 treatment was sufficient to abolish luciferase activity driven from the −6904/−5995 enhancer element of the Sox10 promoter in SLK knockout cells (Fig. 4e). Knockdown of AKT1, 2 or 3 showed that a ~50% knockdown of AKT1 reduced Sox10 levels by about 50%. However, knockdown of AKT2 by 50–70% reduced Sox10 levels to about 20% of controls. Knockdown of AKT3 did not show a marked downregulation of Sox10. Together, these data suggest that AKT2 preferentially regulates Sox10 expression and that direct AKT-mediated activation of Sox9 regulates Sox10 transcription from the −6904/−5995 enhancer element.

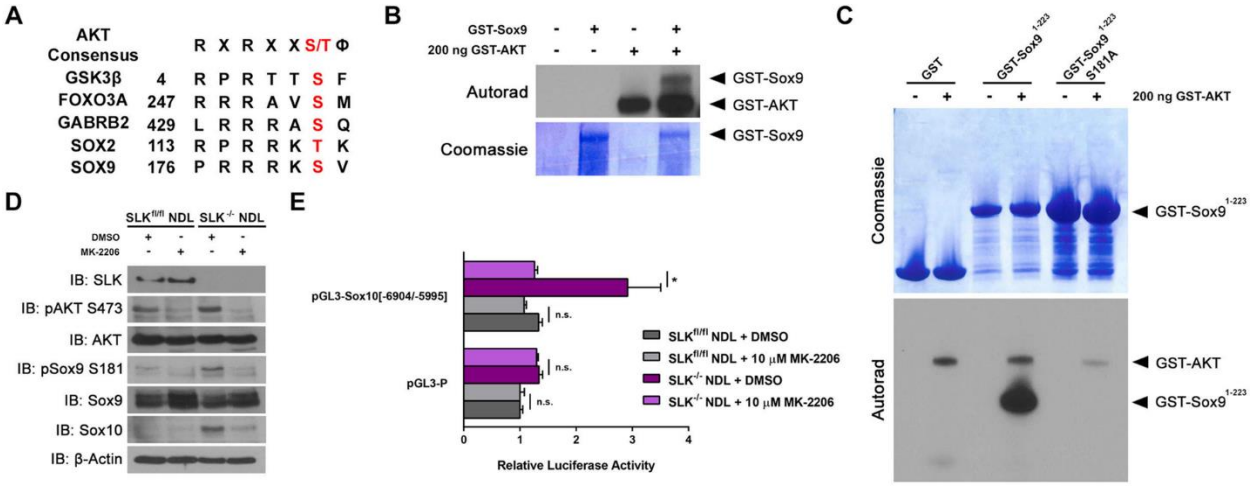
A
AKT Consensus R X R X X S/T Φ
GSK3β 4 R P R T T S F
FOXO3A 247 R R R A V S M
GABRB2 429 L R R R A S Q
SOX2 113 R P R R K T K
SOX9 176 P R R R K S V
B
GST-Sox9
200 ng GST-AKT
Autorad
Coomassie
GST-Sox9
GST-AKT
GST-Sox9
C
GST
GST-Sox9 1-223
GST-Sox9 1-223 S181A
200 ng GST-AKT
Coomassie
Autorad
GST-Sox9 1-223
GST-AKT
GST-Sox9 1-223
D
SLKfl/fl NDL
SLK-/- NDL
DMSO
MK-2206
IB: SLK
IB: pAKT S473
IB: AKT
IB: pSox9 S181
IB: Sox9
IB: Sox10
IB: β-Actin
E
pGL3-Sox10[-6904/-5995]
pGL3-P
n.s.
SLKfl/fl NDL + DMSO
SLKfl/fl NDL + 10 μM MK-2206
SLK-/- NDL + DMSO
SLK-/- NDL + 10 μM MK-2206
Relative Luciferase Activity

Figure 4. AKT directly phosphorylates Sox9 at serine 181. a The consensus AKT target sequence is provided aligned to bona fide AKT substrates (GSK-3b, FOXO3A, GABRB2, and SOX2) and the putative consensus sequence within SOX9 at serine 181. Within the consensus sequence X represents any amino acid, the phosphorylated serine (S) or threonine (T) is in red and ϕ is any hydrophobic residue. A recombinant kinase assay was performed using 200 ng of recombinant active GST-AKT and GST-Sox9 as substrate (**b**) or a GST-Sox9 S181A mutant (**c**). **d** Phosphorylation of Sox9 at serine 181 was assessed by Western blot analysis in SLKfl/fl and SLK-/- NDL cells treated with DMSO or MK-2206 for 72 hours. **e** Luciferase assays were performed in the presence or absence of MK-2206 using the responsive −6904/−5995 element of the Sox10 promoter. Raw light units from the luciferase constructs were normalized to Renilla for each technical sample. Data is represented as the mean luciferase activity from three independent biological replicates +/− SEM. ns: no statistical difference, *$p < 0.05$

Phosphorylation of Sox9 at serine 181 is required for maximal transcriptional activity

To assess the effect of Sox9 phosphorylation on Sox10 transcriptional regulation, we first tested whether phosphorylation of Sox9 was required for direct binding to the Sox10 promoter. SLK-/- NDL cells were transfected with an empty vector, myc-Sox9 or myc-Sox9 S181A and subjected to anti-myc ChIP on the Sox10 promoter (Fig. 5a). No differences were observed in DNA binding activity for the Sox9 S181A mutant (Fig. 5a), suggesting that S181 phosphorylation is not required for enhancer binding. Next, we investigated whether Sox9 S181A expression could impair luciferase expression driven from the Sox10 promoter. Transfection of myc-Sox9 into SLK-/- NDL cells with the Sox10 −6904/−5995 enhancer element resulted in a 2.5-fold increase in luciferase activity above a Myc control vector and myc-Sox91-223, lacking the C-terminal transactivation domain (Fig. 5b). Albeit significantly lower than wildtype Sox9, overexpression of the Sox9 S181A mutant also resulted in an increase in luciferase activity (Fig 5b). As Sox9 can homodimerize when bound to DNA (38), one possibility is that the Sox9 S181A mutant can form a complex with endogenous Sox9, resulting in reduced transcriptional activity imparted by the mutant Sox9.

Since Sox9 is present on the Sox10 promoter of both cell lines, we hypothesized that the activation of AKT results in DNA-bound Sox9 phosphorylation and increased transcriptional activity. To test this, we transiently overexpressed myc, myc-Sox9, or myc-Sox9 S181A in SLK-/- NDL cells and performed luciferase assays using the −6904/−5995 fragment of the Sox10 promoter. Consistent with our previous data, we observed a two- to three-fold increase in luciferase activity from the Sox10 promoter fragment with the Myc vector control (Fig. 5c) lanes 1 and 2). Additionally, we observed an AKT-dependent increase in luciferase activity following heregulin-stimulation in these cells (Fig. 5c, lanes 3 and 4). These controls further support the notion that Sox10 induction

from the −6904/−5995 promoter element is dependent on Neu signaling through AKT. To validate that these signals are dependent on Sox9 transcriptional activity (34), we assessed luciferase activity in the presence of myc-Sox9 or a myc-Sox9 S181A mutant with reduced transcriptional activity. As observed in Fig. 5b, in unstimulated cells, both wildtype and mutant Sox9 were sufficient to increase luciferase activity four-fold above background (Fig. 5c, lanes 5 and 6 compared to lanes 9 and 10). However, following stimulation with heregulin, a two-fold increase in luciferase activity was observed in myc-Sox9 expressing cells, whereas no significant change was observed in cells expressing the myc-Sox9 S181A mutant (Fig. 5c, lanes 6 and 7 compared to lanes 10 and 11). As for myc control-transfected cells, the increased luciferase activity following heregulin-stimulation in myc-Sox9 transfected cells was completely dependent on AKT activity (Fig. 5c, lanes 7 and 8). Together, these data show that the −6904/−5995 region of the Sox10 promoter is an AKT5

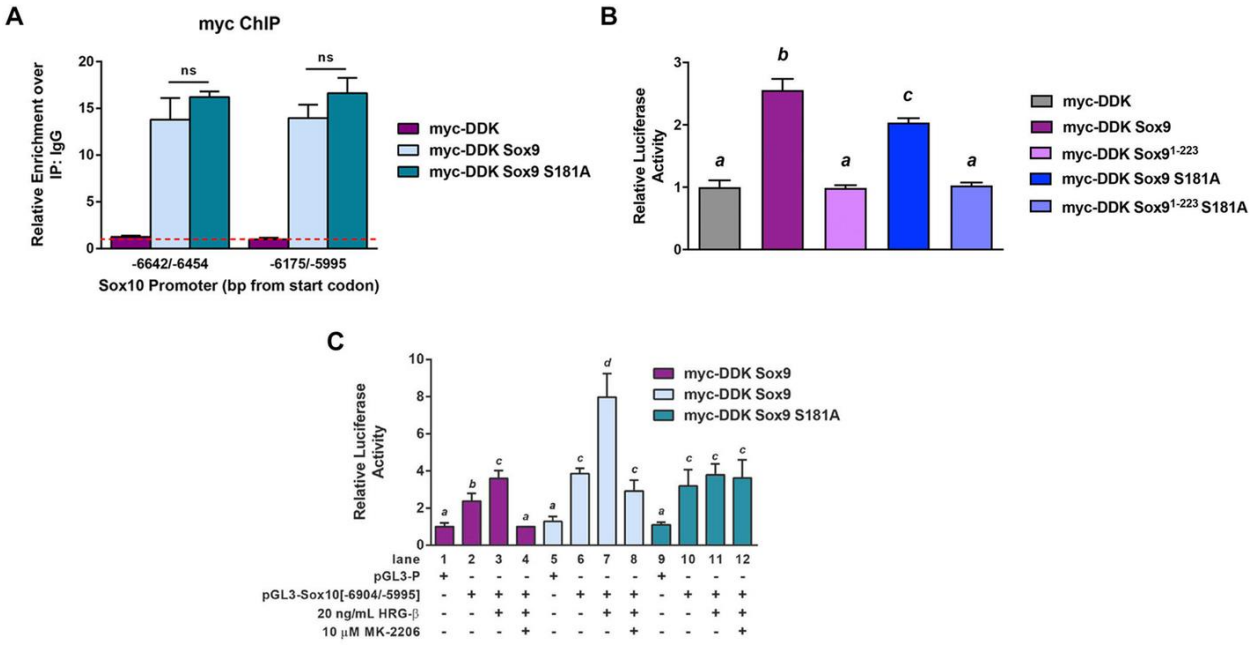
A
myc ChIP
Relative Enrichment over IP: IgG
ns
ns
-6642/-6454
-6175/-5995
Sox10 Promoter (bp from start codon)
myc-DDK
myc-DDK Sox9
myc-DDK Sox9 S181A
B
Relative Luciferase Activity
a
b
a
c
a
myc-DDK
myc-DDK Sox9
myc-DDK Sox9^1-223
myc-DDK Sox9 S181A
myc-DDK Sox9^1-223 S181A
C
Relative Luciferase Activity
myc-DDK Sox9
myc-DDK Sox9
myc-DDK Sox9 S181A
lane 1 2 3 4 5 6 7 8 9 10 11 12
pGL3-P + - - - + - - - + - - -
pGL3-Sox10[-6904/-5995] - + + + - + + + - + + +
20 ng/mL HRG-β - - + + - - + + - - + +
10 μM MK-2206 - - - + - - - + - - - +

Figure 5. Sox9 phosphorylation at serine 181 is required for maximal transcriptional activation of the Sox10 promoter. a Anti-myc ChIP was performed on SLK-/- NDL cells transiently transfected with myc-DDK, myc-DDK-Sox9, or myc-DDK-Sox9 S181A. Following anti-myc ChIP, qPCR analysis was performed across two SoxE binding sites within the −6904/−5995 fragment of the Sox10 promoter. qRT-PCR data was normalized to an IgG ChIP (dashed red line). ns: no statistical difference. **b** Luciferase assays were performed on SLK-/- NDL cells that were transiently transfected with the indicated plasmids along with the responsive −6904/−5995 element of the Sox10 promoter. Raw light units from the luciferase constructs were normalized to Renilla for each technical sample. Data is represented as the mean luciferase activity from three independent biological replicates +/− SEM. All bars with the same letter are not statistically significant from each other. a compared to b: $p < 0.005$; a compared to c: $p < 0.005$; b compared to c: $p < 0.05$. **c** SLK-/- NDL cell were transfected with the indicated plasmids along with the responsive −6904/−5995 element of the Sox10 promoter for 48 h. Cells were treated with heregulin-β (HRG-β), AKT inhibitor (MK-2206), or vehicle control for 2 h prior collecting the cell lysate. Raw light units from the luciferase constructs were normalized to Renilla for each technical sample. Data is represented as the mean luciferase activity from three independent biological replicates +/− SEM. All bars with the same letter are not statistically significant from each other. a compared to b: $p<0.05$, a compared to c or d: $p<0.005$, b compared to c: $p<0.05$, b compared to d: $p<0.005$ and c compared to d: $p<0.05$

DISCUSSION

Here, we have shown that the observed induction of Sox10 in SLK-/- NDL tumor cells is dependent on a novel enhancer located at about −7kb upstream of the putative Sox10 start site. Our data show that Sox10 expression is also directly correlated with Sox9 phosphorylation and activity in our SLK-/- NDL mouse model and human tissue microarrays. We demonstrate that AKT can directly phosphorylate DNA-bound Sox9 at serine 181, increasing its transcriptional activity on the −7kb Sox10 enhancer. These data also extends the growing list of AKT substrates.

Our data demonstrate that an AKT-dependent pathway regulates Sox10 transcription specifically through an enhancer fragment located between −6904 and −5995 from the putative start site. Scanning of this enhancer revealed three SoxE sites. Although we have observed some variability, no significant differences were found in Sox9 binding to those SoxE sites, suggesting that Sox9 is bound equally to these elements in both SLKfl/fl and SLK-/- NDL cells. This suggests that Sox9 phosphorylation at S181 activates transcription without altering its DNA binding activity. Given the large increase in Sox10 expression in the SLK-/- cells, it is likely that, in addition to Sox9 binding to SoxE sites, other transcriptional mechanisms are activated. One possibility is that phosphorylation at this site is required to recruit transcriptional cofactors which may be required for maximal activity.

Using amino acid alignment and kinase assays, we have shown that AKT can directly phosphorylate Sox9 in vitro and that enhancer activity is lost following AKT inhibition (Fig. 4). This suggests that the inability for AKT to phosphorylate Sox9 prevents its activation and Sox10 induction. Although we predict that AKT directly phosphorylates Sox9 at serine 181, this remains to be demonstrated in vivo. However, this may be more challenging as a number of other kinases have been shown to phosphorylate that site in other contexts (33–36). Alternatively, it is possible

that AKT directly phosphorylates and inhibits the activity of an unknown phosphatase that targets pSox9 S181. It is also possible that this phosphorylation may be mediated by another kinase in the AKT pathway such as S6 kinase (S6K). S6 Kinase is activated by mTOR downstream of AKT and has a consensus phosphorylation motif matching that of Sox9 S181 (39). Combined with in vitro kinase assays, rapamycin treatment to inhibit mTOR would address the potential role of S6K in Sox9 activation and Sox10 expression.

To validate the role of Sox9 in regulating the transcription of Sox10, we performed luciferase assays using the AKT-responsive element from the Sox10 promoter. Surprisingly, myc-Sox9 or the myc-Sox9 S181A mutant is both capable of activating luciferase expression from the −7kb enhancer under basal conditions (Fig. 5). This was also observed for the collagen II promoter, where the induction by both Sox9 constructs is relatively high above background (34). In the context of the collagen II promoter, wildtype Sox9 was sufficient to boost luciferase activity following co-transfection with the catalytic subunit of PKA, whereas the Sox9 S181A mutant failed to do so (34). Similarly, treatment of the myc-Sox9 transfected cells with heregulin increased luciferase activity two-fold above the untreated sample (Fig. 5c, lanes 6 and 7). However, expression of the phospho-deficient mutant abrogated this effect (Fig. 5c, lanes 10 and 11). One possibility is that Sox9 activity through phosphorylation at S181 and/or S211 can be further increased by specific signals while bound to DNA as a homodimer. This would explain the slight reduction in enhancer activity when a myc-Sox9 S181A is expressed in SLK-/-NDL cells. The S181A mutant may have a dominant negative effect on a Sox9/Sox9 S181A dimer.

We have previously shown that Sox10 is biomarker for the TNBC subtype and is induced following the mammary gland-specific deletion of SLK in a MMTV-Neu mouse model, inducing a basal-like phenotype in a HER2+ model (23). The induction of Sox10 is accompanied by

increased stemness and accelerated tumorigenesis (23). Recently, Sox10 has been shown to be expressed in mammary progenitor cells in vivo (21) and be critical to maintain stemness in breast cancer(22). Interestingly, Sox2 and Sox9 have been shown to be critical for the persistence of quiescent stem-like breast cancer cells (19). It is not clear whether those Sox9+ stem-like cells also express Sox10.

Supporting our findings in murine mammary tumors, we have also observed a correlation between pSox9 S181 levels and Sox10 expression in a proportion of HER2+ human tumor samples (23). In addition, Fig 3c shows that a high proportion of Sox10hi TNBC samples also show a Sox9hi phenotype (blue dots in the SOX9/SOX10 high quadrant of the data set), suggesting that high Sox9 activity could occur without increased Akt activity. Similarly, Sox9 is highly phosphorylated in human triple-negative breast cancers expressing high levels of Sox10 (see Fig. 3 and (37)). Therefore, it is possible that a similar mechanism exists in breast cancers that display high level of PI3K/AKT pathway activation. In fact, oncogenic activation of the PI3K/AKT signaling pathway is frequent in TNBC and most commonly occurs following PIK3CA gain-of-function mutations or P53 inactivation (40,41). Treatment of triple-negative breast cancer cell lines with the allosteric AKT inhibitor, MK-2206, inhibits tumor growth and increases sensitivity to other chemotherapeutic agents (42–44). Clinical trials for TNBC have shown that AKT inhibitors, including MK-2206, have a synergistic effect with paclitaxel and significantly improve progression-free and overall survival (42,43). In addition to regulating cell survival and promoting tumor growth, we have shown that AKT controls the expression of Sox10. Therefore, we believe that the therapeutic targeting of AKT could decrease mammary tumor stem/progenitor activity by downregulating SOX10 expression in TNBC.

A recent murine model for TNBC has identified a high frequency of both Egfr and Fgfr2 amplifications (21,30). FGF-signaling has previously been shown to induce the expression of both Sox9 and Sox10 (21,30). In light of our observations, Fgfr2 amplifications in TNBC (41) may be sufficient to upregulate Sox9 expression. Combined with gain-of-function mutations in PIK3CA, this would be sufficient to increase Sox9 activity in an AKT-dependent manner. Therefore, the combinatorial treatment of triple-negative breast cancers with FGFR and AKT inhibitors may target two distinct signaling pathways that drive SOX10 expression by blocking both the induction and activation of Sox9.

One of the largest barriers to the effective treatment of HER2-positive breast cancers is the rapid acquisition of Herceptin-resistance (45,46) often accompanied by significantly elevated levels of phosphorylated active AKT (47). As both chronic Herceptin treatment and SLK deletion result in the hyperactivation of AKT, we speculate that these Herceptin-resistant tumors may have also acquired SOX10 expression. Therefore, it is possible that Herceptin-resistant tumors with high levels of AKT activity may be dependent on the oncogenic and stem/progenitor activities of Sox10.

Conclusion

We and others have reported that triple-negative and basal/stem-like breast cancers can be defined by a high level of SOX10 expression (20,48–51). Here, we have uncovered a novel link between constitutive activation of AKT, Sox9 phosphorylation, and the induction of Sox10 gene expression. Our studies have identified Sox9 as a novel AKT substrate. As recently highlighted (20,22), Sox10 transcriptional reprogramming may be a hallmark of TNBCs. This raises the possibility that targeted therapies to the Sox9-Sox10 axis could represent an important first step in the treatment of TNBCs. This might also have major implications in the targeting of tumor stem cells in TNBCs and our understanding of the role of Sox9 and Sox10 during development.

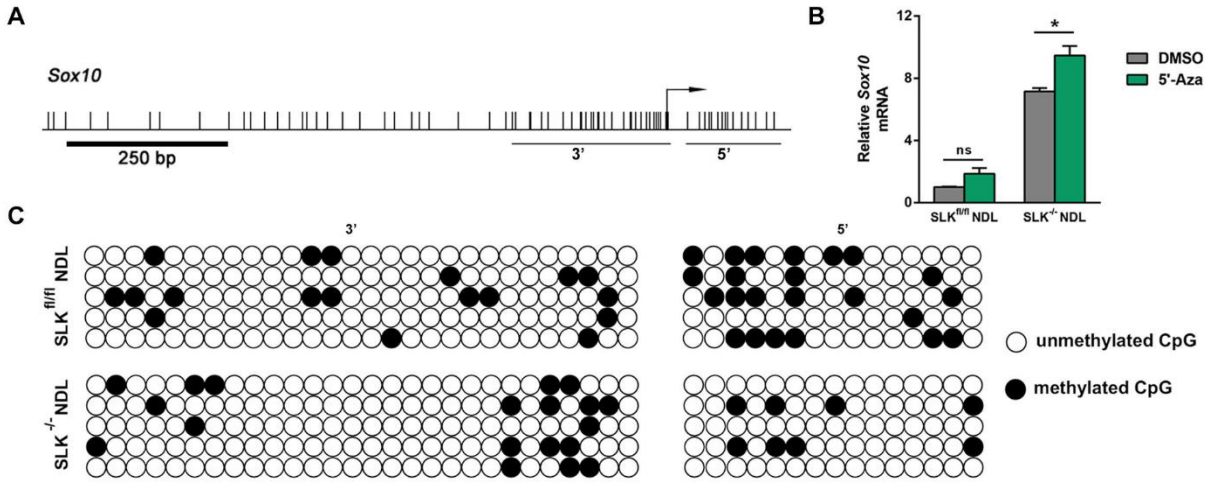

Supplementary Figure 1. Induction of *Sox10* following *Slk* deletion is not due to promoter demethylation. A, Schematic representation of the murine *Sox10* gene. The transcriptional start site is indicated by the forward arrow. The location of all CG dinucleotides are represented as individual vertical lines. Methprimer CpG prediction software was used to identify potential CpG islands and are shown as the underlined regions. **B,** $SLK^{fl/fl}$ and $SLK^{-/-}$ NDL cells were treated with 5-aza-2'-deoxycytidine (5'-Aza) for five days. The levels of *Sox10* transcript was assessed by qPCR analysis. **C,** Bisulfite sequencing of genomic DNA from $SLK^{fl/fl}$ and $SLK^{-/-}$ NDL cells was performed. Five independent clones from each cell line was sequenced. A representative plot of unmethylated (open) and methylated (filled) CpG repeats from two putative CpG islands identified in (**A**) is presented. ns: no statistical difference, * $p < 0.05$.

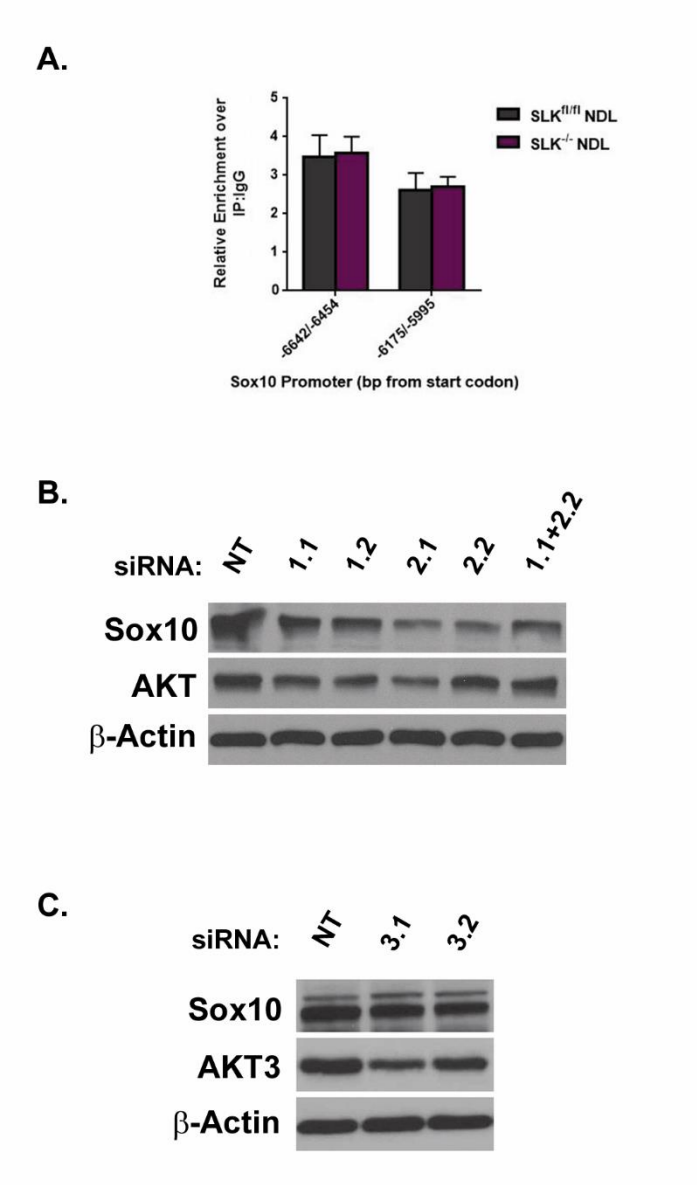

Supplementary Figure 2. Sox10 induction is preferentially mediated by AKT2. (**A**) Chromatin immunoprecipitation (ChIP) was performed on SLKfl/fl and SLK-/- NDL cells to assess K27 Acetylated histone H3 binding to the Sox10 enhancers. Following ChIP, qPCR analysis was performed across two putative SoxE binding sites within the -6904/-5995 fragment of the Sox10 promoter. qRT-PCR data was normalized to an IgG ChIP or a negative control element within exon one (-150/+103) as in Fig 2. No statistical differences were observed between the cell lines. N=3. (**B**) Knock down of AKT1 or AKT2 results in Sox10 downregulation. AKT1 knockdowns

were ~50% at best with two independent siRNAs. AKT2 knockdowns with two siRNAs ranged from 50-70% with a marked downregulation (80-90%) of Sox10. (**C**) AKT3 knockdowns from 40-60% did not show any appreciable reduction in Sox10 levels. Underexposed blots were subjected to ImageJ densitometry and normalized to β-actin and NT controls. NT= non targeting siRNA control.

References

1. Perou CM, Sørile T, Eisen MB, Van De Rijn M, Jeffrey SS, Ress CA, et al. Molecular portraits of human breast tumours. Nature. 2000 Aug 17;406(6797):747–52.

2. Sørlie T, Perou CM, Tibshirani R, Aas T, Geisler S, Johnsen H, et al. Gene expression patterns of breast carcinomas distinguish tumor subclasses with clinical implications. Proc Natl Acad Sci U S A. 2001 Sep 11;98(19):10869–74.

3. Mansour EG, Ravdin PM, Dressier L. Prognostic factors in early breast carcinoma. Cancer. 1994;74(1 S):381–400.

4. Guy CT, Webster MA, Schaller M, Parsons TJ, Cardiff RD, Muller WJ. Expression of the neu protooncogene in the mammary epithelium of transgenic mice induces metastatic disease. Proc Natl Acad Sci U S A. 1992;89(22):10578–82.

5. Dankort DL, Wang Z, Blackmore V, Moran MF, Muller WJ. Distinct Tyrosine Autophosphorylation Sites Negatively and Positively Modulate Neu-Mediated Transformation. Mol Cell Biol. 1997 Sep 1;17(9):5410–25.

6. Gullick WJ, Srinivasan R. The type 1 growth factor receptor family: New ligands and receptors and their role in breast cancer. Breast Cancer Res Treat. 1998;52(1–3):43–53.

7. Harari D, Yarden Y. Molecular mechanisms underlying ErbB2/HER2 action in breast cancer. Oncogene [Internet]. 2000 Dec 11 [cited 2023 Aug 24];19(53):6102–14. Available from: https://pubmed.ncbi.nlm.nih.gov/11156523/

8. Role of HER2 gene overexpression in breast carcinoma [Internet]. [cited 2023 Aug 24]. Available from: https://onlinelibrary-wiley-com.proxy.bib.uottawa.ca/doi/epdf/10.1002/%28SICI%291097-4652%28200002%29182%3A2%3C150%3A%3AAID-JCP3%3E3.0.CO%3B2-E

9. Al-Zahrani KN, Baron KD, Sabourin LA. Ste20-like kinase SLK, at the crossroads: A matter of life and death. Cell Adh Migr. 2013;7(1):1–10.

10. Quizi JL, Baron K, Al-Zahrani KN, O'Reilly P, Sriram RK, Conway J, et al. SLK-mediated phosphorylation of paxillin is required for focal adhesion turnover and cell migration. Oncogene. 2013 Sep 26;32(39):4656–63.

11. Wagner S, Storbeck CJ, Roovers K, Chaar ZY, Kolodziej P, McKay M, et al. FAK/src-family dependent activation of the Ste20-like kinase SLK is required for microtubule-dependent focal adhesion turnover and cell migration. PLoS One. 2008 Apr 2;3(4).

12. Conway J, Al-Zahrani KN, Pryce BR, Abou-Hamad J, Sabourin LA. Transforming growth factor β-induced epithelial to mesenchymal transition requires the Ste20-like kinase SLK independently of its catalytic activity. Oncotarget. 2017;8(58):98745–56.

13. Wang K, Hong RL, Lu JB, Wang DL. Ste20-like kinase is upregulated in glioma and induces glioma invasion. Neoplasma. 2018;65(2):185–91.

14. Roovers K, Wagner S, Storbeck CJ, O'Reilly P, Lo V, Northey JJ, et al. The Ste20-like kinase SLK is required for ErbB2-driven breast cancer cell motility. Oncogene. 2009 Aug 6;28(31):2839–48.

15. Manning BD, Toker A. AKT/PKB Signaling: Navigating the Network. Cell. 2017 Apr 20;169(3):381–405.

16. Bondurand N, Sham MH. The role of SOX10 during enteric nervous system development. Dev Biol. 2013 Oct 1;382(1):330–43.

17. She ZY, Yang WX. SOX family transcription factors involved in diverse cellular events during development. Eur J Cell Biol. 2015 Dec 1;94(12):547–63.

18. Xu YR, Yang WX. SOX-mediated molecular crosstalk during the progression of tumorigenesis. Semin Cell Dev Biol. 2017 Mar 1;63:23–34.

19. Malladi S, MacAlinao DG, Jin X, He L, Basnet H, Zou Y, et al. Metastatic Latency and Immune Evasion through Autocrine Inhibition of WNT. Cell. 2016 Mar 24;165(1):45–60.

20. Al-Zahrani KN, Cook DP, Vanderhyden BC, Sabourin LA. Assessing the efficacy of androgen receptor and Sox10 as independent markers of the triple-negative breast cancer subtype by transcriptome profiling. Oncotarget. 2018 Sep 1;9(70):33348–59.

21. Dravis C, Spike BT, Harrell JC, Johns C, Trejo CL, Southard-Smith EM, et al. Sox10 Regulates Stem/Progenitor and Mesenchymal Cell States in Mammary Epithelial Cells. Cell Rep. 2015 Sep 29;12(12):2035–48.

22. Dravis C, Chung CY, Lytle NK, Herrera-Valdez J, Luna G, Trejo CL, et al. Epigenetic and transcriptomic profiling of mammary gland development and tumor models disclose regulators of cell state plasticity. Cancer Cell [Internet]. 2018 Sep 9 [cited 2023 Aug 24];34(3):466. Available from: /pmc/articles/PMC6152943/

23. Al-Zahrani KN, Abou-Hamad J, Cook DP, Pryce BR, Hodgins JJ, Labrèche C, et al. Loss of the Ste20-like kinase induces a basal/stem-like phenotype in HER2-positive breast cancers. Oncogene. 2020 Jun 4;39(23):4592–602.

24. Tong X, Li L, Li X, Heng L, Zhong L, Su X, et al. SOX10, a novel HMG-box-containing tumor suppressor, inhibits growth and metastasis of digestive cancers by suppressing the wnt/β-catenin pathway. Oncotarget. 2014;5(21):10571–83.

25. Jin SG, Xiong W, Wu X, Yang L, Pfeifer GP. The DNA methylation landscape of human melanoma. Genomics. 2015 Dec 1;106(6):322–30.

26. Li LC, Dahiya R. MethPrimer: Designing primers for methylation PCRs. Bioinformatics. 2002 Nov 1;18(11):1427–31.

27. Antonellis A, Huynh JL, Lee-Lin SQ, Vinton RM, Renaud G, Loftus SK, et al. Identification of neural crest and glial enhancers at the mouse Sox10 locus through transgenesis in zebrafish. PLoS Genet. 2008 Sep;4(9).

28. Betancur P, Bronner-Fraser M, Sauka-Spengler T. Genomic code for Sox10 activation reveals a key regulatory enhancer for cranial neural crest. Proc Natl Acad Sci U S A. 2010 Feb 23;107(8):3570–5.

29. Betancur P, Sauka-Spengler T, Bronner M. A sox10 enhancer element common to the otic placode and neural crest is activated by tissue-specific paralogs. Development. 2011 Sep 1;138(17):3689–98.

30. Chen Z, Huang J, Liu Y, Dattilo LK, Huh SH, Ornitz D, et al. FGF signaling activates a Sox9-Sox10 pathway for the formation and branching morphogenesis of mouse ocular glands. Development (Cambridge). 2014;141(13):2691–701.

31. Dutton JR, Antonellis A, Carney TJ, Rodrigues FSLM, Pavan WJ, Ward A, et al. An evolutionarily conserved intronic region controls the spatiotemporal expression of the transcription factor Sox10. BMC Dev Biol. 2008;8.

32. Werner T, Hammer A, Wahlbuhl M, Bösl MR, Wegner M. Multiple conserved regulatory elements with overlapping functions determine Sox10 expression in mouse embryogenesis. Nucleic Acids Res. 2007 Oct;35(19):6526–38.

33. Coricor G, Serra R. TGF-β regulates phosphorylation and stabilization of Sox9 protein in chondrocytes through p38 and Smad dependent mechanisms. Sci Rep. 2016 Dec 8;6.

34. Huang W, Zhou X, Lefebvre V, de Crombrugghe B. Phosphorylation of SOX9 by Cyclic AMP-Dependent Protein Kinase A Enhances SOX9's Ability To Transactivate a Col2a1 Chondrocyte-Specific Enhancer . Mol Cell Biol. 2000 Jun 1;20(11):4149–58.

35. Kumar D, Lassar AB. The Transcriptional Activity of Sox9 in Chondrocytes Is Regulated by RhoA Signaling and Actin Polymerization. Mol Cell Biol. 2009 Aug 1;29(15):4262–73.

36. Malki S, Nef S, Notarnicola C, Thevenet L, Gasca S, Méjean C, et al. Prostaglandin D2 induces nuclear import of the sex-determining factor SOX9 via its cAMP-PKA phosphorylation. EMBO Journal. 2005 May 18;24(10):1798–809.

37. Ma Y, Shepherd J, Zhao D, Bollu LR, Tahaney WM, Hill J, et al. SOX9 is essential for triple-negative breast cancer cell survival and metastasis. Molecular Cancer Research. 2020 Dec 1;18(12):1825–38.

38. Huang YH, Jankowski A, Cheah KSE, Prabhakar S, Jauch R. SOXE transcription factors form selective dimers on non-compact DNA motifs through multifaceted interactions between dimerization and high-mobility group domains. Sci Rep. 2015 May 27;5.

39. Pei JJ, An WL, Zhou XW, Nishimura T, Norberg J, Benedikz E, et al. P70 S6 kinase mediates tau phosphorylation and synthesis. FEBS Lett. 2006 Jan 9;580(1):107–14.

40. Cossu-Rocca P, Orrù S, Muroni MR, Sanges F, Sotgiu G, Ena S, et al. Analysis of PIK3CA mutations and activation pathways in triple negative breast cancer. PLoS One. 2015 Nov 5;10(11).

41. Liu H, Murphy CJ, Karreth FA, Emdal KB, Yang K, White FM, et al. Identifying and targeting sporadic oncogenic genetic aberrations in mouse models of triple-negative breast cancer. Cancer Discov. 2018 Mar 1;8(3):354–69.

42. Costa RLB, Han HS, Gradishar WJ. Targeting the PI3K/AKT/mTOR pathway in triple-negative breast cancer: a review. Breast Cancer Res Treat. 2018 Jun 1;169(3):397–406.

43. Kim SB, Maslyar DJ, Dent R, Im SA, Espié M, Blau S, et al. Ipatasertib plus paclitaxel versus placebo plus paclitaxel as first-line therapy for metastatic triple-negative breast cancer (LOTUS): a multicentre, randomised, double-blind, placebo-controlled, phase 2 trial. Lancet Oncol. 2017 Oct 1;18(10):1360–72.

44. Sangai T, Akcakanat A, Chen H, Tarco E, Wu Y, Do KA, et al. Biomarkers of rsponse to Akt inhibitor MK-2206 in breast cancer. Clinical Cancer Research. 2012 Oct 15;18(20):5816–28.

45. Gajria D, Chandarlapaty S. HER2-amplified breast cancer: Mechanisms of trastuzumab resistance and novel targeted therapies. Expert Rev Anticancer Ther. 2011 Feb;11(2):263–75.

46. Wolff AC, Hammond MEH, Schwartz JN, Hagerty KL, Alfred DC, Cote RJ, et al. American Society of Clinical Oncology/College of American Pathologists guideline recommendations for human epidermal growth factor receptor 2 testing in breast cancer. Arch Pathol Lab Med. 2007 Jan;131(1):18–43.

47. Chan CT, Metz MZ, Kane SE. Differential sensitivities of trastuzumab (Herceptin®)-resistant human breast cancer cells to phosphoinositide-3 kinase (PI-3K) and epidermal growth factor receptor (EGFR) kinase inhibitors. Breast Cancer Res Treat. 2005 May;91(2):187–201.

48. Cimino-Mathews A, Subhawong AP, Elwood H, Warzecha HN, Sharma R, Park BH, et al. Neural crest transcription factor Sox10 is preferentially expressed in triple-negative and metaplastic breast carcinomas. Hum Pathol. 2013 Jun;44(6):959–65.

49. Feng W, Liu S, Zhu R, Li B, Zhu Z, Yang J, et al. SOX10 induced Nestin expression regulates cancer stem cell properties of TNBC cells. Biochem Biophys Res Commun. 2017 Apr 1;485(2):522–8.

50. Krings G, Joseph NM, Bean GR, Solomon D, Onodera C, Talevich E, et al. Genomic profiling of breast secretory carcinomas reveals distinct genetics from other breast cancers and similarity to mammary analog secretory carcinomas. Modern Pathology. 2017 Aug 1;30(8):1086–99.

51. Min L, Zhang C, Qu L, Huang J, Jiang L, Liu J, et al. Gene regulatory pattern analysis reveals essential role of core transcriptional factors' activation in triple-negative breast cancer. Oncotarget. 2017;8(13):21938–53.